FIRE DYNAMICS AND FORENSIC ANALYSIS OF LIQUID FUEL FIRES

Final Report

Grant No. 2008-DN-BX-K168

Prepared by:

Christopher L. Mealy, Matthew E. Benfer, and Daniel T. Gottuk

Hughes Associates, Inc.
3610 Commerce Drive, Suite 817
Baltimore, MD 21227
Ph. 410-737-8677 FAX 410-737-8688

February 18, 2011

ABSTRACT

Liquid fuel spill/pool fires represent the initiating fire hazard in many applications ranging from accidents at industrial plants using combustible liquids to residential arson fires involving flammable fuels. Given the relevancy of such fires and broad range of potential scenarios, it is important to understand how liquid fuel fires develop and how to accurately calculate the fire size based on knowledge of the fuel type, quantity and the surface it is poured on. In addition, it is important to quantitatively correlate fire size to spill area and burn patterns. This understanding will afford the fire protection and investigation communities the ability to properly assess the potential hazards and forensically evaluate damage from fuel spill fire events. The purpose of this study is to expand the fundamental understanding of liquid fuel fire dynamics, establish the utility of forensic tools, and validate empirically-based correlations used to model spill fire scenarios. A multitude of small-, intermediate-, and large-scale non-combustible liquid spill and fuel spill fire tests were conducted using a total of six different liquid fuels and eight different substrates. The results of these tests provide insight into the differences in fire dynamics between pool and spill fires (i.e., thick and thin fuel depths), provide a methodology by which liquid fuel fire events can be assessed, and identify forensic indicators that can be used in the analysis of liquid fuel fire events.

TABLE OF CONTENTS

LIST OF FIGURES

LIST OF TABLES

EXECUTIVE SUMMARY

Liquid fuel spill/pool fires can be defined as a diffusion flame established over top of a horizontal liquid fuel surface. The primary variables in a liquid fuel fire are the quantity of fuel and the area over which the liquid is permitted to spread. These variables will dictate whether it is confined to a fixed area (i.e., pool) or simply bounded by the equilibrium forces controlling the motion of the fluid (i.e., spill). The nature of a spill fire is highly variable, depending on the source of the release, the thermal characteristics and surface features of the substrate that the fuel is spilled on (e.g., concrete, ground, water), and the point and time of ignition. Given the relevancy of such fires and broad range of potential scenarios, it is important to have an understanding of the evolution of fuel spill fires from inception to extinguishment. Developing such an understanding requires the identification of key parameters governing the progression of a spill (i.e., area and depth) as well as the burning dynamics of the spill once ignited. Key parameters include properties of the fuel, properties of the substrate, and inherent interfacial properties developed between the liquid and substrate. To date, most assessments of fuel spill fires are based upon data obtained from confined pool fire experiments. The aptness of assuming equivalent burning rates between spills and pools has not been fully vetted. Data available in the literature indicates that significant differences in mass burning rates exist between spill and pool fires, which dramatically affects how fire size is calculated, resulting in a factor of five difference. However, since these findings are based on only two studies with limited fuels, additional work with a wider range of fuels and substrates was warranted.

The objectives of this research were achieved by way of small- and full-scale experiments combined with analytical testing and empirical-based analyses. A summary of the tests conducted and the rationale for their execution is provided in Table E.1. In this study, a wide variety of liquids and spill substrates were evaluated. The selection of these liquids and spill substrates was based upon their prevalence and relevancy in real-world fire scenarios. A total of 8 liquids were considered, including: 3 flammable, 3 combustible, and 2 aqueous-based samples. In addition to the liquid fuels used, three different Class A materials were tested in order to characterize fire pattern similarities/differences between liquid fuel and Class A sources. Similarly, a total of 8 spill substrates were selected, 4 concrete finishes, 2 wood flooring materials, a vinyl flooring material, and a base grade carpet with pad. Other variables considered in this work included fuel depth, ignition delay, and substrate temperature.

The results of these tests allowed for the examination of the effects of various parameters (i.e., fuel quantity, substrate, ignition delay) on both the spill and fire dynamics of scenarios resulting from the release of various quantities of liquid. This work also provided insight into the forensic fire patterns developed from both liquid and Class A fuel fires atop a variety of surfaces.

Table E.1. Summary of Testing Conducted

Test Series Name	**Rationale for Testing**
Cone Calorimeter Pan Fires	**Primary:** Characterize the effective heat of combustion of test fuels under free-burning, ambient conditions. **Secondary:** Characterize impact of fuel depth on burning rate in convectively dominated burning regime.
Pan Fires	Benchmark and characterize impact of fuel depth on burning rate.
Diked Fires	Characterize impact of substrate on fuel burning rate.
Spill Dynamics	Characterize spill area and depth of various liquids.
Spill Fire Dynamics	Characterize fuel spill dynamics and spill fire dynamics of fuels on various substrates.
Continuous Spill Fires	Characterize the steady state burning rate of spill fires (approximately 1 mm depth).
Class A Fires	Characterize fire patterns from Class A fires.
Physical Properties Analysis	Characterize physical properties of liquids.
Combustion Properties Analysis	Characterize combustion properties of fuels.

Based upon a statistical analysis of the fluid depths measured in the spill dynamics testing for all spill quantities, liquid types (except lube oil), and substrates, the average depth was 0.72 mm with a standard deviation of 0.34 mm. This value is consistent with the values currently recommended in the literature for minimum liquid spill depths. The range of spill depths measured was from 0.22 mm up to 2.4 mm depending upon the specific liquid/substrate scenario. This relatively wide range of empirical depths demonstrates the importance of understanding key variables governing fluid spread such that an appropriate spill depth is used when performing an analysis. The primary two factors governing the spread of a fuel and the equilibrium spill depth reached are the surface tension of the liquid and the surface characteristics of the substrate. However, given that the surface tensions of most fuels of interest are relatively similar; this parameter is generally not as influential, when considering the characteristics of a spill. The more dominant variable to consider is the substrate surface topography which can have a substantial impact on the spread and equilibrium spill depth, both of which play an important role in predicting the fire hazard resulting from the spill. It is for this reason that an understanding of the surface on which a spill occurs is far more important than understanding the fuel that was spilled, from a spill dynamics standpoint.

The experimental data set was also used to investigate correlations between equilibrium spill depth and both liquid properties and initial spill volumes. Equilibrium spill depth correlated relatively well with the surface tension of the liquid and as surface tension decreased, so did the equilibrium spill depth. When examining the relationship between initial spill volume and equilibrium spill depth, an increasing trend was also observed (i.e., as spill volume increased, so did the measured equilibrium spill depth). Currently, there are inconsistencies between the empirical and theoretical data presented in the literature. These inconsistencies are attributed to the variability in the surface characteristics that are not accounted for in the theoretical solution. These differences could lead to ancillary effects that cause the spilled liquid to slow in its progression or stop all together, leading to localized pooling of the liquid.

In addition to fire diameter, the burning rate of a fuel was shown to be dependent upon several factors including, but not limited to, fuel quantity, substrate, and ignition delay. Fuel quantity was identified as a factor because it can be directly related to the depth of fuel for fixed quantity/fixed area fires and can be applied to scenarios in which the fires are continuously-fed. For fixed quantity scenarios, the volume of liquid spilled is proportional to the depth of liquid within the area of coverage. For these scenarios, a depth of 5 mm was established as the minimum depth for which a steady-state peak mass burning rate can be achieved for fuel on steel, water, concrete, and vinyl substrates. At depths less than 5 mm, the peak burning rates were consistently less than the diameter dependent, steady-state maximum burning rate. The mass burning rate associated with fixed quantity 1 mm fuel depths was on the order of 70–80 percent of the steady-state maximum. Based upon the data collected, correlations were developed for both gasoline and kerosene that can be used to predict the reduction on peak mass burning rate as a function of fuel depth. The product of these correlations when coupled with the diameter dependent mass burning rate correlation available in the literature can be used to predict more appropriate mass burning rates for thin fuel layer scenarios. Although this 5 mm depth criterion was found to be appropriate for all fixed quantity scenarios, the same was not true for continuously-fed fire scenarios. In these scenarios, fuel depths on the order of 1 mm were maintained while still achieving peak mass burning rates that were comparable to the diameter dependent maximum steady-state mass burning rates. These results demonstrated that it is not the depth of fuel that impacts the peak mass burning rate but that it is the quantity of fuel available to burn (i.e., burn long enough to achieve steady-state). At the beginning of this project, one hypothesis was that the reduction in mass burning rate for a thin layer fuel compared to pool fires was attributed to enhanced heat transfer between the substrate and the thin fuel layer. However, as described above, the main reason for the difference was due to thin, fixed quantity fuel spills not being able to burn long enough to reach maximum steady-state burning rates.

The second parameter identified as having an impact on the mass burning rate of a fuel was the substrate on which the fuel is burning. The data shows that mass burning rates of a fuel is different when burned atop surfaces with differing thermal properties. The rank order of the mass burning rates for each fire size were consistent with the highest burning rates occurring on the vinyl flooring and the lowest on concrete. For the scenarios evaluated, no specific thermal property of the substrates (i.e., thermal conductivity, thermal inertia, thermal effusivity, and thermal diffusivity) could be directly correlated to the rank order of burning rates. In general, less thermally conductive materials (i.e., vinyl and water) produced mass burning rates higher than those achieved in tests with more thermally conductive substrates (i.e., steel and concrete). However, the ranking of mass burning rates with respect to the thermal conductivity of the substrates was not appropriate when evaluating the case of the concrete and steel. In this case, the mass burning rates measured on the concrete were consistently lower than those measured on the steel despite the fact that the thermal conductivity of the steel is an order of magnitude larger than that of the concrete. This discrepancy may be attributed to the reflectivity of the steel and the resulting re-radiation from the steel substrate to the fuel layer. This reflected heat was then transferred into the fuel layer thus raising the mass burning rate of the fuel. In general, the influence of the substrate was only found to be significant for fuel depths less than 5 mm.

Typically, when discussing the impact of a substrate on the mass burning rate of a fuel, it is assumed that the substrate is acting as a heat sink (i.e., removing heat from the fuel layer), thus

reducing the peak burning rate. However, a small subset of tests in which the fuel substrate was heated to temperatures greater than ambient conditions demonstrates that an opposite affect can occur and have significant impact. These tests, while limited, showed that an elevated substrate temperature can increase the peak mass burning achieved during a spill fire scenario. This increase is attributed to the heated substrate pre-heating the fuel layer prior to ignition, reducing heat loss from the fuel to the substrate and reducing the amount of energy required to volatize the fuel, thus more fuel can be evaporated.

The results from the spill fire tests also identified the third parameter impacting the peak mass burning rate achieved. This parameter was the ignition delay time (i.e., the time between the initial spill and ignition of the spilled liquid). Ignition delay times of 30 and 300 seconds were evaluated. In general, the 300 second ignition delay tests resulted in larger areas with reduced peak mass burning rates per unit area. However, the differences in the average increase in spill area from the 30-second to the 300 second ignition delay times ranged from 8–76 percent with an average value of 36 percent. The percent decrease in the average peak heat release rates range from 25 to 74 with an average of 52 percent, respectively. Although the effects resulting from delayed ignition could not be fully explained using the data collected, substrate cooling and evaporative fuel losses were shown to account for some of the changes in peak mass burning rate.

It should be noted that for all tests conducted on all substrates and all fuel depths, the impact of diameter on peak mass burning rate per unit area was evident and followed a power-law correlation as well established in the literature. Furthermore, on average the maximum mass burning rate achieved by the multi-constituent fuels (i.e., gasoline and kerosene) were approximately 20 percent lower than the data currently available in the literature; whereas for the pure fuel evaluated (heptanes), the mass burning rate was equivalent to literature values. The reduction in mass burning rate for the multi-constituent fuels was attributed to the reduction in volatility and inclusion of more alcohols in the multi-constituent blends.

Using the data collected in this study, an analytical methodology was developed. The analytical framework can be used in two capacities: 1) to predict the fire hazard associated with a fuel spill fire scenario, and 2) provide a tool that can be used to gain insight into a fuel spill scenario based upon the fire patterns produced by the event.

With respect to the fire analysis of both the fuel spill and Class A fires, the fuel spill fire patterns were generally comparable in area to the areas measured for the spills prior to ignition. For non-combustible substrates, the pre- and post-fire pattern areas were nearly identical; while for the combustible substrates, except carpet, fire pattern areas were up to 14 percent larger than initial spill areas. For carpet scenarios, the area of pattern involvement was time dependent due to the fact that the fire pattern areas continued to increase as the flame front moved outwards from the spill due to sustained burning of the carpet and carpet padding. After the liquid fuel was consumed, flame spread rates over the carpet surface, ranged from 1.1–1.4 cm/min. (0.41–0.55 in./min). Substrate damage from the liquid fuel spill fires was generally minimal, primarily consisting of thermal discoloration and staining of the material. The damage to the substrate was mostly superficial with some evidence of the early stages of thermal decomposition of the wood. Damage resulting from the Class A fuels varied depending upon the fuel, with some fuels

resulting in complete burn-through of the substrate and others resulting in thermal damage with large quantities of oily residue being deposited atop the substrate.

Several types of patterns were consistently identified for certain fuel types. Liquid fuel spill fires consistently resulted in irregularly-shaped burn patterns with minimal thermal damage to the substrate, except in the case of carpet scenarios. Class A fuels constructed from plastic and foam materials consistently left an oily residue on the substrate after self-extinguishing upon fuel consumption. Based on visual pattern shapes, there were no clear indicators to differentiate between Class A and flammable liquid fuel fires. However, the extent of damage (i.e., char depths and burn through) was greater for the Class A fires compared to fuel spill fires.

In summary, this research provides new insight into the effects of various parameters on the spill and burning dynamics of fuel spill scenarios. A variety of fuels, substrates, and conditions were evaluated to capture a wide range of potential scenarios. From this set of spill fire data an analytical methodology was developed to serve as a tool for the fire protection and forensic communities.

1.0 INTRODUCTION

Liquid fuel spill/pool fires represent the initiating fire hazard in many applications ranging from accidents at industrial plants using combustible liquids to residential arson fires involving flammable fuels. All of these scenarios can be defined as a diffusion flame established over top of a horizontal fuel surface. However, the primary variable in a liquid fuel spill is whether or not it is confined to a fixed area (i.e., pool) or simply bounded by the equilibrium forces controlling the motion of the fluid (i.e., spill). Pool fires are generally defined as a confined body of fuel having a depth of greater than 1 cm [Gottuk et al., 2008]. A pool can result due to a spill that collects in a low spot, such as a trench, or can exist as a result of normal storage of fuels in tanks and containers. The nature of a spill fire is highly variable, depending on the source of the release, the thermal characteristics and surface features of the substrate that the fuel is spilled on (e.g., concrete, ground, water), and the point and time of ignition.

Given the relevancy of such fires and broad range of potential scenarios it is important to have an understanding of the evolution of fuel spill fires from their inception to the time at which they extinguish. Developing such an understanding requires the identification of key variables governing the progression of a liquid fuel spill as well as the burning dynamics of the spill once ignited. These key variables include properties of the fuel, properties of the substrate, and inherent interfacial properties developed between the liquid and substrate. A summary of these variables is provided in Table 1.1.

Table 1.1. Summary of Variables Governing Liquid Fuel Spill Progression and Burning Rate

Fuel Properties	**Substrate Properties**	**Interfacial Properties**
• Surface Tension • Viscosity • Density • Flashpoint • Mass Burning Rate	• Surface Contour • Surface Roughness • Surface Permeability • Thermal Inertia • Combustibility	• Contact Angle

Understanding the development of fuel spill fires will afford the fire protection community the ability to properly assess the potential hazards and resulting forensic damage from these events. To date, most assessments are developed based upon the assumption that data obtained from confined pool fire experiments are applicable to spill fire scenarios. The aptness of this assumption has not been fully vetted, thus reinforcing the need to understand the fire dynamics of fuel spill fires. The work of Gottuk et al. [2000] and Putorti [2001] indicate that significant differences in mass burning rates exist between spill and pool fires. These findings dramatically affect how fire size is calculated, resulting in a factor of five differences. However, since these findings are based on only two studies with limited fuels, additional work with a wider range of fuels and substrates is warranted. The research presented in this paper was designed to characterize the burning dynamics of fuels of various depths, to develop an in-depth understanding of the spill progression and burning dynamics of fuel spill fires, and to evaluate the utility of currently available forensic analysis tools as they relate to these fire events.

1.1 Literature Review

1.1.1 Pool Fire Dynamics

This section summarizes the findings of key works from the pool fire literature whose experimental focus was the understanding of pool fire burning dynamics. More specifically, the works summarized herein provide insight and data describing the pool fire mass burning rates and governing parameters for pool fires that were used throughout this study. Parameters such as pool diameter, mass burning rate, and fuel depth are discussed. It is not the intent of this section to provide a historical review of the study of pool fires. For such a description the reader is referred to the works of Joulain [1998] and Steinhaus et al. [2007].

1.1.1.1 Pool Geometries and Burning Rates

The earliest and most extensive study of hydrocarbon pool fire burning dynamics is that of Blinov & Khudyakov [1961] further analyzed by Hottel [1959]. In this work, the authors studied a variety of parameters influencing the burning rates of liquid hydrocarbon pool fires. One such parameter was the geometry of the pool (i.e., the physical dimensions). Pool fires ranging in size from 3.7 mm–22.9 m in diameter were evaluated using a variety of different fuels. From these tests, two distinct burning regimes were identified. The regimes identified from the work of Blinov & Khudyakov [1961] were a radiatively dominated regime for large diameter fires and a convectively dominated regime for small diameter fires. Based upon additional analysis of available data sets, Babrauskas [1983] further divided each of these burning regimes into two burning modes based upon the governing modes of heat feedback to the fuel surface. A summary of the four burning modes identified by Babrauskas [1983] are provided in Table 1.2.

Table 1.2. Pool Fire Burning Modes as Identified by [Babrauskas, 1983]

Diameter (m)	**Burning Mode**
< 0.05	Convective, Laminar
0.05–0.2	Convective, Turbulent
0.2–1.0	Radiative, Optically Thin
>1.0	Radiative, Optically Thick

The burning regimes identified by Blinov & Khudyakov [1961] and Babrauskas [1983] are based upon changes in the dominant mode of heat feedback to the fuel surface that occurs as the diameter of a pool fire increases. An illustration of the impact of these changes was first presented by Blinov & Khudyakov [1961] for a variety of fuels and is presented below in Figure 1.1. Unfortunately, due to the scale of some of the tests conducted mass loss rate data was not collected. Instead the authors documented the burning rate of the fuel as a function of the fuel regression rate in the separate fuel metering tanks being used to maintain a constant fuel depth for the pool fire.

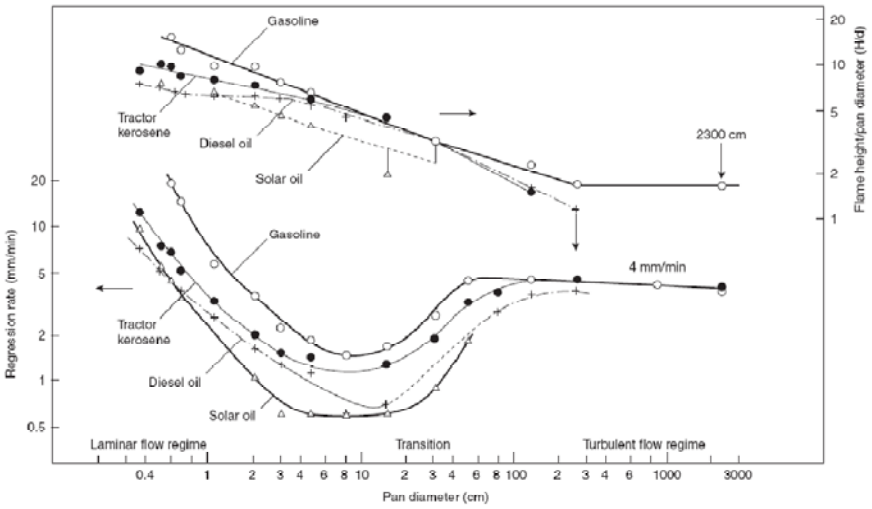

Figure 1.1. Summary of regression rate data compiled from the work of [Blinov & Khudyakov, 1961]

Based upon the foundation provided by Blinov & Khudyakov [1961] and Hottel [1959], a relationship characterizing the effects of these changes on the burning rate was first developed by Burgess et al. [1960] and is presented in Eq. 1.

$$\dot{m}'' = \dot{m}''_{max}[1 - \exp(-k\beta D)] \qquad \text{Eq. 1}$$

In this relationship k, β, and $\dot{m}''_{max}$, are all fuel specific parameters. Furthermore, $\dot{m}''_{max}$, is often referred to as the mass burning rate for an infinite-diameter pool (this term also represents a steady-state value). The parameters k and β are typically determined jointly with k being the extinction-absorption coefficient of the flame and β the mean beam length corrector. The most complete collection of this data has been compiled by Babrauskas [1983]. A subset of this data compilation is provided in Table 1.3 for fuels related to this study.

Table 1.3. Summary of Relevant Pool Fire Burning Dynamics Data [Babrauskas, 1983]

Fuel Description	**Density (kg/m^3)**	**Heat of Combustion (MJ/kg)**	**Avg. Maximum Burning Rate per Unit Area (kg/s-m^2)**	**kβ**
Gasoline	740	43.7	0.055	2.1
Kerosene	820	43.2	0.039	3.5
Diesel	N/A	N/A	N/A	N/A
n-Heptane	675	44.6	0.101	1.1
Methanol	796	20.0	0.017	N/A
Ethanol	794	26.8	0.015	N/A

N/A–Data not provided

It should be noted that the data sets used to develop the relationship described in Eq. 1 and the data provided in Table 1.3 originate from the steady state burning of relatively deep pools of fuel

(i.e., typically greater than 1 cm); thus, their application is only appropriate in confined scenarios in which a fuel can achieve a sufficient depth.

In addition to the effects of diameter on the mass burning rate of fuels, the impacts of the boundaries of pool fires have also been studied. However, the conclusions from the studies identified are not consistent. Blinov & Khudyakov [1961] determined that the rim height surrounding a fully turbulent fire has little effect on the burning rate provided the rim height is less than the diameter. However, both Emmons [1961] and deRis [1976] later concluded that the geometry and thermal properties at the pool rim can significantly alter pool burning rates for diameters as large as 0.8 m (2.6 ft). After further study deRis [1978] found that increasing rim height from flush with the fuel (i.e., no freeboard) up to 13 mm (0.5 in.) freeboard can increase burning rates by as much as 60 percent.

1.1.1.2 Fuel Depth

To date, most liquid fuel fire studies have focused on characterizing the steady-state burning rates of fuels. This characterization generally requires the presence of a relatively deep fuel layer in order to be able to establish and maintain a steady-state temperature gradient within the fuel. The majority of the studies conducted utilized fixed area pans constructed from either steel or concrete and a continuous-feed fuel supply system to maintain a constant fuel level within the confined area. These tests generally require the burning of significant quantities of fuel for relatively long periods of time. In the event that the release of a fuel results in a fuel depth less than required to achieve steady-state burning, understanding the impacts of fuel depth becomes of great importance. However, there has been little systematic testing to understand the impacts of fuel layer depth on fire development.

Garo et al. [2007] conducted a study of the burning characteristics of a liquid fuel layer floating on water. In this study, various single and multi-component fuels were evaluated in pool fires of varying size and initial depth. From this work the authors found that the burning rate of fuel on top of water varied based on the initial depth of fuel. In general, the burning rate tended to decrease as the depth of fuel decreased. The smallest depth of fuel that was tested in this study was 2 mm, a value that is close to that of commonly attributed to liquid fuel spill. The findings of Garo et al. [2007] generally agreed with the spill fire burning rate data collected by Gottuk et al. [2000] and Putorti [2001]. A hypothesis provided by Garo et al. [2007] for the differences in burning rate was that the water substrate acted as a heat sink for the fuel layer.

1.1.2 Spill Dynamics

The progression of a fuel spill prior to ignition is dictated by the forces controlling the motion and equilibrium of the fluid. As a liquid is spilled and spreads, it will undergo three physical regimes governing the motion and equilibrium state of the fluid. These regimes, as outlined by Putorti [2001], are gravity-inertia, gravity-viscous, and viscous-surface tension. The regimes are identified by the force that tends to spread the liquid and the force that tends to oppose spread, respectively.

Currently, there are two approaches that can be used to predict the characteristics of a liquid spill on a surface: 1) transient predictions in which the development and equilibrium state of a spill

are described and 2) steady-state solutions in which only the equilibrium condition of the spill is given. Analytical equations describing the time dependent fluid spread over a flat surface have been developed by Raj et al. [1974], Grimaz [2007], and others. These analytical solutions assume the spill occurs on a perfectly flat, impermeable surface. The solutions obtained using this approach tend to be similar and require fluid properties (density, viscosity, etc.) as well as the spill configuration (flow rate, source geometry, etc.). The more simplified approach is to consider only the equilibrium condition of the spill. Solutions for this approach were developed by Bradley [2002] and Simmons et al. [2004] with minor differences in the two approaches. The basis for these derivations is a balance of surface tension and pressure forces at a fluid's curved surfaces taken from work by Batchelor [1960]. Such an analysis requires the density and surface tension of the liquid as well as the contact angle of the liquid-substrate interface. This is the main difference between the two methods of analytically predicting spill dynamics: one approach requires liquid and spill configuration properties, while the other requires liquid and liquid-surface properties.

It should be noted that the two approaches described above generally yield different results: either a transient spill depth or an equilibrium spill depth. The liquid spread equations of Raj et al. [1974] and Grimaz [2007] yield liquid spread that eventually reaches a quasi-equilibrium spill depth. However, using this approach, the quasi-equilibrium spill depth is not independent of the volume spilled. This is directly contradictory to solutions obtained from the equilibrium spill depth equations which explicitly show that there is no impact of volume of the spill on the spill depth. The independence of equilibrium spill depth and spill volume is supported by the fact that the governing parameters of the third regime identified by Putorti [2001] are properties of the liquid, thus in no way dependent on the quantity of fuel present. Furthermore, other sources ([Modak, 1981], [Simmons et. al, 2004], [Putorti, 2001]) confirm that spill depth on perfectly flat, impermeable surfaces is independent of the amount of liquid spilled. One beneficial part of the transient models by Raj et al. [1974] and Grimaz [2007] is that they show how certain liquid properties influence the spread of a liquid. For instance, keeping all other parameters constant, increasing the fluids viscosity will tend to slow the liquid spread. However, viscosity differences will ultimately have little effect on the equilibrium spill depth.

The contact angle of the liquid-substrate interface has a large impact on the equilibrium spill height equation from Bradley [2002]. A contact angle is the angle that the liquid edge makes with the substrate. An illustration of this principle is provided in Figure 1.2. As the liquid height decreases, the contact angle approaches zero. As the liquid approaches the shape of a perfectly spherical drop sitting on the surface, the contact angle will be 180 degrees.

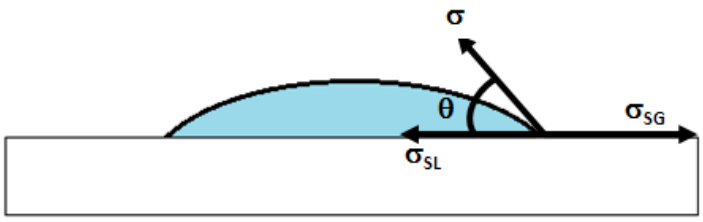

Figure 1.2. Illustration of liquid/substrate contact angle

Batchelor [1960] explained that contact angles occur because the liquid surface naturally tends to form a shape such that the free energy is minimized. Contact angle is typically determined

experimentally, but can be calculated through Young's law, when knowing interfacial tensions of the liquid-air (σ), liquid-solid (σ_{SL}), and the surface free energy of the substrate (σ_{SG}). The liquid-air interfacial tension is typically referred to as the surface tension of a liquid and is the only one of these three values that is typically known for a liquid-substrate system. Therefore, using the contact angle to describe the liquid-substrate interface is much more convenient. Furthermore a variety of standardized test methods exist to measure the contact angle [ASTM D7334-08]. Contact angles can be determined using optical measurement techniques for a sessile liquid drop on a surface.

Realizing that most surfaces are not ideal, it is important to understand the affect that the various surface and liquid characteristics (i.e., surface permeability, surface topography, liquid volatility, etc.) can have on the spread of the liquid. Keller et al. [2005], Simmons et al. [2004], and Belore [1988] studied the effects of substrate permeability on liquid spread. These studies were mainly concerned with pavements, soils and snow as substrates, but the results obtained can be applied to most permeable surfaces. The permeability, or tendency for a certain liquid to penetrate into a porous surface, is a property determined by the surface and liquid characteristics/properties. These studies were aimed at modeling the amount of infiltration of the spreading liquid into the sub-surface area. This infiltration model could then be coupled with a spreading model to determine the impacts of permeable surfaces. Keller et al. [2005] also noted that capillary effects could not be neglected when determining infiltration into a permeable surface. The most notable difference between liquid spread on a permeable surface and an impermeable surface is that it is possible for the entire liquid volume to be imbibed in the subsurface when a permeable surface is concerned. This means that liquid spread on permeable surfaces tends to be much more transient than on impermeable surfaces. Therefore, it is more difficult to determine an accurate spill depth on a permeable surface.

Surface topography is also a key parameter when considering the spread of a liquid. The topography of a surface can include, but is not limited to, levelness, roughness, and uniformity. Each of these characteristics will affect the extent to which a liquid spreads across a surface, and thus the final area and depth of the spill. Surface roughness can be described as a measure of the texture of a surface. The measure of roughness takes into account the amount of vertical variations of a surface from its average. If these variations are large and plenty, the surface can be considered rough, else it would be considered smooth. The main difference between rough and smooth surfaces is that for the same geometric area, a rough surface will have more microscopic surface area due to the increased number of small peaks and valleys Roughness will impact the spread of liquid over a surface in two ways. The peaks and valleys serve as barriers inhibiting the progression of the spill front, and the valleys extract small quantities of volume from the bulk flow of the liquid thus reducing the potential energy of the spill volume. Uniformity can be thought of as the overall flatness, that is, without macroscopic peaks and valleys. Non-uniformity impacts a spill because liquid flow will be directed by macroscopic peaks and valleys and liquids will pool in low spots of a surface, thus making the spill depth non-uniform. Non-levelness in a substrate presents much the same problem as a non-uniform surface in that liquids will move towards low spots, or towards the bottom of an inclined (non-level) surface. Spills on non-level substrates were addressed by Simmons et al. [2004]. Simmons showed that even small inclines on the order of 1^o can over time affect the behavior of a liquid spill. However, spill creeping introduced by a small incline would tend to be slow. Obviously, for a larger incline there will be a larger impact on spill behavior.

Evaporation during spread is another complication that is not taken into account in some liquid spread models. For more volatile fuels such as gasoline, evaporation can have an effect on the equilibrium spill area and depth, whereas for less volatile fuels, these effects will be negligible.

DeHaan [1999] performed small-scale testing to study the impact of pool size, substrate, and temperature on the evaporation rate of several pure hydrocarbons. In this work, ambient temperatures ranging from 5–35^{o}C (41–95^{o}F) were shown to impact (i.e., enhance/retard) fuel evaporation rates by as much as fifty percent. The substrate was also shown to have a significant impact on evaporation rates. Several different porous substrates (i.e., carpet, foam, plaster, sand, aluminum granules) were evaluated with enhanced evaporation observed in all cases when compared to the impermeable substrate baseline (i.e., glass). Substrate characteristics dictated the degree of enhancement with more densely packed substrates resulting in greater evaporation rates. This impact was attributed to the varying degrees of capillary action occurring within the different porous substrates. Finally, the author characterized the evaporation rates for various size pools with sizes ranging from 0.15–0.35 m (5.9–11.8 in.). It was shown that as pool area increased, evaporation rates fell. This relationship was further investigated using thermal imaging, and DeHaan reports that the majority of evaporation occurs at the edges of the pool. Thus, evaporation rates are the highest when the edges represent the majority of the surface area.

The evaporation rates of gasoline and multi-component liquids were evaluated in the works of Okamoto et al. [2009 and 2010]. In these works, the authors characterized changes in the evaporation rates and vapor pressures of various fuels at various fuel depths as a function of their decay. The author demonstrated that the time required to evaporate approximately 70 percent of the liquid was over 2, 4, and 6 hours for 1, 2, and 3 mm depths of high-octane gasoline, respectively. Okamoto et al. [2009] found that the evaporation rate of gasoline decreased rapidly over time and that the decrease is more rapid in the case of decreasing fuel depth. Okamoto et al. [2009] postulated that the reason for this behavior was that, per unit area, a shallow depth of gasoline has a smaller mass of low-boiling point constituents. It is these constituents that evaporate the quickest, causing a high evaporation rate until they are not present. Although over extended periods of time it can be shown that significant quantities of fuel can be lost due to evaporation, it is expected that the over the time periods in which spills generally occur (i.e., minutes) the fraction of gasoline lost would be small and the consequent change in spill area would be insignificant.

Liquid spread on a perfectly flat and impermeable surface can be described by various models and equations presented in the literature. However, for practical liquid-surface combinations, the simpler approach is more feasible. The equations presented by Bradley [2002] and Simmons et al. [2004] are examples of this approach, which uses a balance of gravitational and surface tension forces to determine a spill height. This approach also takes into account the interfacial interactions between the liquid and solid, which are not present in most transient models. The spill depth parameter can easily be determined from one equation using a combination of liquid and liquid-surface properties. When combined with the assumption that spill height is independent of volume spilled, knowing a spill depth one can determine a spill area from a known quantity of liquid spilled.

1.1.3 Spill Fire Dynamics

An unconfined fuel spill is generally associated with fuel that is released with no physical boundaries and results in a liquid layer that is thin compared to a pool. Although there are a number of studies that address liquid pool fires, there is limited work documenting the fire dynamics of unconfined fuel spill fires.

1.1.3.1 Spill Area & Fuel Layer Depth

Several studies have attempted to quantify the layer depth of fuel spills, and in general, unconfined spills on relatively level substrates tend to be less than 2 mm deep. Chambers [1977] first evaluated fuel spill depths using spills ranging in volume from 3.8 L to 189 L (1 to 50 gallons) of JP-4 spilled over a concrete runway. Modak [1981] evaluated a total of four different fuels on steel, unfinished concrete, and coated concrete surfaces and calculated spill depths ranging from 0.22–0.84 mm for volumes ranging from 5 mL to 30 mL. Other studies including that of Gottuk et al. [2000] (1 L to 3 L spills) and Putorti [2001] (250 mL to 1000 mL spills) provide similar spill depths ranging from 0.5–1.1 mm for various fuels. Work by Hill et al. [1999] was cited by Gottuk [2000] as indicating fuel spill depths as large as 4.4 mm for larger quantity spills (up to 114 L); this data indicated a dependence of spill depth on spill quantity. However, after reviewing video footage from the tests by Hill et al. [1999], it was found that these spills may not have reached their full potential (i.e., maximum area) prior to ignition due to seams and boundaries on the spilled surface. Thus the reported spill depths of 4.4 mm are not representative of the spill dynamics being investigated in this study. Currently, the limited data set described above is the majority of data available describing the spill behavior of fuels.

Based upon these data sets Gottuk and White [2008] developed ‘rules of thumb’ to assess the expected spill area per unit volume of liquid. These rules are provided below;

- Spill Qty. $\leq$ 95 l (25 gal.): Area per Unit Volume = 1.4 m^2/l (57 ft^2/gal.)
- Spill Qty. $\geq$ 95 l (25 gal.): Area per Unit Volume = 0.36 m^2/l (14.5 ft^2/gal.)

1.1.3.2 Mass Burning Rate/Fuel Regression Rates

To date, the majority of research into liquid fuel mass burning rates has been focused on characterizing the burning dynamics of fuels at steady-state. The general approach used to achieve and maintain steady-state burning has been either to conduct tests with a sufficiently thick fuel layer in a pool configuration or to use a continuous feed system capable of maintaining a fixed fuel depth for an extended period of time. Both of these approaches result in the development of relatively thin layer of fuel at the boiling temperature backed by a ‘thermally thick’ fuel substrate. Work conducted by Gottuk et al. [2000] found that substantial differences existed between the burning characteristics of JP-5 and JP-8 fuel spills on concrete when compared to confined pool fires of the same fuels. The unconfined spill fire burning rates reported by Gottuk et al. [2000] were approximately twenty percent of the maximum burning rates of confined pool fires as reported by Babrauskas [1983]. Putorti [2001] observed a similar reduction in burning rate for gasoline spilled on wood parquet and vinyl tile floors.

Prior to the current study, the hypothesis postulated to explain the burning rate differences reported by Gottuk [2000] and Putorti [2001] was based on the differing thermal properties of the substrates. Spills are generally considered to have fuel layer depths on the order of 1–2 mm (0.04–0.08 in.) whereas most pool fire data, on which burning rates from the literature are based, was generally measured from pools with depths ranging from 1 to several centimeters. Furthermore, it was found that in a majority of the pool fire research the burning pools of fuel were continuously fed in order to achieve long durations of steady-state burning. Consequently, since concrete has a higher thermal conductivity (1.4 W/m-K) than a thick fuel layer (0.11 W/m-K), more heat is lost to the substrate, which would otherwise contribute to heating the fuel. In other words, the deep fuel layer of a pool serves as a greater insulator to the fuel surface than does the concrete, resulting in the fuel surface heating up more quickly, vaporizing and burning at a higher rate. As mentioned earlier, similar conclusions were developed by Garo et al. [2007] for decreasing fuel spill depths on water having smaller burning rates. Modak [1981] discussed the thermal effects of substrates on the ignition of high flash point fuel spills, but did not investigate the effect on burning.

1.1.3.3 Flame Spread

Due to the relatively high likelihood that fuel spill scenarios will result in fuel layer depths on the order of 1–2 mm (0.04–0.08 in.) it is necessary to understand the impacts that this can have on the spread of flame over a fuel surface. The two primary parameters that govern flame spread are the fuels flashpoint and the temperature of the fuel [Gottuk and White, 2008]. When the temperature of the fuel spill is lower than the fuels flashpoint, flame spread is driven by the physical properties of the fuel (e.g., surface tension). This flame spread regime is often identified as liquid-phase spread. On the other hand, fuel temperatures greater than the flashpoint of the fuel spilled result in gas-phase spread. Liquid-phase flame spread can be further dissected to identify underlying parameters which can affect the rate of spread of flame over a fuel surface. The most relevant parameter affecting the liquid-phase flame spread is the depth of the fuel layer. Studies performed by Mackinven et al. [1970] and Burgoyne et al. [1968] determined that flames do not spread from the point of ignition for fuel layer depths of less than 1.5 mm (0.06 in.). It is important to note that under most ambient conditions, combustible fuels will only support liquid-phase flame spread thus heating of the fuel substrate is required in order to spread flame over the liquid surface.

1.1.4 Forensic Fire Pattern Analysis

The current standard of care in the forensic investigation of fires is NFPA 921 [2008]. The core of the 921 methodology is the application of the scientific method to fire investigation. In the context of fire investigation, this involves the collection of data, the formulation of hypotheses from that data, and the testing of hypotheses. Fire investigation data collection often involves the identification and documentation of fire patterns followed by the collection of material samples from within the identified patterns, if the use of accelerants is suspected. Section 6.3 of NFPA 921 [2008] provides an inventory of fire patterns and the associated fire phenomena which cause them. Furthermore, Section 16.5.4 provides several methods for the collection of evidence for accelerant testing. Unfortunately, the information provided in these sections is primarily based upon the documentation of singular events due to the fact that there have been

very limited systematic investigations of fire patterns. Only information specific to floor patterns will be discussed herein.

1.1.4.1 Fire Patterns

The analysis of floor patterns is often the primary method used to substantiate that a fire scenario involved the use of an accelerant. A comprehensive discussion of the historical evolution and utility of floor patterns is provided by Beyler [2009]. To date, there has been relatively limited study of floor patterns resulting from the spill and consequent ignition of ignitable liquids on different substrates. However, the studies that have been conducted have given insights into the types of patterns formed and the quantity of liquid required to create the patterns. Putorti [2001] investigated spill fires in the context of arson scenarios on both hard surfaces and carpeted surfaces. In this study the author presented the following conclusions related to the forensic analysis of fuel spill fire patterns:

1) In all but one scenario, the nonporous flooring gasoline burn areas were found to be the same as the spill areas within the experimental uncertainty.
2) Initial carpet burn areas were found to be the same as the carpet spill areas, within the experimental uncertainty.
3) The quantity of gasoline spilled could be determined from the burn pattern area on nonporous flooring.

1.1.4.2 Ignitable Liquid Residue Sampling Techniques

As described by Beyler [2009], the visual identification of a fire pattern on flooring material is not sufficient data to affirm an arson event. It is well established within the fire investigation community that such a claim can only be supported with the positive identification of an ignitable liquid residue (ILR), such as via ASTM E1412 [2007] and ASTM E1618 [2010] testing. These standards of practice provide guidance for how a fire debris sample should be stored and analyzed but provide no insight related to how and where potential ILR samples should be collected from a fire scene. Consequently, it is left up to the fire investigator to make these determinations based upon experience and guidance provided in the literature (e.g., [IAAI, 1999], [Dolan et al., 2008], [Putorti, 2001]). However, in general, only qualitative rationale for recommended sampling locations is provided in these texts. Furthermore, there are two different schools of thought as to where an ILR sample should be collected based upon the substrate/scenario. For non-carpet substrates, it is recommended that fire debris samples be collected along the perimeter of a potential floor pattern based upon the assumption that the center of a fire is exposed to the highest radiant heat flux thus residual fuel in this area, if any at all, will be the most depleted. For a carpet substrate, Putorti [2001] observed what is termed as the ‘donut’ affect whereby the saturation of the carpet in the immediate vicinity of the pour results in the potential that more fuel/fuel residue being present in this area after a fire has been extinguished/consumed.

1.2 Motivation

1.2.1 Forensic Fire Investigation

The utility of the patterns resulting from a spill and ensuing fire event in both pre-flashover fires as well as open fires has not been fully characterized. Although studies such as that conducted by Shanley, [1997] and Putorti [2001] have provided some insight into the patterns formed and quantity of liquid required to create the patterns, additional work is required to expand this work to other types of substrates and identify additional indicators.

1.2.2 Industrial Fire Protection

One of the most challenging aspects of industrial fire protection is the assessment of the hazards associated with large, open hydrocarbon fires. The primary concern stemming from these types of events is generally the duration and severity of the thermal radiation emitted by the fire. A detailed review of the state of the art with respect to the prediction of thermal radiation hazards from liquid hydrocarbon pool fires is provided by Beyler [2008]. However, as noted by Beyler [2008], the prediction of the duration and severity of the thermal radiation from a fire is highly dependent upon the characterization of the geometry and burning dynamics of the fire. As indicated above, correlations and models have been developed to predict expected spill areas; however, there is limited validation of these prediction methods. The ability to accurately predict the development and duration of a fire resulting from an unconfined fuel spill has not been well studied. Current methods of fire hazard analysis [NRC, 2004] that are based upon empirical data [SFPE, 2008] typically utilize the steady-state burning rate of a fuel and apply this value to a specified spill area to quantify the potential fire size, duration, and corresponding thermal radiation threat. Based upon the results of Gottuk et al. [2000] and Putorti [2001], this methodology could result in gross over-estimates of severity and under-estimate of the duration of the fire and thermal hazard. An illustration of these differences in the predicted and expected behavior of an unconfined hydrocarbon fire is provided in Figure 1.3.

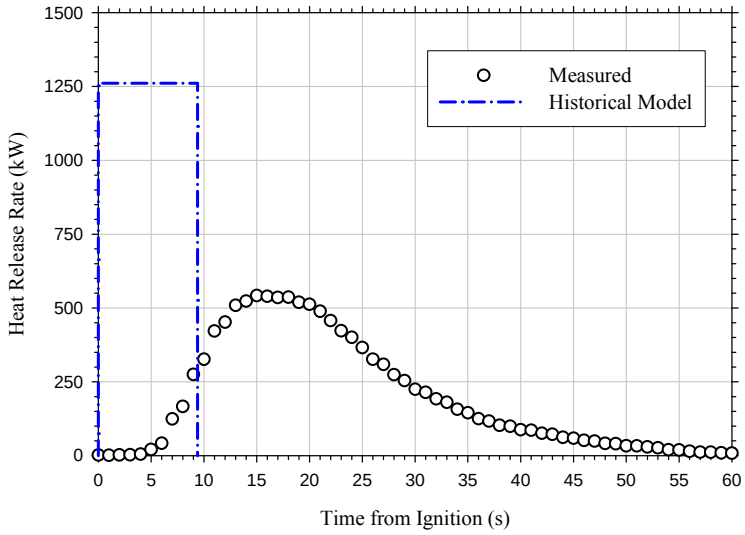

Figure 1.3. Illustration comparing current FHA methodology and measured spill fire data

As shown in Figure 1.3, there is the potential for vast differences between the current fire hazard analysis methodologies and the actual fire growth, peak fire size, and fire duration. Comparison of these plots indicates that using simple empirical calculations can result in an over-estimation of the peak fire size by more than a factor of 2. The figure also illustrates that the fire hazard analysis method typically assumes immediate full involvement which leads to the spill fire burning out just as the experimental 1 L gasoline spill fire is peaking. This could have significant impact on fire exposure, suppression and egress analyses and designs. Consequently, there is a need for additional research to investigate spill fire dynamics and to develop tools to assist in more accurate characterization of these events. Being able to more accurately predict the actual behavior of spill fires also improves forensic fire analyses, providing better tools for hypothesis testing.

1.3 Objectives

It is important to understand how liquid spill fires develop and to be able to quantitatively characterize these fires in order to be able to estimate the size of spills based on burn patterns and to be able to accurately calculate the fire size based on knowledge of the fuel type, quantity and the surface it is poured on. The purpose of this study was to expand the fundamental understanding of fuel spill fire dynamics, establish the utility of forensic tools, and validate empirically-based correlations used to model spill fire scenarios. There were two main subject areas investigated: 1) spill depth determination relative to fuel type, quantity, and substrate and 2) burning dynamics, including mass burning rate, duration of burn, and heat flux from the fire as it relates to the potential to ignite other items.

This testing also provided a means to further develop an understanding of the patterns resulting from fuel spills on various substrates. This included the characterization of spill patterns as they relate to the original spill and the identification of indicators, if any, that can be used to differentiate between liquid accelerants and Class A fuels burning on a floor substrate. Preliminary work was also conducted on the collection of ignitable liquid residue samples from various locations within a pattern to evaluate the optimum location for sample collection.

2.0 EXPERIMENTAL APPROACH

The objectives of this research were achieved by way of small- and full-scale experiments combined with analytical testing and empirical-based analyses. Small-scale testing consisted of pan fires conducted beneath an [ASTM E1354, 2009] cone calorimeter. These tests were designed to characterize the combustion properties of the fuels considered in this study as well as develop an understanding of the burning dynamics in the laminar burning regime with varying fuel depth. Full-scale experimental testing was executed in six different test series designed to evaluate liquid spill depths, the burning dynamics of fuel spill fires, and the forensic patterns generated by both liquid fuels and Class A fuels. The first series of tests consisted of fixed area pan fires. These tests were used to establish baseline burning rate data for various fuels at various depths as well as to provide comparisons to data previously reported in the literature. The second series of tests consisted of fixed area, diked substrate fire tests designed to characterize the impact of substrate on burning rates of various fuels at various depths. The third series of tests consisted of spill dynamics testing which was used to characterize the progression (area and depth relative to time) of liquid spills on various substrates. The fourth series of tests

consisted of spill fire testing designed to characterize the spill fire dynamics over a wide range of substrates and fuels. The fifth series of tests consisted of a small set of continuous spill fires conducted to characterize the steady-state burning conditions of an unconfined fuel spill. Lastly, a small set of Class A fires were conducted on several substrates in order to identify similarities and differences in the forensic indicators resulting from Class A and fuel spill fires. In addition to the testing previously described, a variety of analytical tests were used to measure the governing physical properties of both the liquids and solids (i.e., spill substrates) evaluated in this research. These governing material properties included the surface tension, low shear viscosity, and densities of all liquids considered in this study as well as the contact angle for several of the liquid/solid interfaces. A reference table summarizing the testing described above is provided in Table 2.1.

Table 2.1. Summary of Testing Conducted

Test Series Name	**Number of Tests Conducted**	**Rationale for Testing**
Cone Calorimeter Fires	15	**Primary:** Characterize the effective heat of combustion of test fuels under free-burning, ambient conditions. **Secondary:** Characterize impact of fuel depth on burning rate in convectively dominated burning regime.
Pan Fires	129	Characterize impact of fuel depth on burning dynamics.
Diked Fires	48	Characterize impact of fuel substrate on burning dynamics of fuels.
Spill Dynamics	78	Characterize spill area and depth of various liquids and bound vast majority of fuels using fuel stimulants.
Spill Fire Dynamics	104	Characterize spill fire dynamics of various fuels on various substrates.
Continuous Spill Fires	3	Characterize the steady state burning dynamics of spill fires.
Class A Fires	9	Characterize fire pattern similarities/differences between fuel spill fires and Class A sources.
Physical Properties Analysis	11	Characterize physical properties of liquids used in testing.
Combustion Properties Analysis	11	Characterize combustion properties of fuels used in testing.

2.1 Experimental Variables

The selection of liquids and spill substrates for this study was based upon their prevalence and relevancy in real-world fire scenarios. A total of 8 liquids were considered including, 3 flammable, 3 combustible, and 2 aqueous-based samples. Similarly, a total of 7 spill substrates were selected, 3 concrete finishes, 2 wood flooring materials, a vinyl flooring material, and a base grade carpet with pad. A detailed description of each of the liquids and spill substrates is provided below. A summary of the test liquids and substrates evaluated in this research is presented in Table 2.2 and Table 2.3, respectively.

Table 2.2. Summary of Test Liquids

Liquid Name	**Liquid Description**	**Liquid Classification**
Gasoline	87 octane, automotive grade gasoline	Flammable
Kerosene	K-1 dyed kerosene	Combustible
Diesel	Automotive grade diesel	Combustible
Denatured Alcohol	SLX Klean Strip Denatured Alcohol	Flammable
n-Heptane	Tilley Chemical Grade n-Heptane	Flammable
Lube Oil	BP Turbinol Select AS 32	Combustible
3% AFFF Solution	Lower Bounding Fuel Simulant	Aqueous-based
3% FP Solution	Upper Bounding Fuel Simulant	Aqueous-based

Table 2.3. Summary of Spill Substrates

Substrate Name	**Substrate Description**	**Substrate Classification**
Coated Concrete	Type I concrete sealed w/ Epoxy coating	Impermeable
Smooth Concrete (NIJ)	Type I concrete w/ Float finish	Permeable
Smooth Concrete (ATF)	Type I concrete w/ Float finish	Permeable
Brushed Concrete	Type I concrete w/ Broom finish	Permeable
Vinyl Flooring	Residential vinyl w/ plywood subfloor	Impermeable
Plywood	14.7 mm (0.578 in.) plywood	Permeable
Oriented Strand Board	14.7 mm (0.578 in.) OSB	Permeable
Carpet Flooring	25 oz. carpet w/ PU foam padding	Permeable

2.1.1 Test Liquids

The primary fuels used in this study were chosen from common household and industrial fuels and included gasoline, kerosene, diesel, and denatured alcohol. These fuels encompass a wide range of flammability and fluid dynamic properties (presented later in Table 4.1). A subset of tests was also conducted using n-Heptane and lube oil. N-Heptane was evaluated not only for its applicability to industrial applications but also because it is a pure fuel. This characteristic ensures that the properties of the fuel have not changed over time thus allowing data from the current test series to be compared to historical data sets. Furthermore, the fact that n-Heptane is a pure fuel simplifies the analysis needed to understand the burning dynamics of the fuel because it has a constant boiling temperature, vapor pressure, heat of combustion, etc. Whereas for multi-constituent fuels, such as gasoline, liquid composition can vary from year to year and between manufacturers. In addition, the combustion properties of multi-constituent fuels change as the fuel burns due to the composition changing (e.g., the preferential burning of lower molecular weight components first). Lube oil was considered in order to extend the findings of this research to liquids with viscosities significantly greater than those commonly attributed to liquid fuels.

In addition to the fuels identified above, two fuel simulants were used to provide bounding scenarios for the vast majority of liquid fuels with respect to spill dynamics. These bounding liquids were chosen based upon their surface tensions and the knowledge that surface tension has

been identified as a governing parameter to characterize different liquids relative to spill dynamics [Gottuk and White, 2008].

All of the primary fuels considered were readily available to the public and are present in a variety of residential and industrial applications in various quantities. Furthermore, due to the potential differences in fuel chemistries from one distributor to another, all fuels tested were purchased in bulk from a single distributor or at one time from a single distributor. All fuels were purchased in July of 2009. Samples from each of the fuel batches were collected, identified, and stored for analytical testing and reference purposes. The gasoline used was 87 Octane, regular, unleaded gasoline purchased from Carroll Independent Fuel Company, a local fuel distributor. The gasoline was stored in a UL 142 rated above-ground storage tank with a capacity of 1136 L (300 gal.). The tank was constructed from 12Ga steel with 1.5 m (60 in.) length and 0.76 m (30 in.) diameter. The gasoline was stored in this tank throughout testing. The kerosene used was K-1 type, dyed kerosene purchased from Carroll Independent Fuel Company and stored in a UL 142 rated above-ground storage tank with a capacity of 1893 L (500 gal.). The diesel and denatured alcohol were not purchased in bulk; however, these fuels were purchased from a single distributor at the same time. The diesel fuel was seasonal diesel fuel, also known as diesel No. 2, obtained from a local filling station. The diesel fuel was stored in 5 gallon fuel storage cans that remained sealed until it was required for testing. The denatured alcohol, manufactured by W.M. Barr Company, and distributed under the product name Klean-Strip SLX Denatured Alcohol was purchased from a local hardware store and stored in 3.8 L (1 gal.) cans. The other liquid fuels considered were n-Heptane and BP Turbinol Select AS 32 lube oil. The n-Heptane used was chemically pure and manufactured by the Exxon Corporation. The fuel was purchased from Tilley Chemical Company as product code HEP315. Experiments conducted with n-Heptane and lube oil provided data sets for a pure fuel with well defined combustion properties and a highly viscous fuel with vastly different physical properties than any other fuel considered, respectively.

The fuel simulants used were a Buckeye BFC-3.1 3 percent aqueous film forming foam (3% AFFF) concentrate and an Ansul 3 percent fluoro-protein foam concentrate (3% FP). The AFFF concentrate was purchased from Buckeye as part number 50340. The FP concentrate was purchased from Ansul as part number 73973. These solutions were mixed by test personnel per manufacturer requirements. Both solutions consisted of mixing 2.25 L (0.6 gal) of foam concentrate with 72.75 L (19.2 gal) of water yielding a total volume of 75 L (19.8 gal). Solution concentrations were verified using an Oakton Model ECTestr 11 electrical conductivity meter. In order to enhance the visibility of the 3% AFFF, the solution was dyed with 49 mL of McCormick black food coloring.

2.1.2 Spill Substrates

The spill substrates evaluated in this study included coated concrete, two types of hard-trowel-finished concrete, brushed concrete, 14.7 mm (0.578 in.) plywood, 14.7 mm (0.578 in.) oriented-strand board (OSB), vinyl sheet flooring over plywood, and carpet over pad. Photographs of each of the eight substrates are provided in Figure 2.1. These substrates are generally the most common types of flooring in residential, commercial, and industrial applications. Three different types of concrete finishes were used to explore the effects of surface roughness on fuel spill dynamics.

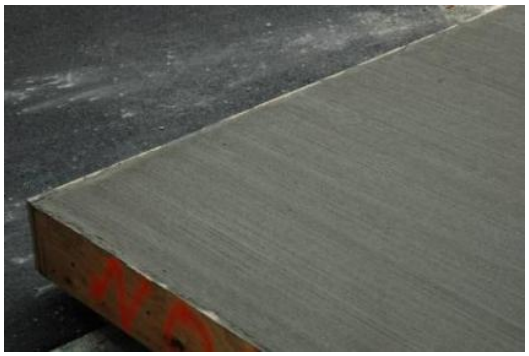

(a) – Brushed Concrete

(b) – Smooth Concrete (NIJ)

(c) – Coated Concrete

(d) – Smooth Concrete (ATF)

(e) – Oriented Strand Board

(f) – Plywood

(g) – Vinyl on Plywood

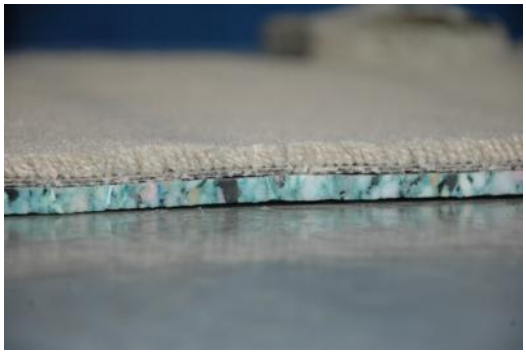

(h) – Carpet with Foam Pad

Figure 2.1. Photographs of various spill substrates evaluated

2.1.2.1 Concrete

A total of six concrete pads were poured for this research ranging in size from 0.09 m^2 (1 ft^2) up to 12.9 m^2 (139 ft^2). Although concrete slabs are generally poured to depths ranging from 0.1–0.2 m (4–8 in.), the pads used in this study were poured to a thickness of 0.05 m (2 in.). This reduction in slab thickness resulted in significantly lighter, more manageable pads while still providing a thermally thick substrate on which fuel spill fires could be conducted. The multi-dimensional, heat transfer code [HEATING 7.2, 1993] was used to verify this thermally thick assumption. All concrete substrates were constructed from Type I concrete, using a 6.5 bag mix (i.e., 6.5 bags of Portland cement per cubic yard of concrete). This mixture produces concrete with a compressive strength between 2500–3000 psi which is required in the majority of concrete construction. [IBC, 2009] The pads were professionally poured at the same time and finished per the specifications of this study (i.e., smooth or brushed finish).

Three of the six pads were poured in steel forms with a plywood base for diked fire testing. The remaining three pads were poured into plywood forms of various sizes including, two pads poured into 2 m (6.5 ft) square forms and a single pad poured into a 3.4 m x 3.8 m (11.2 ft by 12.33 ft) form. The 2 m (6.5 ft) square concrete pads were used for uncoated concrete substrates with smooth- and brushed finishes. The larger pad was used as a coated concrete substrate, as were all of the diked pads. A summary and description of the concrete pads poured for this testing is provided in Table 2.4.

Table 2.4. Description of Concrete Pads Poured

Side Length (m (ft))	**Finish**	**Test Series Used**
0.3 (1)	Epoxy Coated	Diked Fires
0.6 (2)		
1.2 (4)		
2 (6.5)	Smooth	Spill/Spill Fires
	Brushed	Spill/Spill Fires
3.4 (11.2)	Epoxy Coated	Spill/Spill Fires

The smooth-finish and coated concrete pads were finished using a 0.46 m (18 in.) aluminum bull-float. The brush finish concrete pad was finished using a standard concrete brush. Once completed, all concrete substrates were permitted to cure for a minimum of 28 days prior to any testing. Once cured, the surface of the coated concrete pad was finished using an Eco-HPS Urethane Topcoat. This high-solid, one-component, aliphatic, moisture-cure urethane coating was applied over an epoxy primer and was used as a typical smooth coating and to minimize fuel absorption into the concrete pad. The coating was applied in a three step process whereby the pads were first etched with a Formula 409 cleaning agent, rinsed, and allowed to dry overnight. Next, a two part epoxy basecoat (Tennant Co. ECO-MPE) was applied with an average coverage rate of 60 ft^2/gal. Finally, within 24 hours of basecoat application, the topcoat (Tennant Co. ECO-HPS) was applied and allowed to dry for over 24 hours. Both the basecoat and topcoat were applied using 3/8 in. nap paint rollers. Final coating system thicknesses were measured using a Defelsko Positector 200 ultra-sonic thickness gauge and found to have an average thickness of 0.62 mm (24.4 mils).

In addition to the pads poured specifically for this research, the existing concrete floors of the test facility were used to investigate large scale spill dynamics. The test facility concrete pad used had an approximate foot print of 12.2 m (40 ft) square and was located beneath the 4 MW hood calorimeter. The floor was characterized as a smooth finish, polished concrete pad that was unsealed and uncoated.

2.1.2.2 Wood

The wood substrates considered were plywood and OSB. These two types of wood are most commonly found in residential sub-flooring applications. The plywood substrate used was Georgia Pacific plywood with a thickness of 14.7 mm (0.578 in.). The OSB used was a Georgia Pacific Blue Ribbon product with an actual thickness of 14.7 mm (0.578 in.). Both the glued and unfinished sides of the OSB were evaluated in this testing. All wood substrate material was stored in the conditioned laboratory environment prior to testing. Both the plywood and OSB substrates were attached to a wood stud frame with screws spaced 0.41 m (16 in.) on center in order to level the substrate material.

2.1.2.3 Vinyl

The vinyl flooring was Congoleum Prelude vinyl sheeting with a nominal thickness of 1.2 mm (0.04 in.). The vinyl sheet was applied to 14.7 mm (0.578 in.) plywood using Robert's Premium vinyl adhesive. The vinyl adhesive was applied using a 1/16 x 1/16 x 3/32 in. notch trowel. Once applied, the adhesive was permitted to become tacky prior to the application of the vinyl sheet. Vinyl (with plywood backing) was chosen for its prevalence as a residential and commercial material. In addition, the vinyl would provide a relatively impermeable substrate on which to spill.

2.1.2.4 Carpet

Although carpeting presents the most challenges with respect to the characterization of spill dynamics and fuel spread, it was deemed necessary that this substrate be included in the study due to its prevalence in the residential setting. The carpet used was a Portico Royale Plus (BP724) 100% nylon cut pile Saxony with an approximate mass per unit area of 0.85 kg/m^2 (25 oz. /yd^2) and pile height of 12.5 mm (0.493 in.). The backing material of the carpet was a woven polypropylene. The carpet used was in compliance with all federally mandated flammability standards including 16CFR-1630.4 (Pill Test), ASTM E648 (Critical Radiant Flux), and ASTM E662 (Smoke Density). All carpet was backed using PS53P bonded urethane foam pad with a nominal thickness of 9.5 mm (0.375 in.) and density of 88.1 kg/m^3 (5.5 lb/ft^3).

2.1.3 Fuel Quantities

The quantity of fuel used and rationale for use was test series dependent. All fuel quantities, other than those used in cone testing, were measured on a mass basis using an Ohaus Explorer Model E1K210 load cell with 12 kg (26.5 lb) capacity and 0.1 g (0.0002 lb) resolution. Cone calorimeter fuel quantities were measured using a Sartorius Model FBG16EDE-HOUR load cell with 16 kg (35.3 lb) capacity and 0.1 g (0.0002 lb) resolution.

For the confined fires (i.e., pan and diked configurations), the fuel quantities were designed such that the initial fuel depths within the pan ranged from 1–40 mm (0.04–1.57 in.). A total of eight fuel depths were evaluated including 1, 2, 3, 4, 5, 10, 20, and 40 mm. Initially, depths of 1, 5, 10 and 20 mm were tested. The 1 mm depth was considered to be representative of spill scenarios. The 5 and 10 mm depths were chosen as intermediate values between expected spill and pool fire depths. The 20 mm depth was in the range considered to be a pool. After the initial testing, a small subset of 40 mm depths was evaluated in order to ensure steady state burning was achieved at the 20 mm depth. In addition, depths of 2, 3, and 4 mm were evaluated to fully characterize the transition between spill and pool burning behavior. A complete list of depths and the required fuel quantities for each of the three pan/diked configurations are provided in Table 2.5.

Table 2.5. Summary of Fuel Volumes Used in Pan/Diked Fire Tests

Fuel Depth (mm)	**Pan Side Length (m (ft))**		
	0.3 (1)	**0.6 (2)**	**1.2 (4)**
1	0.093 L	1.486 L	3.457 L
2	0.186 L	2.972 L	6.914 L
3	0.279 L	4.458 L	10.371 L
4	0.372 L	5.944 L	13.828 L
5	0.465 L	7.432 L	17.29 L
10	0.929 L	14.86 L	34.57 L
20	1.858 L	29.73 L	69.140 L
40	3.716 L	59.46 L	N/A

The intent of the selected liquid quantities for the unconfined (i.e., spill dynamics and spill fire) scenarios was to develop spills that could spread freely but still remain on the substrate being evaluated. Based upon fluid dynamics theory, the depth of a spill should be independent of the volume of the spill when spilled on a non-absorbing surface. This has been verified in the literature by Modak [1981] and Simmons [2003] who stated that the spill depth is primarily a function of the liquid properties and liquid / substrate interactions. Consequently, the majority of the spill dynamics tests utilized a single volume (i.e., 0.5 L [0.13 gal.]). However, a subset of tests was also conducted with larger liquid volumes to verify the above findings. Larger quantities of fuel were also used in a subset of spill fire tests to ensure that the effective diameter of the resulting spill fire was larger enough to be considered within the radiative, optically thick burning mode as defined by Babrauskas [1983]. These larger quantities included fuel spills ranging from 1 to 5 L (0.26 to 1.3 gal.). It should be noted that larger spills were originally planned for this test program; however, due to lab scheduling issues these tests were not able to be conducted.

2.1.4 Class A Sources

A total of three different Class A fuels were tested on three different substrates. The substrates used were plywood, vinyl flooring, and carpet. Concrete substrates were not considered in this test series since it was not combustible. The Class A fuels evaluated included a polyurethane foam chair mock-up, an infant baby seat, and a wood crib. These sources were selected because they represent materials and fuel packages commonly found in residential fire scenarios that

when consumed in a fire can result in patterns similar to those commonly attributed to fuel spill patterns.

Photographs of each of the Class A fuels used are provided in Figure 2.2. The polyurethane foam source consisted of a chair mock-up constructed from non-fire retarded, low density (19.2 kg/m^3 [1.2 lbs/ft^3]) flexible polyurethane foam. The polyurethane foam was purchased from Tedco Industries as material description number 2110. The 0.9 m x 0.6 m x 0.15 m (3 x 2 x 0.5 ft) piece of foam was placed atop the steel chair frame. The bottom of the foam was located 0.2 m (9 in.) above the substrate. On average, the polyurethane foam used in this scenario had a total mass of 1.3 kg (2.9 lbs). The infant baby seat was selected because it provided a multi-component fuel package that was comprised of both plastic, cloth and padding materials. The infant baby seats tested had an average total mass of 3.0 kg (6.6 lbs). The wood crib fuel package was selected because it is representative of a variety of cellulosic fuels commonly found in residential settings (i.e., end tables, book cases, etc.). The crib selected was a UL 1254 wood crib comprised of 8 tiers of four 5 cm (2 in.) square sticks. The sticks were spaced 12 cm (3.75 in.) on center and the wood crib was elevated 5 cm (2 in.) above the substrate. The average mass of the wood cribs was 6 kg (13 lbs).

For all Class A fire scenarios, the ignition source was two and a half full sheets of newspaper crumpled into a nominally 0.15 m (6 in.) diameter ball and ignited using a small propane flame. For the chair mock-up and baby seat scenarios the newspaper was placed on top of the center of the fuel package. For the wood crib, the newspaper was twisted and inserted into the center vertical flue of the wood crib. In all configurations, the newspaper was ignited using a 2 second exposure from a propane torch applied to the top of the newspaper.

(a) (b) (c)

Figure 2.2. Photographs of the Class A sources on a plywood substrate: (a) wood crib, (b) infant baby seat, and (c) polyurethane foam chair mock-up

2.2 Naming Convention

In order to efficiently present and discuss the results from the large number of tests conducted in this research, a naming convention was developed to fully-describe the pertinent variables considered in each test. An alpha-numeric code was developed to identify the following parameters;

1. Test type and identification number
2. Confined or unconfined scenario

3. Substrate
4. Liquid type
5. Liquid Depth (confined scenarios) or Quantity (unconfined scenarios)
6. Liquid Area (confined scenarios) or Spread Time (unconfined scenarios)

The alpha-numeric key is provided in Figure 2.3. This alpha-numeric code will be used to identify all tests within the report.

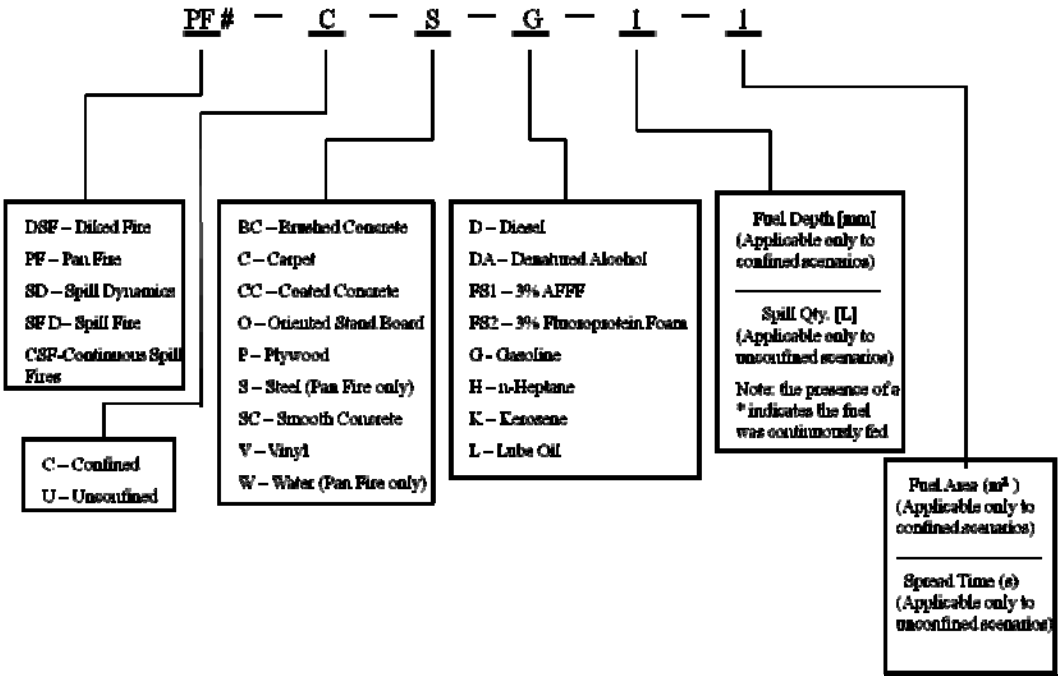

Figure 2.3. Key to Alpha-Numeric Test Identification Code

2.3 Test Matrices

Due to the large number of tests conducted, the test matrices executed in this research are not presented in the body of the report. A summary of the test matrices executed are provided in Appendix A. These matrices were designed to systematically evaluate the experimental variables identified in Section 2.1.

3.0 EXPERIMENTAL DESIGN

Experimental testing was conducted in several test series designed to investigate different phenomena relating to liquid spills and fuel spill fire dynamics. All tests, with the exception of analytical testing and cone calorimeter experiments, were conducted at the Bureau of Alcohol, Tobacco, and Firearms (ATF) Fire Research Laboratory (FRL) located at the National Laboratory Center in Beltsville, Maryland. Data for all tests, other than cone calorimeter testing, was measured using the existing ATF FRL data acquisition system. Control of test equipment and acquisition systems was achieved using iFix Intellution, a Supervisory Control and Data Acquisition system (SCADA). The data collection and cataloging was performed through

FireTOSS, a software package unique to the ATF FRL. Instrumentation was connected to the SCADA using Yokogawa DA 100 and DS 600 data acquisition units. A sampling frequency of 1 Hz was used for all tests.

3.1 Analytical Testing

Analytical test methods were used to characterize liquid and surface properties identified as key variables governing fuel spill progression and burning dynamics. These properties included surface tension, viscosity, contact angle, flash point, specific gravity, and fuel chemistry in the case of multi-constituent fuels. All analytical testing was conducted at contract laboratories in controlled test environments. Liquid/substrate properties were measured by Augustine Scientific Laboratories in Newbury, OH. Fuel combustion property testing was conducted by Intertek Automotive Research Laboratories in San Antonio, TX.

The surface tension of the 8 liquids considered was measured in triplicate using Wilhelmy plate measurements on a Kruss Tensiometer K100 at room temperature (22^{o}C). Liquid viscosities were measured using a low shear falling ball viscometer from Gilmont Instruments Type GV-00. Given that a total of six spill substrates and eight liquids were considered in this research, a total of 48 different permutations existed for liquid/solid contact angle analysis. This matrix of tests was optimized based upon similarities in fuel properties and by testing only liquids whose properties bound the remainder of the fuels considered. The first liquid selected for contact angle analysis was diesel fuel which provided a relatively non-volatile liquid whose surface tension and viscosity bounds all other fuels considered, excluding lube oil. The second liquid selected was gasoline due to its highly volatile nature at ambient temperatures as well as the fact that the properties of gasoline (i.e., surface tension and viscosity) are also at the lower end of the fuels considered. These liquids were identified for contact angle analysis on each of the six substrates utilized in this research. Contact angles for the diesel and gasoline liquids were measured using static and dynamic sessile drop methods. Dynamic sessile drop tests were required for all contact angle analyses conducted on permeable surfaces (i.e., smooth concrete, brushed concrete, plywood, and OSB), while static tests were required for contact angle analyses on impermeable surfaces (i.e., coated concrete and vinyl). Dynamic sessile drop tests were designed to characterize the evolution of the liquid contact angle from the time of impact to the time of complete absorption thus providing bounding contact angles for spills on permeable surfaces. Static sessile drop tests were appropriate all impermeable surfaces because the volume of liquid resting atop the substrate did not change with time. A summary of the aforementioned tests is provided in Table 3.1.

The flashpoint of each of the five fuels was measured in accordance with [ASTM D93, 2008], *Standard Test Methods for Flash Point by Pensky-Martens Closed Cup Tester*. In addition to flashpoint, the chemistry of each of the multi-component hydrocarbon fuels (i.e., gasoline, kerosene, and diesel) was characterized in accordance with [ASTM D86, 2009], *Standard Test Method for Distillation of Petroleum Products at Atmospheric Pressure* and [ASTM D287, 2006], *Standard Test Method for API Gravity of Crude Petroleum and Petroleum Products (Hydrometer Method)*. These tests were selected based upon existing fuel characterization procedures [Bardon & Rao, 1984] that require ASTM distillation curves and fuel density to construct important fuel properties (e.g., vapor pressure). Using these procedures, the aforementioned tests can be used to provide detailed information regarding the chemical

composition of the hydrocarbon fuels; the distillation data can also be used to derive valuable physical properties including boiling point, heat of vaporization, heat of combustion, vapor pressure, etc. A summary of the analytical testing performed to characterize the combustion properties of the fuels is provided in Table 3.2.

Table 3.1. Summary of Liquid and Substrate Contact Angle Testing

Test No.	Substrate	Liquid	Test Method
1	Coated Concrete	Gasoline	Static
2	NIJ Smooth Concrete		Dynamic
3	Plywood		
4	OSB		
5	Vinyl		Static
6	NIJ Smooth Concrete	3% AFFF	Dynamic
7	Coated Concrete	Diesel	Static
8	NIJ Smooth Concrete		Dynamic
9	Plywood		
10	OSB		
11	Vinyl		Static

Table 3.2. Summary of Liquid Combustion Property Testing

Test No.	Fuel	Test Method
1	Gasoline	ASTM D86, Distillation Curve
2	Diesel	
3	Kerosene	
4	Gasoline	ASTM D287, API Specific Gravity
5	Diesel	
6	Kerosene	
7	Gasoline	ASTM D93, Closed Cup Flashpoint
8	Diesel	
9	Kerosene	
10	Denatured Alcohol	
11	n-Heptane	

3.2 Cone Calorimeter Experiments

A series of cone calorimeter experiments were conducted to characterize the combustion properties of each of the fuels considered in this study. During this characterization, tests were also conducted to evaluate the impact of fuel depth on burning dynamics for fires whose equivalent diameter is between 0.05 m and 0.2 m, thus resulting in a burning mode commonly referred to as convective/radiative [Babrauskas 1983]. These cone calorimeter tests were conducted on fuel samples collected from the batch of fuels used throughout the test series.

All tests were conducted at the Hughes Associates Laboratory beneath a calorimeter constructed and maintained in general accordance with the requirements of ASTM E1354 [2009], *Standard Test Method for Heat and Visible Smoke Release Rates for Materials and Products Using an Oxygen Consumption Calorimeter*. The experiments conducted were performed without an incident heat flux exposure imposed by the cone. The fuels evaluated were contained within a steel fuel pan constructed from 6.25 mm (0.25 in.) steel plate, with a side length of 0.01 m (4 in.), and an internal vertical lip height of 25.4 mm (1 in.). The bottom of the pan was backed by a single layer of 25.4 mm (1 in.) Duraboard LD insulation. A photograph of the experimental setup for this test series is provided in Figure 3.1. Data collection for this test series was achieved using a National Instruments SCXI-1000 data acquisition chassis with one SCXI-1303, 32-channel isothermal terminal block, and a SCXI-1327, 8-channel high-voltage attenuator terminal block. The National Instruments hardware was interfaced with Labview 8.1 data acquisition software using a 16-bit PCMCIA converter. The data acquisition system was set to a sampling rate of 1 Hz.

Figure 3.1. Photograph of ASTM E1354 cone calorimeter

3.3 Pan Fires

The pan fires conducted in this research were designed to establish baseline burning rate data for various fuels at various depths as well as provide comparisons to data previously reported in the literature. Three different size fuel pans were designed and fabricated for this test series. All fuel pans were constructed from 6.3 mm (0.25 in.) steel plate with two pieces of 6.3 mm (0.25 in.) x 0.064 m (2.5 in.) angle iron welded to opposite sides of the pan for reinforcement. The wall thicknesses and side wall reinforcement were used to minimize expected thermal deflections due to the heating and cooling of the pans during testing. The design proved successful and the pans did not change shape during all testing. The fuel pans were square in geometry with side lengths of 0.3 m (12 in.), 0.6 m (24 in.), and 1.2 m (48 in.). The internal vertical lip height was 6.4 cm (2.5 in.) for all pans. As shown in Table 3.3, the pan sizes chosen were designed such that their equivalent diameters result in burning modes that range from

radiative/optically thin ($0.2 < D < 1.0$ m) to radiative/optically thick ($D > 1$ m) as defined by Babrauskas [1983]. These sizes are also consistent with data in the literature.

Table 3.3. Summary of Pan Size Selection and Expected Mode of Burning

Side Length (m [ft])	Equivalent Diameter (m [ft])	Burning Mode
0.3 [1]	0.34 [1.1]	Radiative, Optically Thin
0.6 [2]	0.69 [2.3]	Radiative, Optically Thin
1.2 [4]	1.4 [4.6]	Radiative, Optically Thick

The primary two fuels evaluated in this test series were gasoline and kerosene. These fuels were selected due to the differences in a variety of fire properties between them including, flashpoint, $k\beta$ values, maximum mass burning rate, and boiling point. Furthermore, these differences are generally large enough that the evaluation of these two fuels will provide bounding characteristics for most liquid hydrocarbon fuels. It is important to note that denatured alcohol was also evaluated in a small subset of the pan fire test series. This fuel was tested in place of the kerosene for the 1.2 m (4 ft) square pan testing due to the inability to readily ignite the kerosene fuel in this configuration. This subset of alcohol tests provides insight into the behavior of alcohol as opposed to strictly hydrocarbon fuels.

Instrumentation used in the pan fire test series included hood calorimetry, mass loss, incident heat flux, and temperature. The heat release rate of all pan fires was characterized using oxygen consumption calorimetry via either a 1 or 4 MW calorimeter, depending upon the expected fire size. All 0.3 m (1 ft) and 0.6 m (2 ft) pan fire tests were conducted beneath the 1MW calorimeter, while all 1.2 m (4 ft) pan fire tests were conducted beneath the 4 MW calorimeter. The construction and calibration of the hood calorimeters used in all tests as well as a list of instrumentation used is summarized in Appendix B. For all tests, fuel pans were placed atop a 50.8 mm (2 in.) thick layer of gypsum wall board (GWB). The GWB substrate provided a well characterized backside boundary condition for all tests conducted. The fuel pan and GWB substrate were placed atop a Sterling Scale, Model 810-N4 load cell with a maximum capacity of 453.6 kg (1,000 lb) with 0.05 kg (0.1 lb) resolution.

The fuel pans were fabricated with several threaded instrumentation ports incorporated into the base of the pans in order to accommodate heat flux gauges. These gauges were used to characterize the incident heat flux to the fuel surface as well as to the base of the pan (i.e., heat transmitted through the fuel substrate). Schmidt-Boelter type, water-cooled heat flux gauges were used to characterize the incident heat flux impinging upon the fuel surface and substrate. Gauges mounted in the fuel pans were oriented vertically (i.e., the gauge face was parallel with fuel surface). The measuring surface of the gauges was positioned such that it was at the same elevation as either the fuel surface or substrate. The pans were designed such that heat flux values could be obtained at nominally the center of the pan and at a distance of one-half the effective radius (0.5 R) from the center. The exact locations of the gauges depended upon pan size. A schematic of the gauge locations for all three pan sizes is provided in Figures 3.2 and 3.3.

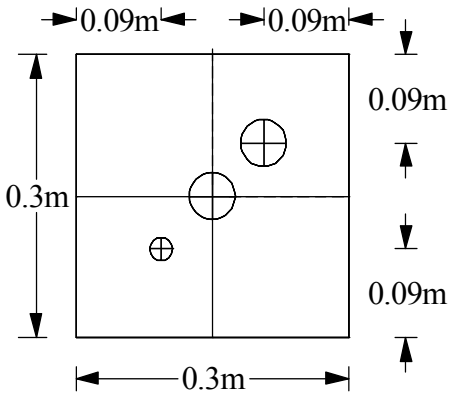

0.3 m (1 ft) square pan

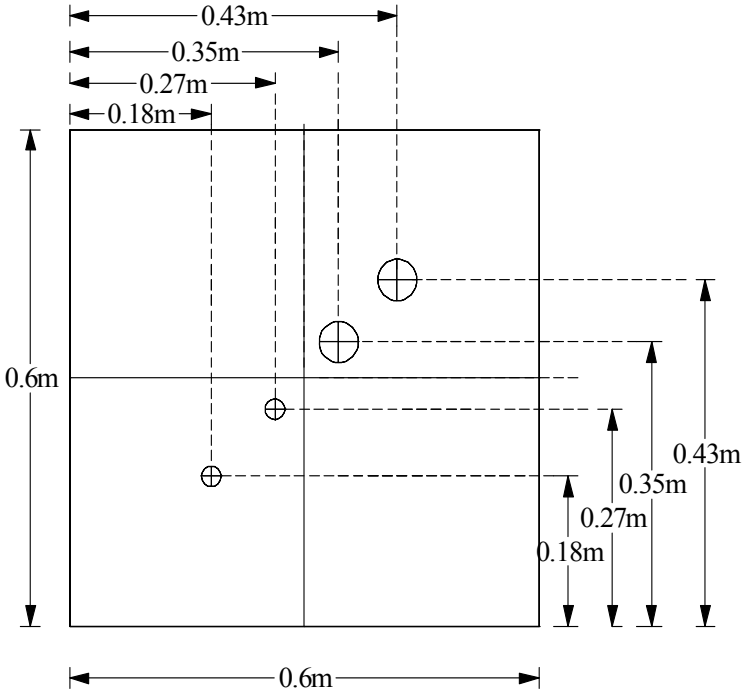

0.6 m (2 ft) square pan

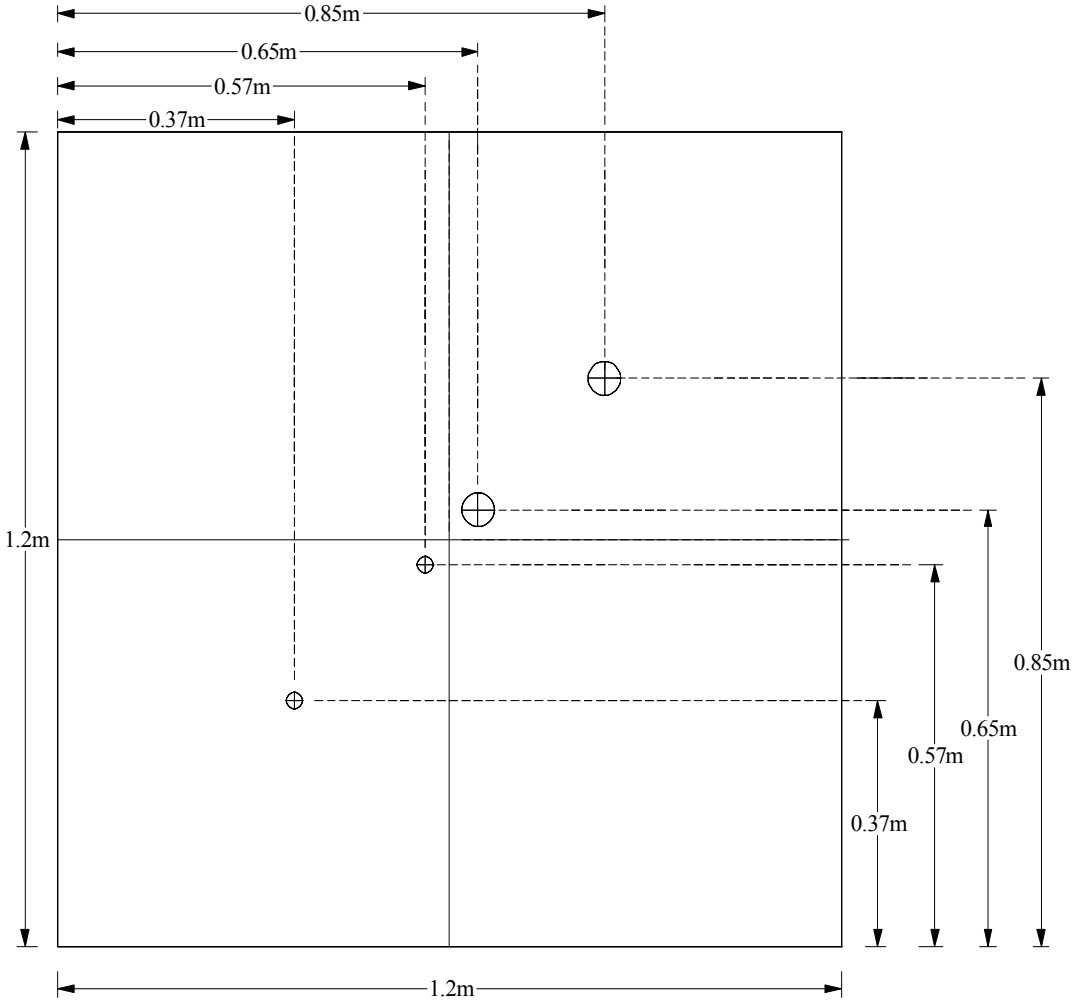

(a) 1.2 m (4 ft) square pan

Figure 3.2. Schematic of heat flux gauge locations in the 0.3, 0.6, and 1.2 m (1, 2, and 4 ft) fuel pans

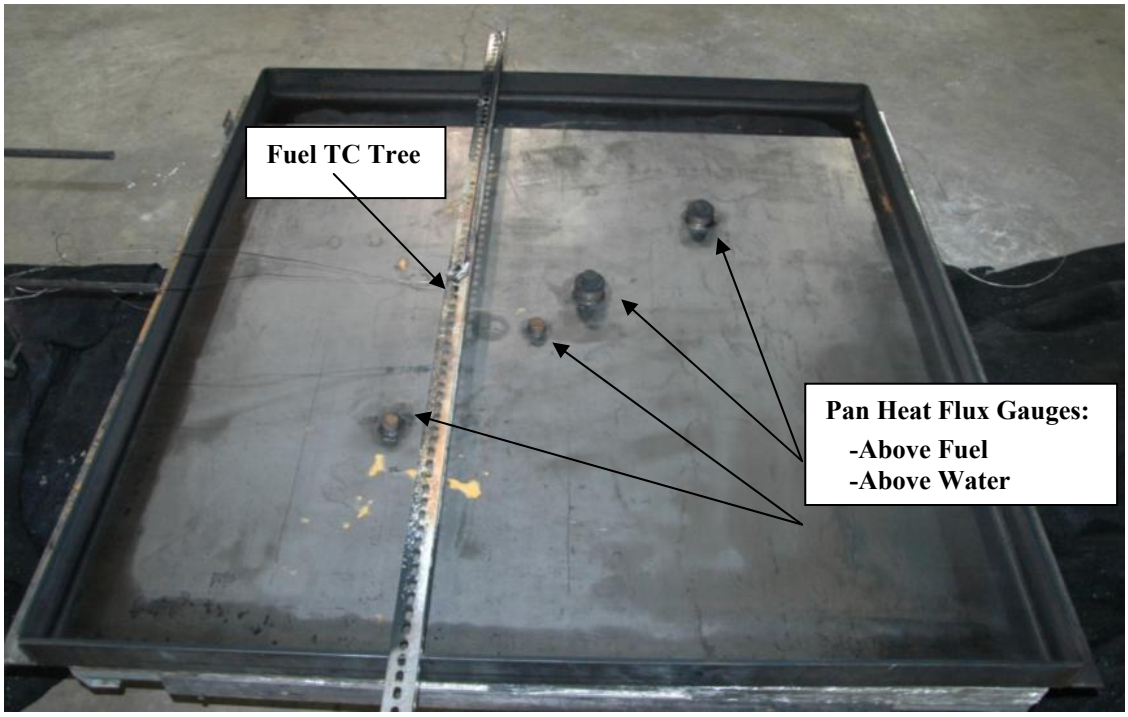

Figure 3.3. Photograph of 1.2 m (4 ft) fuel pan with heat flux gauges installed

Heat flux to the environment was also characterized using a total of three combination radiation / total heat flux gauges. These instruments were used to assess the thermal radiation hazard produced by the various liquid fuel fires (pool and spill). The measuring surface of these gauges was oriented horizontally (i.e., the face of the gauge perpendicular to the fuel surface). These heat flux gauges were located at distances of 1 R, 2 R, and 4 R from the center of the pan, where R is the equivalent radius of the square pan (shown in Table 3.4). These gauges were installed such that the face of the instrument was perpendicular to the fuel surface at a height of 1 m (39 in.) above the fuel level. A photograph of the heat flux gauge (HFG) installation for the 0.3 m (1 ft) pan fire testing is provided in Figure 3.4. All heat flux gauges were attached to a central circulating water bath maintained at a temperature of 40^{o}C (104^{o}F).

Table 3.4. Summary of Equivalent Radial Distances for Pan Sizes Used

Pan Side Length (m)	Equivalent Diameter (m)	HFG Location 1 (m)	HFG Location 2 (m)	HFG Location 3 (m)
0.30	0.34	0.17	0.34	0.69
0.61	0.68	0.34	0.69	1.38
1.22	1.38	0.69	1.38	2.75

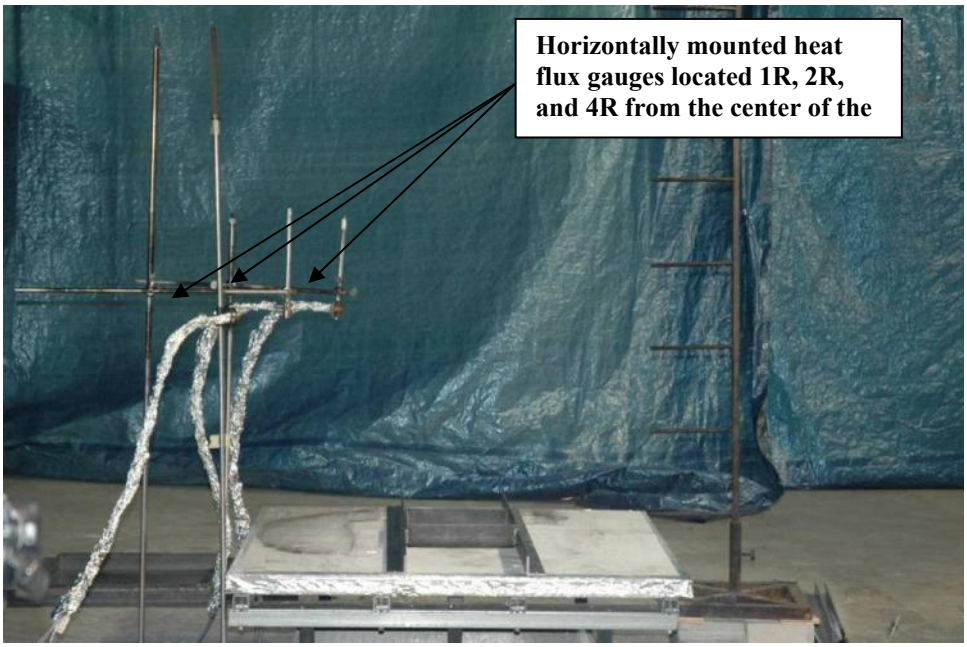

Figure 3.4. Photograph of horizontally mounted heat flux gauges located 1.0 m (3 ft–4 in.) above the surface of the pan at distances of 1R, 2R, and 4R

A total of ten temperature measurements were also collected at depth within the pan. These measurements were collected at 2 mm (0.08 in.) intervals originating 2 mm from the base of the pan. These measurements were obtained using a vertical tree of 24 Ga, glass-braid, type K thermocouples positioned at the center of the pan. An additional thermocouple was welded to the bottom of the pan to measure the backside pan temperature.

All tests were recorded using two video cameras offset 90 degrees from one another. Flame height indicators, with markers spaced at intervals of 0.2 m (9.8 in.), were positioned within the view of each camera for flame height references. A FLIR ThermaCAM Model P640 infrared camera positioned at 45 degrees between the video cameras was also used to record the events of each test. Infrared cameras were used as a secondary means of assessing the fire plume characteristics of the various pool/spill fires conducted.

3.4 Diked Fires

The diked fire test series was designed to characterize the impacts of varying fuel depth and substrate on fuel burning dynamics. The diked pan sizes, fuel types, and fuel quantities used in this test series were identical to those described in Section 3.1 for pan fire tests. The primary difference between the two test series is the substrate onto which the test fuels were burned. The substrates evaluated in this test series were coated concrete and vinyl. Photographs of the 1.2 m (4 ft) diked concrete and vinyl assemblies are provided in Figure 3.5. The primary rationale for selecting these substrates was their impermeability. A primary objective of this test series was to characterize changes in burning dynamics with varying fuel height, thus it was critical that fuel heights be independent of substrate. This could not be achieved if one substrate was absorbent and the other impermeable. Furthermore, the characterization of substrates absorbencies can be highly complex; thus it was decided that impermeable substrates be used. The coated concrete

substrate was also selected based upon its applicability to a broad spectrum of real-world scenarios in which concrete could be present.

(a) Coated Concrete Pad (b) Vinyl Substrate

Figure 3.5. Photographs of 1.2 m (4 ft) diked fire test setup

Similar to the pan fire test series, oxygen consumption calorimetry was used to characterize fire size in all diked fire tests conducted. The construction and calibration of the hood calorimeters used as well as identification of the instrumentation used in all tests are summarized in Appendix B. The instrumentation layouts used in this test series were slightly different than those used in the pan fires, as shown in Figure 3.6. The diked assemblies were instrumented with only two Schmidt-Boelter type, water-cooled heat flux gauges. For all diked fire tests these embedded gauges were installed at the center and at a distance of 1 R from the center. The faces of the heat flux gauges were installed flush with the top of the substrate. Heat flux to the environment was characterized in a manner identical to that described in Section 3.3, Pan Fires. All heat flux gauges were attached to a central circulating water bath maintained at a temperature of 40°C (104°F).

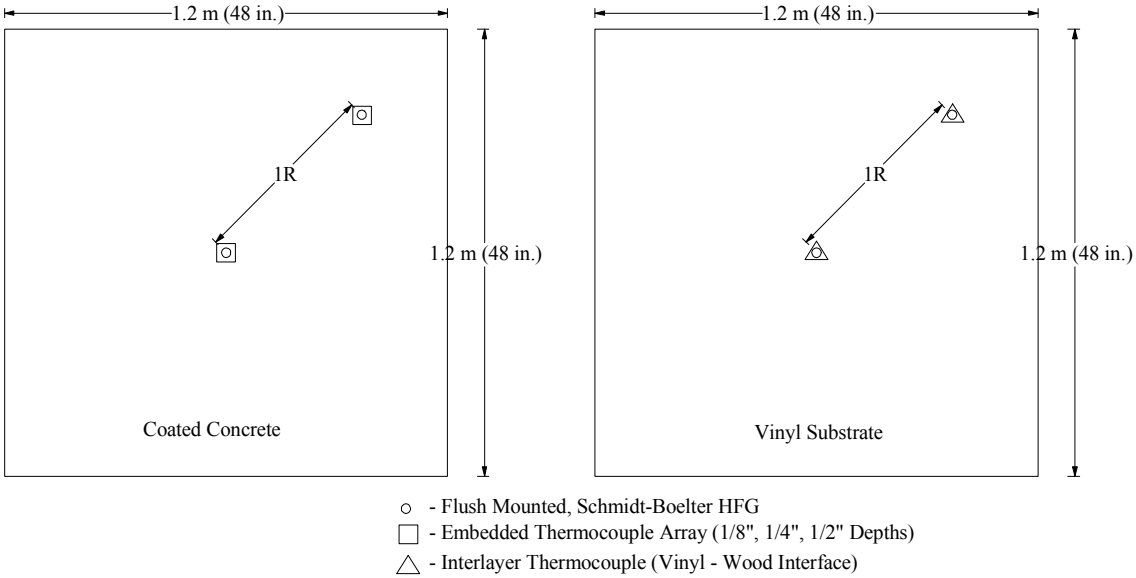

Figure 3.6. Schematic showing embedded thermocouple and heat flux gauge locations for (a) diked concrete and (b) diked vinyl substrates

In addition to the installation of the fuel thermocouple tree described in Section 3.3, diked fire tests also included thermocouples embedded within the substrates to characterize the heat losses from the fuel. Temperature profiles were collected at the center and half-radius locations of the diked assembly diagonally outward from the center of the specimen. For the concrete specimen, 1.6 mm (0.0625 in.), type K, closed-head, grounded thermocouples were embedded at depths of 0.32 cm (0.125 in), 0.64 (0.25 in), and 1.3 cm (0.5 in). For vinyl substrate testing, 24 Ga, glass-braid, type K thermocouples were placed at the vinyl-plywood interface at the center and half-radius locations. Video and thermal imaging cameras were located at the same locations as described in Section 3.3, Pan Fires.

3.5 Spill Dynamics

The spill dynamics tests were designed to characterize the progression of liquid fuel spills over various substrates. However, in order to mitigate the potential hazards of flammable vapor clouds and to determine maximum expected spread areas, all spill dynamics tests were conducted using fuel simulants whose relevant properties bound the vast majority of common fuels. Spill dynamics testing was conducted in two different locations dependent upon the quantity of liquid being spilled.

The majority of the tests conducted were executed using a liquid quantity of 0.5 L (0.13 gal). However, smaller quantities of liquid were used when spills reached the edge of the substrate being evaluated. Larger quantities of liquid were also investigated on substrates with larger foot prints in order to examine the dependence of spill depth upon spill volume. A summary of the various sizes of substrates used in this test series is provided in Table 3.5.

Table 3.5. Summary of Substrates and Sizes Evaluated

Substrate	**Sizes Evaluated (m [ft])**
Vinyl, Plywood, OSB, Carpet	1.2 [4]
Brushed Concrete, Smooth Concrete	2 [6.5]
Coated Concrete, Vinyl	3.5 [11.5]
Smooth Concrete	12.2 [40]

The primary data collected in these tests was visual and infrared video of the progression of each liquid spill and the maximum area covered. The infrared camera used was a FLIR ThermaCAM Model P640. The experimental setup used to capture these videos was dependent upon the quantity of liquid being spilled. For spills of 2 L (0.53 gal) or less, test cameras were mounted 8.9 m ± 0.15 m (29.5 ± 0.5 ft) directly above the spill substrate. See Figure 3.7 for a schematic of this configuration. This elevation combined with the view angles of the cameras resulted in the ability to capture the entire spill substrate within the frame of view.

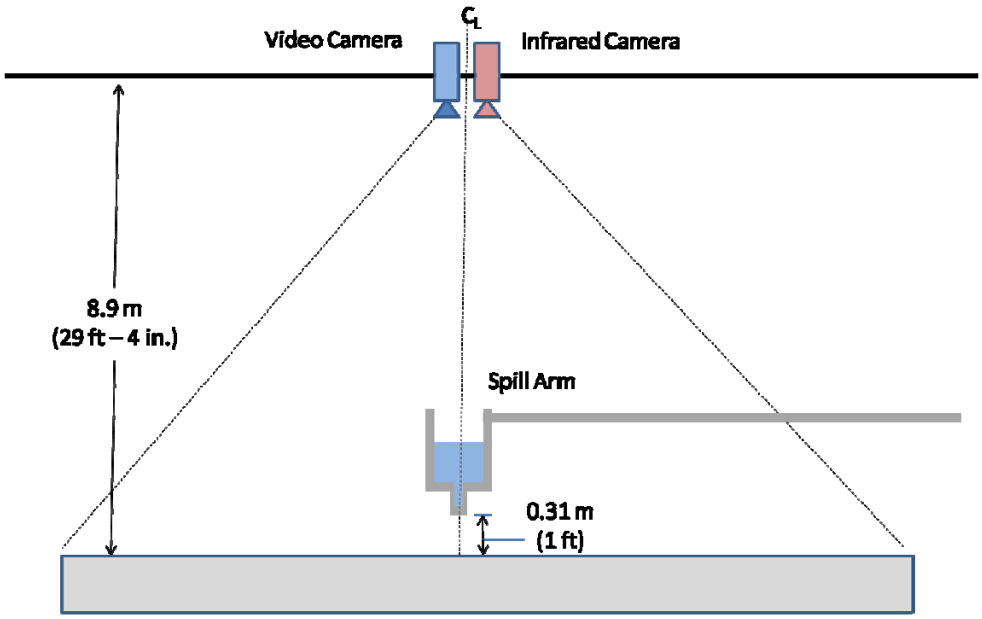

Figure 3.7. Experimental setup for spill dynamics tests of less than 2 L (0.53 gal.)

For spills greater than 2 L (0.53 gal), a different experimental setup was required due to the size of the spill substrate needed to accommodate the progression of the unconfined spill. For these scenarios, the cameras were mounted at an off-axis location due to the inability to be directly above the center of the spill. In this setup the cameras were installed 7.9 m (26 ft) above the spill substrate and 11.6 m (38 ft) off-center. A schematic of this experimental setup is provided in Figure 3.8.

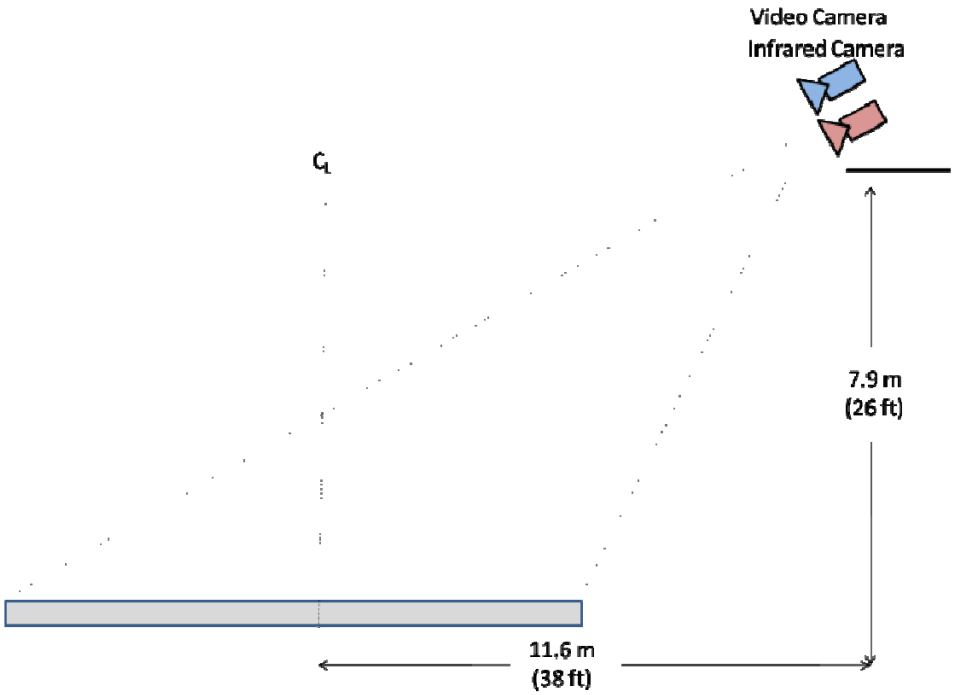

Figure 3.8. Experimental setup for spill dynamics tests of greater than 2 L (0.53 gal.)

All spills were executed using a unique spill arm designed specifically for this test series. The spill arm was designed to release up to 25 L (6.6 gal) of liquid from a distance of 4.6 m (15 ft). The spilling orifice had an internal diameter of 0.05 m (2 in.) and the spilling reservoir was a gravity-fed system. The initiation of a spill was manually accomplished using a quarter-turn valve located at the base of the reservoir. For all spill tests the spilling orifice was located 0.3 m ± 0.05 m (12 ± 2 in.) above the substrate being evaluated. A schematic of a typical spill scenario is provided in Figure 3.7.

3.6 Spill Fires

The spill fire dynamics tests were designed to evaluate the burning dynamics of spill fires resulting from different fuels spilled over various substrates. These tests were conducted on substrate surfaces ranging in size from 1.5 m^2 (16 ft^2) up to 12.9 m^2 (139 ft^2) using liquid quantities ranging in volume from 0.5 L (0.13 gal) up to 5 L (1.3 gal).

Instrumentation used in this test series included hood calorimetry, incident heat flux, and temperature. The heat release rates for all tests were characterized using oxygen consumption calorimetry via 1 and 4 MW calorimeters, depending upon expected fire size. The construction details and calibration of the hood calorimeters, as well as the instrumentation used, are summarized in Appendix B. Heat fluxes to the fuel substrate were measured using Schmidt-Boelter type, water-cooled heat flux gauges. All heat flux gauges were embedded in the substrate such that the measurement surface was flush with the substrate surface. The gauges were installed in 25 mm (1 in.) holes within each of the substrates at set locations. After installation, the perimeter of the gauge was sealed with a high temperature RTV silicone to prevent leaking. All gauges were attached to Haake Model B12 circulating water baths maintained at a temperature of 40°C (104°F).

The number and location of heat flux measurements was dependent upon the size of the substrate being evaluated. For smaller substrates (i.e., 1.2 m (4 ft) square), a total of two heat flux gauges were installed. Heat flux measurements collected during spill fires on substrates other than concrete (i.e., vinyl, plywood, OSB) were measured at the same locations shown in Figure 3.6 for spill fires conducted except carpet. These gauges were located at the center and at a distance of 1 R from the center. For the 3.5 m (11.5 ft) coated concrete pad, a total of five surface mounted heat flux gauges were installed at various radial distances from the center of the pad (i.e., the point of spill origin). A schematic of the heat flux gauge locations for the coated concrete pad is provided in Figure 3.9.

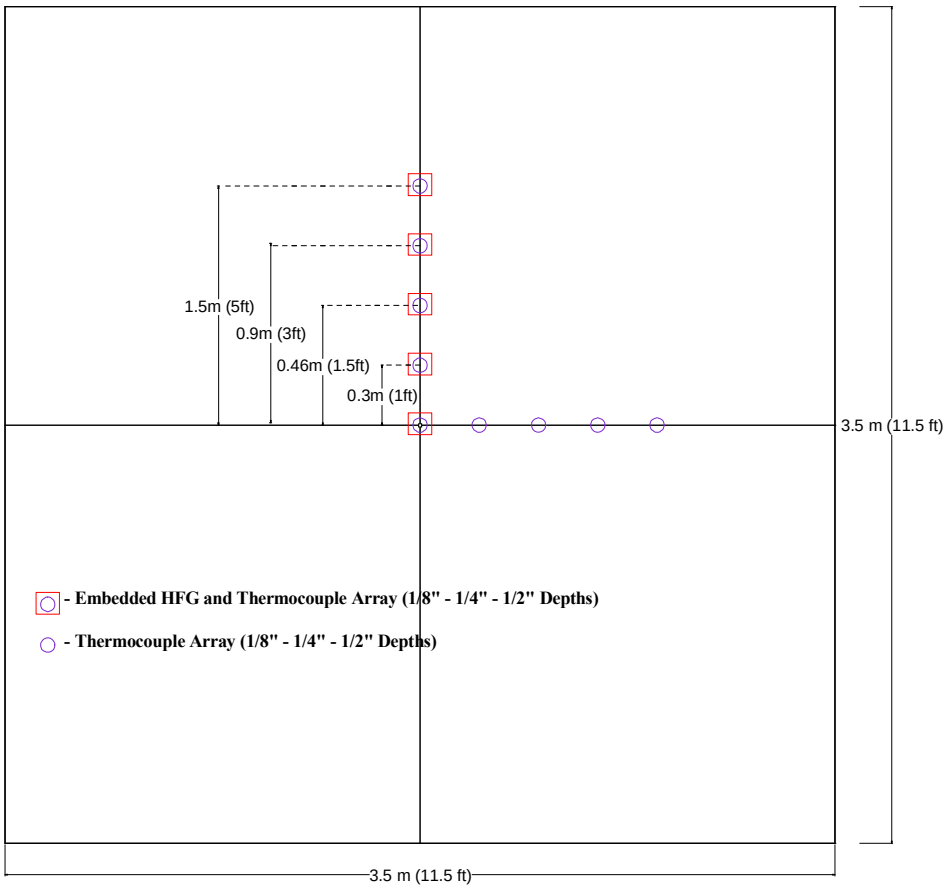

Figure 3.9. Schematic showing thermocouple and heat flux gauge installation locations for 3.5 m (11.5 ft) coated concrete pad

Heat fluxes to the environment were measured using horizontally oriented (i.e., the face of gauge is perpendicular to fuel surface) heat flux gauges. These gauges were installed at fixed distances of 1.8 m (6 ft), 3.0 m (10 ft), and 4.3 m (14 ft) from the center of the spill. All three gauges were mounted 1 m (3 ft–4 in.) above the fuel surface and were off-set from one another to prevent any blockage of the incident heat flux from the fire.

The migration of heat into the fuel substrates was measured using embedded thermocouples for all spill fire tests. For the coated concrete substrates, 1.6 mm (0.0625 in.), type K, closed-head, grounded thermocouples were embedded at depths of 0.32 cm (0.125 in.), 0.64 cm (0.25 in.), and 1.3 cm(0.5 in.). These thermocouple profiles were located at the center of each pad as well as at distances of 0.30, 0.46, 0.91, and 1.5 m (1, 1.5, 3, and 5 ft) for the 3.5 m (12 ft) from the center along two perpendicular axes. These locations were selected based upon expected distances for the half radii and full radii of the spills. Thermocouple locations were co-located with the aforementioned embedded heat flux gauges and these locations are presented in Figure 3.9.

Both visual and infrared video were used to record the progression of each fuel spill as well as the fire size and flame height. The configuration of the cameras used to document the progression of each spill was dependent upon the quantity of liquid being spilled. Due to the ensuing fires after fuels were spilled, both scenarios required that the cameras be mounted at an

angle. A schematic of the camera mounting used for spill fires conducted beneath the 4 MW hood was provided previously in Figure 3.8. For all other spill fires (i.e., those conducted beneath the 1 MW hood) a schematic of the camera setup is provided in Figure 3.10. In this setup the cameras were installed 3.9 m (13 ft) above the spill substrate and 6.4 m (21 ft) off-center.

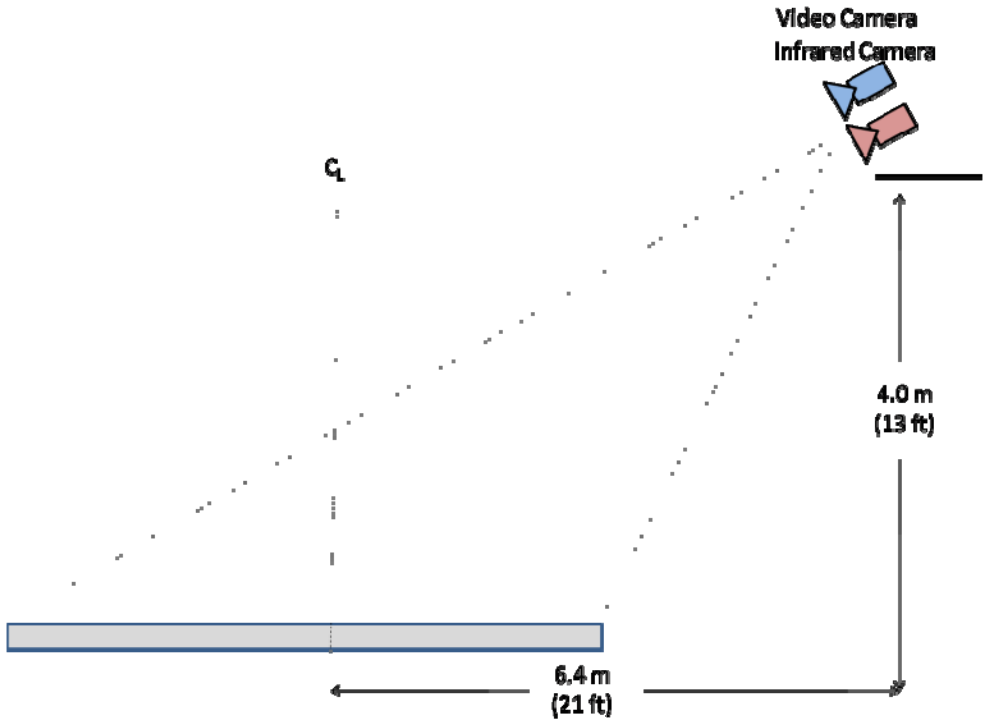

Figure 3.10. Experimental setup for spill fire dynamics tests conducted beneath 1MW (round) hood calorimeter

In addition to the elevated cameras used to document spill progression, two floor cameras were installed 90 degrees from one another for all spill fire tests. These cameras were used to record each test and document flame height and volume. In order to do so, each camera was positioned behind a 6.3 mm (0.25 in.) grid, wire screen mesh designed to divide each video frame into cells of a known area. The area captured in each grid cell was determined using a calibration image with a known area. Video images of the tests conducted beneath the 1 MW hood calorimeter were divided into 0.08 m (3 in.) square cells while images of the tests conducted beneath the 4 MW calorimeter were divided into 0.15 m (6 in.) square cells.

3.7 Continuously Fed Spill Fires

Due to the highly transient nature and relatively short duration of spill fires, steady-state behavior is seldom achieved for these types of fire scenarios. In order to develop steady-state conditions for spill fires (i.e., thin liquid depths) it is necessary to maintain the spill via a continuous fuel supply system. The continuously fed spill fire tests were designed to evaluate the steady-state burning characteristics of both gasoline and denatured alcohol spill fires. These tests were conducted on a modified version of the 2 m (6.5 ft) smooth concrete pad used in previous testing. The pad was modified in that it was instrumented with a total of five

thermocouples and a 12.7 mm (0.5 in.) fuel delivery tube was installed in the center of the pad. This delivery tube was connected to a piping system tied to a pressurized fuel reservoir. A schematic of the continuous spill system is provided in Figure 3.11.

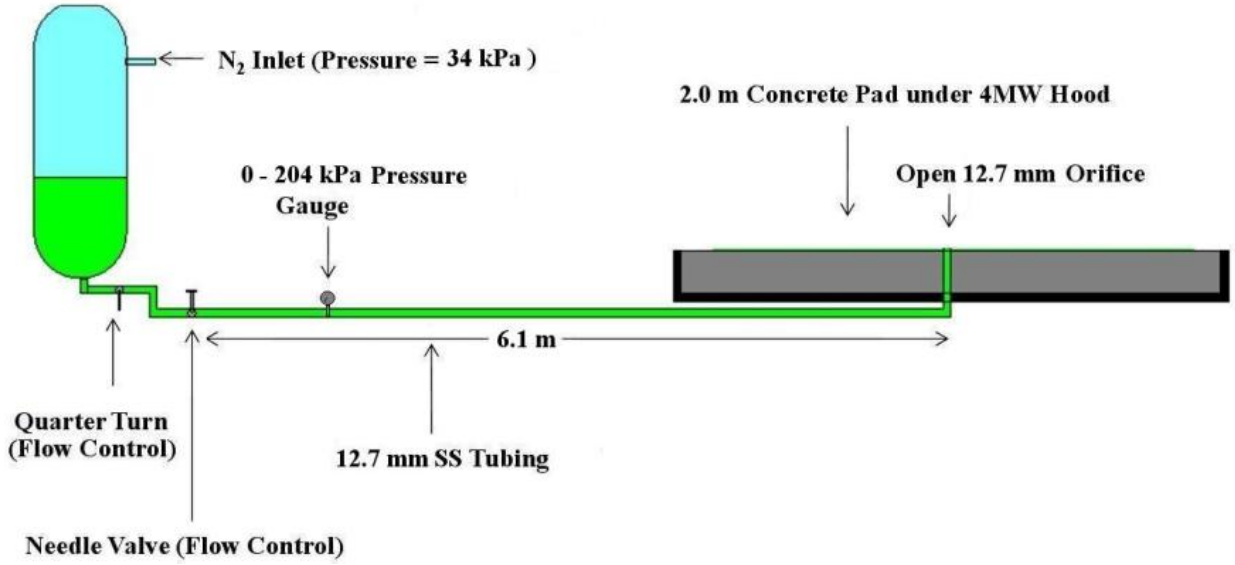

Figure 3.11. Schematic of fuel delivery system used in continuous spill fire testing (not drawn to scale)

Prior to each test, approximately 20 L (5.3 gal) of fuel was added to the fuel reservoir. Based upon the mass burning rates measured in previous spill fire tests, it was determined that this volume of fuel would provide a burning duration of approximately 5 minutes if a 1 m^2 (10.8 ft^2) spill was maintained. The ullage space within the fuel reservoir was pressurized to 34 kPa (5 psi) using nitrogen. The fuel was delivered to the pad via 6.1 m (20 ft) of 12.7 mm (0.5 in) stainless steel tubing. A quarter-turn and a needle valve were installed in line to provide flow control along with a 0–30 psi pressure gauge to provide discharge pressure measurements. The fuel was delivered to the surface of the concrete through a 12.7 mm (0.5 in.) tube opening installed flush with the pad surface.

The instrumentation for these tests included hood calorimetry and embedded temperature measurements. All continuous spill fire tests were conducted beneath the 4 MW hood. The construction and calibration of the hood calorimeter used in these tests as well as the instrumentation used is summarized in Appendix B. Temperature measurements were collected using five 1.6 mm (0.0625 in.), type K, closed-head, grounded thermocouples embedded at a depth of 1.3 cm (0.5 in). These thermocouples were located at the center of the pad as well as at distances of 0.3 m (1 ft) from the center along each of four diagonals of the pad (see Figure 3.12). Thermocouples were installed on a 0.3 m (1 ft) radius because the goal of this testing was to develop a spill fire with an approximate diameter of 1.2 m (4 ft); thus, the temperature measurements would be collected from within the continuous spill area. Both video and thermal imaging cameras were used to document theses tests and were installed at the same locations and orientations as described for spill fire tests conducted beneath the 4 MW hood calorimeter.

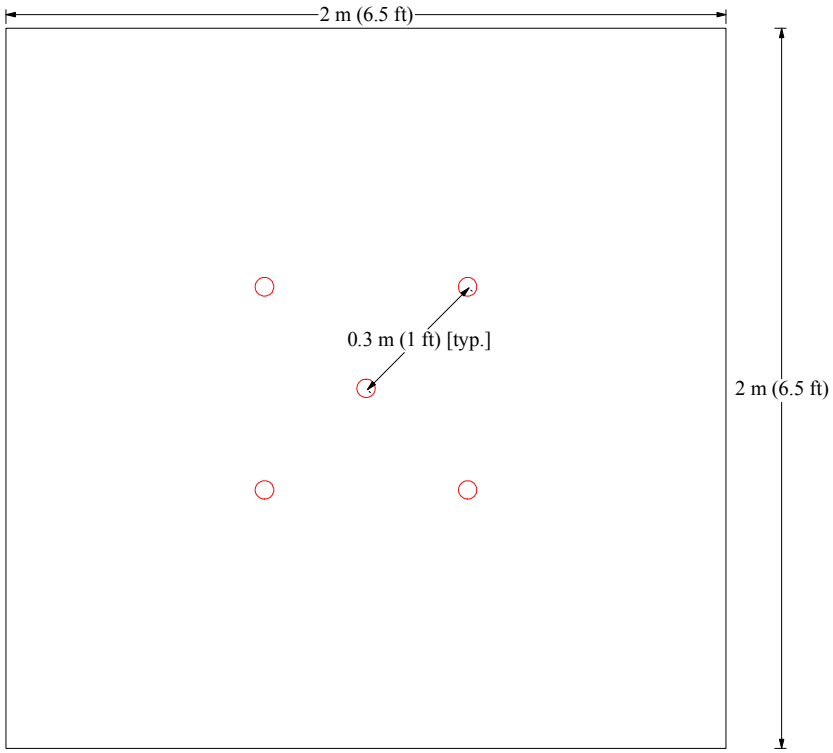

Figure 3.12. Schematic of thermocouple locations installed in 2 m (6.5 ft) smooth concrete pad used in continuous spill fire tests

4.0 TEST PROCEDURES AND RESULTS

4.1 Analytical Test Results

Material properties for both the liquids/fuels and substrates used in this study are presented in Tables 4.1(a) and (b). It should be noted that the properties presented are comprised of both measured values as well as those obtained from the literature. In Table 4.1(a), the only material property that was not measured specifically for this testing was the specific heat capacities of the various liquids. In Table 4.1(b) all material properties were obtained from the literature.

In addition to the initial contact angles presented in Table 4.1(a), transient contact angle measurements were also collected for each of the permeable substrates (i.e., smooth concrete, plywood, and OSB). These transient contact angle measurements are shown in Figure 4.1 and Figure 4.2 for smooth concrete and the cellulosic substrates (i.e., wood and OSB), respectively. These absorption times are for a 5 µL test drop and not a large liquid spill, where overall absorption effects would be different. The data in Table 4.1 and the graphs show that the fuels have lower initial contact angles on the permeable surfaces than for non-permeable substrates. The graphs also show that gasoline tends to soak into the permeable surfaces (with the exception of smooth concrete) more quickly than the diesel fuel. This is most likely due to the gasoline having a lower surface tension than the diesel fuel. This hypothesis is supported by the fact that, on the smooth concrete, the 3% AFFF penetrates even faster than the gasoline as it has a lower

surface tension than gasoline. In terms of surfaces, both fuels soak into plywood the quickest, then OSB, and into the smooth concrete the slowest.

Table 4.1a. Summary of Liquid/Fuel Properties

	Gasoline	Kerosene	Diesel	Denatured Alcohol	n-Heptane	Lube Oil	3% AFFF Solution	3% FP Solution
Surface Tension (mN/m)	21.9	26.1	27.2	22.3	19.9	29.2	17.2	27.0
Viscosity (cp)	0.6	2.4	2.8	1.1	0.4	43.0	1.2	1.1
Coated Concrete Contact Angle (degrees)	24.4	N/M	33.4	N/M	N/M	N/M	N/M	N/M
NIJ Smooth Concrete Contact Angle (degrees)	19.7	N/M	28.1				14.2	
Plywood Contact Angle (degrees)	9.7	N/M	23.2				N/M	
OSB Contact Angle (degrees)	10.4	N/M	24.7					
Vinyl Contact Angle (degrees)	25.7	N/M	35.9					
Density (kg/m^3)	742	798	823	790	671	844	990	1000
Specific Heat Capcity (kJ/kg-K)[1]	2.2	2.0	1.7	2.5	2.2	1.9	4.2	4.2
Flash Point (^{o}C)	-4	58	71	7	13	N/M	N/A	N/A
Initial Boiling Point (^{o}C)	45.0	169.9	185.8	N/A	N/A			
Final Boiling Point (^{o}C)	211.7	256.7	347.5	N/A	N/A			
API Specific Gravity	57.7	45.6	35.1	N/M	N/M			
Measured Effective Heat of Combustion (MJ/kg)	37.6	40.2	38.6	22.2	40.3			

N/M - Not measured N/A - Not applicable

1 - Not measured experimentally.

Table 4.1b. Summary of Substrate Properties

Substrate	Thermal Condcutivity (W/m-K)	Specific Heat Capacity (kJ/kg)	Density (kg/m^3)	Thermal Intertia	Thermal Effusivity	Thermal Diffusivity
Concrete [Incropera et al., 2002]	1.4	0.88	2300	2.83E+03	53	6.92E-04
Vinyl [IEA, 1991]	0.19	1.47	1200	3.35E+02	18	1.08E-04
Wood (Plywood/OSB) [Incropera et al., 2002]	0.17	2.38	545	2.21E+02	15	1.31E-04
Steel [Incropera et al., 2002]	60.5	0.43	7854	2.06E+05	454	1.77E-02
Water [Incropera et al., 2002]	0.59	4.20	1000	2.48E+03	50	1.40E-04
Gasoline [Eaton, 1991]	0.19	2.22	742	3.13E+02	18	1.15E-04

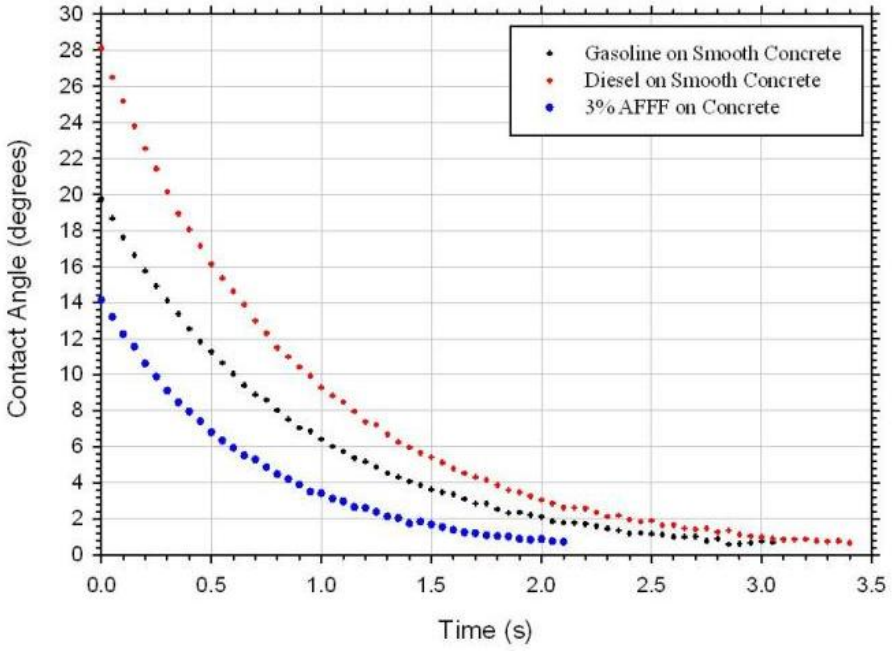

Figure 4.1. Transient contact angles measured on NIJ smooth concrete

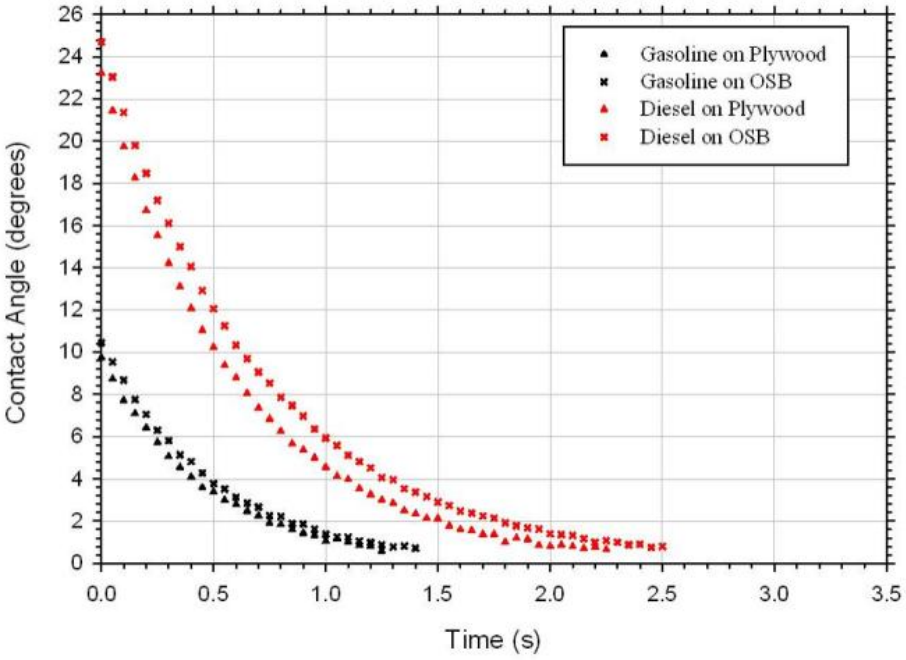

Figure 4.2. Transient contact angles measured on plywood and OSB substrates

The distillation curves for each of the multi-constituent hydrocarbon fuels considered in this study were also characterized. These curves are presented in Figure 4.3. The gasoline was analyzed at the beginning and end of the test program. As the curves show, there was no appreciable change in fuel composition over the 10 month time frame.

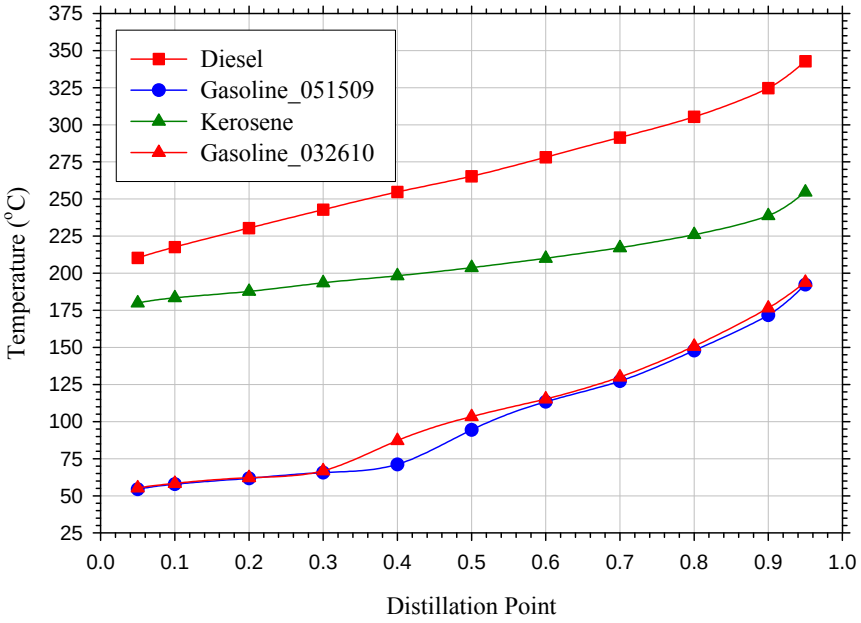

Figure 4.3. Distillation curves for the gasoline, diesel, and kerosene measured in accordance with ASTM D287

4.2 Cone Calorimeter Procedures and Results

All cone calorimeter tests were conducted in general accordance with the procedures provided in ASTM E1354 [2009]. A total of 15 individual cone calorimeter tests were conducted. A summary of these test results is provided in Table 4.3.

The primary objective of conducting cone calorimeter tests was to determine average effective heat of combustion values for each of the fuels. These values were calculated by averaging the heat of combustion values reported above for each fuel at all fuel depth levels. These calculated values along with literature values are reported in Table 4.4. The measured average effective heats of combustion for each fuel were within 15 percent of literature values for all fuels.

The heat of combustion values measured in the cone calorimeter were consistently lower than those reported in the literature. This difference is most likely an artifact of the differing calorimetry methods used to measure the heat of combustion of the fuels. The values reported in the literature are typically measured in a high-pressure oxygen atmosphere designed to drive the reacting fuel to complete combustion (i.e., no inefficiencies). The heat of combustion values obtained in this study were measured at ambient pressure with combustion efficiencies of less than 1 which can result in lower average effective heats of combustion. However, these inefficiencies in combustion are similar to those expected during realistic spill fire events thus the values obtained in the cone calorimeter were used throughout this study. It is also possible that the lower heat of combustion values measured in the cone calorimeter are a result of heat losses from the pan playing a larger role in the burning dynamics of the fuel.

Table 4.3. Summary of Cone Calorimeter Test Results

Sample ID	Fuel Depth (mm)	Average Effective Heat of Combustion (MJ/kg)	Test Avg. HRR (kW/m^2)	Peak HRR (kW/m^2)	Peak HRR (kW)	Total HRRPUA (MJ/m^2)	Average Specific Extinction Area (m^2/kg)
Gasoline	1	35.9	305	459	4.68	27	641
	5	37.5	395	515	5.25	139	664
	10	39.5	427	728	7.42	301	483
Kerosene	1	39.7	246	349	3.56	32	568
	5	38.8	366	467	4.76	156	750
	10	42	415	1121	11.43	339	593
Diesel	1	40.6	177	266	2.71	34	769
	5	36.6	301	384	3.92	156	1121
	10	38.6	327	386	3.93	330	1082
Denatured Alcohol	1	16.5	205	303	3.09	13	0
	5	20.6	334	450	4.59	85	2
	10	22.2	338	463	4.73	179	10
n-Heptane	1	35.5	362	564	5.75	25	175
	5	42.5	425	561	5.72	145	218
	10	42.8	443	534	5.45	301	220

Table 4.4. Comparison of Measured and Literature Heat of Combustion Values

Fuel	Heat of Combustion (MJ/kg)		% Difference
	Measured	Literature	
Gasoline	37.6 ± 1.8	44.1 [SFPE, 2002]	(15)
Kerosene	40.2 ± 1.7	43.1 [SFPE, 2002]	(7)
Diesel	38.6 ± 2.0	42.9 [Cameo, 1999]	(10)
Denatured Alcohol	22.2 ± 2.9	26.8 [SFPE, 2002]	(17)
n-Heptane	40.3 ± 4.1	44.4 [SFPE, 2002]	(9)

In addition to heat of combustion measurements, cone calorimeter results were also used to investigate the impact of fuel layer depth on heat release rate with a fire in the convective, turbulent burning mode (i.e., 0.05 m ≥ D ≥ 0.2 m) as described by Babrauskas [1983]. Cone calorimeter results show that in this mode of burning, a 1 mm fuel layer results in a lower average heat release rate than a 5 or 10 mm case. As shown in Figure 4.4, this holds true for all fuels considered in this study. Such a conclusion can also be made, for the majority of fuels evaluated, based upon comparisons of the peak heat release rate values presented in Figure 4.5. Unlike all other fuels evaluated, the trend observed for the n-Heptane fuel was found to be

relatively flat with no increasing trend in heat release rate with increasing fuel depth. In fact, a decrease in peak heat release rate values was observed when comparing fuel depths of 5 and 10 mm. Justification for this behavior was not identified in the analysis of the data sets and additional testing would be required to fully-understand whether this data is real or an artifact of experimental error.

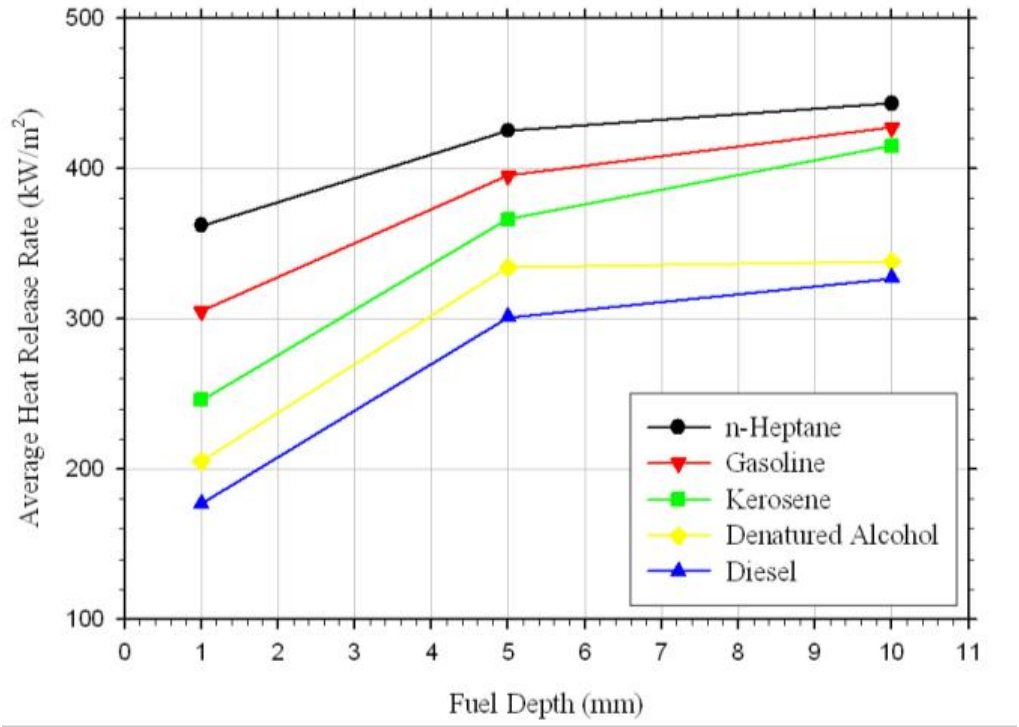

Figure 4.4. Summary of average heat release rate as a function of fuel depth for fires in the convective, turbulent burning mode

In the cone tests conducted, the measured heat release rate, both peak and average values, were found to generally increase with increasing fuel depth. Based upon average heat release rate data, the increase observed when transitioning from 1 to 5 mm was generally larger than that observed for the 5 to 10 mm transition suggesting that the impact of the fuel depth on heat release rate diminishes once a fuel depth of 5 mm is reached.

Conducting these cone calorimeter tests in general accordance with ASTM E1354 [2009] also provided the mass loss rate data for each of the fuels considered at each of the fuel depths being investigated. A summary of the average mass burning rate for each of the fuel type/fuel depth tests conducted is provided in Table 4.5.

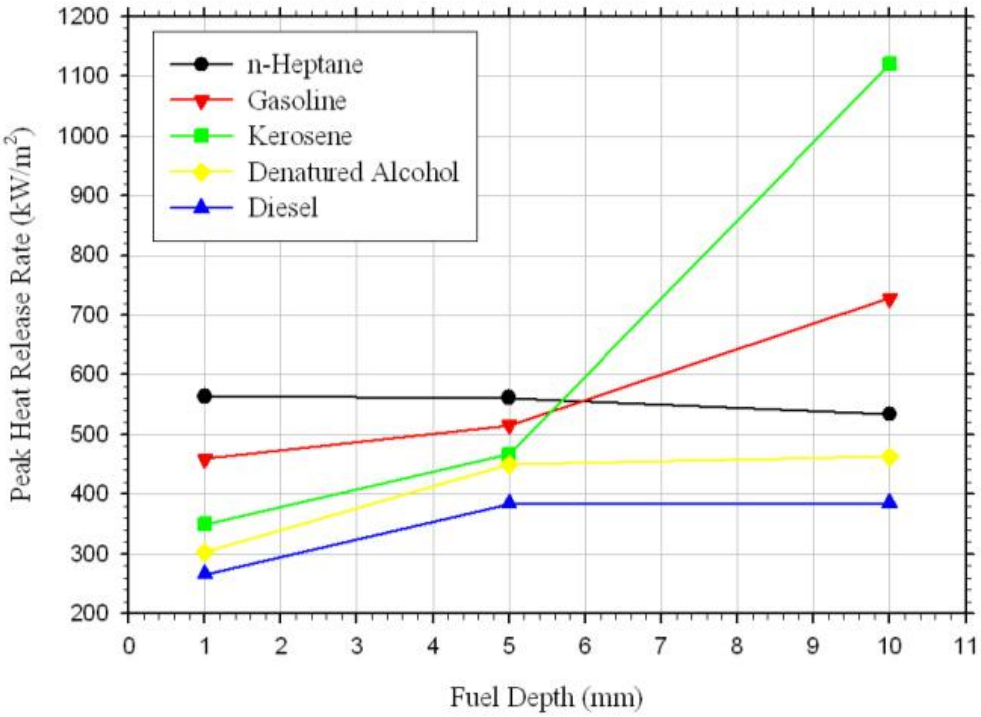

Figure 4.5. Summary of peak heat release rate as a function of fuel depth for fires in the convective, turbulent burning mode

Table 4.5. Average Mass Burning Rates Measured in ASTM E1354 Testing

Fuel	**Fuel Depth (mm)**	**Mass Burning Rate (g/m^2-s)**
Gasoline	1	11
	5	11
	10	14
Kerosene	1	6
	5	9
	10	12
Diesel	1	3
	5	6
	10	7
Denatured Alcohol	1	12
	5	12
	10	16
n-Heptane	1	11
	5	14
	10	14

4.3 Pan Fires

4.3.1 Pan Fire Procedure

Prior to testing, the instrumentation incorporated into the pans (i.e., threaded heat flux gauges) were sealed using a high temperature sealant to prevent fuel leakage. Once instrumented, the fuel pan was leveled to within 3.2 mm (0.125 in.) over a distance of 1.2 m (4 ft). The load cell was then zeroed and the initial mass and volume of the fuel as well as ambient conditions were recorded. The data acquisition system, cameras, and FLIR camera were initiated prior to the fuel being poured into the pan. Two minutes of background data were collected prior to each test. Once poured, the fuel was ignited using a propane torch. In the case of gasoline, the fuel was easily ignited at the edge of the pool. However, for kerosene, the propane torch was applied for a longer period of time until sustained ignition was observed on the kerosene fuel layer. Both the time of ignition and the time to sustained ignition were recorded. For the purpose of any subsequent calculations and discussions, the time of sustained ignition was considered the beginning of a test. The flame extinguishment time was also recorded at the end of each test. In these tests the flame extinguishment time was defined as the time at which only localized areas of small flamelets were observed, typically occurring along the edges of the fuel pans. The data, cameras, and FLIR camera continued recording until the last flame extinguished.

The transition between tests consisted of cooling the pan assembly and removing any fuel residue, if present, from the previous burn. In these tests, a temperature threshold of 30°C (86°F) was established as the minimum pan temperature at which the next test could be started. In the case of tests conducted on water substrates, fresh water was used in each test. The water substrate was 25.4 mm (1 in.) in the test pan.

4.3.2 0.093 m^2 (1 ft^2) Pan Fire Results

A total of 80, 0.093 m^2 (1 ft^2) pan fire tests were conducted with gasoline and kerosene. Forty-six tests were conducted using gasoline with fuel depths ranging from 1–40 mm (0.04–1.57 in.) on both water and steel substrates. The remaining thirty-four tests were conducted with kerosene under similar conditions. At a minimum, all tests were conducted in duplicate.

In general, the variation between tests with identical test parameters was found to be excellent. The coefficient of variation (CoV) for 33 of the 34, 0.093 m^2 (1 ft^2) data sets was less than 10 percent. The only data set whose CoV was larger than 10 percent was the 1 mm (0.04 in.) kerosene on steel scenario. This scenario presented a significant challenge with respect to repeatability because of the fuel's high flash point and the resulting difficulty of the fuel to support flame at such a shallow depth. Based upon the generally good repeatability between tests, the graphical results presented throughout the remainder of this section will be representative subsets of the entire population of data collected in the 0.093 m^2 (1 ft^2) pan fire test series. A complete summary of the data collected in this test series is presented in Appendix C.

The primary objective of the pan fire test series was to understand the impact of fuel depth on the heat release rates of liquid fuels. Representative heat release rates as a function of time for each of the fuel depths considered in the 0.093 m^2 (1 ft^2) pan are presented in Figure 4.6. For both

fuels considered, similar trends were observed with respect to heat release rate as a function of fuel depth. In general, the fire growth rates observed for all fuel depths were comparable. The impact of fuel depth was observed when evaluating the peak heat release rates achieved and the duration of the burning observed during each test. For the 0.093 m^2 (1 ft^2) pan fire tests, the 1 mm fuel depth resulted in maximum fire sizes 40 to 50 percent less than that observed for all depths of 5 mm or greater. The 1 mm fuel depths were generally unable to support any period of steady-state burning. The heat release rates obtained for depths of 5 mm or greater were generally similar with some evidence of slight increases with fuel depth, but these increases were relatively small when compared to that observed from 1 to 5 mm.

Using the heat of combustion data reported in Table 4.1(a) and the heat release rate per unit area (HRRPUA) data presented in Figure 4.6, mass burning rates for each fuel at each fuel depth were derived. Due to the brevity of the 1 mm (0.04 in.) fuel fires and the lack steady-state conditions therein, it was necessary to establish an approach for calculating and comparing mass burning rates that was applicable not only to the short duration tests but also those of longer burning durations. The approach used consisted of the following; first the peak 10-second average heat release rate was calculated using Eq. 4-1.

$$Q_{10s\ Average-Peak} = \max\left[\frac{Q_{i-5} + \ldots Q_i + \ldots Q_{i+5}}{10}\right] \quad \text{Eq. 4-1}$$

Once the peak 10-second average heat release rate value was calculated, it was divided by the area of the fire (Eq. 4-2),

$$Q^{"}\left(\frac{kW}{m^2}\right) = \frac{Q_{10s\ Average-Peak}}{A} \quad \text{Eq. 4-2}$$

where A is the measured area of the spilled liquid just prior to ignition. Finally, the mass burning rate per unit area was determined by simply dividing the solution of Eq. 4-2 by the fuel specific effective heat of combustion measured in the cone calorimeter testing as shown in Eq. 4-3.

$$\dot{m}^{"}\left(\frac{g}{s-m^2}\right) = \frac{\dot{Q}^{"}}{\Delta h_c} \quad \text{Eq. 4-3}$$

Based upon this approach, peak average mass burning rates for each fuel on each substrate, at each fuel depth are presented in Table 4.6. The values presented in Table 4.6 represent the average mass burning rates for a minimum of two replicate tests but in some cases represent the average of up to four replicate tests. The variance in mass burning rates when comparing replicate tests was generally on the order or 1–2 g/s-m^2. Using this variation, any differences in mass burning rate that were larger than this were assumed to be the result of an influencing factor.

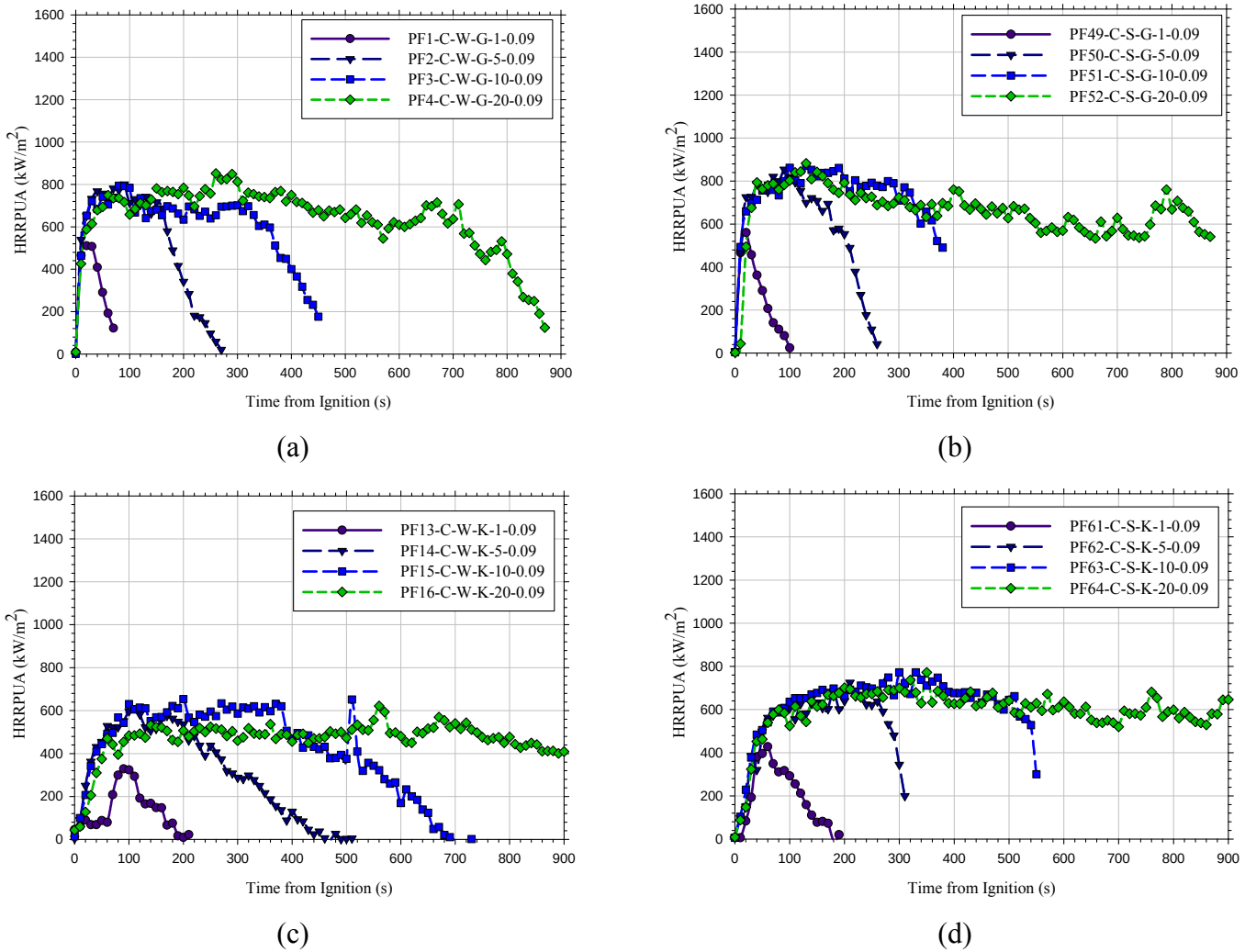

Figure 4.6. Representative 0.093 m^2 (1 ft^2) pan fire heat release rate per unit area data measured for varying fuel depths (1, 5, 10 and 20 mm) for (a) gasoline on water, (b) gasoline on steel, (c) kerosene on water, and (d) kerosene on steel

Table 4.6. Summary of 10 s – Average Peak Mass Burning Rates for 0.093 m^2 (1 ft^2) Pan Fires

Fuel Type	Substrate	Fuel Depth (mm)	10 s-Average Peak Mass Burning Rate (g/s-m^2)
Gasoline	Water	1	17
		5	21
		10	20
		20	22
	Steel	1	12
		5	20
		10	22
		20	22
Kerosene	Water	1	7.5
		5	15
		10	17
		20	17
	Steel	1	7.8
		5	17
		10	18
		20	17

The impacts of fuel depth as well as fuel substrate are evident from the data presented above for the 0.093 m^2 (1 ft^2) pan fires. For each of the four fuel/substrate combinations considered in Table 4.6, the average mass burning rates for a fuel depth of 1 mm (0.04 in.) was generally a factor of two less than that measured for any of the 20 mm deep fuel scenarios. The results also demonstrate that the substrate beneath a thin (i.e., 1 mm or less) gasoline layer can impact the mass burning rate of the fuel. At depths greater than 1 mm (i.e., 5, 10, 20 mm) there was no difference in mass burning rate when comparing the different substrates. Data from the 1 mm gasoline fires show that the presence of steel as the fuel substrate reduced the mass burning rate by 29 percent. However, data from 1 mm kerosene tests show very little difference. This reduction for gasoline is most likely due to the volatility of gasoline and the steel substrate acting as a larger heat sink than water with respect to the burning fuel layer. This heat sink effect effectively reduces the extent to which the unburned fuel can be heated prior to being vaporized.

4.3.3 0.372 m^2 (4 ft^2) Pan Fire Results

A total of 54, 0.372 m^2 (4 ft^2) pan fire tests were conducted with gasoline and kerosene. Thirty tests were conducted using gasoline with fuel depths in the pan ranging from 1 to 20 mm (0.04–0.79 in.) on both water and steel substrates. The remaining twenty-four tests were conducted with kerosene under similar conditions. At a minimum, all tests were conducted in duplicate with some tests repeated up to four times.

Similar to the results achieved in the smaller pan fires, the repeatability between the 0.372 m^2 (4 ft^2) pan tests was found to be excellent. The coefficient of variation (CoV) for all 16 data sets was less than 10 percent. Based upon the repeatability of the pan tests conducted, representative plots are presented in this section. A complete summary of the data collected in this test series is presented in Appendix C.

In general, the observations made for the 0.093 m^2 (1 ft^2) pan fires were applicable to this the results of this pan size as well. Representative heat release rates as a function of time for each of the fuel depths considered in the 0.372 m^2 (4 ft^2) pan are presented in Figure 4.7. For both fuels considered, similar trends were observed with respect to heat release rate as a function of fuel depth. The fire growth rates observed for all fuel depths were comparable with the exception of the 1 mm layer of kerosene on water which developed at a much slower rate than any other fuel depth. The impacts of fuel depth were observed when comparing the maximum heat release rate achieved during each test. For the 0.372 m^2 (4 ft^2) pan fire tests, the 1 mm fuel depth resulted in maximum fire sizes that were approximately half of those measured for all depths of 5 mm or greater. The 1 mm fuel depth layers were unable to support any period of sustained steady-state burning while at fuel depths of 5 and 10 mm some period of steady-state burning was observed and similar heat release rates were measured. It should be noted that in this larger pan, the 20 mm fuel depth resulted in slightly larger peak heat release rates than measured in the 5 and 10 mm pools. This trend is contrary to that observed in the 0.093 m^2 (1 ft^2) pan fires in which all fuel depths greater than 5 mm resulted in comparable heat release rates. The peak values measured for the 20 mm, 0.372 m^2 (4 ft^2) pools were on average 30 percent higher for gasoline and 60 percent higher for kerosene when compared to the 5 and 10 mm heat release rates.

Using the measured effective heats of combustion and the heat release rate per unit area (HRRPUA) data presented in Figure 4.7, average mass burning rates for each fuel at each fuel depth were derived. The approach described previously for the 0.093 m^2 (1 ft^2) pan fires was also adopted to derive the data presented in Table 4.7. The variance in mass burning rates between replicate tests for the 0.372 m^2 (4 ft^2) pan fires was comparable to that observed in the smaller pan size (i.e., 1–2 g/s-m^2).

For each of the four fuel/substrate combinations considered for the 0.372 m^2 (4 ft^2) pan fires in Table 4.7, the average mass burning rates for a fuel depth of 1 mm (0.04 in.) were found to be 2–5 times smaller than that measured for the 20 mm deep fuel scenarios. It should also be noted that that the effects of the substrate were not as evident in the 0.372 m^2 (4 ft^2) mass burning rate data. In these tests, the effect of substrate on the mass burning rate of a 1 mm gasoline fire was negligible and for kerosene the value measured on water was lower than that measured for steel.

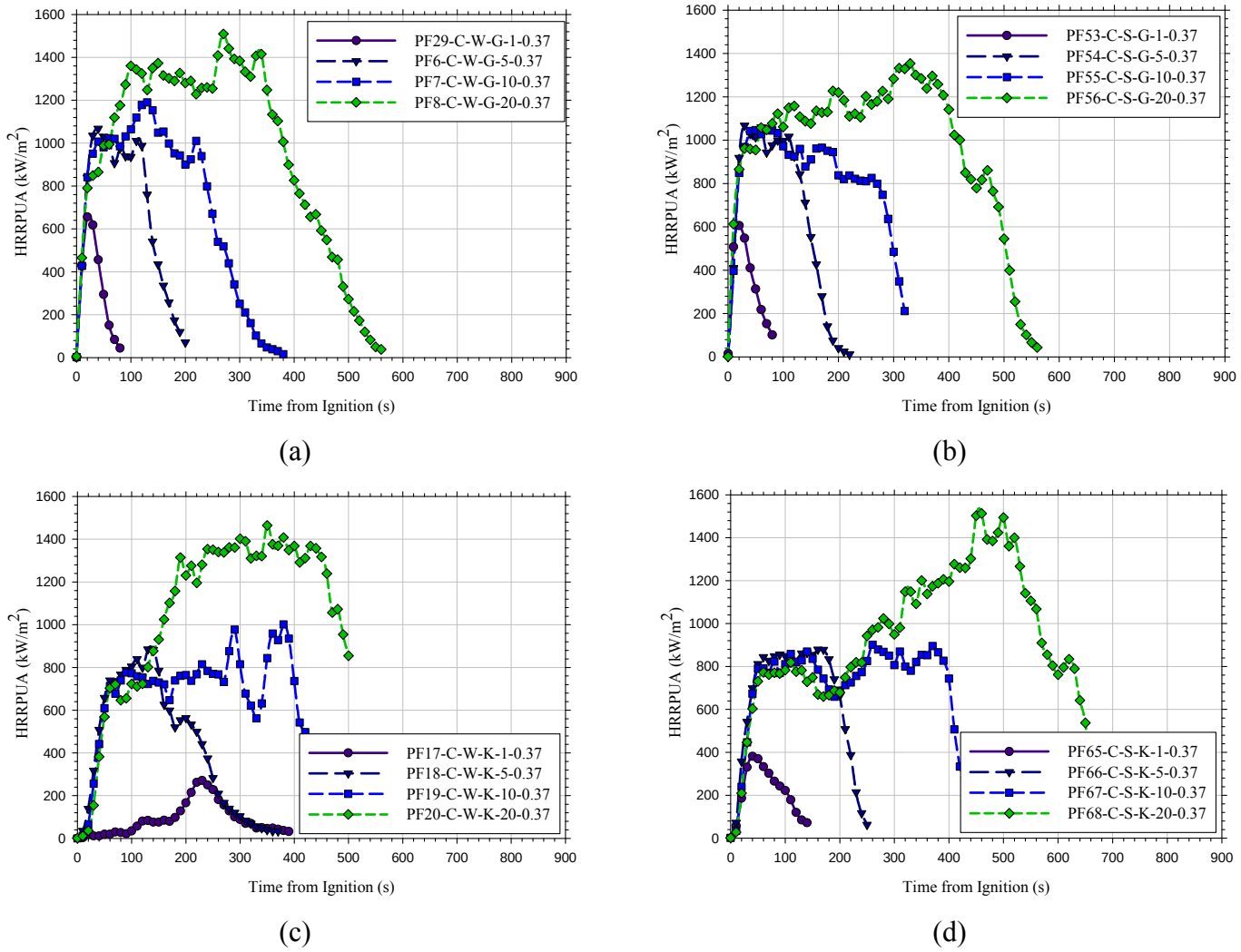

Figure 4.7. Representative 0.372 m^2 (4 ft^2) pan fire HRR per unit area data measured for varying fuel depths (1, 5, 10 ad 20 mm) for (a) gasoline on water, (b) gasoline on steel, (c) kerosene on water, and (d) kerosene on steel

Table 4.7. Summary of Peak 10 s-Average Mass Burning Rates for 0.372 m^2 (4 ft^2) Pan Fires

Fuel Type	Substrate	Fuel Depth (mm)	Peak 10 s-Average Mass Burning Rate ($g/s\text{-}m^2$)
Gasoline	Water	1	17
		5	28
		10	31
		20	40
	Steel	1	16
		5	28
		10	29
		20	35
Kerosene	Water	1	7.1
		5	22
		10	24
		20	35
	Steel	1	9.6
		5	22
		10	23
		20	36

4.3.4 1.6 m^2 (16 ft^2) Pan Fire Results

Based upon the results from the 0.093 m^2 (1 ft^2) and 0.372 m^2 (4 ft^2) fires, a different approach was taken during the execution of the 1.49 m^2 (16 ft^2) pan fire test series. A total of 27 tests were conducted with six different fuel depths. The results of the smaller pan fire test series demonstrated that the mass burning rates being achieved with a 1 mm (0.04 in.) fuel layer were approximately half of those expected during steady state burning. Furthermore, these tests demonstrated that the 5 mm (0.2 in.) fuel layer was sufficient to reach quasi-steady state mass burning rates for both fuels considered. Based upon these data, fuel depths of 1, 2, 3, 4, 5, and 18 mm (0.04, 0.08, 0.12, 0.16, 0.20, and 0.76 in.) were evaluated in order to better resolve the minimum fuel depth at which steady state burning can be achieved. These tests were conducted using both gasoline and denatured alcohol. The gasoline was tested atop both water and steel substrates while the denatured alcohol was only tested atop steel due to the miscibility of the fuel with water. It should be noted that kerosene was initially considered at this pan size, but due to the inability of the fuel to spread flame over the large area pool, denatured alcohol was used as a more volatile fuel. Although gasoline was tested on both substrates, only two different depths (i.e., 1 and 5 mm) were evaluated on the steel substrate. Only the 1 and 5 mm depths were tested on steel because this data set alone provided sufficient insight into the differences that exist between the mass burning rates of a 1 mm gasoline fire on the two substrates as well as demonstrating the negligible impact of the substrate at depths of 5 mm or greater. The denatured alcohol tests were not only used as verification tests in identifying the minimum fuel depth at which steady state burning can be achieved, but they also demonstrated the applicability of this concept to non-hydrocarbon based fuels. A summary of the HRR per unit area (HRRPUA) for the gasoline and denatured alcohol 1.49 m^2 (16 ft^2) pan fires conducted atop water and steel are

provided in Figure 4.8 and Figure 4.9, respectively. Furthermore, a comparison of the gasoline data from testing conducted atop the steel and water substrates is provided in Figure 4.10.

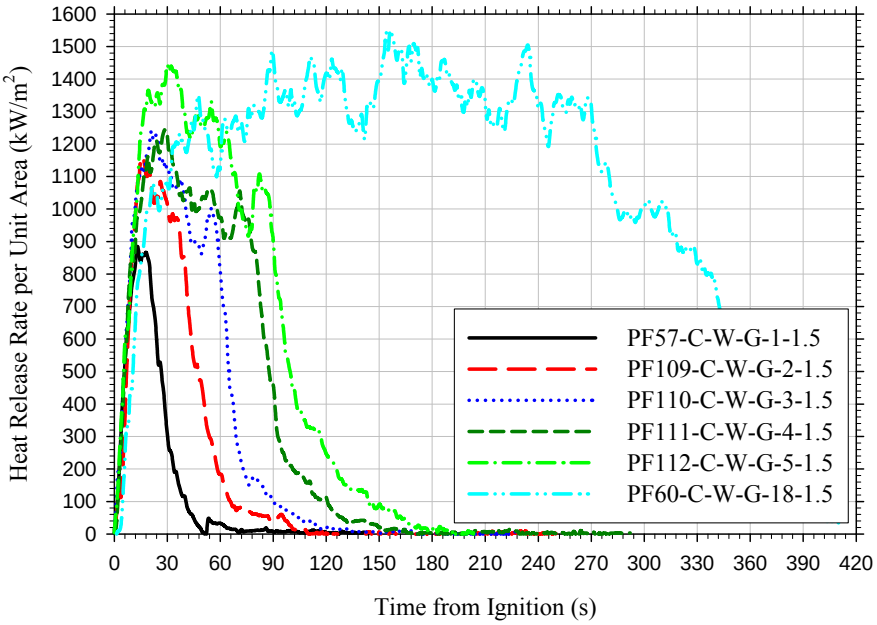

Figure 4.8. Summary of HRRPUA data measured for gasoline on water in the 1.49 m^2 (16 ft^2) pan fire tests with fuel depths of 1, 2, 3, 4, 5 and 18 mm

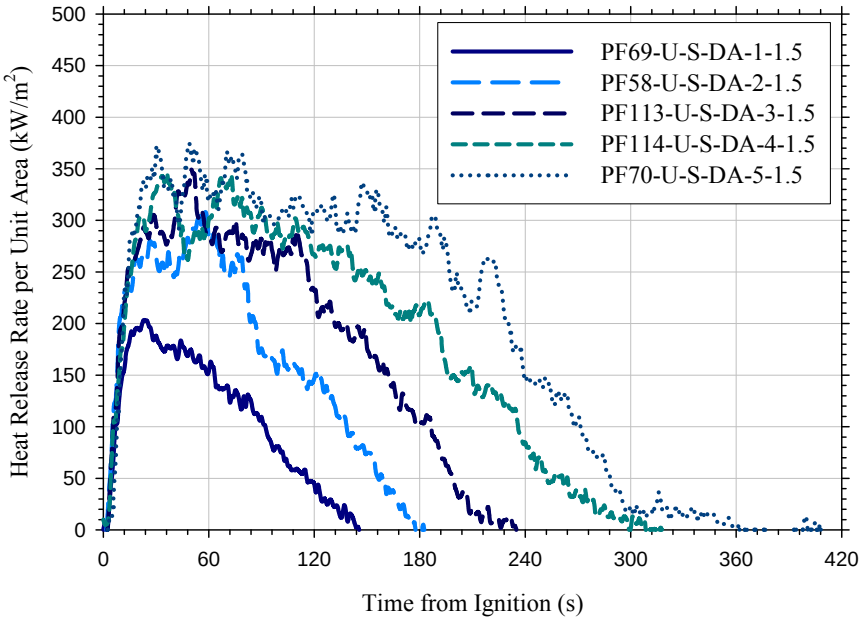

Figure 4.9. Summary of average HRRPUA data measured for denatured alcohol on steel in the 1.49 m^2 (16 ft^2) pan fire tests with fuel depths of 1, 2, 3, 4, and 5 mm

As reported for all smaller pan sizes, the rate of growth (i.e., the initial HRRPUA slope) of the pool fires for all fuel depths was equivalent for the data shown in Figure 4.8 and Figure 4.9. After this initial growth phase, the HRRPU curves peak at different values dependent on the fuel depth and then decay as the fire burns out. It is not until a fuel depth of approximately 4 to 5 mm is reached that a peak heat release rate value comparable to that observed in the 18 mm case is achieved. This is true for both fuels evaluated. Table 4.8 presents the peak ten second average mass burning rates for the 1.49 m^2 (16 ft^2) pan fire tests.

Table 4.8. Summary of Peak 10-second Average Mass Burning Rates for 1.49 m^2 (16 ft^2) Pan Fires

Fuel Type	**Substrate**	**Fuel Depth (mm)**	**Peak 10 s-Average Mass Burning Rate (g/s-m^2)**
Gasoline	Steel	1	20
		5	41
	Water	1	27
		2	36
		3	38
		4	39
		5	42
		18	47
Denatured Alcohol	Steel	1	10
		2	15
		3	18
		4	18
		5	19

As shown in Table 4.8, the peak heat release rates measured for the 4 and 5 mm gasoline and denatured alcohol spill depths were approximately a factor of 2 larger than that measured for the 1 mm depth. Based upon the data shown in Figure 4.8 and Figure 4.9, once a fuel depth greater than approximately 4–5 mm is reached, the addition of fuel (i.e., increasing fuel depth) simply prolongs the duration of steady-state burning without increasing peak fire size.

The comparisons provided in Figure 4.10 demonstrate the impact of the substrate on the mass burning rate of a fuel at relatively thin depths and the negligible effect of the substrate at deeper depths. As can be seen in the figure, at a 1 mm depth (blue lines), the gasoline reaches a higher peak HRRPUA when burning atop the water substrate compared to the steel (solid v dashed, respectively). This agrees with the data collected in the smaller pan fire test series. Also in agreement with the smaller pan fire test data is the fact that at a depth of 5 mm (red lines), the impact of the substrate is negligible in that there is relatively no difference between the HRRPUA data from the fires on steel and water.

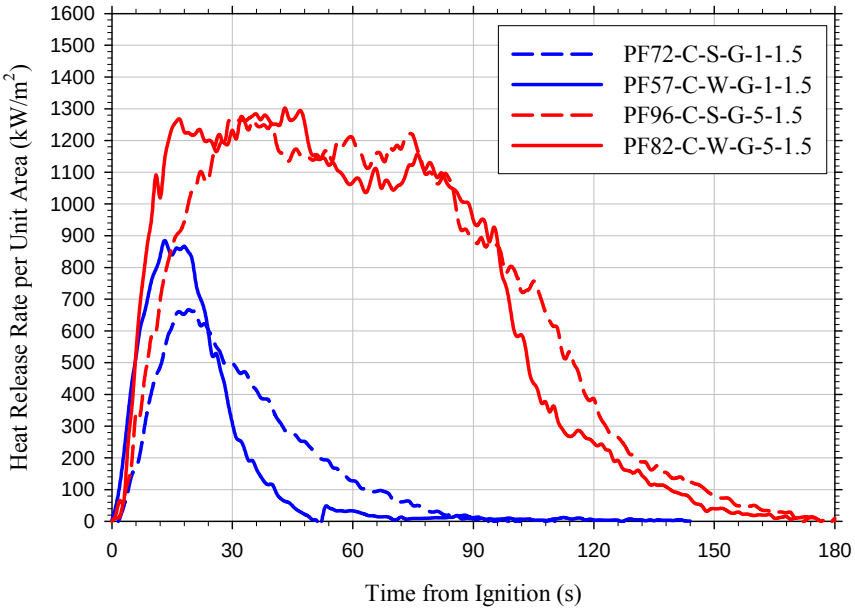

Figure 4.10. Comparison of HRRPUA for 1.49 m^2 (16 ft^2) gasoline pan fires on steel and water substrates for fuel depths of 1 and 5 mm

Figure 4.10 also demonstrates the potential effect of the substrate on the initial growth rate of these fires. For both 1 and 5 mm fuel depths, the fuel burning on steel grew at a slightly slower rate than that occurring on the water. It is likely that this is due to the more conductive nature of the steel removing heat from the fuel layer, thus reducing the rate at which the fuel is heated and vaporized.

4.4 Diked Fires

4.4.1 Procedures

Prior to testing, the edges and instrumentation seams of each diked assembly were sealed using a high temperature sealant (Permatex Ultra Black RTV Silicone Gasket Maker) to prevent fuel leakage. Once instrumented, the fuel pan was leveled to within 3.2 mm (0.125 in.) over a distance of 1.2 m (4 ft). The load cell was then zeroed and the initial mass and volume of the fuel as well as ambient conditions were recorded. The data acquisition system, cameras, and FLIR camera were initiated prior to the fuel being poured into the pan. Two minutes of background data were collected prior to each test. Once poured, the fuel was ignited using a propane torch. In the case of gasoline, the fuel was easily ignited at the edge of the pool. For kerosene pools in these diked scenarios, care was taken to only apply the torch to the fuel surface in order to not damage the substrate. In order to accomplish this, when needed, the torch was applied parallel to the fuel surface just above the surface of the fuel. Both the ignition time and the time to sustained ignition were recorded. The flame extinguishment time was also recorded at the end of each test as the time at which only localized areas of small flamelets were observed, typically occurring along the edges of the fuel pans. The data, cameras, and FLIR camera continued recording until the last flame extinguished.

Test transition for the concrete substrate consisted of cooling the diked assembly with ice and cold water until the subsurface TCs were all below 30°C (86°F). The remaining liquid in the pan was removed with a shop vacuum and the pan was dried before running the next test. The test setup was inspected in between tests for leaks and alignment of the fuel thermocouple tree.

The transition procedure between vinyl substrates consisted of the removal of the previous vinyl and plywood substrate and the installation of a pre-cut and glued sample. The virgin sample was then instrumented and sealed as previously described. The sealant was permitted to cure for a minimum of 1 hour prior to testing.

4.4.2 0.093 m^2 (1 ft^2) Diked Fire Results

A total of 16, 0.093 m^2 (1 ft^2) diked fire tests were conducted: 8 tests on a coated concrete substrate and 8 tests on a vinyl substrate. A summary of the peak mass burning rates obtained in these tests is provided in Table 4.9. Figure 4.10 presents the HRR per unit area for each of the tests.

Table 4.9. Summary of 0.093 m^2 (1 ft^2) Diked Fire Test Data and Influence of Substrate

Substrate	Area (m^2)	Fuel Depth (mm)	Peak 10 s Average Mass Burning Rate (g/s-m^2)		Influence of Substrate (% Difference b/n substrates)	
			Gas	Kerosene	Gas	Kerosene
Concrete	0.093	1	10	10	38	38
Vinyl			16	16		
Concrete		5	19	16	5	16
Vinyl			20	19		
Concrete		10	19	17	5	15
Vinyl			20	20		
Concrete		20	19	23	21	8
Vinyl			24	25		

The data presented in Table 4.9 indicates that the fuel substrate has the largest effect with a fuel depth of 1 mm (0.04 in.). At this fuel depth, tests conducted atop the vinyl substrate were 38 percent larger for both fuels evaluated. The influence of the substrate was not as significant for each of the three greater fuel depths evaluated. For these depths, the differences between the burning rates on each substrate ranged from 5–21 percent. Although in some cases only by a very small margin, the mass burning rates measured on the vinyl substrate were consistently greater than those measured on the coated concrete surface. This could be due to the lower thermal conductivity of the vinyl material compared to the concrete substrate, thus keeping a larger fraction of the heat at the fuel surface.

The HRRPUA data for each of the 0.093 m^2 (1 ft^2) diked fire tests are presented in Figure 4.11 below. In general, for a given fuel and substrate pair, the steady-state values achieved were comparable for fuel depths greater than 1 mm. The only exceptions were the 20 mm fuel depths conducted atop vinyl (Plots b & d), in which an increase in HRRPUA was observed at the end of the test. This increase is most likely a result of the involvement of the substrate material as well

as the rapid boiling of the residual kerosene remaining atop the substrate. Both of these phenomena would result in an increased heat release rate over the same burning area.

4.4.3 0.37 m^2 (4 ft^2) Diked Fire Results

A total of 16, 0.37 m^2 (4 ft^2) diked fire tests were conducted: 8 tests on a coated concrete substrate and 8 tests on a vinyl substrate. A summary of the peak mass burning rates obtained in these tests is provided in Table 4.10. Figure 4.11 presents the HRR per unit area for each of the tests.

Table 4.10. Summary of 0.37 m^2 (4 ft^2) Diked Fire Test Data and Influence of Substrate

Substrate	Area (m^2)	Fuel Depth (mm)	Peak 10 s Average Mass Burning Rate (g/s-m^2)		Influence of Substrate (% Difference b/n substrates)	
			Gas	Kerosene	Gas	Kerosene
Concrete	0.372	1	13	10	46	47
Vinyl			24	19		
Concrete		5	28	23	10	0
Vinyl			31	23		
Concrete		10	28	25	15	29
Vinyl			33	35		
Concrete		20	33	28	13	26
Vinyl			38	38		

Similar to the 0.093 m^2 (1 ft^2) diked fires, the fuel substrate has the largest effect on the 0.37 m^2 (4 ft^2) diked fires with a fuel depth of 1 mm (0.04 in.). For this fuel depth, the differences in burning rates between the concrete and vinyl substrates were nearly 50 percent. At thicker depths, the differences ranged from 0 up to 29 percent. In general, the percent difference between substrates calculated for the 5, 10, and 20 mm fuel depths were comparable to those calculated in the smaller fire scenarios. For this diked fire size (i.e., 0.37 m^2 [4 ft^2]), a steadily increasing HRRPUA was observed for fires on the vinyl substrate for both fuels at depths of 10 and 20 mm. This steadily increasing trend did not start until after 100–120 seconds of burning and continued for the duration of the fire. It should be noted that these trends are different than the phenomena observed at the end of the 20 mm kerosene fire shown in Figure 4.11 (d) where the increase occurred at the end of the test.

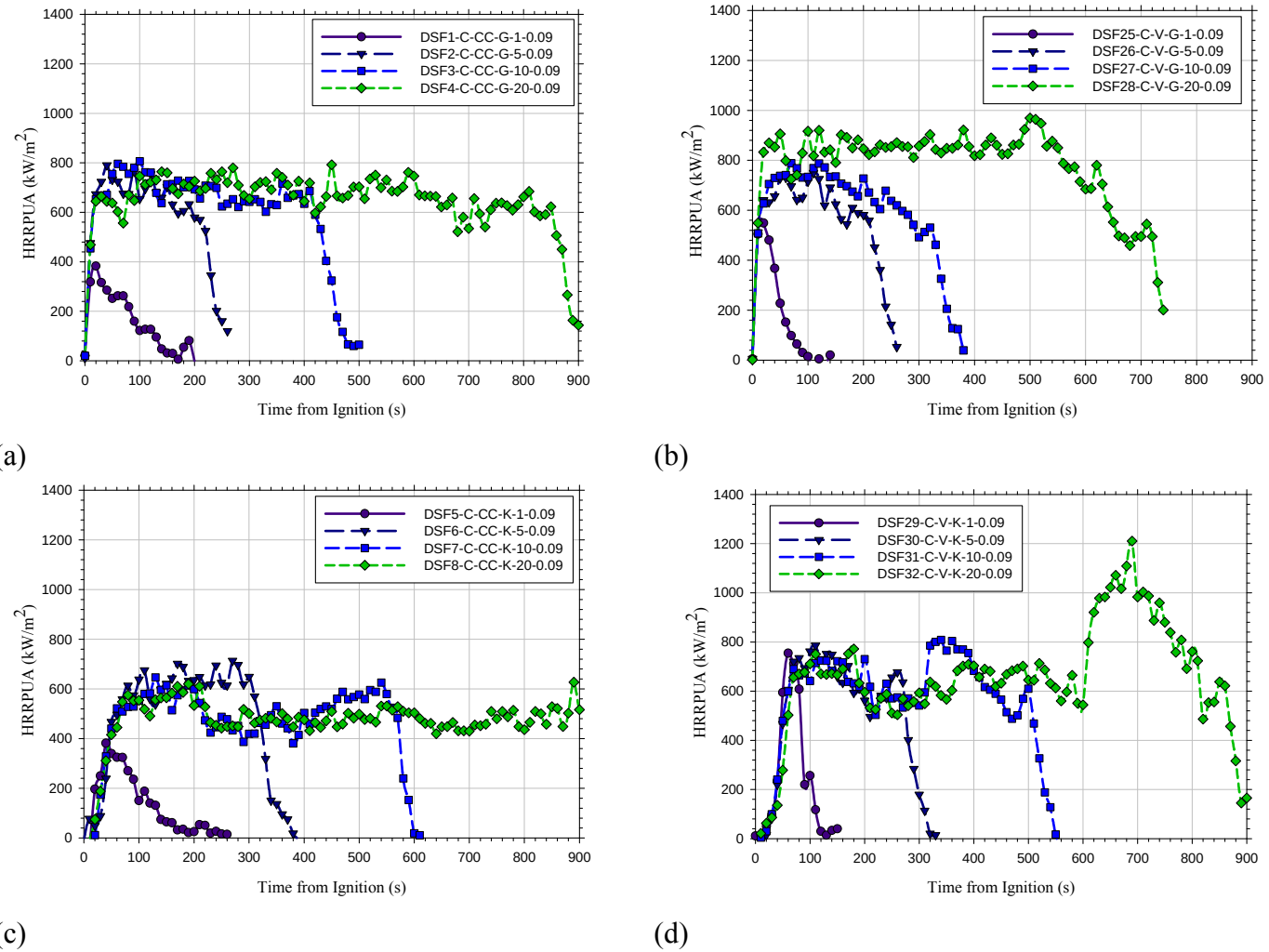

Figure 4.11. 0.093 m^2 (1 ft^2) diked fire HRRPUA measured for varying fuel depths (1, 5, 10 and 20 mm) for (a) gasoline on coated concrete, (b) gasoline on vinyl, (c) kerosene on coated concrete, and (d) kerosene on vinyl.

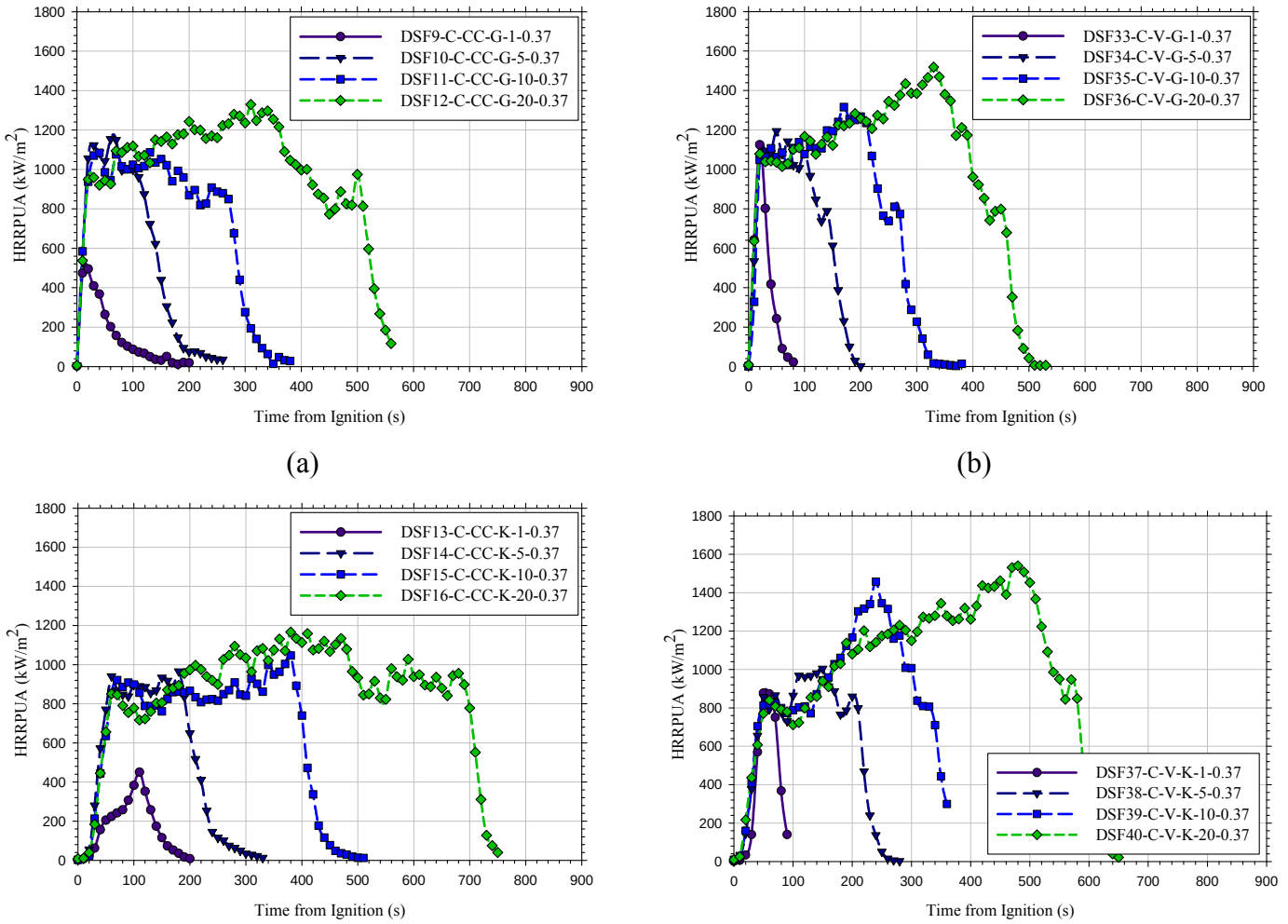

Figure 4.12. 0.37 m^2 (4 ft^2) diked fire HRRPUA measured for varying fuel depths (1, 5, 10 and 20 mm) for (a) gasoline on coated concrete, (b) gasoline on vinyl, (c) kerosene on coated concrete, and (d) kerosene on vinyl

4.4.4 1.49 m^2 (16 ft^2) Diked Fire Results

As described in the 1.49 m^2 (16 ft^2) Pan Fire section, the fuel depths evaluated in the 1.49 m^2 (16 ft^2) diked fire tests were different than those considered in the 0.093 m^2 (1 ft^2) and 0.372 m^2 (4 ft^2) diked fire test series. For the 1.49 m^2 (16 ft^2) diked fires on coated concrete and vinyl, spill depths of 1, 2, 3, 4, 5, and 20 mm (0.04, 0.08, 0.12, 0.16, 0.20, and 0.80 in.) were evaluated. In this test series, only gasoline was used due to the inability of igniting and involving kerosene pools at this size. Again with the intent of identifying the minimum fuel depth needed to achieve steady state mass burning rates on various substrates. As a result, a total of twelve 1.49 m^2 (16 ft^2) diked fire tests were conducted. A summary of the mass burning rate data collected in these tests is provided in Table 4.11. The most substantial differences in peak mass burning rates measured for each substrate was observed for a gasoline depth of 1 and 2 mm with all other differences being less than 10 percent.

Table 4.11. Summary of 1.49 m^2 (16 ft^2) Diked Fire Test Data and Influence of Substrate

Substrate	Area (m^2)	Fuel Depth (mm)	Peak 10 s Average Mass Burning Rate (g/s-m^2)	Influence of Substrate (% Difference b/n substrates)
Concrete	1.49	1	16	11
Vinyl		1	18	
Concrete		2	22	27
Vinyl		2	30	
Concrete		3	29	6
Vinyl		3	31	
Concrete		4	31	3
Vinyl		4	32	
Concrete		5	34	8
Vinyl		5	37	
Concrete		20	40	5
Vinyl		15	42	

A comparison of the HRRPUA data from the various gasoline fuel depths on both a coated concrete and vinyl substrate are presented in Figure 4.13. The general trends with respect to HRRPUA were similar for both substrates in that as fuel depth increased so did the peak HRRPUA. The only difference, as mentioned above, was that the peak values achieved on the coated concrete substrate were consistently lower than those obtained on the vinyl. The differences were relatively minimal at depths of 3 mm or greater but for the 1 and 2 mm depths the differences ranged from 11–27 percent.

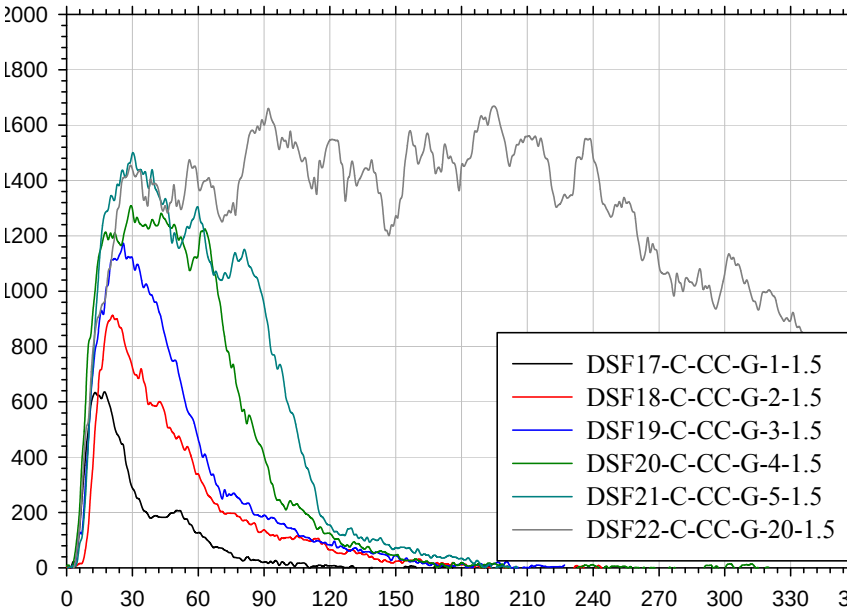

(a)

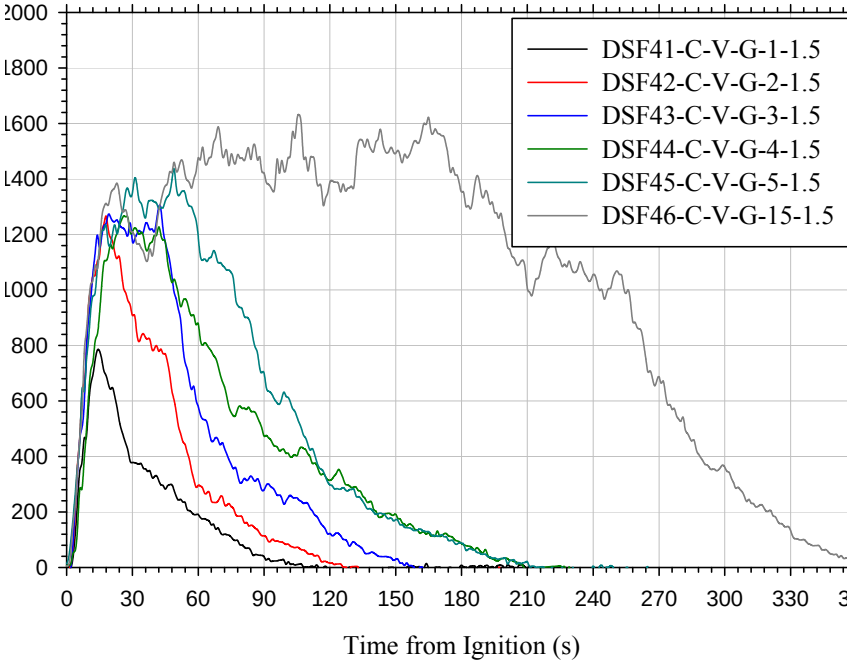

(b)

Figure 4.13. 1.49 m^2 (16 ft^2) diked fire HRRPUA for varying fuel depths for (a) gasoline on coated concrete, (b) gasoline on vinyl

4.5 Spill Dynamics

4.5.1 Test Procedures

Prior to each spill dynamics test, the substrate being evaluated was centered beneath the spill arm. In the case of the vinyl, plywood, and OSB, the substrate was attached to a wood stud frame flooring system with studs spaced 0.41 m (16 in.) on center. This was done to prevent warping of the specimen, which could affect the spill progression. The substrate was leveled to within 3.2 mm (0.125 in.) over a distance of 1.2 m (4 ft).

Prior to filling the spill arm, the volume and mass of the liquid being used were recorded. The spill arm apparatus was then centered 0.3 m (1 ft) above the substrate at which point in time the video image collection was started. After approximately 30-seconds of background video collection, the valve on the spill arm was opened remotely. The contents were allowed to drain for 10-seconds, sufficient for the total amount of liquid to be spilled. The spill arm was then swung out of the field of view of the camera. The spills were allowed to spread for 5 minutes from the time of valve opening. Still photographs were used to capture spill progression at various instances in time. Photographs were also used to capture the height of the spill front moving across each substrate. Spill durations ranged from 5–30 minutes depending upon the quantity of liquid spilled. Larger spill volumes were permitted to progress for extended periods of time such that the maximum spill area could be achieved.

All liquid spills were removed from the substrate surfaces using a shop vacuum and the surfaces of the specimen were allowed to dry. The drying of the porous concrete substrates (i.e., brushed, NIJ smooth, and ATF smooth pads) was expedited using forced air convection provided by fans blowing over the top of these surfaces. Cellulosic substrates such as plywood and OSB were flipped over and their other side was used for the next test before being discarded. Impermeable substrates such as vinyl and coated concrete were wiped dry with towels before repeat testing was conducted. In the case of carpet, the spill and absorption patterns on the different layers were photographed and the specimens were not re-used.

The lube oil was removed using a chemical absorption agent called Chem-Oil Away. This absorbed the oil from the surface and helped to remove some oil if it absorbed into the substrate. The oil impregnated agent was then swept off of the specimen. Then, in the case of brushed and smooth concrete, the pads were hosed down to remove any remaining absorption agent and dried using the above mentioned method.

4.5.2 Results

A total of 86 spill dynamics tests were conducted on eight different substrates using three different fuel simulants. Spill growth rates and maximum spread areas were measured using image analysis of video collected from each test. A complete description of the image analysis procedure used to calculate spread areas is provided in Appendix C. All spill dynamics tests were conducted in triplicate and repeatability between tests was generally good. The coefficients of variance for these tests ranged from 0.01–0.23 with the majority of scenarios having a CoV of less than or equal to 0.1. Larger variances were calculated for spills conducted on the vinyl, brushed concrete, and OSB substrates. A summary of the spill dynamics testing results on

impermeable, permeable, and carpet substrates are provided in Tables 4.12, 4.13 and 4.14, respectively.

Table 4.12. Summary of Averaged Spill Dynamics Data Collected for Impermeable Substrates (Coated Concrete and Vinyl)

Test ID	Liquid	Substrate	Spill Volume (L)	Surface Tension (mN/m)	Average Spill Area (m^2)	Average Perimeter (m)	Average Spill Depth (mm)	Average A/V (m^2/L)
SD28	3% AFFF	Coated Concrete	0.5	17.19	1.47	8.89	0.34	2.93
SD29								
SD30								
SD31	3% FP			27.03	0.57	4.98	0.88	1.13
SD32								
SD33								
SD34	Lube Oil			29.24	0.22	2.55	2.30	0.43
SD35								
SD36								
SD04	3% FP	Vinyl	0.25	27.03	0.35	4.66	0.71	1.40
SD05								
SD06								
SD01B	3% AFFF		0.1	17.19	0.42	3.47	0.25	4.08
SD02								
SD03								
SD7	Lube Oil		0.5	29.24	0.35	2.32	1.42	0.70
SD8								
SD9								
SD61	3% AFFF			17.19	1.71	9.38	0.30	3.36
SD62								
SD63								

Table 4.13. Summary of Averaged Spill Dynamics Data Collected For Permeable Substrates (Smooth Concrete, Brushed Concrete, Plywood, and OSB)

Test ID	Liquid	Substrate	Spill Volume (L)	Surface Tension (mN/m)	Average Area (m^2)	Average Perimeter (m)	Average Spill Depth (mm)	Average A/V (m^2/L)
SDA13	3% FP	Smooth Concrete (ATF)	0.5	27.03	1.26	4.87	0.40	2.51
SDA21								
SDA17								
SDA1	3% AFFF			17.19	1.90	6.66	0.26	3.79
SDA5								
SDA9								
SDA14	3% FP		5	27.03	7.82	19.77	0.64	1.55
SDA18								
SDA22								
SDA2	3% AFFF			17.19	12.03	22.33	0.42	2.40
SDA6								
SDA10								
SDA16	3% FP		20	27.03	24.63	33.73	0.81	1.23
SDA20								
SDA24								
SDA4	3% AFFF			17.19	30.00	34.83	0.67	1.50
SDA8								
SDA12								
SD37	3% AFFF	Smooth Concrete (NIJ)	0.5	17.19	1.19	5.80	0.42	2.36
SD38								
SD39								
SD40	3% FP			27.03	0.92	5.85	0.54	1.84
SD41								
SD42								
SD43	Lube Oil			29.24	0.57	3.75	0.88	1.13
SD44								
SD45								
SD46	3% AFFF	Brushed Concrete	0.5	17.19	0.95	4.02	0.53	1.90
SD47								
SD48								
SD49	3% FP			27.03	0.45	3.19	1.15	0.87
SD50								
SD51								
SD52	Lube Oil			29.24	0.30	2.73	1.69	0.59
SD53								
SD54								

Table 4.13. Summary of Averaged Spill Dynamics Data Collected For Permeable Substrates (Smooth Concrete, Brushed Concrete, Plywood, and OSB) (Continued)

Test ID	Liquid	Substrate	Spill Volume (L)	Surface Tension (mN/m)	Average Area (m^2)	Average Perimeter (m)	Average Spill Depth (mm)	Average A/V (m^2/L)
SD57	3% AFFF	Plywood	0.25	17.19	0.60	3.73	0.42	2.38
SD55A								
SD56A								
SD22	3% FP		0.5	27.03	0.34	4.19	1.50	0.67
SD23								
SD24								
SD25	Lube Oil			29.24	0.39	2.43	1.30	0.77
SD26								
SD27								
SD55A	3% AFFF	OSB	0.35	17.19	0.54	3.36	0.66	1.52
SD57								
4678								
SD58	3% FP		0.5	27.03	0.24	4.03	2.09	0.48
SD59								
SD60								

Table 4.14. Summary of Averaged Spill Dynamics Data Collected for Carpet Substrates

Test ID	Liquid	Substrate	Spill Volume (L)	Surface Tension (mN/m)	Average Area (m^2)	Average Perimeter (m)	Average Spill Depth (mm)	Average A/V (m^2/L)
SD10	3% AFFF	Carpet	0.5	17.19	0.10	1.45	5.27	0.19
SD11								
SD12								
SD13	3% FP			27.03	0.08	1.34	6.70	0.15
SD14								
SD15								

The test results provided above were divided into three categories based upon surface type in order to assess the impacts of this parameter. Surfaces are divided into categories of permeable, impermeable, and carpet. Permeable surfaces include cellulosic materials such as oriented strand board (OSB) and plywood, in addition to brushed and smooth concretes. Impermeable surfaces include ones where absorption should be non-existent such as vinyl and coated concrete. Carpet is separate due to the large amount of absorption and the different surface structure.

Figure 4.14, Figure 4.15, and Figure 4.16 show typical spill fronts for 3% AFFF, 3% FP, and lube oil, respectively. Each group of pictures has one spill on a concrete substrate, one spill on a wood substrate, and one spill on vinyl. Rulers are shown for reference purposes only and are not intended, nor were used to measure spill depth.

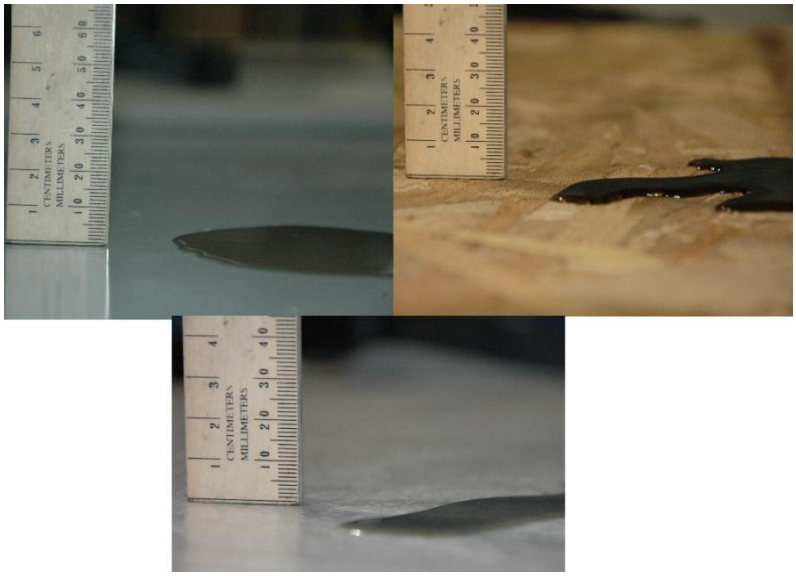

Figure 4.14. Typical spill fronts for 3% AFFF spilled on coated concrete (top left), OSB (top right), and vinyl (bottom) substrates

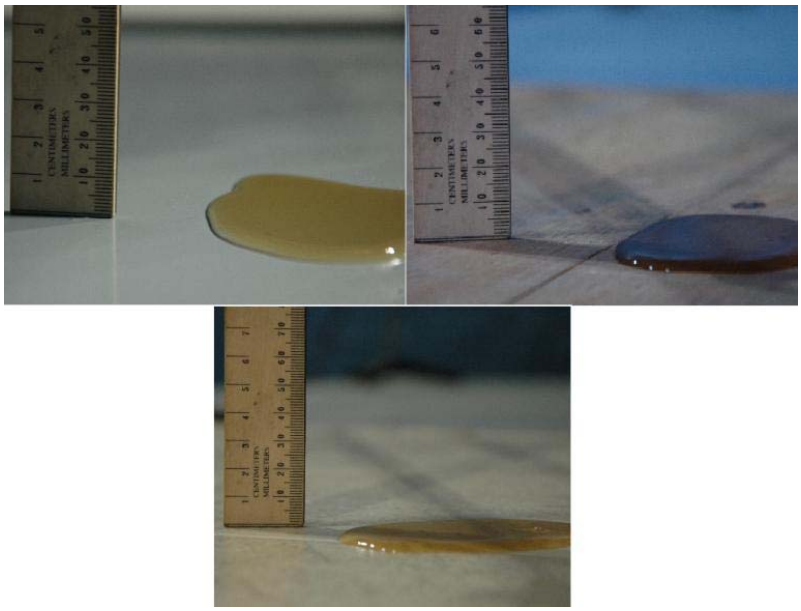

Figure 4.15. Typical spill fronts for 3% FP spilled on coated concrete (top left), plywood (top right), and vinyl (bottom) substrates

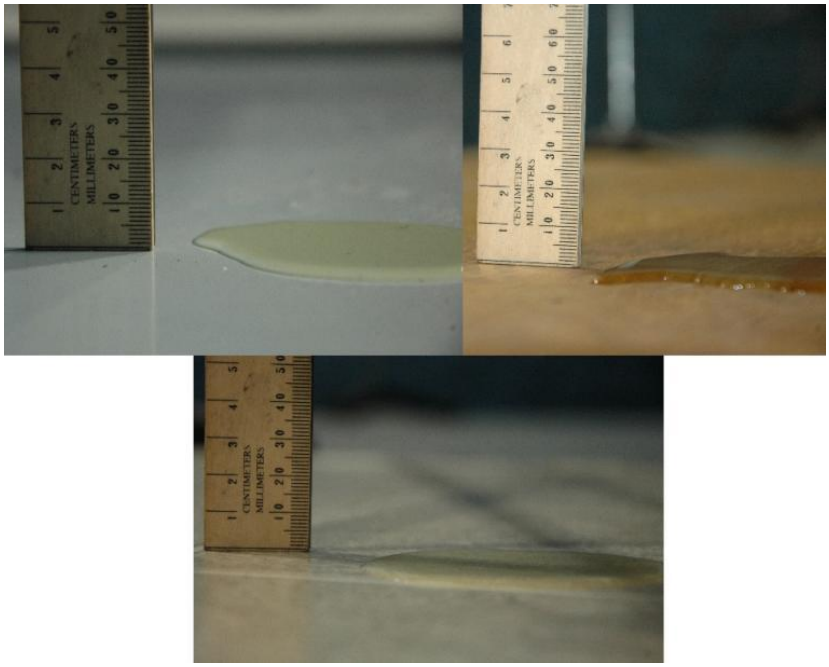

Figure 4.16. Typical spill fronts for lube oil spilled on coated concrete (top left), plywood (top right), and vinyl (bottom) substrates

Initially, some tests were conducted for longer than the 300-second spread time used for the majority of testing. This was done in order to examine whether at 300 seconds, the spill was at or near equilibrium. In general, after 300 seconds, most spills reached approximately 90% or more of their maximum spill area. Thus, it was determined that the 300-second spread time was suitable to allow the spills to reach a quasi-equilibrium spill area as well as allow for multiple tests to be run in an efficient and consistent manner.

The growth in spill area as a function of time was measured for all spills at 30-second intervals. A series of six plots, provided below in Figure 4.17, were constructed from this data to show generalized growth curves for spills of various liquids on various substrates. In these plots, the spill area measured at each time interval was normalized with respect to the maximum spill area observed for that scenario. This normalized value was then plotted against time with t_0 being the point at which the liquid was spilled. In general, the spilled liquids exhibited similar growth trends with an initial period of rapid growth (t_{0s}–t_{30s}) followed by an extended period (t_{30s}–t_{300s}) of substantially slower growth trending towards a quasi-steady-state. This observed behavior is consistent with the physical regimes governing the motion and equilibrium of state of a fluid. As described by Putorti [2001], there are three regimes which govern the development of a liquid spill; gravity-inertia, gravity-viscous, and viscous-surface tension. The rapid spreading of the liquid immediately after being spilled (i.e., t_{0s}–t_{30s}) is a result of the forces described in the first two regimes, while the gradual growth observed later in the spill can be attributed to the third regime. Trends for specific scenarios differed in that the fraction of the spill area reached in the initial 30-seconds was less on some surfaces or with certain liquids.

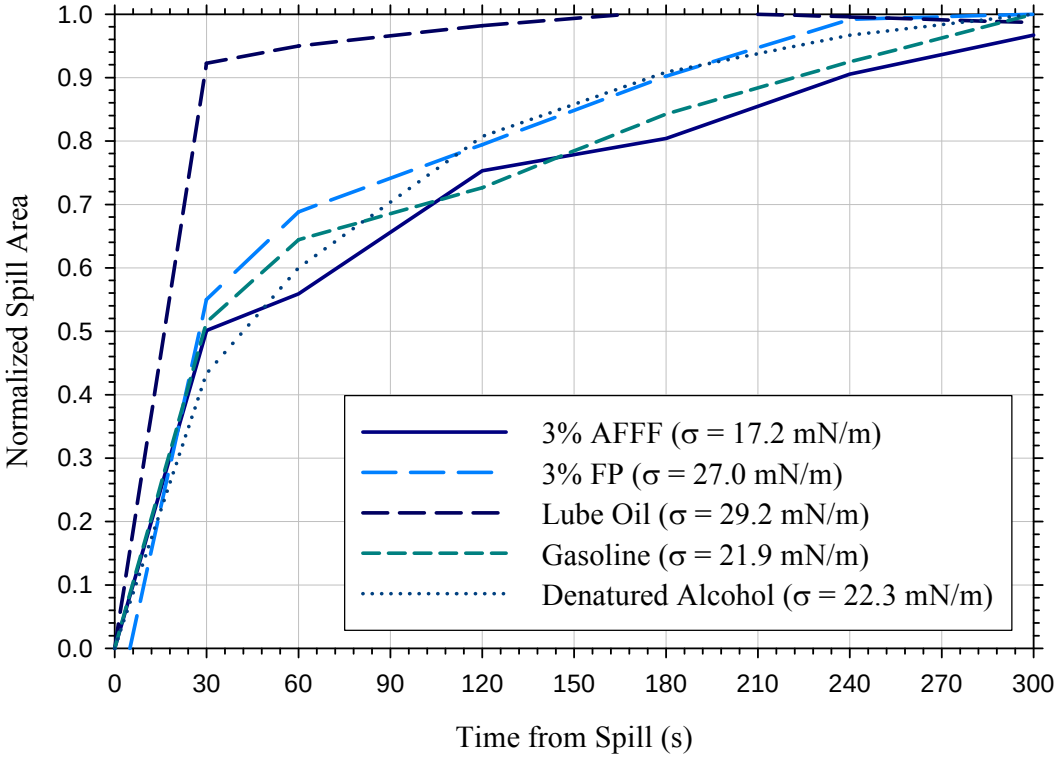

(a) – Various Liquid Spread Rates on Coated Concrete

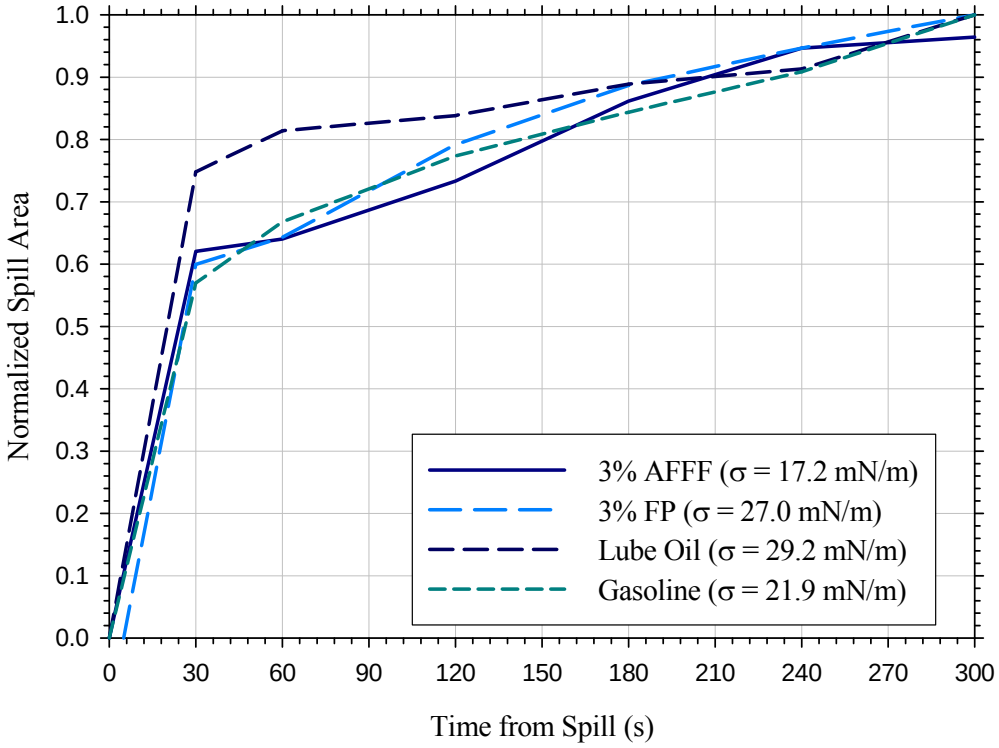

(b) – Various Liquid Spread Rates on Smooth Concrete

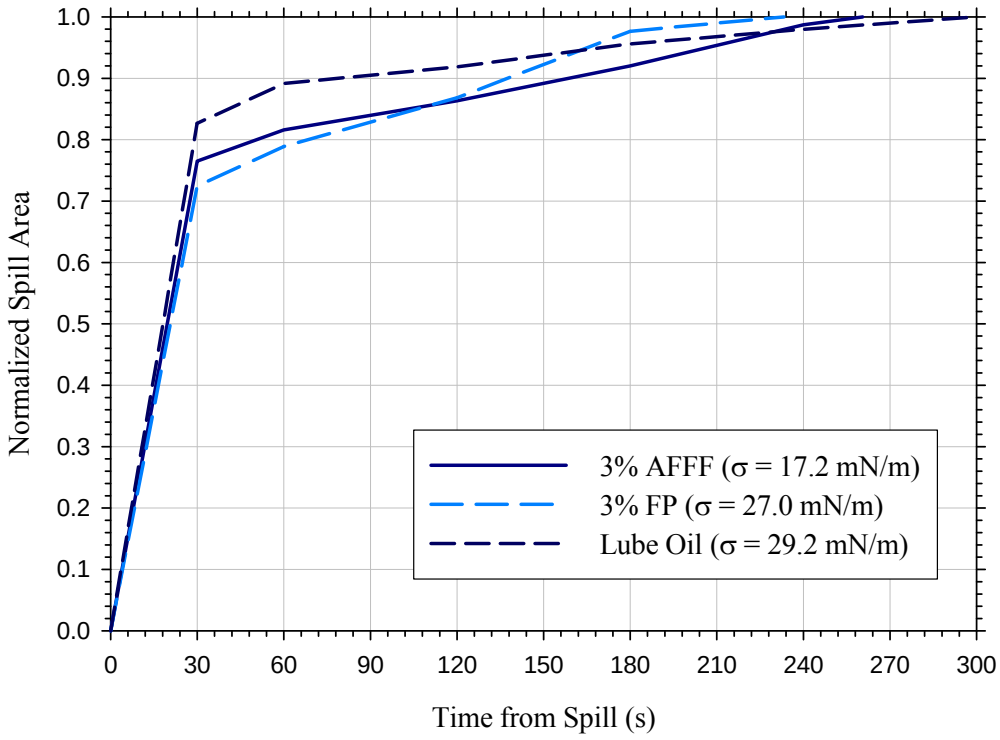

(c) – Various Liquid Spread Rates on Brushed Concrete

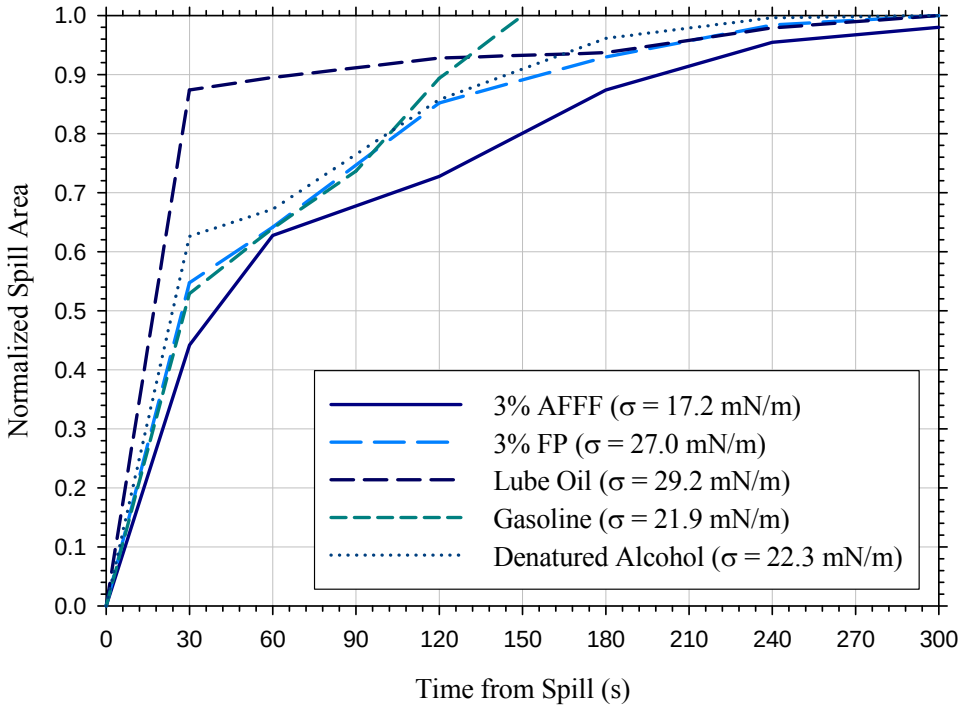

(d) – Various Liquid Spread Rates on Vinyl

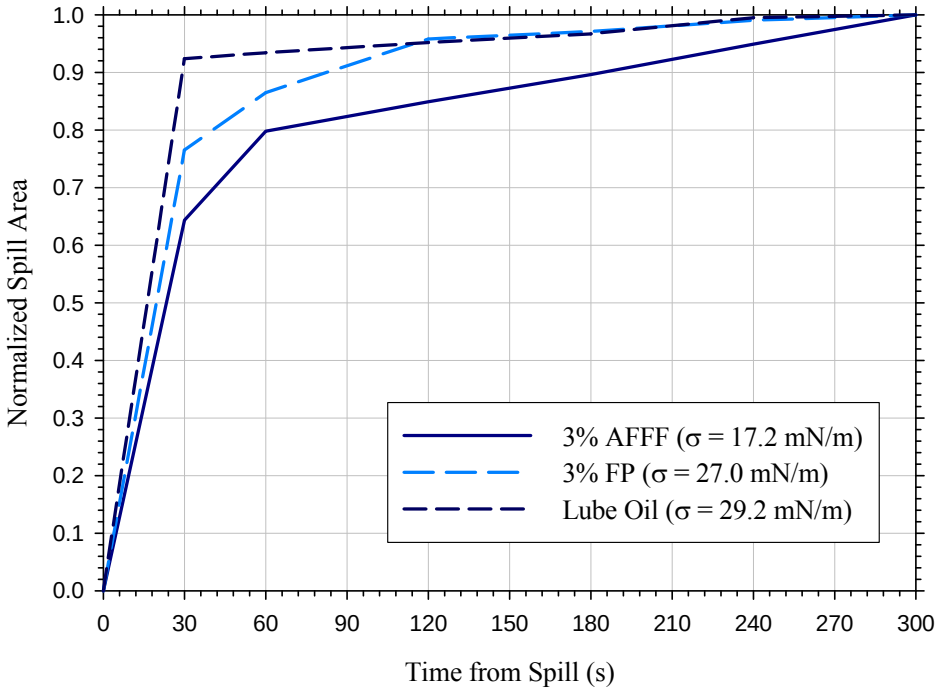

(e) – Various Liquid Spread Rates on Plywood

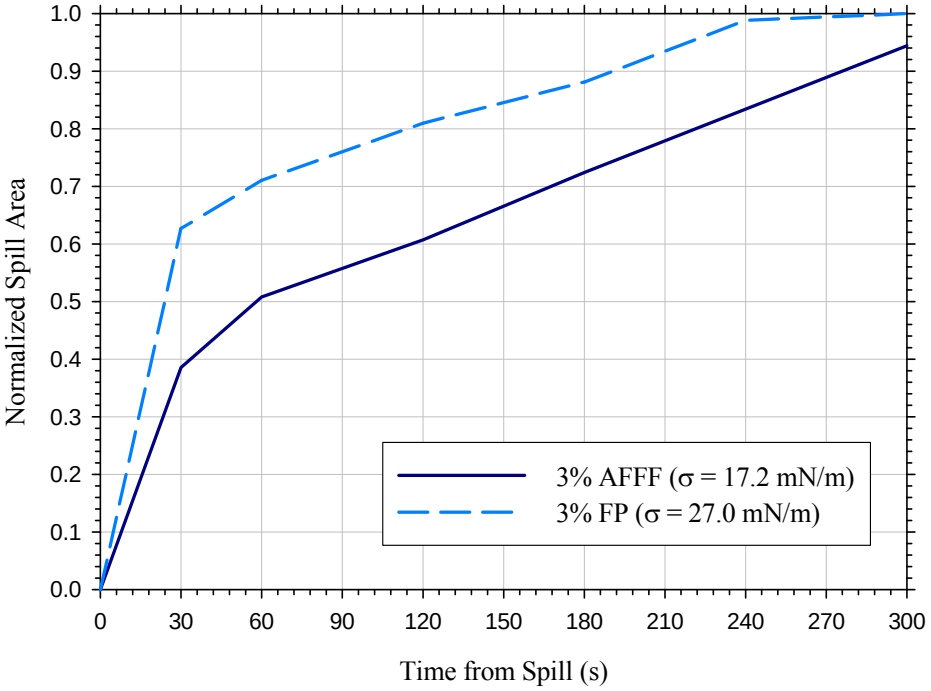

(f) – Various Liquid Spread Rates on Oriented Strand Board (OSB)

Figure 4.17. Normalized spill area as a function of time for various liquids on each substrate

For liquids other than lube oil spilled on smooth, impermeable surfaces (i.e., coated concrete and vinyl); approximately 50–60 percent of the total spill area was achieved in the initial 30-seconds. The remaining spill area was gradually obtained over the next 270 seconds. Similar trends were observed for the smooth concrete substrate although the initial spill area fraction was slightly higher (e.g., 60–65 percent of total area).

On coated concrete, vinyl, and smooth concrete, the lube oil exhibited a slightly different trend then the other liquids, reaching 75–90 percent of the total spill area in the initial 30-seconds. This larger fraction is attributed to the high viscosity of the liquid relative to all other liquids. The high viscosity of the lube oil inhibits the spread of the liquid beyond the initial spill area. The majority of the area covered by the lube oil can be attributed to gravity-inertia forces (i.e., the momentum of the liquid impacting the substrate) and gravity-viscous forces with very little spread occurring due to viscous-surface tension forces. The dichotomy between the lube oil and other liquids was less pronounced with spills occurring on rough/porous substrates (i.e., brushed concrete/plywood). In these cases, all liquids had spill area fractions greater than 65 percent during the initial 30-seconds. This data suggests that the roughness/absorptivity of the surface impeded the progression of the spill beyond the initial area caused by gravity-inertia and gravity-viscous forces.

The trends provided in Figure 4.17 (a)–(f) illustrate the impact that both liquid and substrate characteristics can have on the development of a spill over time. For liquids, other than lube oil, spills on smooth, impervious substrates generally result in an initial period of rapid growth occurring as a result of (gravity-inertia/gravity-viscous forces) followed by a gradual increase in area governed by viscous-surface tension forces. In these scenarios, the momentum of the spilled liquid impacting the substrate causes the liquid to spread rapidly resulting in a quick transition through the first two governing regimes with the majority of the spill duration being dominated by the viscous-surface tension forces.

Spills on rough/absorbent surfaces or spills involving fluids with high viscosities, generally achieve a large fraction of their spill area potential soon after being spilled. The lack of fluid spread after the initial spill can be attributed to several different factors including; the physical characteristics of the substrate impeding the movement of the fluid, the absorbency of the substrate removing liquid from the bulk flow of fluid thus reducing the spill area potential, or the internal forces within the liquid (i.e., viscosity) inhibiting the spread of the spilled volume.

4.5.2.1 Impermeable Surface Results

Out of the 78 spill dynamics tests, 21 were conducted on impermeable surfaces. Table 4.12 shows that for both fuel surrogates on all impermeable surfaces, the spill depths were all less than 1 mm. These values are in agreement with the limited data in the literature values (Section 1.1.3.1). Some variation in spill depth was expected based on the differences in the liquid properties as well as the differences in the liquid-substrate interfacial properties. The data did reveal differences relative to these parameters. Figure 4.18 shows the spill depth versus surface tension for various volume liquid spills on impermeable and permeable substrates.

4.5.2.2 Permeable Surface Results

Fifty one out of 78 spill dynamics tests were conducted on permeable substrates including OSB, plywood, smooth concrete (NIJ and ATF), and brushed concrete. The 18 tests conducted on the large ATF concrete pad were aimed to address the impact of spill volume on spill depth by allowing larger spills than possible on the other substrate pads. One thing to note is that the spill depth calculated was determined by dividing the volume spilled by the visibly wetted area of the substrate. For impermeable surfaces, this technique calculates the fuel depth above the substrate, but for permeable surfaces, it calculates a nominal depth that is a combination of the fuel depth above the substrate as well as a depth of fuel absorbed into the substrate.

A general trend can be seen in Figure 4.18 that for increasing surface tension, spill depth increases for all substrates except plywood. The decreasing trend seen for 0.5 L spills on plywood is not significant because of statistical overlap with error bars of one standard deviation. There is no statistical overlap using error bars of one standard deviation for the average spill depth on all other substrates. The direct relationship between spill depth and surface tension results agrees with the theories presented in the literature. Given the significant spread in the permeable and impermeable spill depth results, it is difficult to make any comparison between the two types of surfaces.

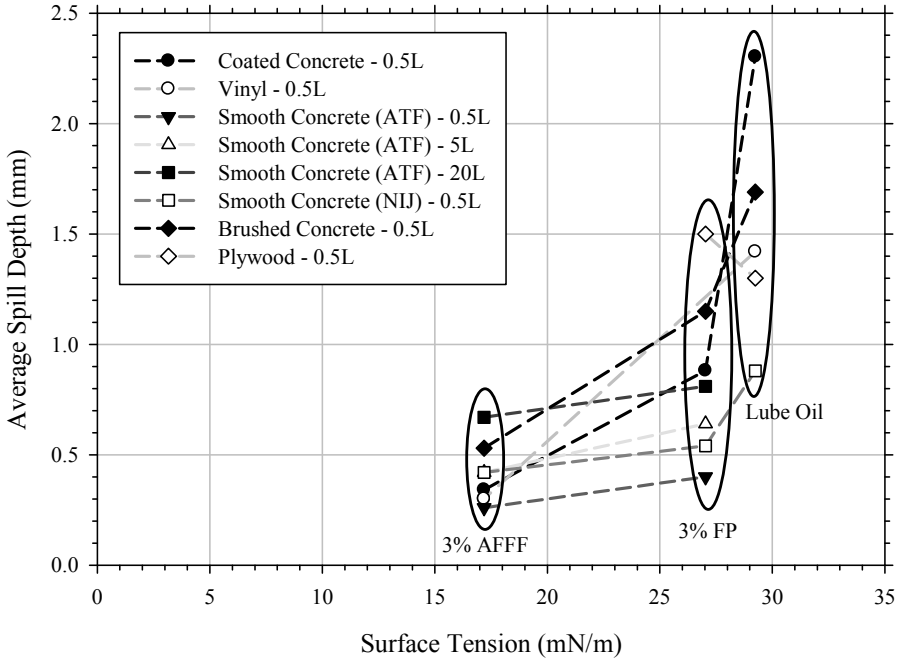

Figure 4.18. Average spill depth vs. surface tension for various volume liquid spills on impermeable and permeable substrates

The subset of 18 tests of different volumes of 3% FP and 3% AFFF solutions spilled on smooth concrete (ATF) shows that for increasing volume, spill depth increases. This is contrary to theories presented in the literature. The larger 20 L spills have a depth almost twice that of the 0.5 L spills on this concrete floor. However, this trend does not necessarily prove that there is in fact a direct relationship between increases in spill depth and increasing volume spilled. The only other test series that had different volumes of the same liquid spilled on the same substrate was 3% AFFF on vinyl. However, the difference in spill depth between the two volumes was not significant relative to the standard deviation in the data. It is possible that the trend established for the smooth concrete (ATF) is a result of the topographical variations in the concrete pad. Pooling of the liquid spills in low spots of the concrete floor was observed during testing, making the spill depth not uniform. This could affect the perceived spill area producing a calculated spill depth that is not accurate for all sections of the spill. However, it is noted that the floor is quite typical of many facilities. The reality may be that theoretically there should be no impact on depth based on the volume of liquid spilled when the surface is ideally smooth and level, but in practice, such surfaces are not representative of actual floors. Therefore, greater depths are expected with larger volumes. In this testing, when comparing spill volumes of 0.5 and 20 L (0.13 and 5.3 gal.) spill depths were almost a factor of three larger for the larger spill volumes.

4.5.2.3 Carpet Results

It was observed during the duration of the carpet spill tests that all of the liquid was eventually absorbed into the carpet and padding materials. Due to the large amount of absorption of liquid into the carpet and padding, the spill depth reported is not representative of a surface spill, but is more closely linked to the absorbed liquid depth. It is interesting to note, however, that carpet spills also follow the trend of decreasing spill depth with increasing surface tension. The spill depths for carpet were larger than those reported for other substrates by a factor of five or more for 3% AFFF and 3% FP liquids.

4.6 Spill Fire Dynamics

4.6.1 Test Procedures

Prior to each spill fire dynamics test, the substrate being evaluated was centered beneath the spill arm. In the case of vinyl, plywood, and OSB, the substrate was attached to a wood stud frame flooring system with studs spaced 0.41 m (16 in.) on center. This was done to prevent warping of the specimen that could affect the spill progression. Once centered beneath the spill arm the substrate was leveled to within 3.2 mm (0.125 in.) over a distance of 1.2 m (4 ft).

Prior to filling the spill arm, the volume and mass of the liquid being used were recorded. The spill arm apparatus was then centered 0.3 m (1 ft) above the substrate at which point in time the video image collection was started. The valve on the spill arm was then opened remotely, which signaled the beginning of the test. Background data was collected for two minutes prior to spilling. The contents were allowed to drain for 10-seconds, sufficient for the total amount of liquid to be spilled. The spill arm was then swung out of the field of view of the camera. The spills were allowed to spread for 5 minutes or 30-seconds from the time of valve opening depending on the test. Still photographs were used to capture spill progression at various

instances in time. Photographs were also used to capture the height of the spill front moving across each substrate.

Ignition of the liquid fuel was done at the end of the spreading time by using a propane torch at the edge of the spill. The fire was considered extinguished at the point where only small isolated flamelets existed inside the original spill area. Data collection was terminated around one minute after this extinguishment time was noted.

After all residual flaming was extinguished on the substrate; photos were taken of any spill pattern. For all substrates other than carpet, these photos were only of the surface patterns. In the case of carpet burns, the remaining layers of carpet and padding were removed individually and all interface burn patterns were documented with photos. The substrates were then hosed down with water to cool them. For carpet, plywood, glued vinyl, and OSB tests, the substrates were not re-used. Concrete pads were cooled and dried by using forced air convection provided by fans blowing over wet towels on the top of these surfaces. A pad was deemed cool enough when the average surface temperature was below 20^{o}C and the range of surface temperatures was less than 3^{o}C. This was determined using an infrared camera.

4.6.2 Spill Fire Results

Spill depths obtained in the flammable liquid spill fires are presented along with other relevant spill fire data in Table 4.15–4.17. Some typical photographs of 0.5 L and 1.0 L spill fires are shown in Figure 4.19 and Figure 4.20. These depths are comparable to those obtained with the fuel surrogates. All spill depths for fuels were less than 1 mm, with the exception of those on carpet and plywood substrates. Spill depths for fuels on plywood were between 1.0 and 1.2 mm, slightly higher than the other fuels. As was seen for the fuel surrogates, fuel spills on carpet produced spill depths much greater than those on the less absorptive substrates. For all fuels, the shorter ignition delay times produced spill depths that were larger than those from the longer ignition delays; the reason being that the 30-second spills had not completely finished spreading to the equilibrium spill depth. For the 300 second ignition delay tests, the spills were closer to equilibrium; having reached approximately 90% of their maximum spill area (see Section 4.5.3).

Table 4.15. Summary of Averaged Spill Fire Dynamics Data Collected on Concrete Surfaces

Test ID	Substrate	Fuel	Qty. (L)	Ignition Delay (s)	Average 10s Peak HRR (kW)	Average 10s Peak HRRPUA (kW/m^2)	Average THR (MJ)	Average Spill Area (m^2)	Average Spill Depth (mm)
SFD1	Coated Concrete	Gasoline	0.5	300	227	304	6	0.75	0.67
SFD21									
SFD21A									
SFD100									
SFD89	Coated Concrete	Gasoline	0.5	30	397	635	9.3	0.63	0.8
SFD91									
SFD89A									
SFD89B									
SFD136	Coated Concrete	Gasoline	0.5	0	452	866	12.2	0.52	0.96
SFD73	Coated Concrete	Heptane	0.5	300	254	233	5.3	1.07	0.47
SFD78									
SFD139									
SFD78A									
SFD93	Coated Concrete	Heptane	0.5	30	501	564	10.4	0.89	0.56
SFD94									
SFD16	Coated Concrete	Denatured Alcohol	0.5	300	108	127	4.6	0.85	0.59
SFD36									
SFD36A									
SFD36B									
SFD90	Coated Concrete	Denatured Alcohol	0.5	30	138	238	6.2	0.58	0.86
SFD92									
SFD11	Coated Concrete	Kerosene	0.5	300	LOCALIZED OR NO IGNITION OBSERVED				
SFD11A									
SFD11				0					
SFD31									
SFD74	Coated Concrete	Heptane	1	30	1169	886	21.4	1.32	0.76
SFD119									
SFD79	Coated Concrete	Heptane	1	300	609	212	11.4	1.92	0.52
SFD121									
SFD79A									
SFD2	Coated Concrete	Gasoline	1	30	923	741	19.6	1.26	0.8
SFD3									
SFD95									
SFD96									
SFD22				150	497	263	12.9	1.89	0.53
SFD22A				300	437	244	9.1	1.79	0.56
SFD23									
SFD17	Coated Concrete	Denatured Alcohol	1	30	323	300	14.3	1.08	0.93
SFD18									
SFD37				300	236	132	7.4	1.79	0.56
SFD140	Smooth Concrete	Gasoline	0.5	30	466	531	11.4	0.88	0.57
SFD122									
SFD142				300	129	136	4.2	0.95	0.53
SFD124									
SFD141			1	30	932	586	18.2	1.59	0.63
SFD123									
SFD83	Brushed Concrete	Gasoline	0.5	30	368	542	11	0.68	0.74
SFD134									
SFD86				300	263	306	9.3	0.86	0.58
SFD136									
SFD84	Brushed Concrete	Gasoline	1	30	743	580	23.1	1.28	0.78
SFD135									
SFD87				300	456	311	14.1	1.47	0.68
SFD137									

Table 4.16. Summary of Averaged Spill Fire Dynamics Data Collected on Vinyl and Wood Surfaces

Test ID	Substrate	Fuel	Qty. (L)	Ignition Delay (s)	Average 10s Peak HRR (kW)	Average 10s Peak HRRPUA (kW/m^2)	Average THR (MJ)	Average Spill Area (m^2)	Average Spill Depth (mm)
SFD62A	Vinyl	Gasoline	1	30	1412	1102	24.2	1.28	0.78
SFD66				30					
SFD68				150	1646	891	25.2	1.85	0.54
SFD69				167					
SFD65	Vinyl	Denatured Alcohol	1	30	457	418	17.6	1.1	0.91
SFD115									
SFD71				300	407	313	12.9	1.3	0.77
SFD117									
SFD63	Vinyl	Gasoline	0.5	30	635	1102	12.9	0.58	0.87
SFD61									
SFD64	Vinyl	Kerosene	0.5	30	469	918	15.5	0.51	0.98
SF156									
SFD67	Vinyl	Gasoline	0.5	300	419	412	7.3	1.02	0.49
SFD126	OSB (Rough)	Gasoline	0.5	30	495	805	10.2	0.62	0.83
SFD127	OSB (Smooth)	Gasoline	0.5	30					
SFD130	OSB (Rough)	Gasoline	0.5	30					
SFD131	OSB (Smooth)	Gasoline	0.5	30					
SFD128	OSB (Rough)	Denatured Alcohol	0.5	30	171	286	6.9	0.6	0.84
SFD132	OSB (Rough)	Denatured Alcohol	0.5	30	171	286	6.9	0.6	0.84
SFD133	OSB (Smooth)	Denatured Alcohol	0.5	30					
SFD129	OSB (Smooth)	Denatured Alcohol	0.5	30					
SFD150	OSB (Rough)	Kerosene	0.5	30	491	961	13.1	0.51	0.98
SFD151	OSB (Smooth)	Kerosene	0.5	30					
SFD154	OSB (Smooth)	Kerosene	0.5	30					
SFD153	OSB (Rough)	Kerosene	0.5	30					
SFD41	Plywood	Gasoline	0.5	30	570	1184	11.1	0.48	1.04
SFD42									
SFD43	Plywood	Kerosene	0.5	30	478	1124	13.7	0.43	1.18
SFD44									
SFD45	Plywood	Denatured Alcohol	0.5	30	172	365	5.5	0.47	1.07
SFD46									

Table 4.17. Summary of Averaged Spill Fire Dynamics Data Collected On Carpet Surfaces

Test ID	Substrate	Fuel	Qty. (L)	Ignition Delay (s)	Average 10s Peak HRR (kW)	Average 10s Peak HRRPUA (kW/m^2)	Average THR (MJ)	Average Spill Area (m^2)	Average Spill Depth (mm)
SFD49	Carpet/Pad/Plywood	Gasoline	0.5	30	140	679	39.4	0.21	2.39
SFD55									
SFD52	Carpet/Pad/Plywood	Kerosene	0.5	30	227	1062	53.3	0.21	2.45
SFD58									
SFD50	Carpet/Pad/Concrete	Gasoline	1	30	304	1354	61.5	0.22	4.47
SFD56									
SFD50A									
SFD56A									
SFD53	Carpet/Pad/Plywood	Kerosene	1	30	290	1245	77.1	0.23	4.29
SFD53A									
SFD59									
SFD51	Carpet/Pad/Plywood	Gasoline	5	30	1160	3035	238.5	0.38	13.07
SFD57									
SFD141A	Carpet/Concrete	Gasoline	1	30	281	1277	32.4	0.22	20.66
SFD152	Carpet/Pad/Plywood	Gasoline	1	300	312	1493	73.6	0.21	22.89
SFD54	Carpet/Pad/Plywood	Kerosene	5	30	1075	2682	273.1	0.4	12.51
SFD60									

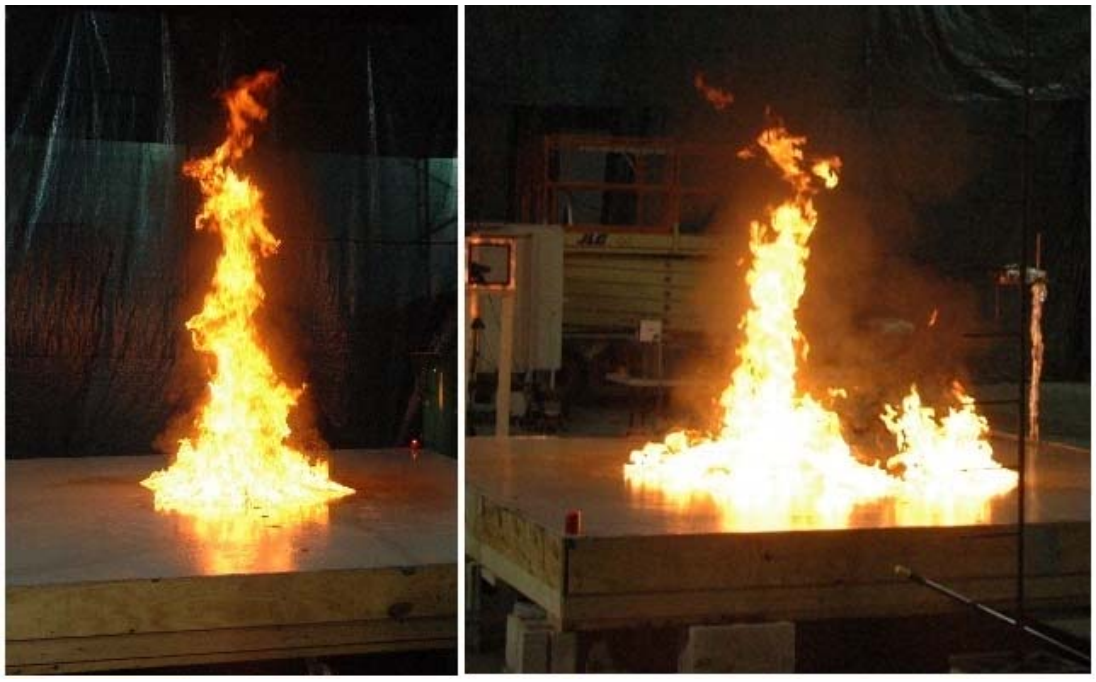

Figure 4.19. Pictures of representative 0.5 L (SFD89-U-CC-G-0.5-30, left) and 1.0 (SFD23-U-CC-G-1.0-30, right) gasoline spill fires on coated concrete

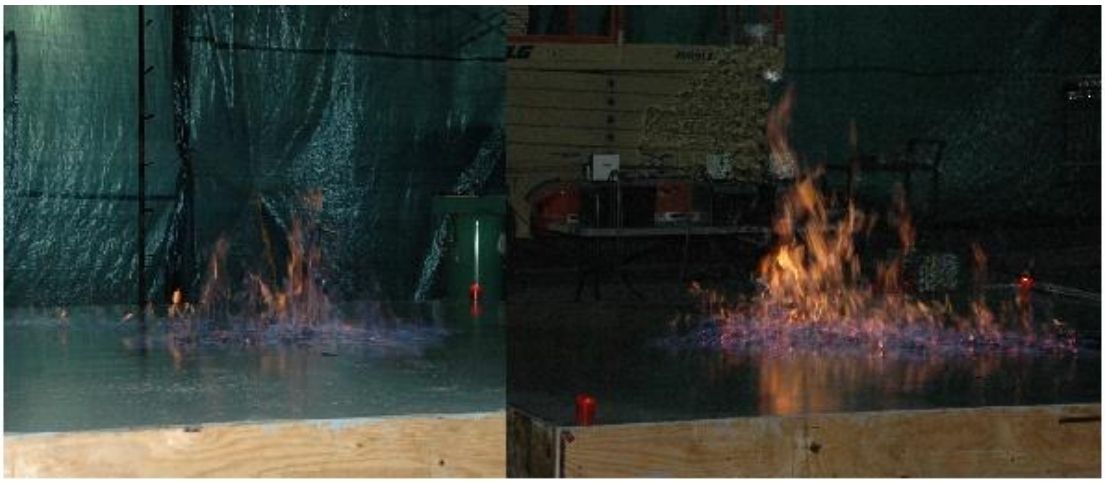

Figure 4.20. Pictures of representative 0.5 L (SFD16-U-CC-DA-0.5-30, Left) and 1.0 L (SFD17-U-CC-DA-1.0-30, Right) denatured alcohol spill fires on coated concrete

Figure 4.21 and Figure 4.22 show the increasing trend in spill depth with increasing surface tension. This increasing trend is similar in magnitude to the non flammable liquid spills. These differences tend to be more pronounced for the impermeable substrates than the permeable substrates. However, the data presented suggests that small differences in surface tension have a correspondingly small impact on spill depth.

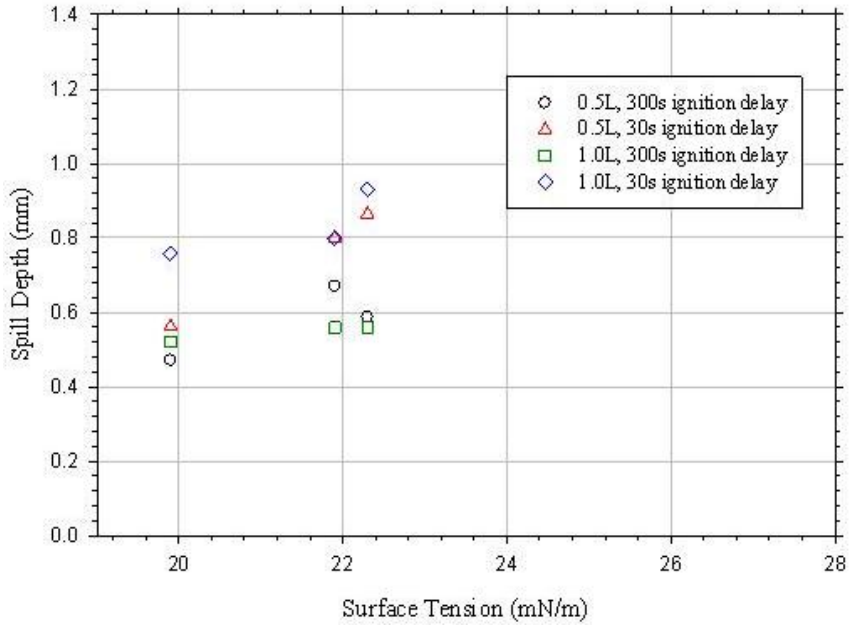

Figure 4.21. Summary of spill depth vs. fuel surface tension for gasoline (21.9 mN/m), denatured alcohol (22.3 mN/m), and n-Heptane (19.9 mN/m) fuels on coated concrete with various volumes and ignition delays

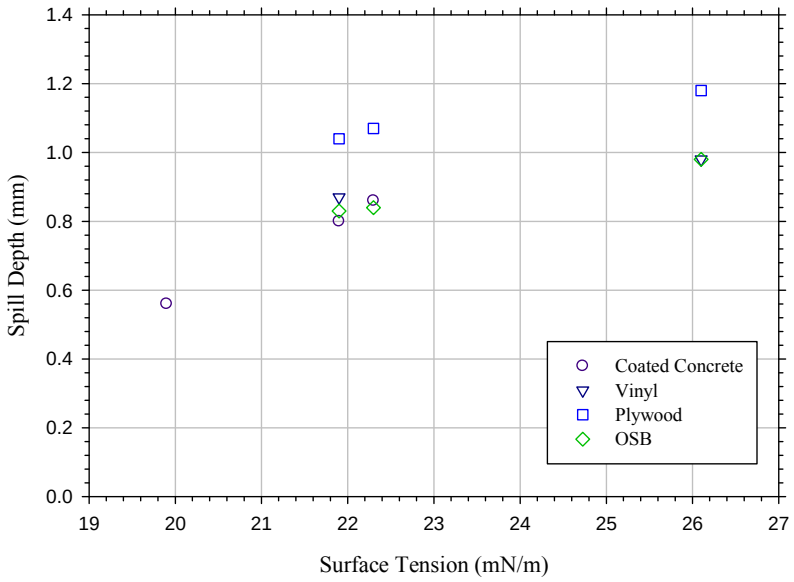

Figure 4.22. Summary of spill depth vs. surface tension for gasoline (21.9 mN/m), denatured alcohol (22.3 mN/m), n-Heptane (19.9 mN/m),and kerosene (26.1 mN/m) fuels on four substrates with 0.5 L spill volumes and 30-second ignition delays

Figure 4.23 shows spill depth versus volume spilled for gasoline spills with 30-second ignition delays on four substrates that were tested with multiple volumes of fuel. There was limited data for large volume spills on the substrates tested because of the size limitations of the substrates. The data in Figure 4.23 and 4.24 does not demonstrate any appreciable impact of spill volume on spill depth. However, due to the limited data for fuels and volumes, no global conclusions on this independence can be made.

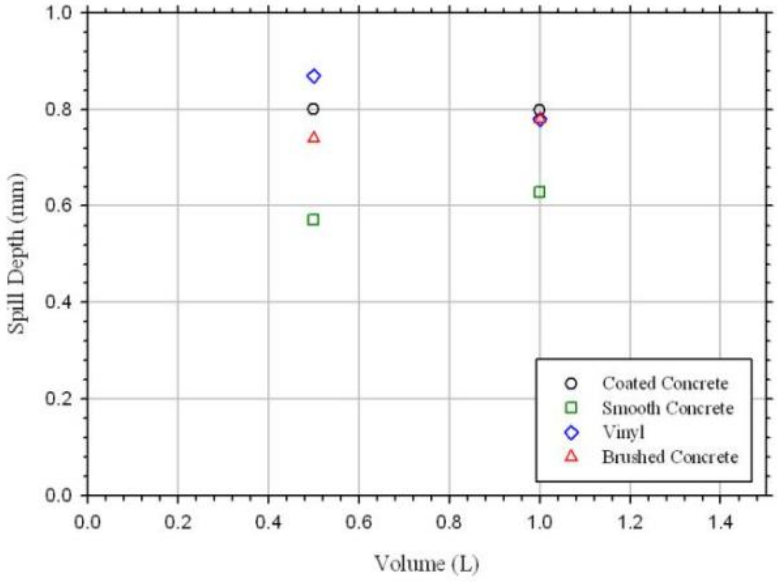

Figure 4.23. Summary of spill depth vs. spill volume data for gasoline on four substrates with 30-second ignition delays

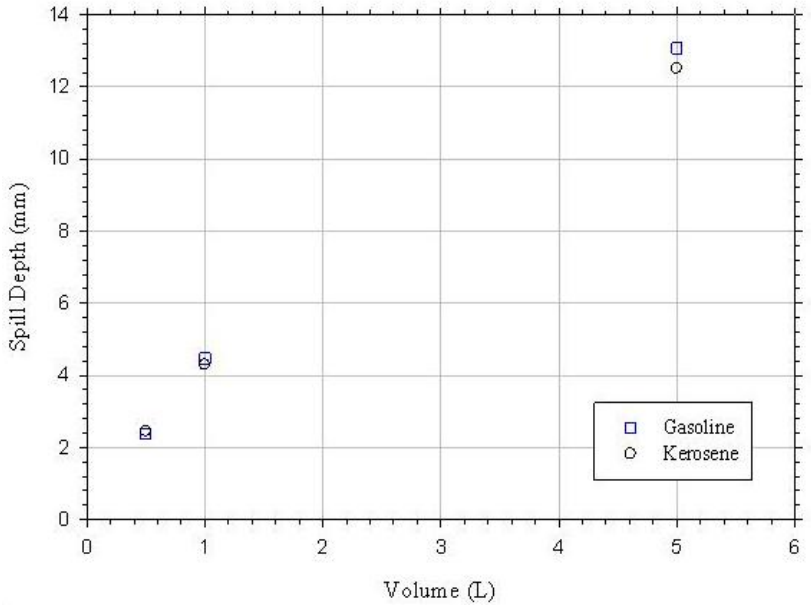

Figure 4.24. Summary of spill depth vs. spill volume for gasoline and kerosene on carpet with 30-second ignition delays

4.6.3 Coated Concrete Results

A total of 41 spill fire tests were conducted on coated concrete. Variables evaluated in these tests included fuel type, spill volume, ignition delay, and substrate temperature. The fuels spilled included gasoline, denatured alcohol, and n-Heptane. Kerosene and diesel fuel were not used due to their inability to propagate flame under the test conditions. Ignition delays of 30 and 300 seconds were used. The impact of substrate temperatures was evaluated based on initial testing when the temperature of the pad was not closely monitored from test to test. Due to changes in environmental conditions, the pad temperature varied from 18–38°C (64–100°F) during this initial series of nineteen tests. These nineteen tests consisted of four gasoline, four denatured alcohol, and eleven n-Heptane spills. All spills except for five n-Heptane tests were conducted using 0.5 L of fuel. For these nineteen tests, the substrate surface temperature was measured using the output from the FLIR camera positioned above the substrate. This data was used instead of the embedded thermocouple data because it provided a surface temperature as opposed to a temperature at depth within the concrete. Furthermore, the FLIR camera has an accuracy of ± 2°C, which is comparable to that of a standard thermocouple thus accuracy is not lost. In this analysis, a fixed area was selected in order to obtain an objective average surface temperature for each scenario evaluated. The area of measurement was a circle whose center was placed at the center of the pad and had an area of 1 m^2 (10.8 ft^2). The measurement area was selected based upon the average spill area for the fuel quantities being evaluated. After preliminary analysis, the impact of substrate temperature was realized and the temperature of the substrate was controlled thereafter. Substrate temperatures for the remainder of the spill fire tests were maintained between 20–25°C (68–77°F).

4.6.3.1 Gasoline on Coated Concrete

The first spill fire tests conducted atop the coated concrete were 0.5 L gasoline spills with 30-second ignition delays (Figure 4.25). In these tests, the pad temperatures ranged from 22–24°C (72–75°F). A total of four identical tests were conducted with a maximum difference in peak heat release rate of 20 percent. The differences in peak heat release rates for these tests were taken to be comparable given the randomness that occurs in the size and shape of a liquid spill on an imperfect substrate as well as the variations common to fire testing. In addition, the initial growth and the decay of these fires agree very well.

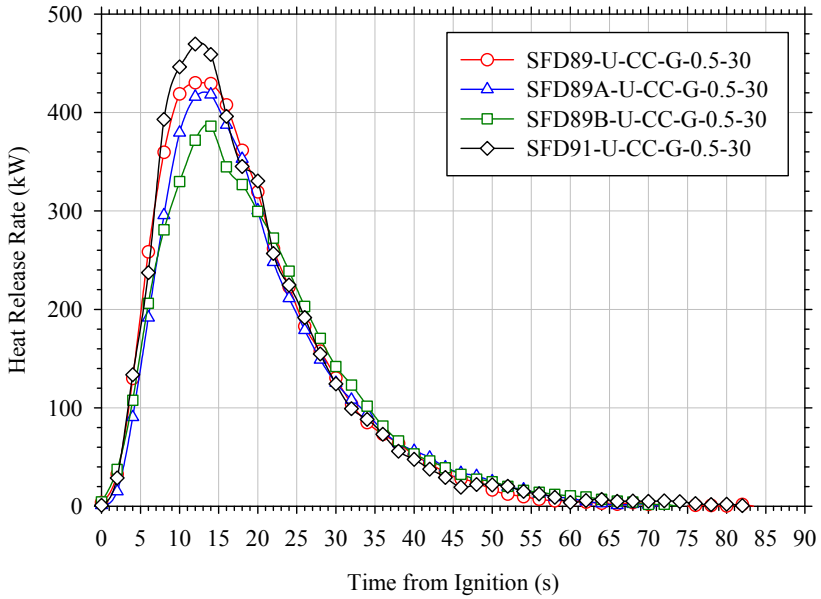

Figure 4.25. Heat release rates for 0.5 L gasoline spills on coated concrete with 30-second ignition delays

The differences measured in the 0.5 L gasoline spills on coated concrete, with 300 second ignition delays, (shown in Figure 4.26) produced results that had substantially more variability than the 30-second ignition delay results. For this spill scenario, there was a maximum difference of about 50 percent between peak heat release rates. In these tests, the initial pad surface temperatures (shown in Table 4.18) ranged from 22–28°C (72–82°F). This temperature range was larger than that measured for the 30-second ignition delay tests and was also spread over a higher temperature range (i.e., 22–28°C as opposed to 22–24°C for the 30 s ignition delay tests). Table 4.18 shows that the tests with higher initial temperatures of 27–28°C had higher heat release rates (~300 kW) compared to the tests with slightly lower pad temperatures 22–24°C that had heat release rates of about 200 kW. As seen in Figure 26, there was also a distinct difference in the initial growth rate of these two sets of fires, with the fires growing faster on the concrete pads with higher temperatures.

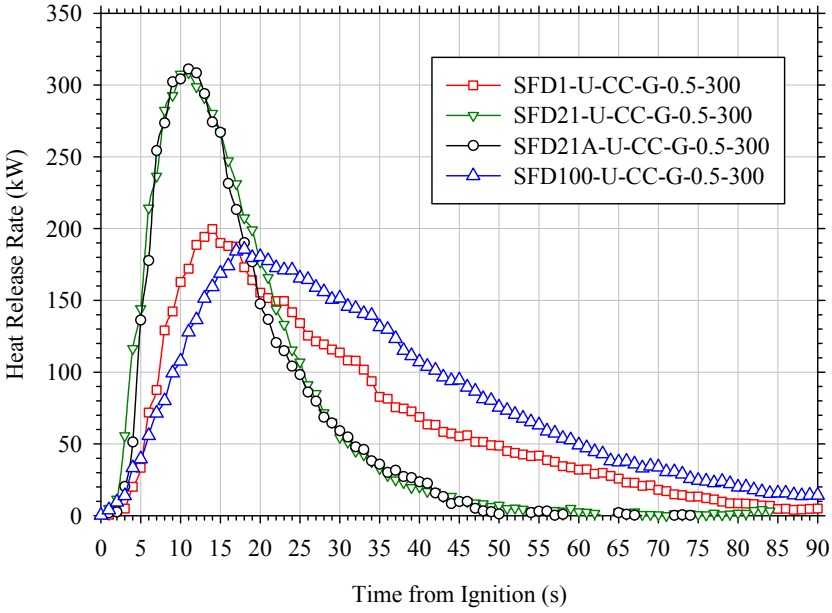

Figure 4.26. Heat release rates for 0.5 L gasoline spills on coated concrete with 300 second ignition delays

Table 4.18. Ambient and Initial Substrate Temperatures for 0.5 L Gasoline Spills On Coated Concrete with 300 Second Ignition Delays

Test ID	Substrate	Fuel	Qty. (L)	Ignition Delay (s)	Ambient Air/Fuel Temp. (°C)	Initial Substrate Temp. (°C)	10 s Peak HRR (kW)
SFD1	Coated Concrete	Gasoline	0.5	300	21	24	199
SFD21					21	28	309
SFD21A					21	27	311
SFD100					18	22	186

The variability observed in the 1.0 L gasoline spills was comparable to that of the 0.5 L gasoline spills on coated concrete. A maximum difference in 10-second peak heat release rates was found to be 14 percent for the 1.0 L, 30-second ignition delay tests. In these tests, the substrate temperatures ranged from 18–20°C (64–68°F), a temperature range similar to that observed for the 0.5 L, 30-second ignition delay gasoline spills in which minimal variability was also observed. Figure 4.27 shows the heat release rate curves for these tests. Three of these tests have almost identical peaks, while the fourth has only a slightly larger peak heat release rate. The peak heat release rates for the 1.0 L, 30-second ignition delay tests were approximately double those of the 0.5 L, 30-second ignition delay spills, corresponding to the larger spill area for the 1 L spills.

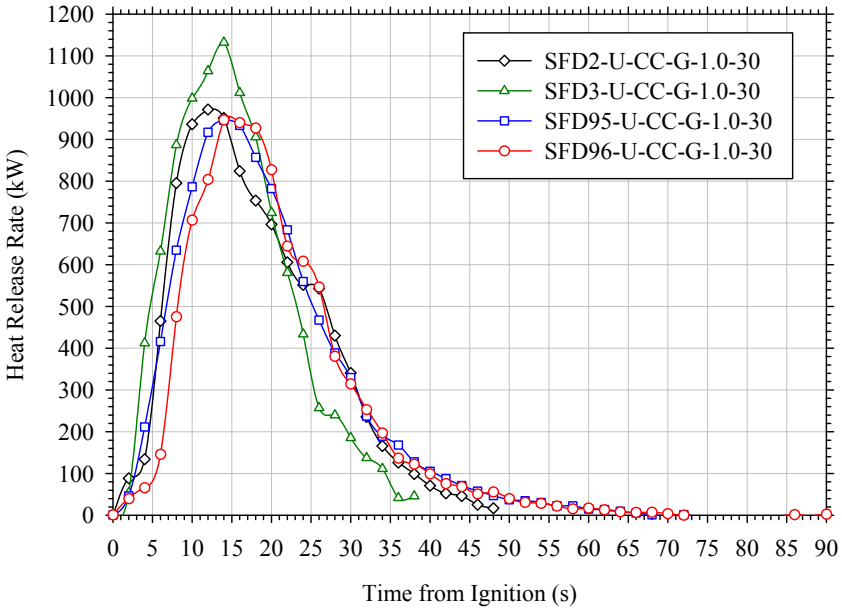

Figure 4.27. Heat release rates for 1.0 L gasoline spills on coated concrete with 30-second ignition delays

In general, the variability in the 10-second average peak heat release rates from the 30- and 300-second ignition delay tests conducted on coated concrete with 1.0 L of gasoline were similar. The maximum difference in 10-second peak heat release rates measured for this spill scenario was 18 percent. The initial pad temperature range for the 150 and 300 second ignition delay tests was 19–22°C (66–72°F). The tests were generally reproducible with similar heat release curves (Figure 4.28).

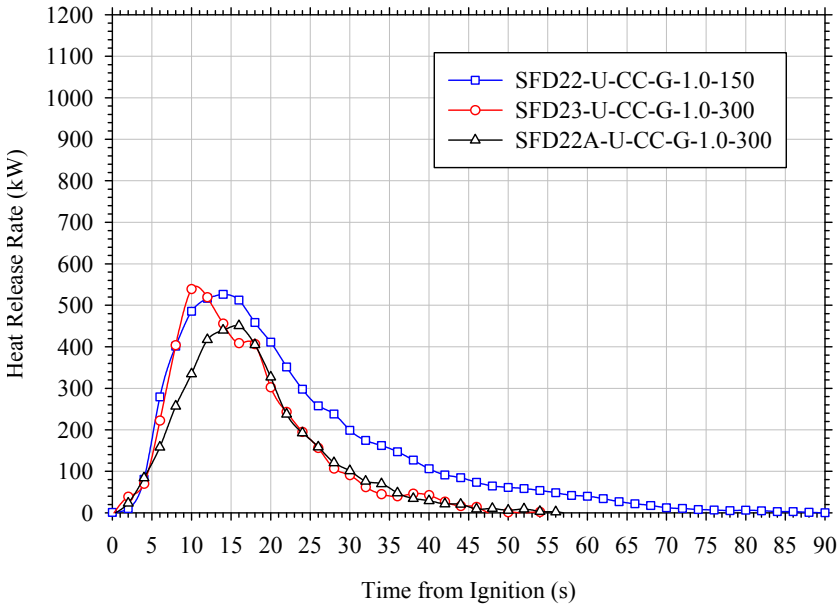

Figure 4.28. Heat release rates for 1.0 L gasoline spills on coated concrete with 150–300 second ignition delays

4.6.3.2 Denatured Alcohol on Coated Concrete

Similar to the gasoline spill fires, for a given spill scenario, the denatured alcohol spills were reproducible (Figure 4.29 to Figure 4.31). The exception to this was the four 0.5 L, 300 second tests that were conducted prior to when the initial concrete surface temperature was closely controlled. In these tests, there was a maximum difference in 10-second peak heat release rates of 46 percent as seen in Figure 4.29. The initial pad temperatures ranged from 20–29°C (68–84°F). Initial pad temperatures, ambient air/fuel temperatures, and 10-second peak heat release rates for these tests are shown in Table 4.19. Contrary to the gasoline tests, the denatured alcohol 0.5 L, 300 second fire sizes do not correlate to the pad temperature. However for this group of tests, the peak heat release rate increases as the difference between the pad temperature and the ambient air/fuel temperature increases.

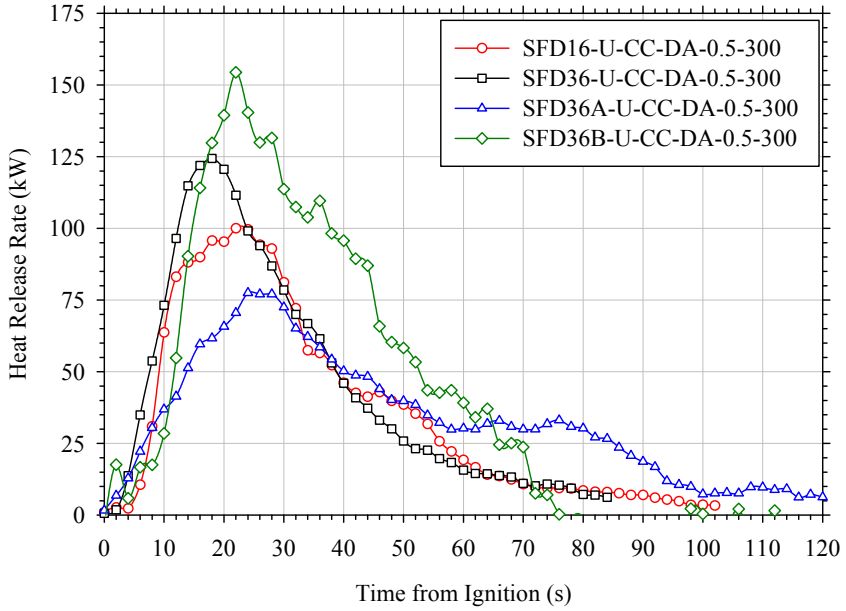

Figure 4.29. Measured heat release rates for 0.5 L denatured alcohol spills on coated concrete with 300 second ignition delays

Table 4.19. Ambient and Initial Substrate Temperatures for 0.5 L Denatured Alcohol Spills On Coated Concrete with 300 Second Ignition Delays

Test ID	Substrate	Fuel	Qty. (L)	Ignition Delay (s)	Ambient Air/Fuel Temp. (°C)	Initial Substrate Temp. (°C)	10 s Peak HRR (kW)
SFD16	Coated Concrete	Denatured Alcohol	0.5	300	21	25	98
SFD36					21	29	118
SFD36A					20	22	75
SFD36B					11	20	140

The 30-second ignition delay tests conducted with 0.5 L of gasoline on coated concrete were highly repeatable as shown in Figure 4.30. In these tests, both the ambient and substrate temperature were within one degree of each other.

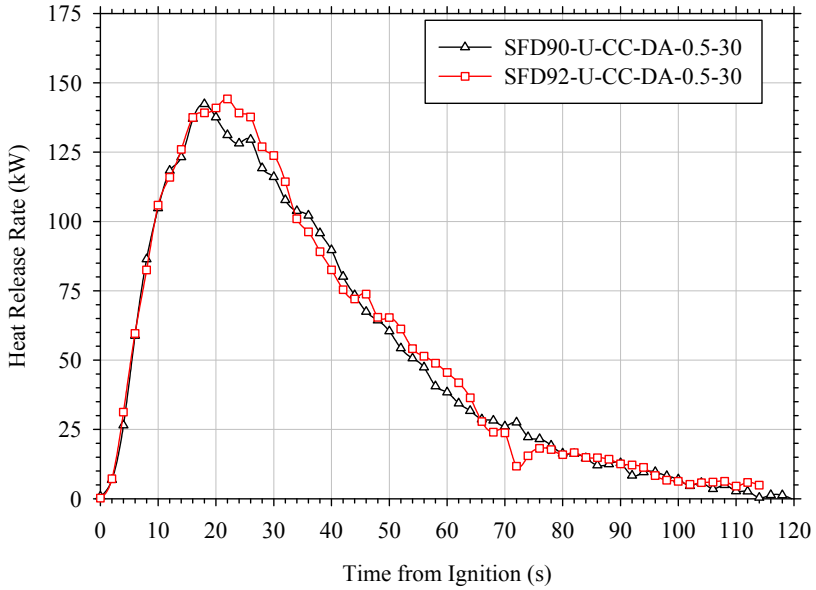

Figure 4.30. Measured heat release rates for 0.5 L denatured alcohol spills on coated concrete with 30-second ignition delays

Similar growth rates and peak heat release rates were observed for the repeat tests of the 1.0 L denatured alcohol spills on coated concrete with ignition delay times of both 30 and 300 seconds. The substrate and ambient temperature conditions in these tests were comparable (i.e., within two degrees for similar spill scenarios). In these tests it was also found that the total heat released (THR) in the 300-second ignition delay tests was approximately 50 percent of that measured in the 30-second ignition delay. This difference is most likely a consequence of a larger quantity of fuel evaporating from the spill over the longer 300-second exposure.

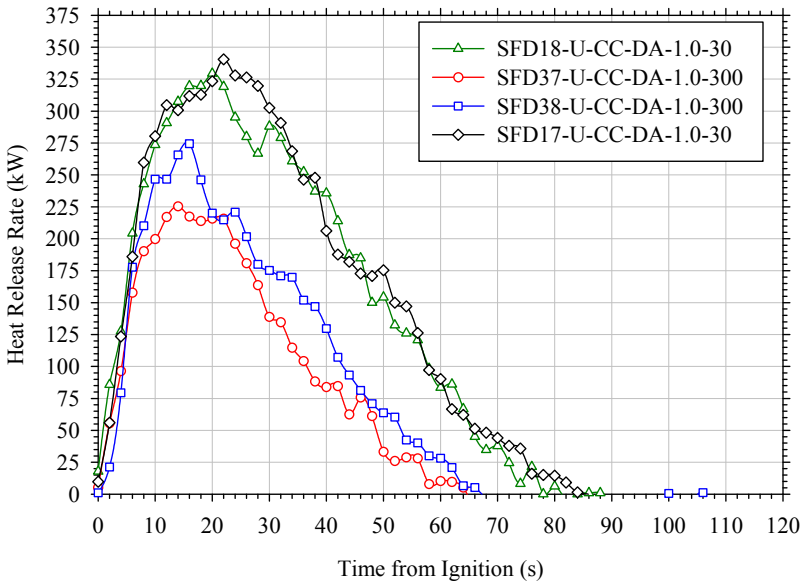

Figure 4.31. Measured heat release rates for 1.0 L denatured alcohol spills on coated concrete with 30 (shown in green and black) and 300 (shown in red and blue) second ignition delays

4.6.3.3 N-Heptane on Coated Concrete

The n-Heptane spill fires on coated concrete had the greatest variability in behavior out of all of the coated concrete spill fire tests. Out of the four n-Heptane spill scenarios evaluated on coated concrete, only the 1.0 L, 30-second ignition delay tests were found to be repeatable. The remainder of the test scenarios had maximum 10-second peak heat release rate differences between 25 to 380 percent. As seen in Figure 4.32, two sets of two 0.5 L, 300 second ignition delay tests have the largest variability. However, the initial pad temperatures (Table 4.20) ranged from 21 to 38°C (70–100°F) for these four tests. Similar to the gasoline tests on coated concrete, there is a correlation between the peak heat release rates and the pad temperatures (i.e., higher pad temperatures corresponded to higher heat release rates). However, this correlation does not include Tests 73 and 78, which had pad temperatures of 37 and 38°C, respectively. A possible explanation for the very low heat release rates for tests SFD73 and SFD78 is that a large amount of pre-ignition evaporation could have taken place on the hot substrate which would have reduced the amount of fuel present on the pad at the time of ignition thus reducing the peak heat release rate achieved during the test. The substantially lower total heat release (see Table 4.20) for these two tests is consistent with this rationale.

Despite the large amount of variability in the heat release rates for the 0.5 L, 300 second ignition delay tests, overall trends seen in prior testing were present. Most notably, a decrease in heat release rate can be seen for increasing ignition delay time. In addition, there was an overall increase in peak heat release between the 0.5 L and 1.0 L tests with similar ignition delays, as shown in Figure 4.32 and Figure 4.33.

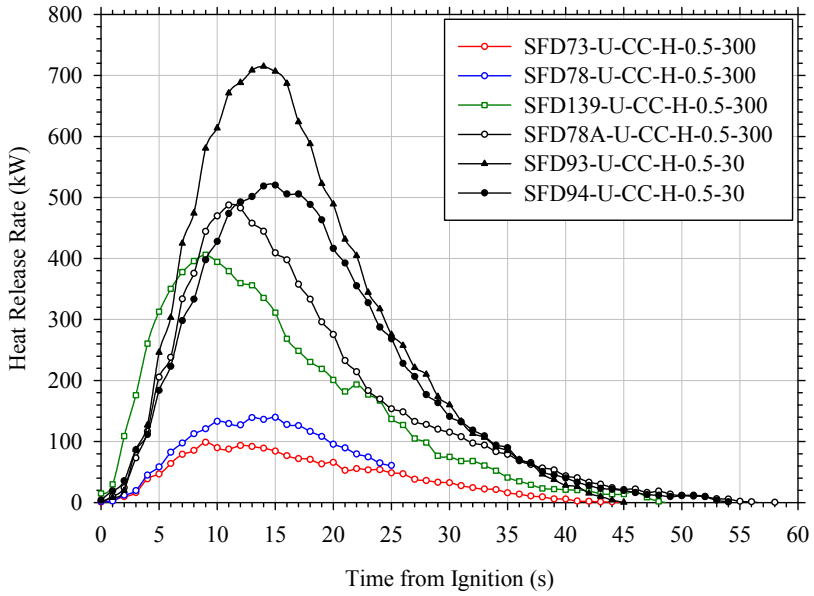

Figure 4.32. Measured heat release rates for 0.5 L n-Heptane spills on coated concrete with 30- and 300-second ignition delays

Table 4.20. Ambient and Initial Substrate Temperatures for 0.5 L N-Heptane Spills On Coated Concrete with 30- and 300-Second Ignition Delays

Test ID	Substrate	Fuel	Qty. (L)	Ignition Delay (s)	Ambient Air/Fuel Temp. (°C)	Initial Substrate Temp. (°C)	10 s Peak HRR (kW)
SFD73	Coated Concrete	n-Heptane	0.5	300	21	37	87
SFD78					21	38	129
SFD139					11	21	367
SFD78A					21	28	431
SFD93				30	21	30	514
SFD94					18	19	489

Significantly less variability was noted in the 1.0 L n-Heptane tests on coated concrete (Figure 4.33) than for the 0.5 L spill fires, when comparing the 30-second ignition delay scenarios. Initial conditions for all of the 1.0 L spill scenarios had temperatures within three degrees of one another (Table 4.21). Despite this fact, the 300-second delay scenarios had a maximum difference in peak heat release rates of 40 percent.

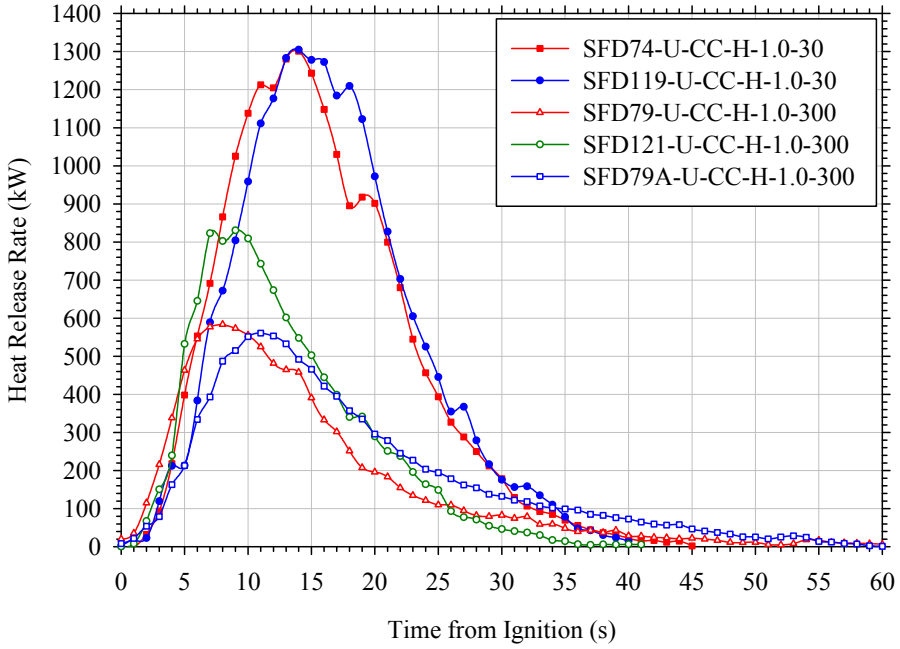

Figure 4.33. Measured heat release rates for 1.0 L n-Heptane spills on coated concrete with 30 and 300-second ignition delays

Table 4.21. Ambient and Initial Substrate Temperatures for 1.0 L n-Heptane Spills on Coated Concrete with 30 and 300-second Ignition Delays

Test ID	Substrate	Fuel	Qty. (L)	Ignition Delay (s)	Ambient Air/Fuel Temp. (°C)	Initial Substrate Temp. (°C)	10 s Peak HRR (kW)
SFD74	Coated Concrete	n-Heptane	1	30	12	19	1146
SFD119					10	20	1191
SFD79				300	11	21	519
SFD121					10	21	699
SFD79A					12	22	497

A few hypotheses have been suggested as to the reason for some large differences in peak heat release rate seen for tests on coated concrete with the same ignition delay and volume parameters. All of these explanations focused on what were thought to be key factors that impacted burning behavior: initial substrate and fuel temperatures. One problem that arises when trying to explain the vast differences in the peak heat release rates through initial substrate and fuel temperatures is how to determine these parameters. The fuel temperature was not specifically measured and was assumed to be equal to ambient temperature. This could lead to small differences between the actual fuel temperature and the assumed temperature. Also, the initial substrate temperature was determined through an average temperature, obtained from FLIR images, over a certain area of the concrete pad. This method can be somewhat subjective in that the size and shape of the area is chosen somewhat arbitrarily based on the residual temperature profile from the previous test. There is not a uniform area over which to obtain this

average temperature because if one were to use the entire pad versus the area of the spill, the differences between the two measures would be significant. And to calculate the average temperature over the exact area of the spill becomes very tedious and again includes a portion of subjectivity. Despite these shortcomings, it is still believed that the initial fuel temperature (or ambient temperature) as well as the initial substrate temperature do have an impact on the heat release rate of a spill fire and that this impact can be quite substantial in some cases. However, these effects are quite difficult to fully assess in this program.

4.6.4 Smooth Concrete Results

A total of six spill fire tests were conducted on smooth concrete using gasoline. Ignition delay times of 30 and 300 seconds were evaluated in addition to 0.5 and 1.0 L spill quantities. Due to pad size limitations, only the 30-second ignition delay time was used for the 1.0 L spill volume. Based upon the results of previous tests performed on the coated concrete substrate, the initial temperature of the smooth concrete was maintained between 20–25°C (68–77°F) for all tests conducted. All tests were performed in duplicate. The peak heat release rates from duplicate tests for the 0.5 L, 30 and 300-second ignition delays were within 17 and 6 percent of one another, respectively. The peak heat release rates for the 1.0 L, 30-second ignition delay tests were less than 5 percent of one another. A summary of the heat release rate per unit area data measured in these tests are provided in Figure 4.34 and Figure 4.35. For this comparison and all comparisons made using HRRPUA it should be noted that the area used is the initial area of coverage. In Figure 4.34 it should be noted that the THR during the 300-second ignition delay tests was substantially less than that measured in the 30-second ignition delay. Some, but not all of this difference can be attributed to the evaporation of the fuel from the surface of the substrate.

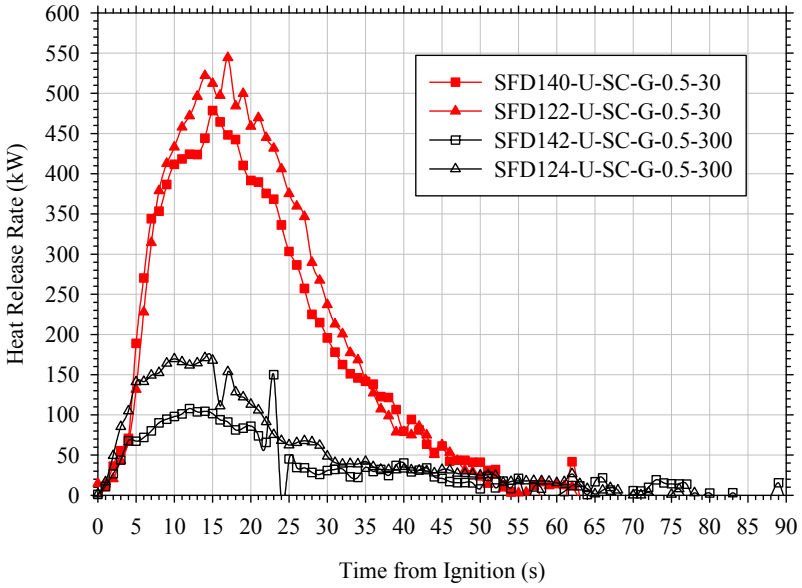

Figure 4.34. Measured HRRPUA for 0.5 L gasoline spills on smooth concrete with 30 and 300-second ignition delays

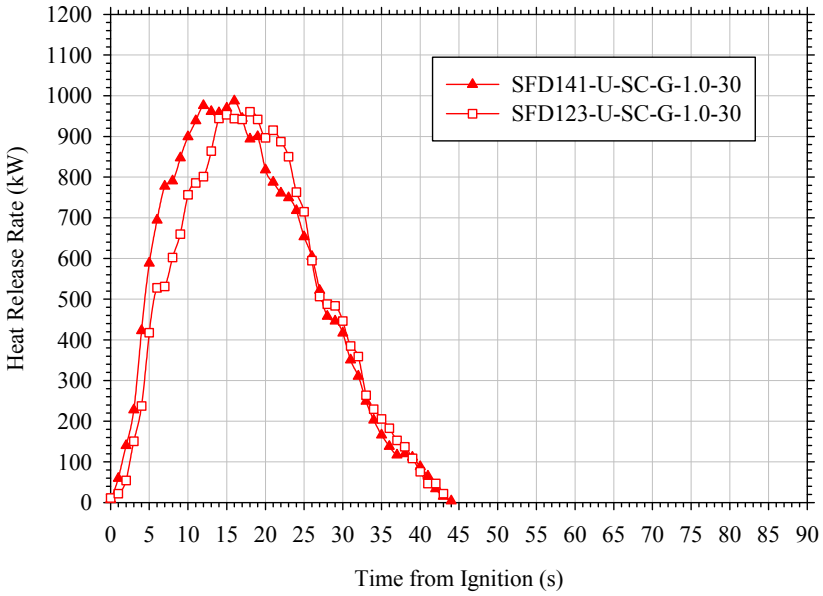

Figure 4.35. Measured HRRPUA for 1.0 gasoline spills on smooth concrete with 30-second ignition delays

The above figures for gasoline spills on smooth concrete reinforce the trends that have been seen in the coated concrete tests. Heat release rate increases for decreasing ignition delay and for increase in volume of liquid spilled. In addition, the control of initial pad temperature limited variability in peak heat release rates of spills with similar parameters.

4.6.5 Brushed Concrete Results

A total of eight spill fire tests were conducted on brushed concrete using gasoline. Ignition delay times of 30 and 300 seconds were evaluated in addition to 0.5 and 1.0 L spill quantities. The initial temperature of the brushed concrete was maintained between 20–25°C (68–77°F) for all tests conducted. All tests were performed in duplicate. Larger spill quantities were not explored due to the size limitations of the concrete pad. A summary of the heat release rate per unit area data measured in these tests is provided in Figure 4.36 and Figure 4.37. The peak heat release rates from similar spill scenarios were generally similar, with maximum differences ranging from 4–17 percent between identical tests, for the 30 and 300-second ignition delays using both the 0.5 and 1.0 L spill volumes. Differences between the 30 and 300-second ignition delays for this substrate ranged from 25 to 37 percent for the 0.5 and 1.0 L spills, respectively. This could be from the rougher surface characteristics of the brushed concrete making the fuel spills themselves more repeatable. This is supported by the spill area data collected for this substrate in which all duplicate spills had less than 5 percent variation.

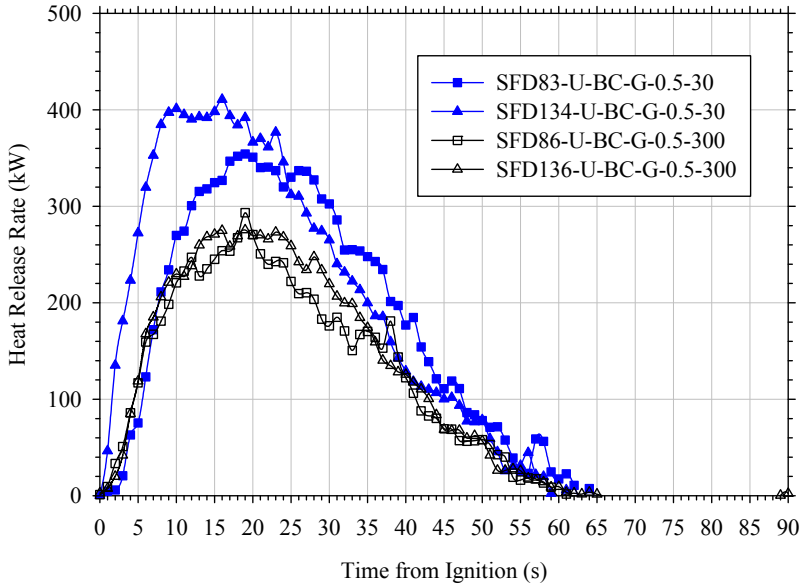

Figure 4.36. Measured HRRPUA for 0.5 L gasoline spills on brushed concrete with 30 and 300-second ignition delays

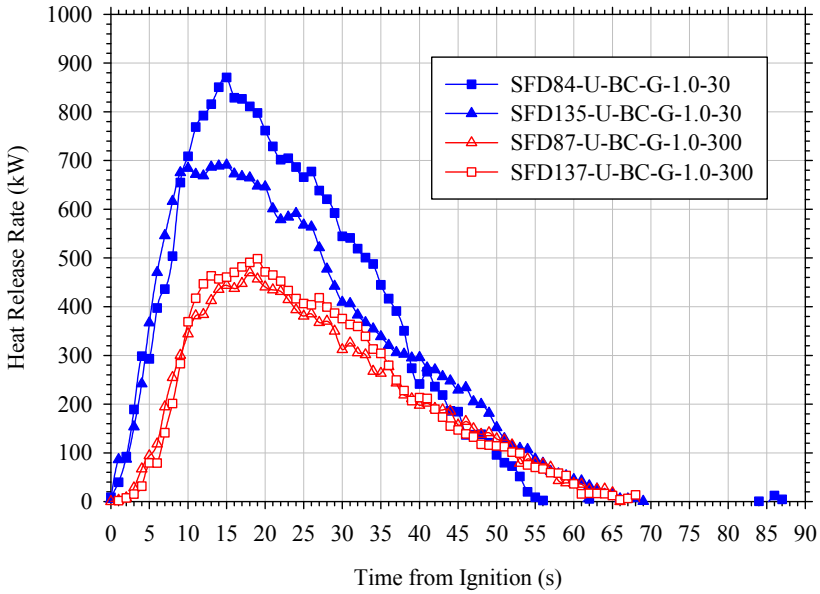

Figure 4.37. Measured HRRPUA for 1.0 L gasoline spills on brushed concrete with 30 and 300-second ignition delays

4.6.6 Plywood Results

A total of six spill fire tests were conducted on plywood using gasoline, kerosene, and denatured alcohol. In these tests the substrate was maintained at ambient conditions until the point at which the spilled fuel was ignited. For these tests ambient temperatures ranged from 20–25°C (68–77°F). These tests were performed in duplicate and all other test variables were held constant: 0.5 L spill volume and 30-second ignition delay. Larger spill quantities and ignition delay times were not explored due to the size limitations of the plywood substrate. Plywood

substrates, without seams, are not available in sizes greater than 1.2 m (4 ft) square; thus only spill scenarios that could fit on this size substrate were explored. Seams can dramatically dictate spill shapes and direction of flow. A summary of the heat release rate per unit area data measured in these tests is provided in Figure 4.38. Duplicate tests were within 13 percent, 17 percent, and 22 percent for gasoline, kerosene, and denatured alcohol, respectively.

The kerosene tests tended to develop slower than the other two fuels. This was due to the fact that for ambient temperatures of approximately 20°C, kerosene is below its flashpoint temperature. For gasoline and denatured alcohol, flame spread across the spill was approximately instantaneous. Kerosene, on the other hand, had to be heated up to its flashpoint locally, thus causing slower flame spread and a slower rise in heat release rate.

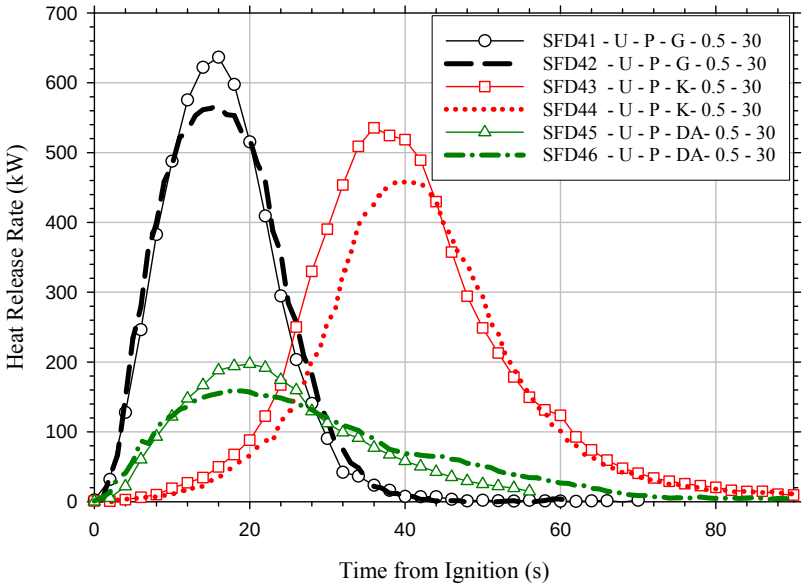

Figure 4.38. Measured heat release rates for 0.5 L fuel spills on plywood with 30-second ignition delays

4.6.7 Oriented Strand Board Results

A total of twelve spill fire tests were conducted on OSB using gasoline, kerosene, and denatured alcohol. In these tests the substrate was maintained at ambient conditions until the point at which the spilled fuel was ignited. For these tests ambient temperatures ranged from 20–25°C (68–77°F). For this substrate, the spill quantity and ignition delay time were held constant at 0.5 L and 30-second, respectively. Larger spill quantities and ignition delay times were not explored on this substrate for the same reason they were not considered on plywood. However, because OSB has two different surface finishes, the impact of this variable was explored by conducting tests on each surface finish (i.e., rough side and smooth side). All spill fire tests on OSB were performed in duplicate. The heat release rate data measured in these tests is provided in Figure 4.39 and Figure 4.40. In general, the heat release rates from the duplicate tests were repeatable. The kerosene tests had peak heat release rates within 23 percent of one another on the rough side and 9 percent on the smooth side, while the gasoline and denatured alcohol tests had variability of less than 5 percent.

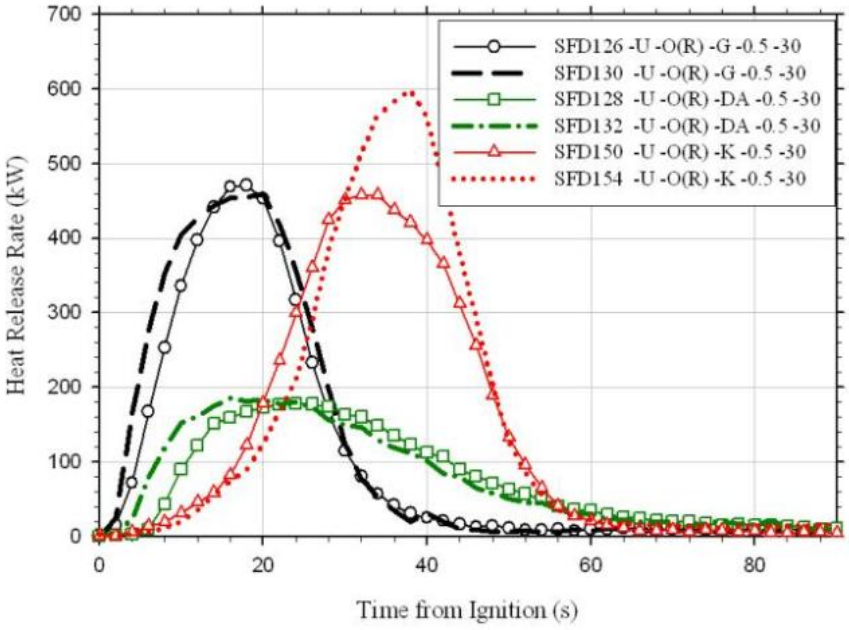

Figure 4.39. Measured heat release rates for 0.5 L fuel spills on rough side of OSB with 30-second ignition delays

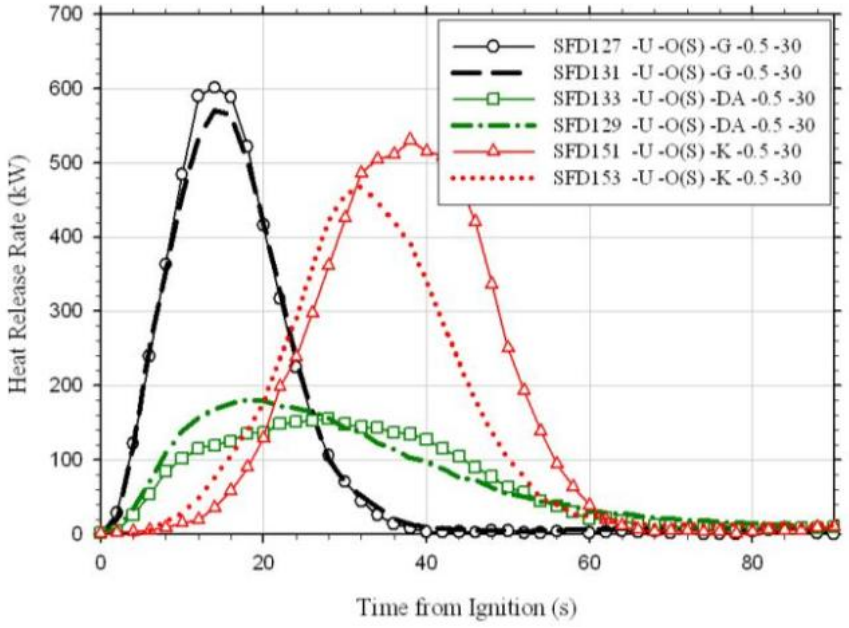

Figure 4.40. Measured heat release rates for 0.5 L fuel spills on smooth side of OSB with 30-second ignition delays

When examining the results of the various fuels spilled on the rough and smooth sides of OSB, it can be seen that there are approximately 10–20% larger spill areas for the smooth side, depending on the fuel. The largest of these differences is for gasoline, which is reflected in the heat release rate data. The heat release rate (Figure 4.40) for gasoline on the smooth side of OSB is approximately 25 percent larger than that on the rough side of OSB (Figure 4.39). However, differences seen for the denatured alcohol and kerosene tests are insignificant.

4.6.8 Vinyl Results

A total of fourteen spill fire tests were conducted on vinyl flooring using gasoline, kerosene, and denatured alcohol. In these tests the substrate was maintained at ambient conditions until the point at which the spilled fuel was ignited. For these tests ambient temperatures ranged from 20–25°C (68–77°F). In addition to various fuels, spill quantities of 0.5 and 1.0 L spills with ignition delay times of 30 and 300 seconds were evaluated. It should be noted that for the 1.0 L gasoline spills, 300-second ignition delays could not be evaluated due to the spill reaching the edge of the substrate; therefore in these tests, the ignition delays ranged from 150 to 167 seconds. In all tests, the vinyl was installed atop a plywood substrate. The heat release rate data measured in these tests is provided in Figure 4.41 and Figure 4.42. In general, the results from the duplicate tests were repeatable.

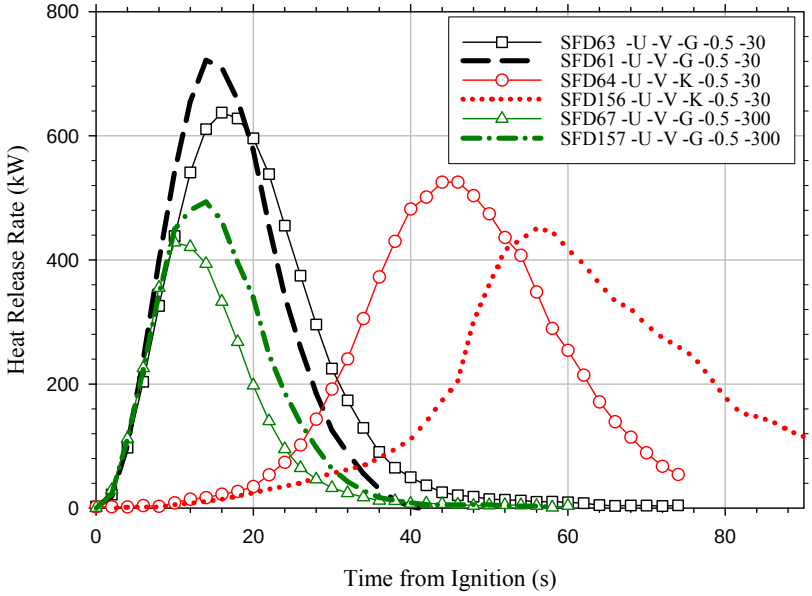

Figure 4.41. Measured heat release rates for 0.5 L fuel spills on vinyl flooring with 30-second and 300-second ignition delays

The heat release rates for 30-second ignition delay tests of gasoline and kerosene on vinyl are similar to their counterparts on OSB and plywood, despite slight differences in spill area between the substrates. Vinyl heat release rate data was only compared to that of the wood substrates due to the fact that the concrete substrates have vastly different thermal properties which have been shown to have some impact on the heat release rate. Figure 4.41 shows the measured heat release rate for the 0.5 L fuel spills on vinyl flooring. The 0.5 L, 300-second ignition delay spill fires on vinyl have peak heat release rates approximately 30% lower than the 0.5 L, 30-second

ignition delay spills, which is consistent with results seen for gasoline on the concrete substrates. Comparisons of the impact of ignition delay to plywood or OSB data could not be made due to the fact that 300-second ignition delay tests were not conducted on these substrates. The growth rate for 0.5 L kerosene tests was slower than that of gasoline. Also, this growth rate was different between the kerosene tests due to the variability of flame progression over the fuel surface from test to test. The kerosene test with a slower fire growth rate had a lower peak, which also occurred later than the other test. For most other tests on vinyl and other substrates, the peak heat release rates occurred at approximately the same time after ignition for duplicate tests.

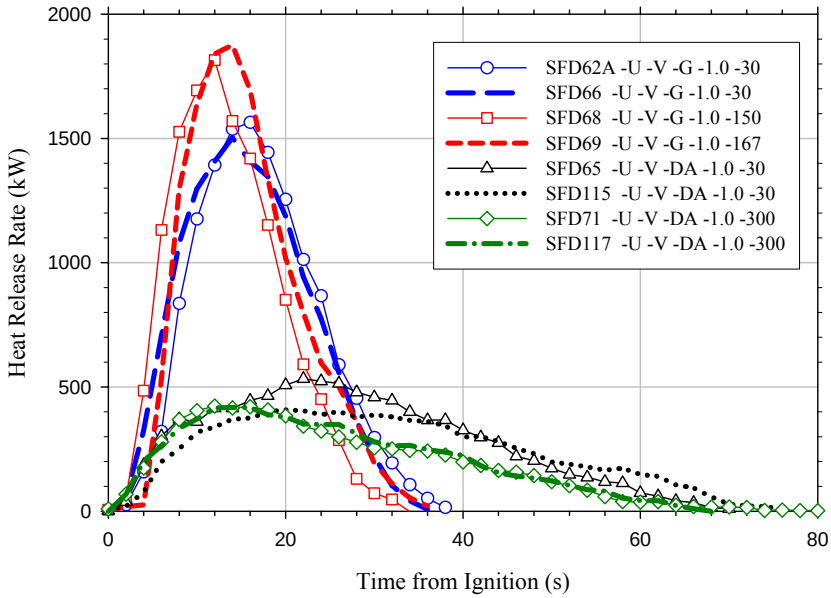

Figure 4.42. Measured heat release rates for 1.0 L fuel spills on vinyl flooring with 30 to 300-second ignition delays

Contrary to spills on concrete substrates, where peak heat release rates decreased as ignition delay increased, the 1.0 L gasoline spills on vinyl resulted in an increase in peak heat release rate of close to 20 percent from 30 seconds to 150 and 167 seconds ignition delays. This could be the result of the fact that in these tests the spills were only permitted to spread for nominally 150 seconds as opposed to the 300-second ignition delay used in most other tests. This modified ignition delay time allowed the spill fire to grow to a larger area, thus increasing the mass burning rate per unit area, without having the issues of substrate properties and fuel evaporation that occur as a result of the 300-second delay time. These influences are discussed in more detail in Section 5.4.1

4.6.9 Carpet Results

Carpet spill fire tests were conducted using both gasoline and kerosene fuels with spill volumes of 0.5, 1.0, and 5.0 L (0.13, 0.26, and 1.3 gal.). Comparisons of gasoline and kerosene spill fire heat release rates at each fuel quantity are presented in Figure 4.43 to Figure 4.46. In general, the results from the duplicate tests were repeatable.

The spill fires on carpet substrates were generally not similar in behavior to those conducted on permeable and impermeable substrates. The heat release rate profile for these tests consisted of two relatively distinct peaks, as shown in Figure 4.43 to Figure 4.46. The initial peak occurring as a result of the rapid combustion of the fuel vapor and liquid fuel absorbed into the carpet material and the second peak occurring as a result of the involvement of the carpet and carpet padding material once ignited by the initial liquid fuel fire. The initial peak heat release rate (liquid fuel burning) tended to be significantly lower for the carpet substrates and the burning durations are much longer. This is due to the absorptive nature of the substrate, which creates a smaller spill area. In general, the carpet spill areas were two to three times smaller than those measured on most other substrates. This reduced spill area would lead to lower peak mass burning rates achieved during the burning duration thus explaining the lower peak heat release rates. In addition to this initial period of fire growth, there was significant contribution of the substrate itself when compared to other combustible substrates. The carpet and carpet padding, once involved, produced fires ranging in size from 150 kW to 1100 kW for spill volumes ranging from 0.5–5.0 L, respectively. Further discussion of the burning dynamics associated with carpet spill fires is provided below. Similar to spill fires on plywood and OSB, growth rate differences between gasoline and kerosene were seen for carpet spill fires, with kerosene lagging slightly behind gasoline. The peak heat release rates were slightly larger for kerosene than gasoline in the 0.5 L tests; however this difference was only about 15 percent. The 1.0 L spill fires exhibited much the same behavior as seen for the 0.5 L tests. There was good repeatability between duplicate tests for 1.0 L spill fires on carpet.

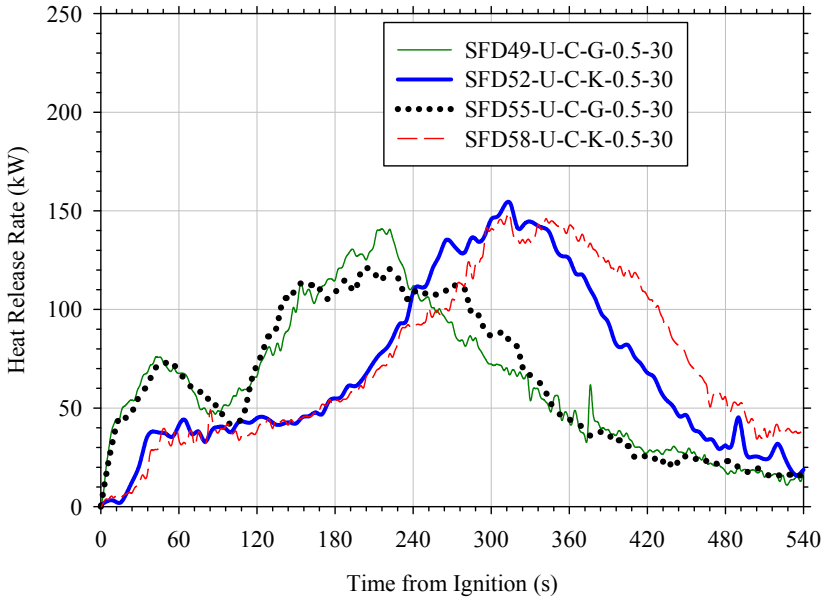

Figure 4.43. Comparison of 0.5 L (0.13 gal.) gasoline and kerosene spill fire heat release rates on carpet

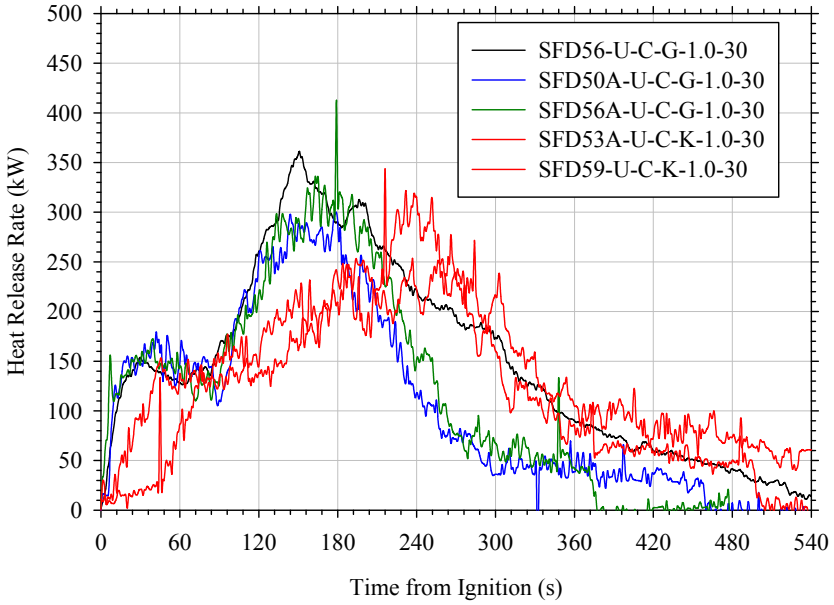

Figure 4.44. Comparison of 1.0 L (0.26 gal.) gasoline and kerosene spill fire heat release rates on carpet

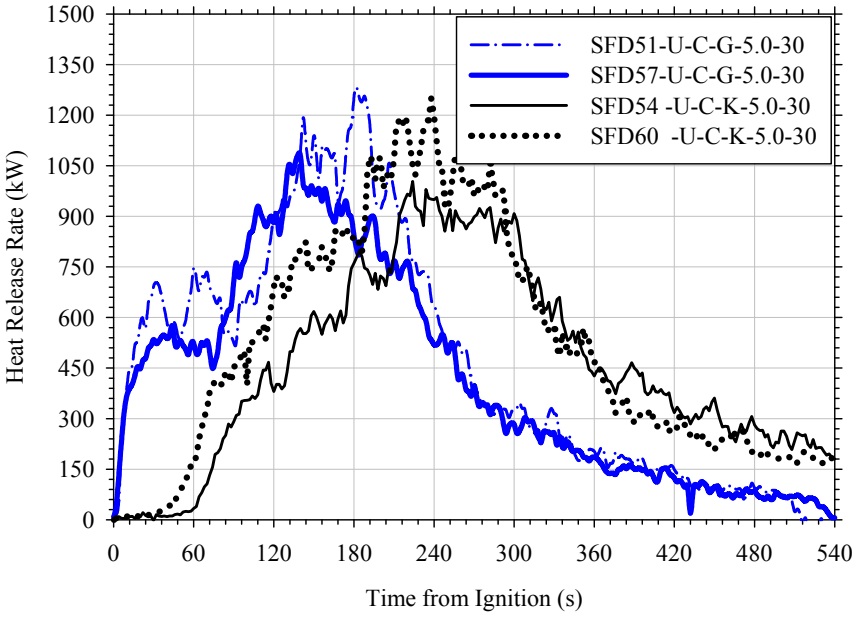

Figure 4.45. Comparison of 5.0 L (0.1.3 gal.) gasoline and kerosene spill fire heat release rates on carpet

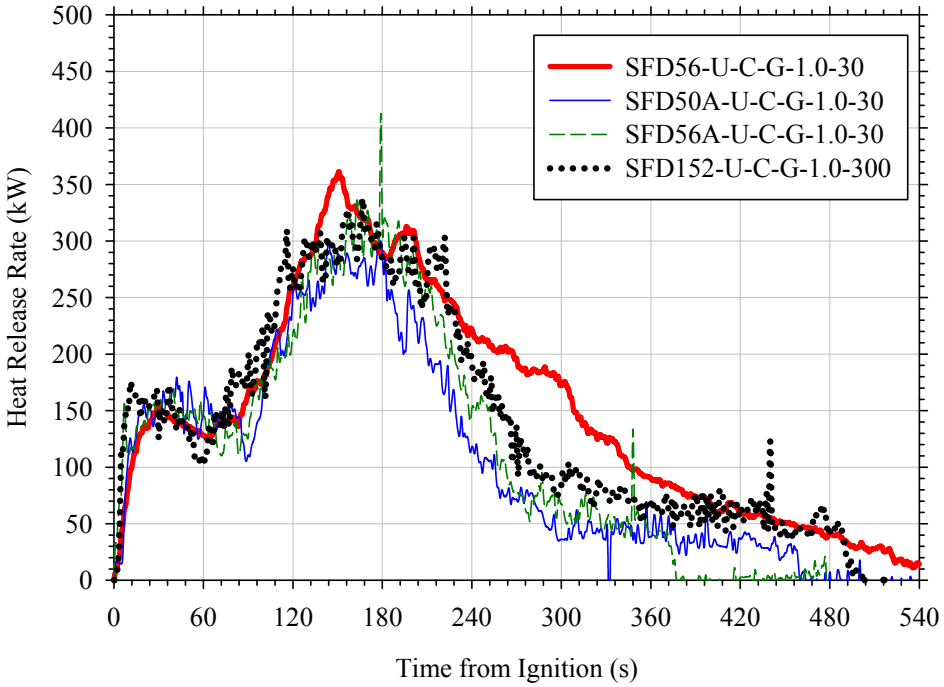

Figure 4.46. Comparison of 1.0 L (0.26 gal.) gasoline spill fire heat release rates from various ignition delay tests on carpet

As was expected, the peak heat release rate increases for increasing volume of liquid spilled. The heat release rate profiles are also very similar between the tests with the same fuels. For gasoline, these heat release rate profiles can be characterized by an initial peak and small steady state period followed by a growth period and a larger second peak. The growth period and second peak are attributed to the growth in fire area as the carpet and padding begin to burn. The kerosene tests have similar heat release rate profiles; however, initially there was not a peak as was seen for gasoline. Instead, the kerosene fires exhibit a growth period and only one later peak, occurring shortly after the time when the gasoline fires peaked. These behaviors can be seen in Figure 4.43 through Figure 4.45.

Due to the findings related to ignition delay for the various other substrates considered in this study, this variable was also considered for a subset of carpet spill fire tests. Figure 4.46 shows the heat release rates from the different ignition delay tests on carpet. Unlike that observed for all of the other substrates, the heat release rates resulting from fuel spills on carpet are independent of the ignition delay time for the time frames considered in this study.

4.7 Continuous Spill Fires

4.7.1 Test Procedures

Prior to filling the fuel tank, the volume and mass of the liquid being used were measured. Once filled, the fuel tank was pressurized with nitrogen to 34 kPa (5.0 psi). At this point, video image recording and data collection were started. The quarter-turn valve was opened to a point where there was a slight spout of fuel coming out of the tube at the center of the concrete pad. After approximately 5 seconds of fuel flow, at which point a spill approximately 0.5 m (20 in.) in

diameter had formed, the flowing fuel was ignited at the edge with a propane torch. Through the use of the needle and quarter-turn valves, the spill fire size was regulated to be approximately 1.2 m in diameter and kept approximately 0.2 m from the edge of the pad. During the initial 60 seconds of each test, fuel flow rates were manually metered until a constant spill size was achieved. After this initial 60 seconds the valves were not adjusted further and the spill fire was allowed to burn for 5 minutes. These 5 minutes were considered to be the steady state burning period because the spill size was constant and the fuel flow was constant. Still photographs were used to capture spill progression at various instances in time. Photographs were also used to capture the height of the spill front moving across the smooth concrete substrate.

After the 5 minutes of steady-state burning finished, the quarter-turn valve was closed and the spill fire self-extinguished. Data collection was terminated approximately 1 minute after self-extinguishment. Any remaining small flames were extinguished manually and photos of the substrate were taken of the surface pattern, if present. The concrete pad was then cooled down by placing buckets of ice on the surface. The pad was deemed cool when all sub-surface thermocouples were at or below a temperature of 22°C (72°F). Any remaining ice was cleaned off of the surface and the pad was dried by hand using towels.

4.7.2 Results

A total of three continuous spill fire tests were conducted on the modified smooth concrete pad. One test used denatured alcohol, while the other two used gasoline. These tests were intended to show the steady-state heat release rate of a spill fire over a period of approximately 4–5 minutes. Figure 4.47 and Figure 4.48 show the heat release rates for the gasoline and denatured alcohol tests, respectively. The results from the duplicate tests were repeatable.

The primary goal of the steady state heat release rates was to be able to compare the results to similar sized pool and non-continuous spill fires. Table 4.22 shows the steady-state average heat release rate, spill area, heat release rate per unit area, and burning duration. The data in the time before the steady-state period is included only to show the adjustments that were made to bring the spill fire to steady-state. This data was not included in any calculations.

Table 4.22. Comparison of Heat Release Rate Data and Spill Area for Continuous Spill Fires on Smooth Concrete

Test No	**Fuel**	**Steady State Burning Duration (s)**	**Area (m^2)**	**Average SS HRR (kW)**	**Average SS HRRPUA (kW/m^2)**
CSF2	Denatured Alcohol	302	1.235	338	274
CSF3	Gasoline	263	0.498	562	1129
CSF4	Gasoline	263	0.522	647	1239

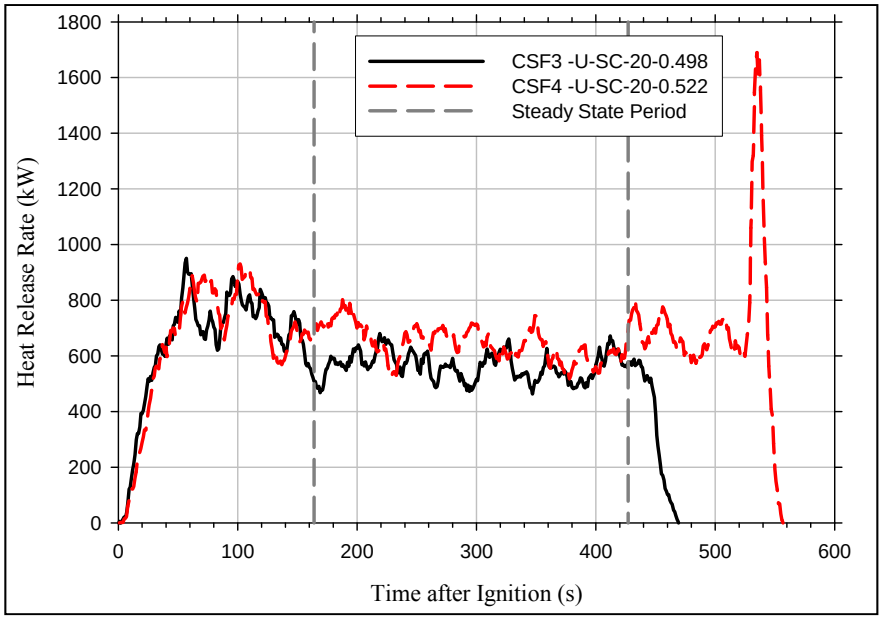

Figure 4.47. Comparison of steady state heat release rates for continuous gasoline spill fires on smooth concrete

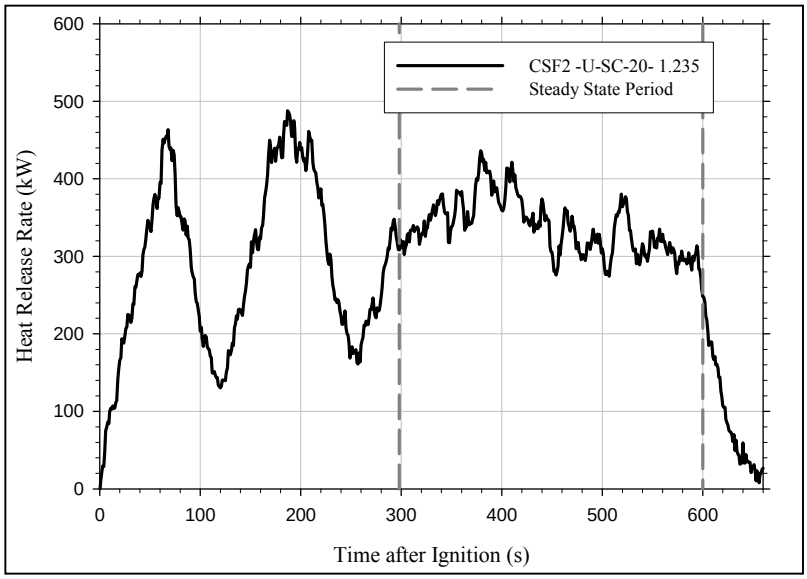

Figure 4.48. Comparison of steady state heat release rates for the continuous denatured alcohol spill fire on smooth concrete

5.0 ANALYSIS

The objective of this study was to characterize the fire dynamics of fuel spill fires under various conditions and on various substrates. A total of 284 fire tests were conducted in order to accomplish this objective. The analysis of this test data, presented in this section, provides an in depth understanding of spill fire dynamics and the dependencies of these dynamics on various parameters. The parameters specifically considered in this analysis were: fuel mass burning rate, fuel depth, substrate properties, and ignition delays.

5.1 Mass Burning Rates of Fuels

To date, the most comprehensive collection of burning rate data has been compiled by Babrauskas [8]. The majority of this data set is now 30–50 years old, which is irrelevant if considering pure fuels. However, when considering multi-constituent fuels (e.g., gasoline, kerosene, etc.) it is reasonable to assume that the components used in these fuels as well as the mixture ratios of these components may have changed with time. Recent surveys of the nation's gasoline by the Environmental Protection Agency (EPA) suggest that the volatility of gasoline has decreased and that the use of alcohols within gasoline mixtures has increased [36]. Consequently, it is important to verify that the data provided in these references, while technically sound, are still representative of the fuels in use today. Given the large set of fuel fire data collected in this study, the mass burning rates of the fuels used were compiled and compared to the data currently available in the literature to address the potential issues identified above.

5.1.1 n-Heptane Burning Rates

Initially, in order to verify that an appropriate and accurate methodology was adopted, the 10-second peak mass burning rate of a 0.093 m^2, 20 mm deep heptane pan fire was measured and compared to literature values. A plot comparing the predicted mass burning rates of heptane as a function of diameter and the experimental mass burning rate is provided in Figure 5.1.

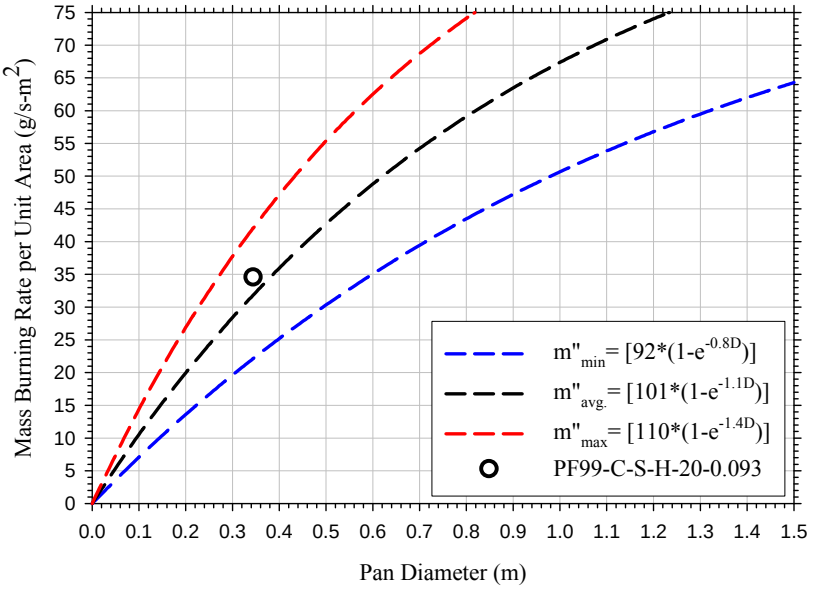

Figure 5.1. Comparison of predicted and experimental mass burning rates for n-Heptane

As expected, given that n-Heptane is a pure fuel, the experimental mass burning rate agreed very well with the predictions of the mass burning rate correlations using the fuel property parameters provided in the literature. The experimental mass burning rate was approximately eight percent higher than that predicted using the average fuel property parameters but fell well within the bounding scenarios developed using the parameters provided [8]. Based upon these results it was concluded that the methodology used to measure fuel mass burning rates was valid and consistent with prior work.

5.1.2 Gasoline Burning Rates

A total of 85 gasoline fires were conducted with fuel layer depths ranging from 0.2–20 mm. A summary of the 10-second peak mass burning rates for these tests are compiled in Figure 5.2. In Figure 5.2, the calculated mass burning rates for gasoline at various fuel layer depths are compared against the empirical correlation developed by Burgess et al. [9] using the maximum mass burning rate and kβ values provided by Babrauskas [8]. This correlation does not take into account any fuel layer depth/fuel quantity effects; thus, an identical trend line is presented in all four plots shown in Figure 5.2.

In general, the 10-second peak mass burning rates achieved in the gasoline fires increased as the quantity of fuel available (i.e., fuel depth) increased for these tests. For all fuel depths, except the 1 mm depths, these values also increased as a function of increasing pool diameter as suggested by the empirical correlation [8, 9]. However in most cases, the gasoline mass burning rates measured in this study were lower than the value predicted by the mass burning rate correlation using the standard input parameters (i.e., 55 g/s-m^2 and 2.1) and were even found to be lower than the predictions made using the bounding values provided by Babrauskas for gasoline. The 1 mm fuel depths resulted in an average peak mass burning rate of 16 g/s-m^2, approximately one-quarter of that predicted by the empirical correlation. These values are consistent with the findings of Putorti [3] who found unconfined gasoline spill fire mass burning rates of 11 g/s-m^2. For the 5, 10, and 20 mm fuel depths, the empirical correlation slightly over-predicted the measured mass burning rates; however, the magnitude of the over prediction decreased as fuel depth increased. A summary of the average 10-second peak mass burning rates measured in this study compared to the range of values predicted by the correlation provided in Eq. 1-1 is provided in Table 5.1.

As shown in Table 5.1 the application of the maximum mass burning rate and kβ values provided by Babrauskas [8] to the mass burning rate correlation generally over-predicted the measured mass burning rates of gasoline for a range of fuel depths and fire areas. The differences between the measured and predicted mass burning rates ranged from 0–38 percent with smaller differences being observed in scenarios with larger quantities of fuel available to burn, which is consistent with the literature in that the data compiled by Babrauskas was solely based upon testing conducted with deep pool fires and large quantities of fuel. In Figure 5.2, the mass burning rates approach the predicted values as the quantity of fuel (i.e., fuel depth) increases. Furthermore, at the largest fire sizes and fuel quantities, the experimental mass burning rates are trending towards the asymptotic value of 55 g/s-m^2.

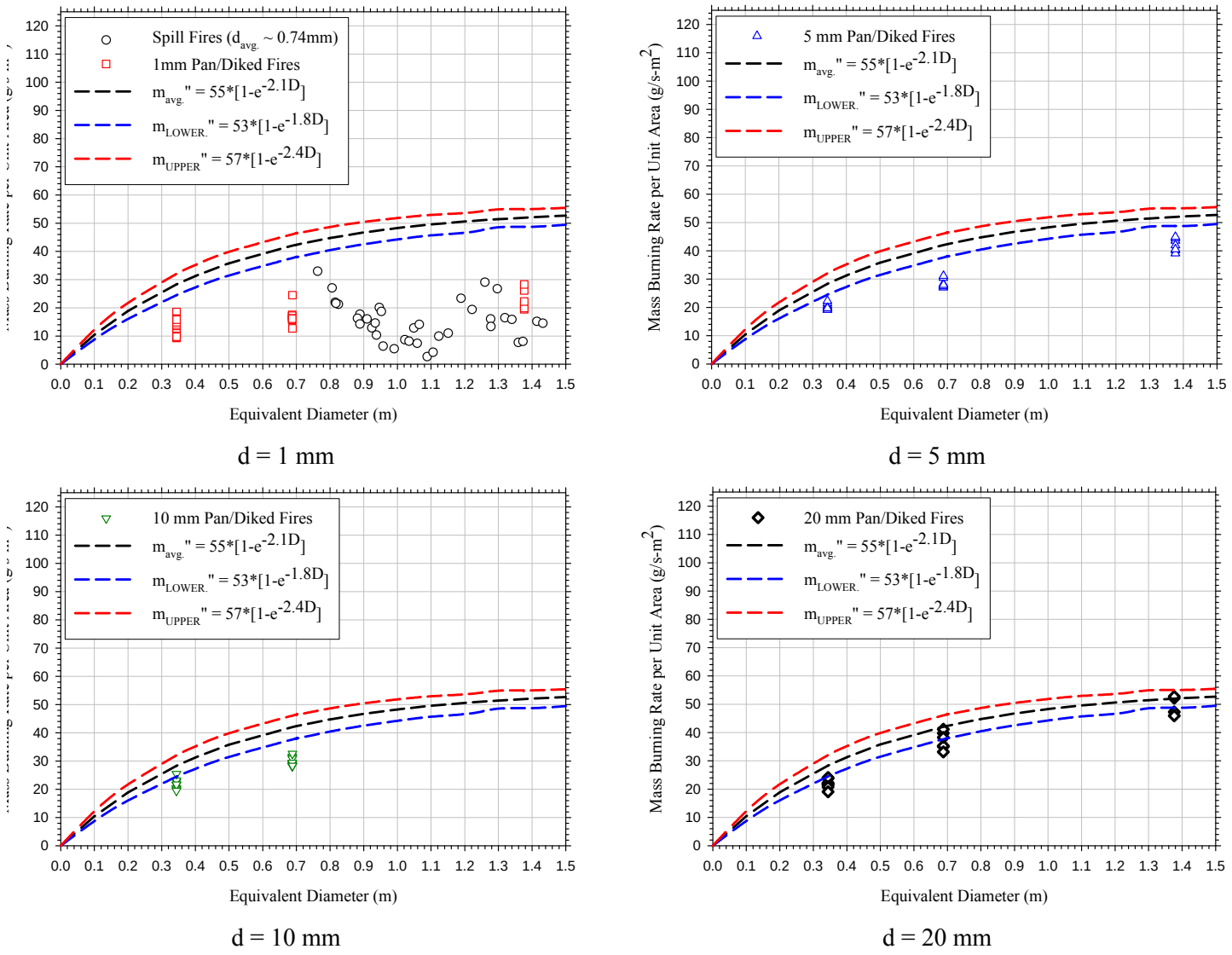

Figure 5.2. Calculated 10-second peak mass burning rates for all gasoline fires conducted compared to empirical mass rate correlation assuming a maximum burning rate of 55 g/s-m^2 and kβ of 2.1 as suggested by Babrauskas [8]

Table 5.1. Comparison of Measured and Predicted Gasoline Mass Burning Rates

Equivalent Fire Diameter (m^2)	**Fuel Depth (mm)**	**10 s Peak Mass Burning Rate ($g/s\text{-}m^2$)**	**Predicted Mass Burning Rate ($g/s\text{-}m^2$)***	**% Difference***
0.34	5	20	24–32	8–38
	10	22		
	20	22		
0.69	5	29	38–46	3–37
	10	30		
	20	37		
1.38	5	42	49–55	0–24
	20	50		

* Range of values presented is based upon standard deviations provided by Babrauskas for maximum mass burning rates for gasoline (53–57 $g/s\text{-}m^2$) and kβ (1.8–2.4) [8].

The tests conducted in this study considered more than just area as a variable; thus it was necessary to develop a means of addressing both area effects as well as fuel depth (fuel quantity) effects for fire scenarios. Given that at deep enough depths (e.g., 20 mm) the existing mass burning rate correlation with the fuel specific input parameters provided in the literature reasonably predict the mass burning rate of gasoline, a leading coefficient for the existing mass burning rate correlation [Burgess et al., 1960] was developed to address the fuel depth (fuel quantity) effects observed in this study. In order to accomplish this, the experimental mass burning rates were normalized with respect to the maximum mass burning rate observed in this study for each fuel and correlated to the initial depth of the burning fuel layer. Correlation of the data was accomplished using power law best fits which were calculated for the average, minimum, and maximum data measured for the varying fuel depths. These equations, shown in Figure 5.3, can be used to calculate a depth coefficient that can be multiplied by the maximum mass burning rate for a specific fuel in order to obtain a mass burning rate that is both fuel depth and spill area specific. For example, the general form of the mass burning rate per unit area as a function of fuel area, D, and fuel depth, δ, is given as

$$\dot{m}''(D,\delta) = C_\delta * (\dot{m}''_\infty(1 - e^{-k\beta D}) \qquad \text{Eq. 5-1}$$

where C_δ is derived from the curve fit shown in Figure 5.3, $\dot{m}''_\infty$ is the maximum mass burning rate of the fuel, $k\beta$ is the product of the extinction coefficient and the mean beam length corrector, and D is the equivalent diameter of the spill.

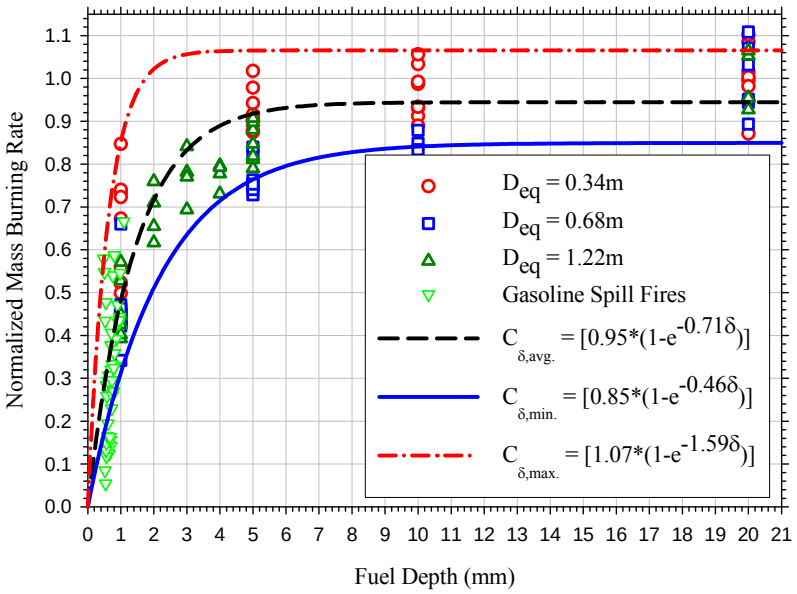

Figure 5.3. Summary of peak mass burning rates and best fit curves for all gasoline fires conducted

As shown in Figure 5.3, the average depth coefficient trend line produces a value of 0.95 at a depth of 5 mm. This is consistent with the conclusion that at depths greater than 5 mm the affect of depth need not be accounted for when calculating the mass burning rate of a fuel. In general, the best fit lines shown in Figure 5.3 capture the vast majority of the mass burning rate data collected.

5.1.3 Kerosene Burning Rates

Figure 5.4 compares the measured 10-second peak mass burning rates of the kerosene spill fires to the empirical correlations developed by Burgess et al. [1960] using the maximum mass burning rate and kβ values provided by Babrauskas [1983]. The mass burning rate correlation over-predicts values for the 1, 5, and 10 mm fuel depths. Only with a fuel layer of 20 mm did the empirical correlation simulate the experimental mass burning rates.

At fire diameters less 0.75 m (2.5 ft), the average kerosene mass burning rate for a 1 mm fuel layer was 10 g/s-m^2, approximately one-quarter that predicted by the empirical correlation. Based upon the limited 1 mm depth fires larger than 0.75 m (2.5 ft) in diameter, an average mass burning rate of 23 g/s-m^2 was measured, approximately one-quarter that predicted by the empirical correlation. For the 5, 10, and 20 mm fuel depths, the empirical correlation slightly over-predicted the mass burning rates, however, the magnitude of the over prediction decreased as fuel depth increased. This finding makes sense, given that the maximum mass burning rate values used in the correlations were primarily developed from 'deep' or continuously fed pan fires. A summary of the average 10-second peak mass burning rates measured in this study compared to the range of values predicted by the correlation provided in Eq. 1-1 is provided in Table 5.2.

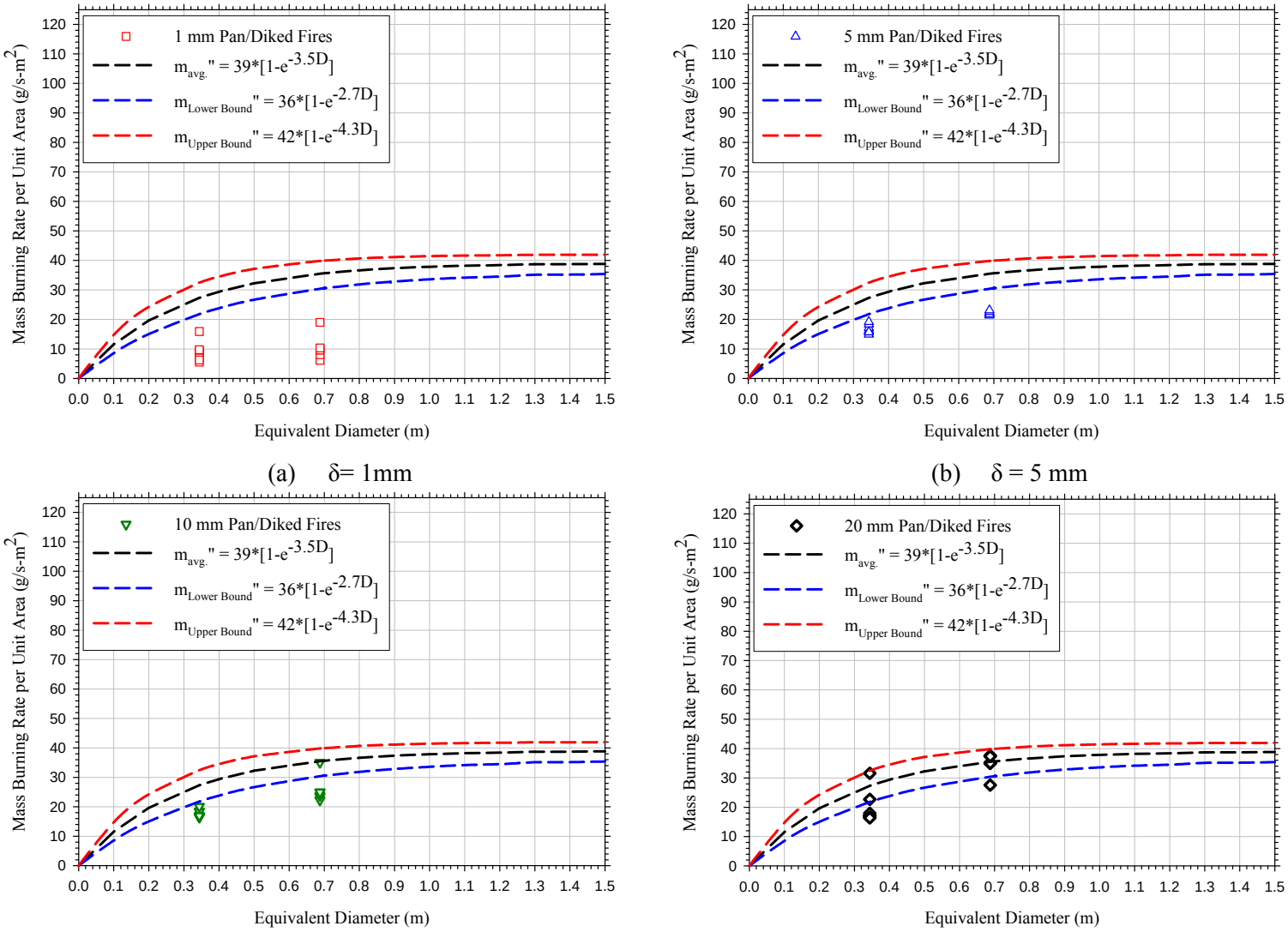

Figure 5.4. Calculated 10-second peak mass burning rates for all kerosene fires conducted compared to empirical mass rate correlation assuming a maximum burning rate of 39 g/s-m^2 and kβ of 3.5 as suggested by Babrauskas [8]

As shown in Table 5.2, the mass burning rate correlation based on literature values [8] generally over-predicted the measured kerosene mass burning rates for the 0.344 m (1.1 ft) and 0.688 m (2.3 ft) diameter fires with the exception of the 20 mm scenario in the larger pan, which is predicted relatively accurately.

Table 5.2. Comparison of Measured and Predicted Kerosene Mass Burning Rates

Equivalent Fire Diameter (m^2)	**Fuel Depth (mm)**	**10 s Peak Mass Burning Rate (g/s-m^2)**	**Range of Predicted Mass Burning Rates (g/s-m^2)***	**Maximum % Difference***
0.344	5	17	22–32	9–47
	10	18		
	20	20		
0.688	5	22	30–40	(17)**–45
	10	26		
	20	35		

* Range of values presented is based upon standard deviations provided by Babrauskas for maximum mass burning rates for kerosene (36–42 g/s-m^2) and kβ (2.7–4.3).

** Values in parentheses indicate the under-prediction of the correlation relative to the experimental mass burning rate.

An approach similar to that taken in the analysis of the gasoline burning rates was undertaken to develop mass burning rate correlations for kerosene that not only account for the effects of varying diameter but also varying fuel depth. The experimental mass burning rates were normalized with respect to the maximum mass burning rate reported by Babrauskas and correlated to the initial depth of the burning fuel layer. Correlation of the data was accomplished using power law best fits which were calculated for the minimum, average, and maximum data measured for the varying fuel depths. These equations, shown in Figure 5.5, were used to calculate a depth coefficient that can be multiplied by the diameter dependent maximum mass burning rate for a specific fuel, as shown in Eq. 5-1. The product of these two values will be a mass burning rate that is both fuel depth and spill area specific.

5.1.4 Denatured Alcohol Burning Rates

The burning rates from the limited number of denatured alcohol pan fires were compared to data available in the literature. All denatured alcohol tests were either conducted in the 1.49 m^2 (16 ft^2) steel pan or conducted as spill fires on various substrates (coated concrete, vinyl, OSB, and plywood). Given that alcohol fires generally produce minimal radiative energy the mass burning rates for these fuels are often considered as constants. However, recent data described by Babrauskas [2008] suggests that the mass burning rates of alcohol fuel fires are diameter dependent and three different burning rate regimes are described. The burning rate regime selected for comparison to the denatured alcohol data collected was 22 g/s-m^2 which was recommended for fire diameters ranging from 0.6–3 m (2–10 ft). This range encompassed all of the diked and spill fire data presented in Figure 5.6.

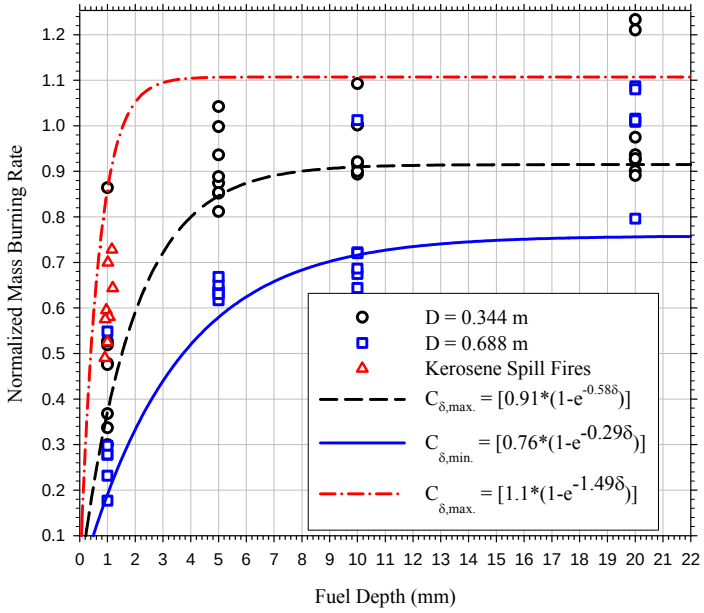

Figure 5.5. Summary of mass burning rates and best fit curves for all kerosene fires conducted

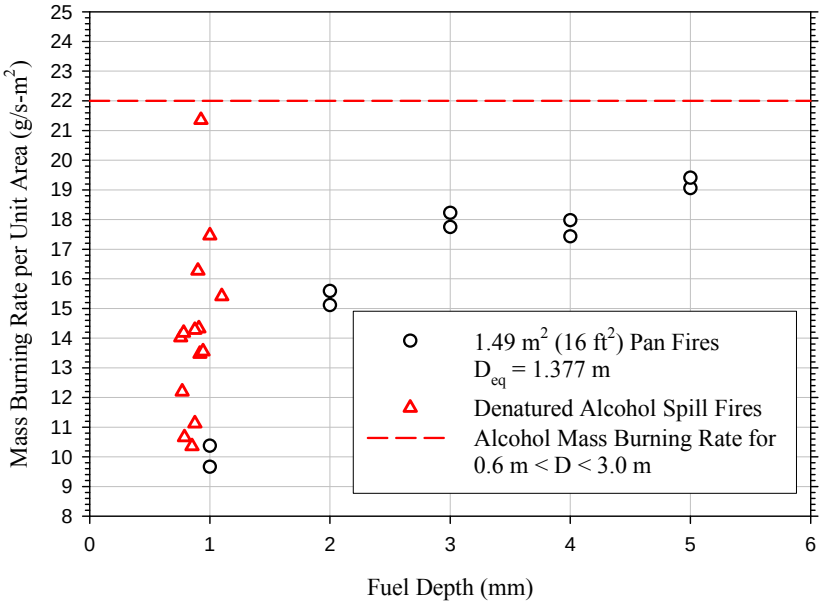

Figure 5.6. Comparison of measured 10-second peak mass burning rates per unit area for all denatured alcohol fires and recommended mass burning rate for alcohol fires with equivalent diameters between 0.6 and 3 m [Babrauskas, 2008]

The 10-second peak mass burning rates measured at the various fuel depths evaluated was consistently less than the recommended mass burning rate for fire diameters ranging from 0.6–3 m. The measured rates ranged from 14–55 percent less than the predicted value; the difference decreased with increasing fuel depth. The significant variability in the mass burning rates measured for the spill fire tests is most likely an artifact of the differing substrates on which the tests were conducted. In general, the lowest mass burning rates were measured on the coated

concrete substrate with larger values obtained for tests conducted on the wood and vinyl substrates. It should also be noted that similar to that observed on both the gasoline and kerosene burning rate analyses, as the fuel depth/fuel quantity was increased, the burning rate per unit area was observed to increase.

5.2 Variables Impacting Mass Burning Rates

At the beginning of this study, one hypothesis was that the reduced fire sizes reported for spill fires with relatively thin (i.e., ≤ 2 mm) fuel depths were a result of heat losses from the burning fuel to the fuel substrate. In other words, the reduced mass burning rates of the thin fuel depth fires was believed to be primarily a function of the thermal properties of the substrate. This hypothesis was based upon testing conducted by Gottuk et al. [2] and Putorti [3] who found that spill fire burning rates were on the order of one-fifth that of traditional pool fire burning rates. Similar findings were also reported by Garo et al. [24] who attributed the reduced mass burning rates of fuels burning atop a water substrate to the 'heat sink effect' of the water sub-layer. Analysis of these data sets resulted in the conclusion that the differences between the burning rates of thin fuel layers and those reported in the literature, typically deep fuel layers, were potentially due to the differing heat transfer phenomena occurring within a deep fuel layer (k = 0.11 W/m-K) versus a thin layer atop a more conductive substrate (i.e., concrete [k = 1.4 W/m-K]). Based upon these data [2, 3, 24] it was concluded that unconfined fuel spills, producing very thin (i.e., ≤ 1 mm [0.04 in.]) fuel depths, experience greater heat losses to the spill substrate thus reducing the amount of heat retained within the burning fuel layer and consequently reducing the fuel mass burning rate [1].

However, further development of this hypothesis resulted in the question that if heat losses were the only factor contributing to the decreased fire size, then it could be expected that fuels burning atop substrates whose thermal properties are comparable to those of a 'deep' pool of fuel would result in fire sizes comparable to those achieved in 'deep' pool burning. For example, consider a wood substrate with a thermal conductivity comparable to that of fuel (k_{wood} = 0.15 W/m-K and k_{fuel} = 0.19 W/m-K). The data reported by Putorti [3] and that measured in this work indicate that the mass burning rate of a fuel spill fire was in fact significantly reduced even when burning atop a wood substrate, just as observed for more conductive materials. These results suggest that additional factors are contributing to the decreased burning rates commonly observed for thin fuel layer fires. Analyses were performed to characterize the impact of fuel substrate, fuel quantity, and spill area regression in order to determine which factors have the most influence on the mass burning rate.

5.2.1 Substrate Effects

The effect of the substrate on the mass burning rate of a fuel is examined in this section. Figure 5.7 presents the average 10 s peak mass burning rates from 1 mm (0.04 in.) gasoline fires burning atop four different substrates at three different fire sizes (i.e., pan and diked fires). The figure also provides comparison of these measured burning rates to the maximum burning rates predicted by the correlation described in Eq. 1-1. For the gasoline fires evaluated, these comparisons show that the substrate influences the peak mass burning rate achieved. The measured burning rates were consistently lower than that predicted using Eq. 1-1 and mass burning rate data provided in the literature. The mass burning rates presented in Figure 5.7

increase with equivalent fire diameter and do so in a qualitative manner consistent with the correlation developed in the literature [Burgess, 1960].

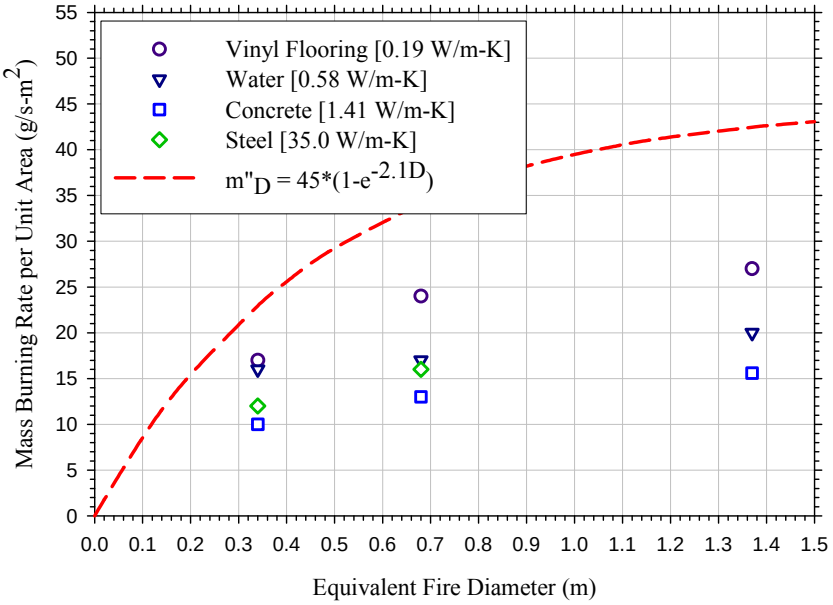

Figure 5.7. Comparison of peak mass burning rates per unit area for 1 mm (0.04 in.) gasoline fires atop substrates with various thermal conductivities

The rank order of the mass burning rates for each fire size were consistent, with the highest burning rates occurring on the vinyl flooring and the lowest on concrete. For the scenarios evaluated, no specific thermal property of the substrates (i.e., thermal conductivity, thermal inertia, thermal effusivity, and thermal diffusivity) could be directly correlated to the rank order of burning rates. In general, less thermally conductive materials (i.e., vinyl and water) produced mass burning rates higher than those achieved in tests with more thermally conductive substrates (i.e., steel and concrete). However, the ranking of mass burning rates with respect to the thermal conductivity of the substrates was not appropriate when evaluating the case of the concrete and steel. In this case, the mass burning rates measured on the concrete were consistently lower than those measured on the steel despite the fact that the thermal conductivity of the steel is an order of magnitude larger than that of the concrete. This discrepancy may be attributed to the reflectivity of the steel and the resulting re-radiation from the steel substrate to the fuel layer. This reflected heat was then transferred into the fuel layer thus raising the mass burning rate of the fuel.

5.2.2 Fuel Quantity Effects

Further analysis was performed to determine if parameters other than substrate have an effect on the mass burning achieved by a fuel for a given fuel spill scenario. The next parameter evaluated and found to have an impact on the peak mass burning rate was the burning duration. The impact of this parameter was first identified in the fixed area pan and diked results and was confirmed using the data obtained in the continuous spill fire testing conducted. Initially this impact was attributed to the depth of fuel present at the time of ignition based upon the fixed area

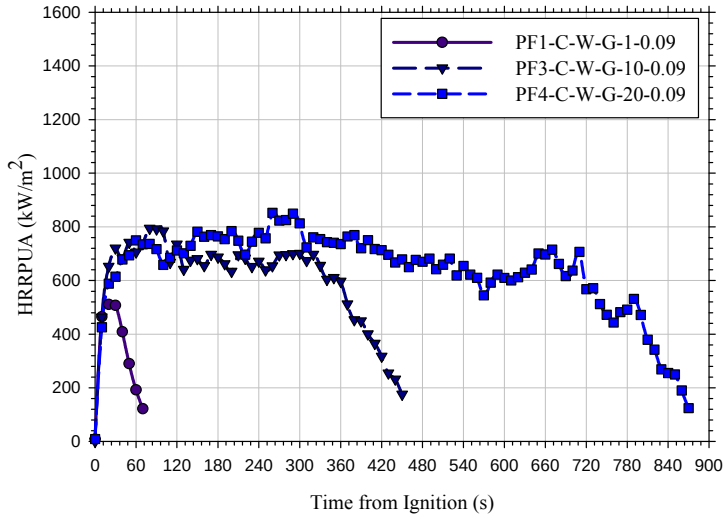

(a) 0.09 m^2 – Gasoline on Water

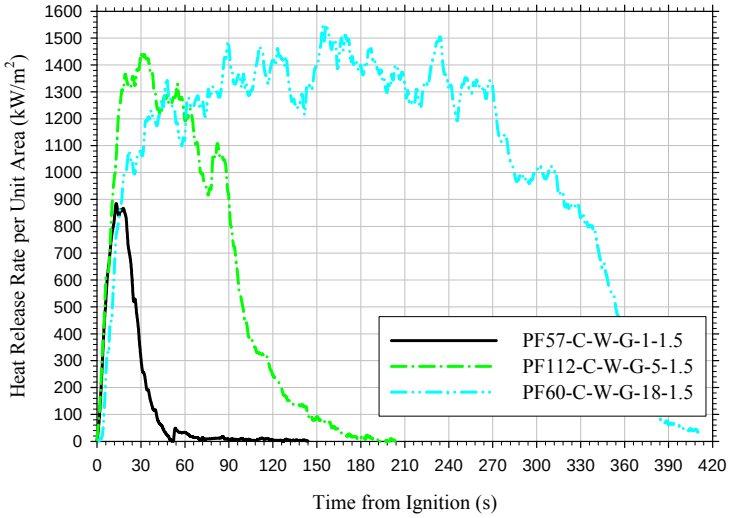

(b) 1.49 m^2 – Gasoline on Water

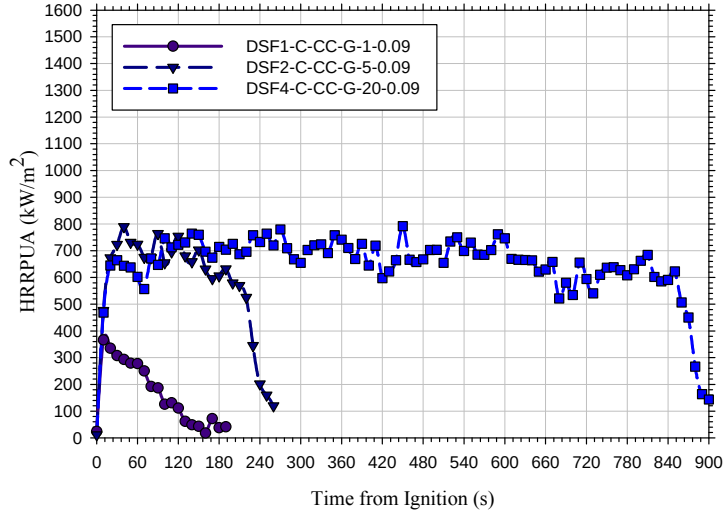

(c) 0.09 m^2 – Gasoline on Coated Concrete

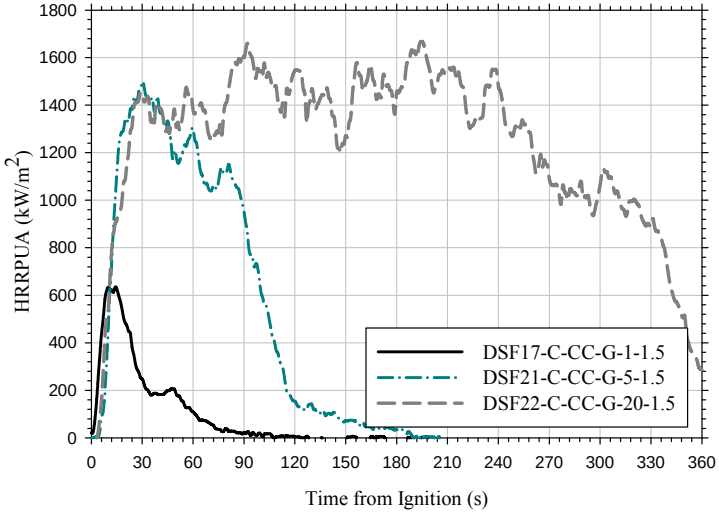

(d) 1.49 m^2 – Gasoline on Coated Concrete

Figure 5.8. Heat release rate per unit area curves for four different fixed area, confined fire scenarios

fire data collected. As presented earlier in Sections 4.3 and 4.4, as well as in the examples provided in Figure 5.8, the results from the range of fuel depths evaluated in these tests suggested that for gasoline depths ≥ 5 mm, the peak mass burning rates achieved are comparable.

However, analysis of the continuous spill fire data set demonstrated that the use of depth as a parameter influencing fuel mass burning rates was not necessarily the governing factor. For the spill fire scenarios, a nominal 1 mm fuel depth with a constant area was maintained for an extended period of time through a continuous supply of fuel that was equal to the mass of fuel being consumed in the fire. The burning rates measured in these scenarios, as shown in Figure 5.9 and 5.10, were found to be comparable to those achieved in 'deep' pool fires (i.e., ≥ 5 mm) not those measured for the thin fuel depth scenarios.

The results of the continuous spill fire tests show that fuel depth is not the actual parameter influencing the peak burning rate achieved. Instead these results indicate that the burning duration is the most influential factor affecting the maximum burning rate in a given fuel fire scenario. Based upon the results from both fixed area and unconfined spill fire testing it was determined that the burning duration dictates what fraction of the maximum mass burning rate can be achieved for a given fire scenario.

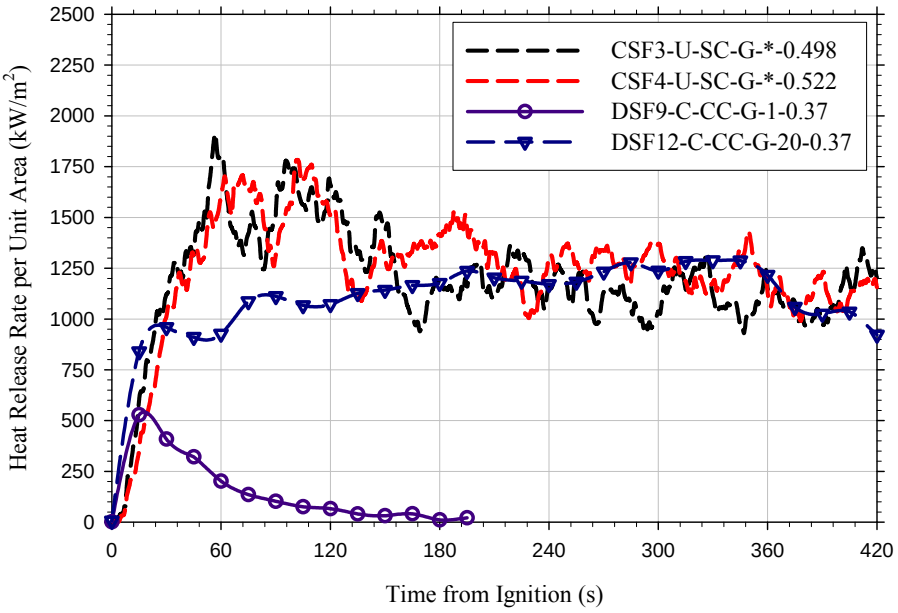

Figure 5.9. Comparison of HRRPUA data from fixed area gasoline fires of varying depth and continuously-fed gasoline spill fires

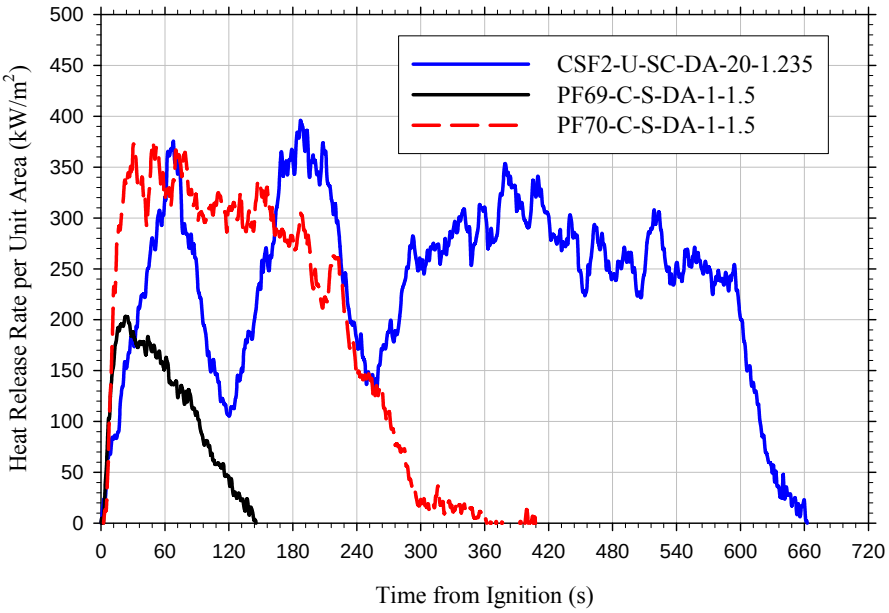

Figure 5.10. Comparison of HRRPUA data from fixed area denatured alcohol fires of varying depth and a continuously-fed denatured spill fire

In order to accurately describe the burning of a thin fuel spill fire it is necessary to understand the point at which a spill with a fixed quantity of fuel will stop growing (i.e., at what fraction of fuel consumption is fire growth inhibited), thus initiating the decay of the fire. An analysis of fixed area fires (i.e., diked and pan fires) was conducted to examine the fraction of fuel remaining at the time of decay for each fire. This fraction was calculated using the transient total heat released and the measured average effective heat of combustion to calculate mass consumed. At each time step, the total heat released was divided by the heat of combustion and subtracted from the initial mass of fuel present in order to quantify the mass of fuel remaining during each fire. Since some fires did not have a distinct single peak before decaying, the time of decay was identified as the time at which the fire reached a heat release rate that was seventy-five percent of its peak during the decay phase of the fire. The results of this analysis are provided in Figure 5.11 which correlates the percent of mass consumed at time of decay to the initial spill depth of the fuel for all fixed area fires. The gasoline and kerosene data presented in Figure 5.11 represent the average of multiple tests conducted on four different substrates for a given fire diameter. Standard deviations for the gasoline tests ranged from 0.04–0.08 and for the kerosene values ranged from 0.04–0.12. Replicate denatured alcohol tests were not conducted; thus statistical analysis could not be performed.

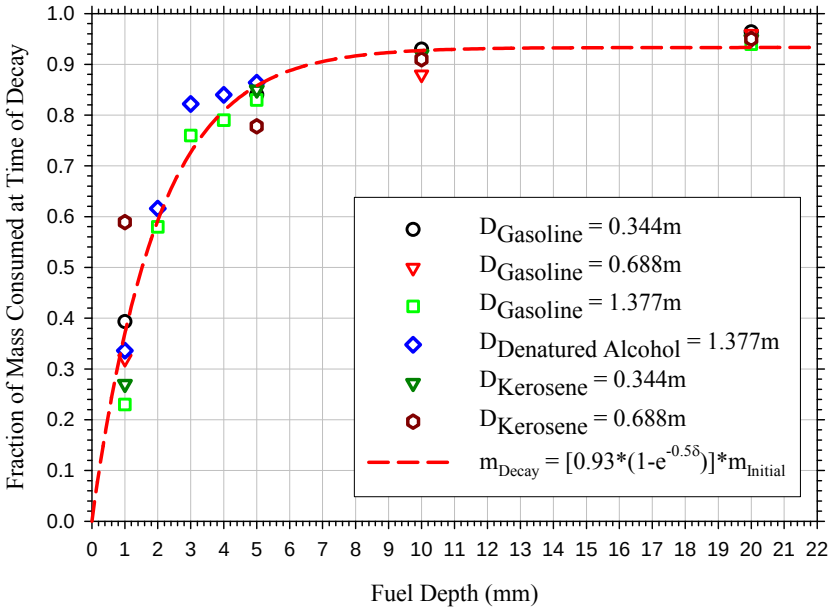

Figure 5.11. Correlation of fraction of mass consumed at time of decay for all fixed area fuel fires to initial fuel depth

As shown in Figure 5.11, the fraction of mass consumed at the time of decay ranged from 0.23–0.96 and generally increased as a function of fuel depths/fuel quantity. In general, it was found that the fraction of mass remaining at the time of decay for all fuel types and fire sizes could be correlated to the initial fuel depth relatively well, regardless of fuel type or fire area. For the thinner fuel depths, the fraction of mass consumed at the time of decay ranged from 0.23–0.62. In all other cases (i.e., depths greater than 2 mm) the fraction of mass consumed was greater than 0.75 with maximum values as high as 0.96. In order to further understand the conditions at which the fires ceased to grow, the fraction of mass consumed at the time of decay was used to derive the mass of fuel remaining.

The mass of fuel remaining was used to calculate the average fuel depth at the time of decay. The fuel depths at the time of decay ranged from 0.22–0.85 mm with an average value of 0.55 mm. It should be noted that the average fuel depth of 0.55 mm assumes a perfectly flat, impermeable surface which in most cases is not representative of real world scenarios. It is likely that it is not the fuel depth of 0.55 mm that causes the decay but instead it is the inability of the remaining fuel to retain a uniform burning surface atop the substrate (i.e., areas of fuel starvation lead to a smaller surface area of burning thus a smaller heat release rate is measured). Despite this fact, the 0.55 mm (0.02 in.) fuel depth does provide a strong indication as to when fire growth ceases for the range of fire sizes and fuels considered in this study and when coupled with an appropriate mass burning rate could be used to predict the growth and decay of a fixed quantity fuel spill fire.

5.2.3 Impact of Carpet as a Substrate

A total of 17 spill fire scenarios were conducted on various configurations of carpet flooring with fuel quantities ranging from 0.5–5 L. These tests were conducted with both gasoline and

kerosene. Comparisons of the 10 s peak mass burning rates to the predicted maximum mass burning rates for both gasoline and kerosene carpet fires are provided in Figure 5.12.

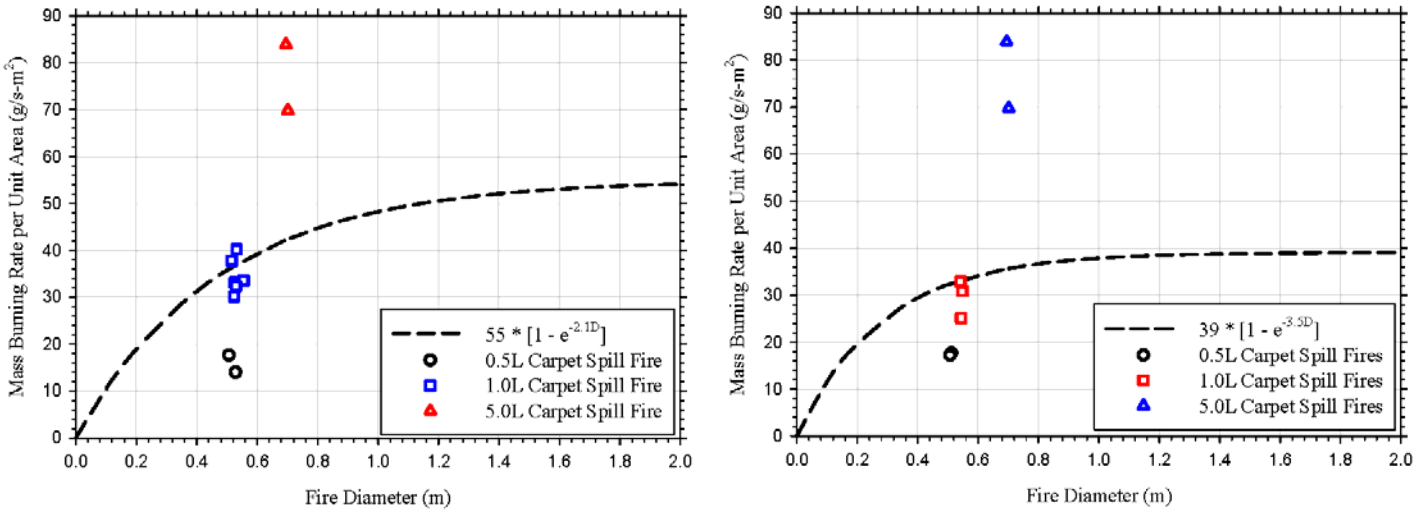

Figure 5.12. Comparisons of carpet spill fire mass burning rates to the maximum mass burning rate correlations (Eq. 1) for gasoline (left) and kerosene (right)

In general, the 1 L (0.26 gal.) spills resulted in mass burning rates that were most consistent with the mass burning rates predicted for free-burning pool fires using the Burgess et al. equation. However, this result should be taken as a uniquely fortuitous of the carpet and spill mechanism used in this testing and is not indicative of all carpet and spill scenarios. The carpet is completely saturated with fuel when 1.0 L is discharged onto the carpet. For the purposes of this discussion, saturation of the carpet is considered to be when the vast majority of the fuel spilled is absorbed into the carpet/padding to the point where the carpet can hold no more liquid. Consequently, the carpet fibers provide an effective means of mass transport (i.e., wicking) which allows the fuel to burn at a rate comparable to that of free-burning pool fires.

For scenarios where only one-half liter was spilled, the maximum mass burning rates were found to be consistently lower than the predicted values for both gasoline and kerosene. Furthermore, for scenarios in which five liters was spilled the mass burning rates were found to be significantly larger than that predicted for both fuels. The reduced mass burning rates obtained in the 0.5 L (0.13 gal.) spills are most likely a result of a reduced degree of mass transfer relative to the 1.0 L tests due to only partial saturation of the carpet. This partial saturation results in fuel vapor concentrations lower than those typically found at the surface of a free-burning liquid pool. With larger quantity spills (i.e., 5 L [1.3 gal]), the carpet becomes over-saturated with fuel (i.e., the carpet is saturated and residual fuel is left in the void spaces of the carpet pile. As a result of this condition, not only is an effective means of mass transport developed via wicking, but the residual fuel is also burning in the form of a fuel layer in the void spaces of the carpet.

Similar findings were reported by Ma et al. [2004] based upon a series of small-scale tests evaluating the burning rates of liquid fuels on porous media. Ma reported that when a sufficient quantity of fuel was supplied, the mass burning rates for the fuel on the carpet were significantly larger than the burning rates of the fuel floating on water. Furthermore, with relatively little fuel in the carpet, the mass burning rates were lower than the fuel on water burning rates. Due to the

fact that these tests were conducted at a relatively small-scale (D = 0.1 m [3.9 in.]) the authors concluded that in addition to the effects of the carpet on the mass burning rate of the fuel (i.e., more efficient mass transfer due to wicking in the carpet fibers) these results were also potentially an artifact of the boundary conditions present during the test.

Although all 1 L (0.26 gal.) spill fires in this study had mass burning rates comparable to that predicted by the Burgess et al. [9] correlation, this should not be viewed as a fuel quantity dependent result. It should be noted that in these carpet spill fire scenarios it is not the quantity of fuel spilled that dictates whether or not the mass burning rate will follow existing correlations, it is the combination of the quantity spilled and the area over which the fuel is dispersed. This spill area per unit volume parameter is potentially a more appropriate parameter to be used, however, it not unreasonable to assume that this parameter is carpet specific thus the results from the carpet used in this study are not necessarily applicable to other carpet types. The correlation between this parameter and the behavior of a fuel mass burning rate on carpet was tabulated and is presented in Table 5.3.

Table 5.3. Summary of Spill Area per Unit Volume Parameter and Mass Burning Rate Data for Carpet Spill Fires of Various Quantities

Fuel	Spill Qty. (L)	A/V (m^2/L)	10 s Peak Mass Burning Rate (g/s-m^2)	Predicted Mass Burning Rate (g/s-m^2)
Gasoline	0.5	4.8	15.8	36
	1.0	4.5	34.3	36
	5.0	2.6	76.8	42
Kerosene	0.5	4.9	17.5	32
	1.0	4.3	29.6	32
	5.0	2.5	63.9	36

As shown in Table 5.3 for both fuels, the spill area per unit volume parameters for the 0.5 and 1.0 L spills are very similar while the 5 L values are significantly less. The fact that the 0.5 L spills had similar spill areas per unit volume supports the hypothesis that the reason for the reduced mass burning rates observed in this scenario was partial saturation. The smaller area per unit volume for the 5 L spills support the hypothesis that the carpet in these scenarios was over-saturated with fuel. In these scenarios nearly double the amount of fuel present in the 1 L spills was available to burn resulting in the burning of the fuel due to the wicking of the carpet fibers as well as the burning of the fuel at the base of the carpet. Although further experimental work would be required, based upon these results, the burning rate of a fuel on a carpet substrate could be correlated to an area per unit volume parameter. However, this would require knowledge of both the fuel quantity and an approximate spill area which are often difficult data points to obtain.

5.3 Spill Dynamics

A variety of fuels and fuel simulants were used to characterize the spill dynamics of liquids spilled onto various substrates. The liquids and substrates used in this testing were selected to bound most real-world spill fire scenarios. The properties used in this selection process were

primarily surface tension/contact angle and viscosity with respect to the liquids and surface energy and absorption with respect to the substrates. In total, 86 spill dynamics tests were conducted.

5.3.1 Spill Depth Analysis

Statistical analyses of the spill dynamics data sets were performed as a group as well for specific data subsets in order to characterize representative spill depths, spill areas, etc. A summary of this analysis is presented in Table 5.4.

Table 5.4. Statistical Analysis of Spill Dynamics Testing

Liquid	Substrate	Average Depth (mm)	Standard Deviation (mm)	Min. (mm)	Max. (mm)
All*	All	0.72	0.34	0.22	2.4
Fuel	All	0.74	0.19	0.45	1.2
Simulants*	All	0.69	0.49	0.22	2.4
All*	Coated Concrete	0.66	0.18	0.32	0.96
All*	Smooth Concrete (NIJ)	0.53	0.08	0.38	0.64
All*	Smooth Concrete (ATF)	0.53	0.20	0.25	0.84
All*	Brushed Concrete	0.76	0.26	0.53	1.5
All*	Vinyl	0.63	0.26	0.22	1.0
All*	Plywood	1.02	0.41	0.38	1.6
All*	Oriented Strand Board	1.04	0.51	0.61	2.4
Gasoline	All	0.71	0.15	0.48	1.1
Denatured Alcohol	All	0.79	0.17	0.56	1.1
Kerosene	All	1.01	0.10	0.91	1.2
3% AFFF	All	0.43	0.15	0.22	0.70
3% FP	All	0.97	0.53	0.37	2.4
Lube Oil	All	1.54	0.55	0.86	2.4

*excluding lube oil

As presented in Table 5.4, the average spill depth measured in this study for all liquids (except lube oil), liquid quantities, and spill substrates was 0.72 mm with a standard deviation of 0.34 mm. The spill depth values obtained in this study ranged from 0.22 mm up to 2.4 mm depending upon the specific liquid/substrate scenario. This average value is consistent with the values currently recommended in the literature [1] to provide conservative minimum depths for fuel spill scenarios.

Although an average spill depth of 0.72 mm was calculated, the range of spill depths measured was from 0.22 mm up to 2.4 mm depending upon the specific liquid/substrate scenario. This relatively wide range of empirical depths demonstrates the importance of understanding key variables governing fluid spread such that an appropriate spill depth is used when performing an analysis. The primary two factors governing the spread of a fuel and the equilibrium spill depth reached are the surface tension of the liquid and the surface characteristics of the substrate. However, given that the surface tensions of most fuels are relatively similar; this parameter is generally not as influential, when considering the characteristics of a spill. The more dominant

variable to consider is the surface topography which can have a substantial impact on the spread and equilibrium spill depth, both of which play an important role in predicting the fire hazard resulting from the spill. The roughness and uniformity of a substrate will dictate the speed and extent to which a liquid spreads and in doing so, will dictate the equilibrium spill depth. For rougher, non-uniform surfaces, it is likely that deeper equilibrium spill depths will be achieved due to the fuel being unable to spread to its full potential. Deeper spill depths result in longer burning durations, resulting in higher peak mass burning rates (i.e., larger fires). It is for this reason that an understanding of the surface on which a spill occurs is far more important than understanding the fuel that was spilled, from a spill dynamics standpoint.

After statistics on the overall data set were calculated, the effects of the various substrates on the spill depth were evaluated. For comparison purposes, the average spill depths and corresponding standard deviations for various spill scenarios were plotted as shown in Figure 5.13 and Figure 5.14.

As shown in Figure 5.13, the effect of the substrate on the spill depth was found to be minimal in most cases. The average spill depths reported for all impermeable substrates (i.e., coated concrete, smooth concrete, and vinyl) were within one standard deviation of one another. Furthermore, the permeable substrates (i.e., plywood, OSB, and brushed concrete) only fell just outside this standard deviation. It should be noted that the higher averages reported for the permeable substrates are most likely an artifact of the measurement technique used to quantify spill areas. As described in Appendix C, this measurement technique assumes that the volume of liquid, from the time spilled to the time the area of the spill is measured, is constant. However, for permeable substrates this is not necessarily true due to the absorption of the spilled liquid into the substrate. The absorption of the liquid by the substrate reduces the depth of liquid present on the surface. However, due to the fact that the depths measured in this work were derived from area measurements thus liquid depth was not directly measured, this loss of liquid volume/reduction in liquid depth was not captured. As a result of this inability to account for absorption losses, the measurement technique could over-predict spill depths for permeable substrates. However, it is generally expected, based upon analytical test results, that these fuel depths are comparable to, if not less than, the values reported for the impermeable substrates. Similar conclusions can be drawn when comparing the fuel specific results presented in Figure 5.14.

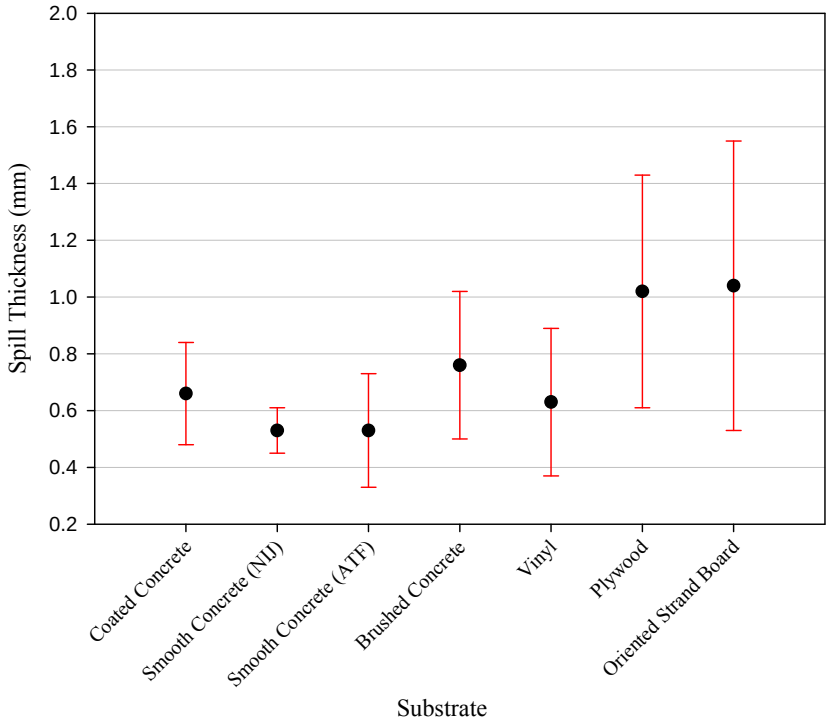

Figure 5.13. Comparison of average spill depths of all liquids, except lube oil, on various substrates

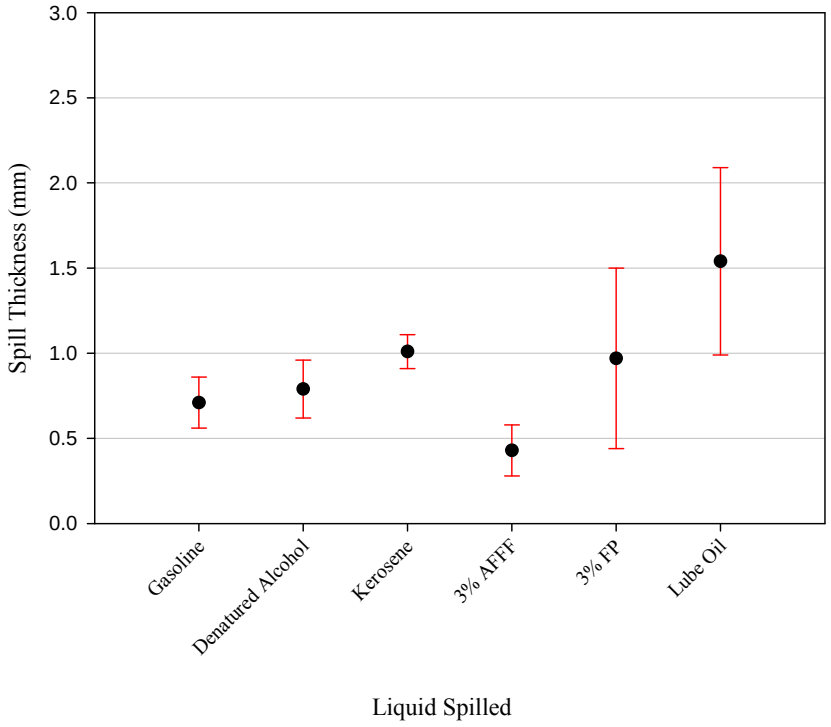

Figure 5.14. Comparison of average spill depths of individual liquids on all substrates

In these comparisons the average depths measured for two of the three fuels, gasoline and denatured alcohol, were very comparable (i.e., within one standard deviation of one another). The kerosene spill depths were slightly higher than those reported for other two fuels, as shown in Figure 5.14. This is most likely due to the fact that kerosene tests were only conducted on a limited set of substrates (i.e., coated concrete, plywood, and OSB), two of which are permeable. As indicated above, the permeability of the substrates was expected to have artificially increased the average spill depths slightly. In general, the spill depths measured for the three fuels (gasoline, denatured alcohol, and kerosene) evaluated were within 0.3 mm of one another.

5.3.2 Fuel Properties and Spill Depths

Simmons et al. [2004] and Bradley [2002] among others suggest that the properties of a liquid, specifically surface tension and viscosity, as well as the interfacial relationship between the liquid and substrate (i.e., contact angle) can be used to gauge the rate of spread and equilibrium depth of a spill. Based upon the statistical data set presented in Table 5.4, the average spill depth of each liquid for all surfaces was plotted against various fuel properties of interest. The relationships between the fuel properties (i.e., surface tension and viscosity) and the average spill depths are provided in Figure 5.15.

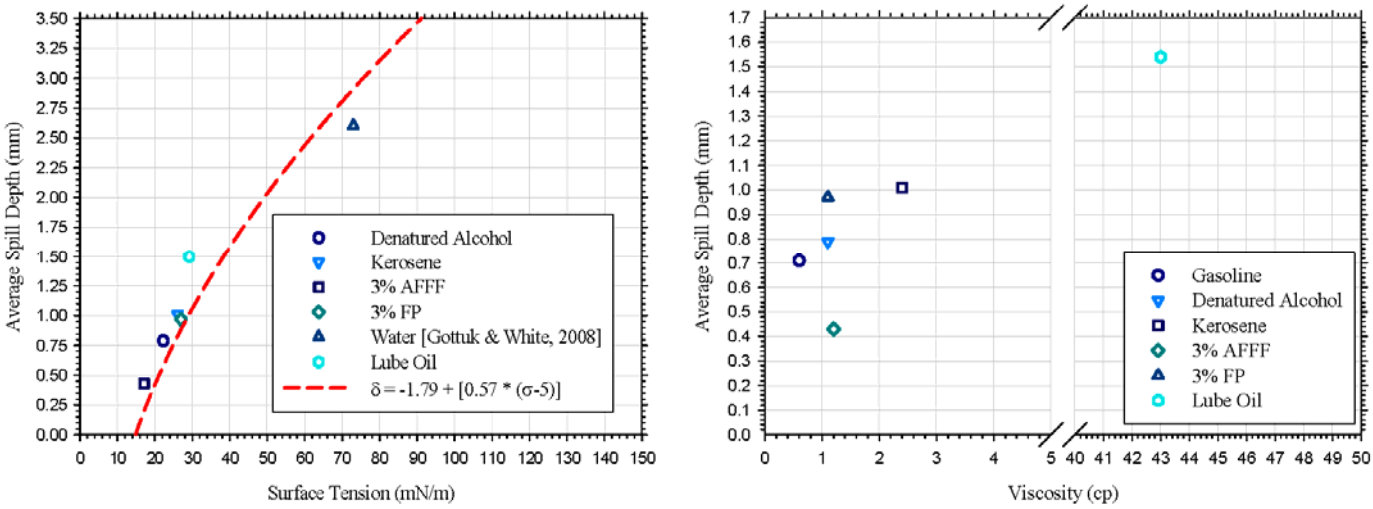

Figure 5.15. Relationship between average spill depth and (a) liquid surface tensiona and (b) liquid viscosity

It is evident from the results presented in Figure 5.15 that the correlation between the liquid surface tension and equilibrium spill depth is relatively strong. Based upon the averages developed from this work, a best-fit exponential regression was developed and presented in Figure 5.15. The liquid spill depths presented in Figure 5.15 (a) and (b) include two fuel simulants, three fuels, and lube oil. It should be noted that the empirical relationship between surface tension and spill depth presented in Figure 5.15 is generally consistent with the theoretical relationships developed by Bradley [2002] and Simmons et al. [2004] whose correlations were derived using a force balance at the liquid surface interface.

On the other hand very little correlation was observed between the viscosity of the liquids and the resulting spill depths. Most of the liquids used in this work, with the exception of the lube oil, had relatively similar viscosities. However, the average spill depths for these liquids differed by as much as a factor of two. Furthermore, the lube oil, having a viscosity more than 35 times greater than any other liquid tested only resulted in a spill depth that was 1.5 to 4 times greater than all other fuels considered. Based upon these results, it was determined that while the viscosity of a liquid may play a role in the transient progression of a liquid spill, it does not control the equilibrium spill depth.

The contact angle, which is related to the liquid surface tension, can be used to predict equilibrium spill depths for various liquid/substrate combinations (see Section 1.1.2). The relationship between liquid/substrate contact angles and equilibrium spill depths is illustrated in Figure 5.16.

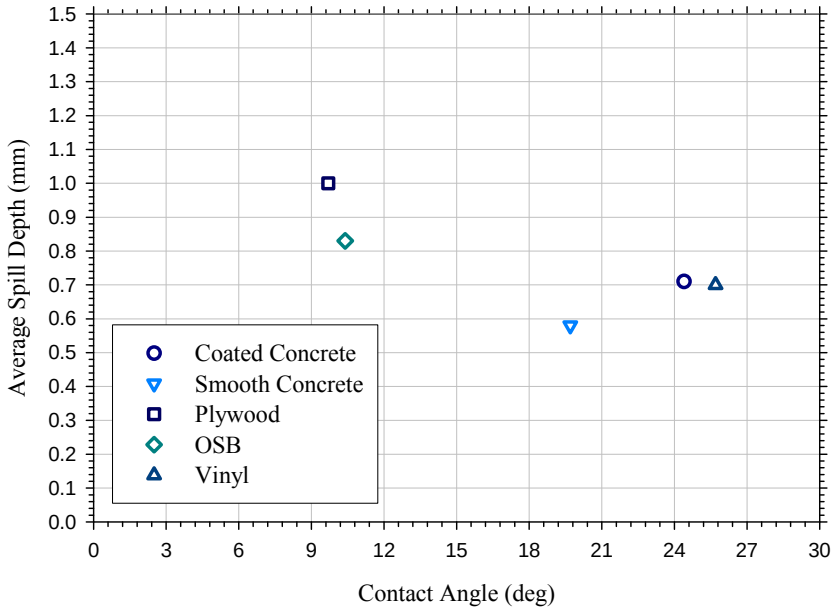

Figure 5.16. Relationship between gasoline/substrate contact angle and equilibrium spill depth

Based on the literature [Bradley, 2002 and Simmons et al., 2004], the contact angle, which characterizes the interaction between a specific liquid/substrate pairing, should provide the best correlation to the equilibrium spill depth. However, a clear correlation was not evident in the data collected in this study. As shown in Figure 5.16, there is no consistent trend in the gasoline data presented. It is expected that as contact angle decreases, so does the equilibrium spill depth of a liquid. If considering only the impermeable substrates (i.e., coated concrete, smooth concrete, and vinyl), a slight decreasing trend can be observed, as would be expected based on theory. However, the plywood and OSB substrates deviate from this decreasing trend significantly. One potential explanation of this lack of correlation, at least for the permeable surfaces (i.e., plywood and OSB) is that the means by which spill depths were derived in this study does not take into account absorption, as described above, which differs from the methodology used to determine contact angles. Neglecting absorption can result in an over-estimation of spill depth, thus explaining the increasing trend shown for the plywood and OSB

substrates. It is unclear as to whether the errors in spill depth measurements for the permeable substrates are significant enough to reduce the average spill depths to values that would be consistent with the downward trend expected. Such a reduction would require the plywood and OSB substrates to absorb approximately 40–60 percent of the liquid spilled onto the surface over a period of known period of time and area. This sort of absorptivity data could be collected using standardized tests methods [ASTM D7433, 2008] but were not collected in this work.

Based upon the results available from this work, the most appropriate parameter for predicting equilibrium spill depths is the surface tension of the liquid. However, if the impact of substrate absorption could be characterized and accounted for in the depth measurements taken for permeable surfaces, it is possible the contact angle could correlate relatively well with equilibrium spill depths. The viscosity of a liquid is not an appropriate fuel property to be used if trying to characterize the equilibrium spill depth.

5.3.3 Fuel Simulant Bounding

As indicated earlier, two fuel simulants were used in this study to provide bounding scenarios with respect to expected spill depths. In order to verify that these simulants provided these bounding scenarios, the average spill depths obtained for simulant and fuel tests on various substrates were made. A summary of these comparisons is provided in Table 5.5.

Table 5.5. Comparison of Fuel Simulant and Fuel Spill Depth Data on Various Substrates

			3% AFFF		**3% FP**	
Fuel	**Substrate**	**Average Fuel Spill Depth (mm)**	**Average Depth (mm)**	**Lower Bound (Y/N)**	**Average Depth (mm)**	**Upper Bound (Y/N)**
Gasoline	Coated Concrete	0.73	0.34	Y	0.88	Y
Denatured Alcohol		0.71		Y		Y
Kerosene		N/D		N/A		N/A
Gasoline	Smooth Concrete	0.58	0.42	Y	0.54	N
Gasoline	Brushed Concrete	0.7	0.53	Y	1.1	Y
Gasoline	Vinyl	0.7	0.27	Y	0.71	Y
Denatured Alcohol		0.84		Y		N
Kerosene		0.98		Y		N
Gasoline	Plywood	1.0	0.42	Y	1.5	Y
Denatured Alcohol		1.1		Y		Y
Kerosene		1.2		Y		Y
Gasoline	OSB	0.83	0.66	Y	2.1	Y
Denatured Alcohol		0.84		Y		Y
Kerosene		0.98		Y		Y

N/D – No data available because scenario was not tested
N/A – Not applicable

In all cases, the 3% AFFF fuel simulant (lower bound) resulted in spill depths that bounded all of the fuels used in this study. The spill depths measured for the 3% AFFF fuel simulant were 25–75 percent that of the fuels spilled on the same substrate. However, the same was not true for the 3% FP fuel simulant (upper bound). This liquid provided upper bounds for fuels spilled on four of the six substrates, including coated concrete, brushed concrete, plywood, and OSB. The 3% FP depths measured on both smooth concrete and vinyl were less than those measured for several of the fuels spilled on these substrates. In the case of the smooth concrete, the gasoline fuel depth was 0.04 mm larger than that of the 3% FP fuel simulant. With respect to the vinyl results for both denatured alcohol and kerosene, the fuel simulant spill depth was 0.13 and 0.27 mm less than the depths measured for the fuels, respectively. In both cases, the differences between the fuel simulant depth and the fuel depths were well within the standard deviations that were calculated for those specific substrates. Based upon these results it was concluded that the 3% AFFF fuel simulant provides a lower bound for all fuels used in this study, which in turn would provide conservative estimates of expected spill areas for a given spill scenario. Similarly, the 3% FP fuel simulant provided a reasonable upper bound for the fuels used in this study.

5.3.4 Dependence of Spill Area on Spill Volume

Currently there are differing opinions as to whether or not the final depth of a spill is dependent upon the initial volume of liquid discharged. The current 'rules of thumb' provided in [1] indicate that the depth of a spill is dependent upon the volume of liquid spilled. Based upon the limited data available at the time, Gottuk & White [2001] identified a break point of 95 L (25 gal.) at which the average fuel thickness for a spill would increase from approximately 0.7 mm to 2.8 mm. However, as described earlier in this report (Section 1.1.3.1), the data on which this break point was developed was not fully representative of the scenarios being considered due to the fact that the spills analyzed were not at their full spread potential. In addition to empirically based correlations, various models have been developed to characterize the progression/final result of a liquid fuel spill. Models have been developed to predict both the final spill depth as well as the transient progression of the liquid spill. The transient spill models provided by Raj et al. [14] and Grimaz et al. [15] show dependence of the final spill depth on the initial volume of the spill as well as a dependence upon the time the liquid is permitted to spread which is consistent with the empirical data provided by Gottuk et al. However, in the equilibrium spill models of Simmons et al. [16] and Bradley [17], it was concluded that the final depth of a liquid on a surface was strictly dependent upon the properties of the fuel and the properties of the substrate. It should be noted that in all of these references [14–17], the spill substrate is idealized (i.e., perfectly flat, perfectly smooth, etc.), and thus, may not accurately represent the possible effects of realistic surfaces. In order to better understand this issue, first the results from a series of tests conducted on the same substrate with varying quantities of fuel being released were compared; secondly, empirical results were compared to the predictions of the various models.

The substrate used in this comparison was smooth concrete (ATF). The quantities spilled consisted of 0.5, 5.0, and 20 L of 3% AFFF and 3% FP were. Larger quantities were not considered due to the constraints of the concrete floor available. The resulting spill areas per unit volume and spill depths from the discharge of the quantities identified above are compared in Figure 5.17.

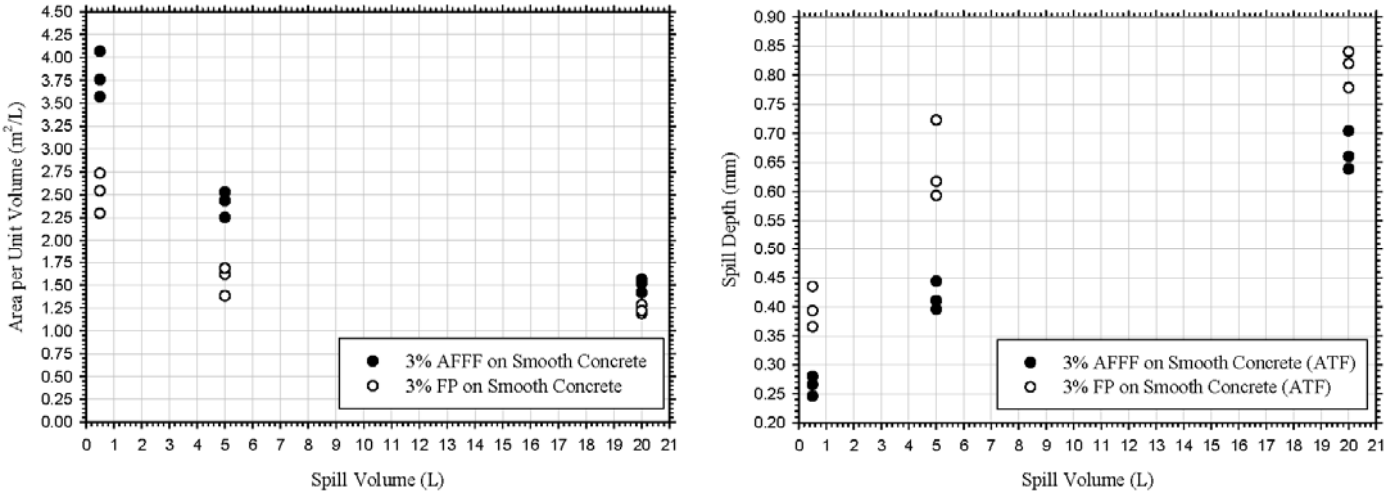

Figure 5.17. Comparison of area per unit volume (left) and spill depth (right) to various quantity spills of 3% AFFF and 3% FP on smooth concrete

As shown in Figure 5.17, the measured area per unit volume for these scenarios consistently decreased with increasing fuel spill quantity, which is indicative of an increasing trend in spill depth. Similar trends were reported by Gottuk and White [2008] for the data sets analyzed. Given that the same liquid was used in all tests conducted in this test series, it is not possible that the differences observed could have been due to the liquid properties. Furthermore, based upon experimental testing in which the liquids were permitted to spread for extended periods of time (i.e., 20–40 minutes depending upon the spill volume), it was demonstrated that the spread times used in these tests were sufficiently long enough for the liquid to reach a quasi-steady state. Consequently, it was concluded the variations in area per volume spilled (or fuel depth) were a result of the substrate surface topography (i.e., levelness, roughness, uniformity, etc.) [Simmons et al., 2004]. It is possible that as a larger area of substrate becomes involved, surface characteristics play a larger role in the development/spread of a liquid. The data trend shown in Figure 5.18 is generally consistent with that presented by Gottuk & White [2008] when relating spill volume and spill area.

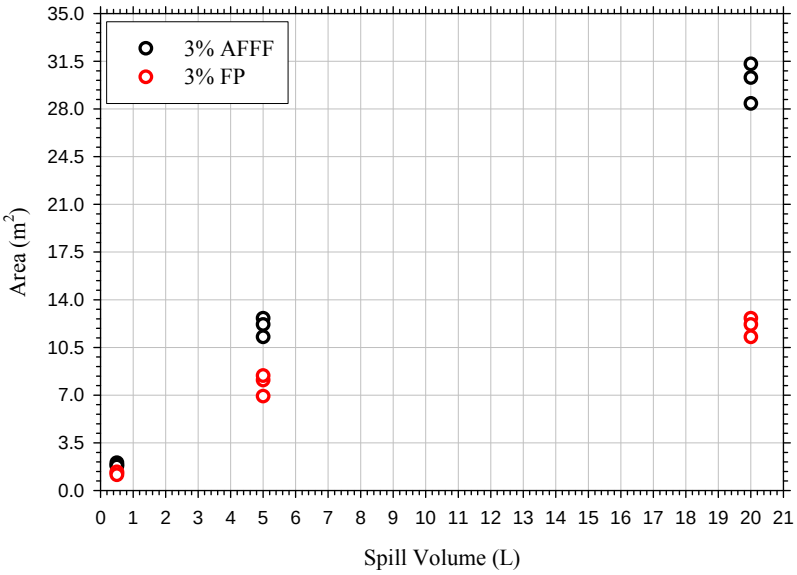

Figure 5.18. Correlation of spill area to spill quantity for 3% AFFF and 3% FP fuel simulants spills on smooth concrete

The uniformity and flatness of the substrate will dictate the direction and extent to which a liquid will spread. Furthermore, a surface that is level, even to within a degree, will result in some bias to the final spill depth achieved/area covered [Simmons et al., 2004]. These peaks and valleys, resulting from slight changes in levelness, result in areas of liquid pooling and liquid creeping. The roughness of a surface will dictate the minimum depth for which spreading can continue, and the roughness of a surface can be highly variable even over a relatively small area of the same substrate.

In order to further understand the factors affecting the spill depth as the volume of the spill increases, the predictions of the various transient and equilibrium spill models were compared for each of the spill volumes discussed above. These comparisons are provided in Figure 5.19.

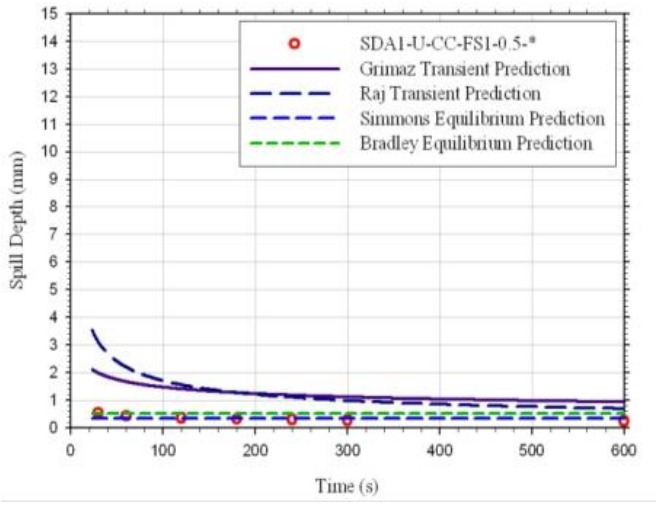

(a) – 0.5L Spill

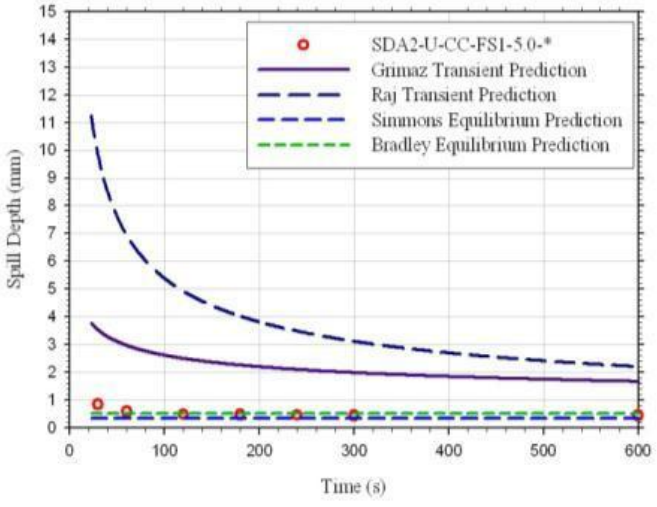

(b) – 5.0 L Spill

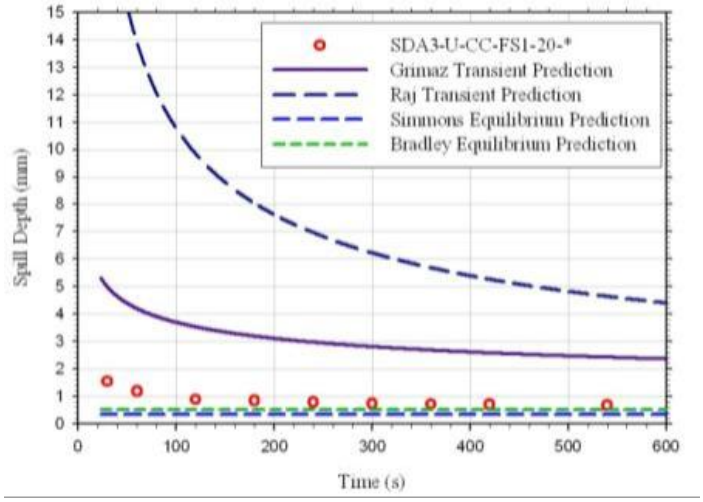

(c) – 20L Spill

Figure 5.19. Correlation of spill depth to spill quantity for 3% AFFF fuel simulant spills on smooth concrete

In general, the transient spill models [Raj et al., 1974 & Grimaz et al., 2007] were found to over-predict spill depths significantly, and as noted by the model developers, depths predicted by these models were dependent upon the initial spill quantity. When considering the 0.5–20 L spills conducted in this work, the transient models predicted quasi-steady state spill depths ranging from 0.75 mm to 4 mm. The equilibrium models did not change as a function of initial spill quantity, consequently, these predictions slightly over-predicted the spill depths achieved in the 0.5 L spills, accurately predicted the spill depths measured for the 1.0 L spills, and under-predicted the spill depths of the 20 L spill. The equilibrium models predicted quasi-steady depths of 0.36 mm to 0.51 mm compared to measured depths of 0.32–0.84 mm for 0.5–20 L, respectively.

Although from an ideal fluid dynamics point of view, there should be no dependence of spill depth on spill quantity, empirical data from this study as well as transient spill models [Raj et al., 1974 and Grimaz et al., 2007] indicate that some dependence exists. As noted earlier, previous empirical data also supported the increase in depths with increases in quantity of liquid spilled.

5.3.5 Implications to Spill Fire Modeling

As discussed above, due to the myriad of variables affecting the spill dynamics of a liquid spreading across a substrate, it is extremely challenging to predict the equilibrium spill depth/spill area. As a result of this, it has become standard practice to adopt an average spill depth value when attempting to characterize the extent of a liquid spill. Based upon the data presented in this work and in previous studies, an appropriate value for the equilibrium depth of an unconfined liquid spill is 0.7 mm. However, given that this is an average value for all fuels on all substrates, it is useful to understand the implications of adopting this value for specific scenarios with available empirical data and the relevance of these implications to the potential hazard of a fuel spill fire.

In order to gain this understanding, the spill depth data provided in Table 1 for each of the substrates evaluated was used to predict approximate mass burning rates for various spill volumes. First, spill areas were calculated using the 68 percent confidence interval values of depths for gasoline for all substrates (i.e., 0.56 and 0.86 mm) and kerosene for all substrates (0.91 and 1.11 mm) as reported in Table 5.4. The volumes used are specified in Table 5.6. These areas were then converted to equivalent diameters, assuming an ideal, circular spread pattern. These equivalent spill diameters were applied to the Burgess et al. [6] burning rate correlation, shown in Equation 5-2, for the two different fuels.

$$\dot{m}'' = \dot{m}''_{\infty}(1 - e^{-k\beta D}) \qquad \text{Eq. 5-2}$$

where $\dot{m}''_{\infty}$ is the peak mass burning rate per unit area measured in this research for the given fuel (g/s-m^2 [lbs./s-ft^2]), kβ is an empirical constant specific to the fuel, and *D* is the effective spill diameter (m [ft]). This pair of data (i.e., minimum and maximum predicted burning rate) was calculated for each spill volume and compared to the mass burning rate predicted using the default 0.7 mm spill depth. The maximum differences at each spill volume for each fuel were then calculated and are presented in Table 5.6. The maximum difference reported in Table 5.6 is the absolute value of the largest difference between the mass burning rates calculated using the default spill depth of 0.7 mm and the mass burning rate calculated using the bounding spill depths.

Table 5.6. Summary of Maximum Differences in Predicted Mass Burning Rates Using 0.7 mm Depth Compared to 68 Percent Confidence Range for Average Measured Fuel Depths on All Substrates

Spill Volume (L)	**Maximum Difference between Mass Burning Rate (%)**	
	Gasoline	**Kerosene**
0.5	17	8.0
1.0	11	3.0
5.0	1.0	0.0
20.0	0.0	0.0

In this analysis, the differences in mass burning rates resulting from the use of an average spill depth of 0.7 mm as opposed to the substrate specific mass burning rate value were generally small and highly dependent upon the quantity of fuel spilled. As shown in Table 5.6, the errors in predicted mass burning rate based upon a 0.7 mm depth diminish as spill volume increases. This is primarily due to the asymptotic nature of the Burgess et al. [1960] correlation for fire diameters greater than approximately 1.0 m (3.3 ft). For gasoline spill volumes of slightly greater than 1.0 L (0.26 gal.), the errors were less than ten percent. Furthermore for kerosene, the volume at which less than ten percent differences were observed was 0.5 L (0.11 gal.). Based upon this assessment, the use of the 0.7 mm spill depth approximation as opposed to a substrate specific spill depth approximation, for spills greater than 1 L (0.26 gal.), will provide baseline mass burning data that is accurate to within ten percent.

5.4 Spill Fire Dynamics

The focus of this section is verify the findings of the diked and spill dynamics analyses presented earlier in the report using real fuel spill fire scenarios, thus providing a better understanding of the appropriateness and applicability of the conclusions to specific fire scenarios. A total of 104 spill fire tests were conducted encompassing a wide variety of fuel types, fuel quantities, and substrates. The results from these tests were compared and explained in this section.

5.4.1 Substrate Effects

The impact of substrate on the mass burning rate of a fuel spill fire was characterized in the fixed area (pan and diked) fire scenarios. The conclusion from Section 5.2.1 was that the substrate does affect the mass burning rate of a fuel but only at depths on the order of a 1 mm (0.04 in.). The thermal conductivity of the substrate was found to provide the best correlation to mass burning rate in that as the thermal conductivity of the substrate increased, the mass burning rate of the burning fuel decreased. The thermal properties of the substrate, when considering a fuel depth of 1 mm, altered the mass burning rate by as much as 50 percent. In general at depths greater than 5 mm it was found that substrate effects become negligible.

5.4.1.1 Concrete Finish Effects

A total of three different surface finishes of concrete were used in this study; coated, smooth, and brushed. Given the different surface finishes, the resulting spill areas varied. Consequently, the comparisons made between the three concrete surface finishes, shown in Figure 5.20, were done on a heat release rate per unit area (HRRPUA) basis.

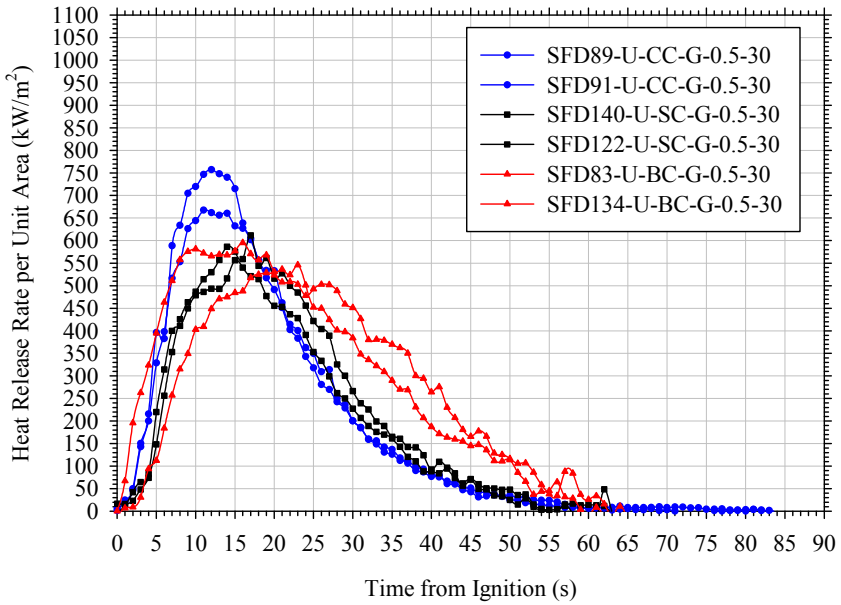

Figure 5.20. Comparison of HRRPUA for 0.5 L gasoline spills on various concrete surfaces: coated concrete (CC), smooth concrete (SC) and brushed concrete (BC)

The brushed and smooth concrete results were very comparable while the coated concrete results had approximately 20 percent higher peak values. The increased heat release rates observed for the coated concrete scenarios are most likely due to the differing surface topography and substrate permeability between the two substrates. The brushed concrete is significantly rougher than the coated concrete, which results in the contact surface area between the gasoline and concrete being larger potentially leading to more heat losses. Furthermore, the brushed concrete is permeable, which could result in absorption of the spilled fuel and a reduction in the overall spill depth. This comparison demonstrates the effects on the mass burning rate of fuel due to differences in the spill dynamics occurring on a substrate with different finishes. However, the fact that the differences observed in Figure 5.20 are relatively small suggests that for a given spill volume, the impact of surface finish is not as influential as the properties of the substrate itself.

5.4.1.2 Wood Finish Effects

Two different types of wood substrates were evaluated in this study: plywood and oriented strand board. Based upon analytical testing, these surfaces have similar contact angles with respect to gasoline. Furthermore, with both substrates being a wood product the thermal properties of the materials are similar. Thus, based upon the conclusions from the fixed area and spill dynamics testing, it was expected that similar fuel spill fire scenarios would be comparable. Verification of this fact is presented in Figure 5.21.

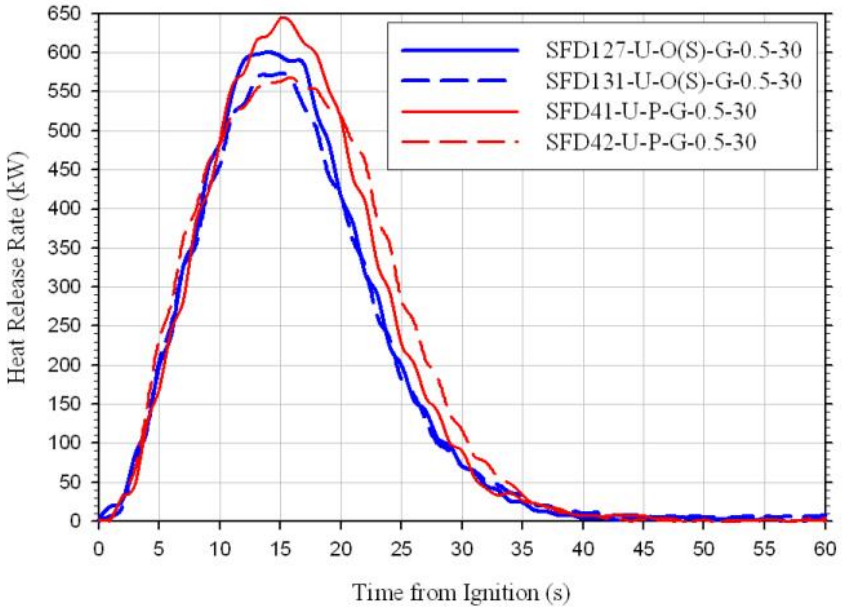

Figure 5.21. Comparison of HRR for 0.5 L gasoline spills on plywood and OSB substrates

As shown in Figure 5.21, the heat release rate profiles from 0.5 L gasoline spills conducted on both plywood and OSB are very similar. Comparable results were achieved for both denatured alcohol and kerosene spills of the same quantity on both of these substrates. These comparisons demonstrates that materials with similar thermal and surface characteristics will result in similar fuel spill fire scenarios, with all other variables held constant.

5.4.1.3 Wood and Concrete Substrates

In order to further assess the effect of substrate thermal characteristics on the mass burning rates of a fuel spill fire, comparisons were made between 0.5 L gasoline and denatured alcohol spill fires conducted on coated concrete, vinyl, and plywood substrates. The heat release rates measured in these fires are presented in Figure 5.22. It should be noted that a 0.5 L denatured alcohol spill fire on vinyl with a 30-second ignition delay was not conducted; thus, spill fire data for this scenario is not presented in the figure.

In general, the results from the 0.5 L gasoline spills on plywood and vinyl are consistent with the conclusions from the fixed area fire tests. The 10-second peak heat release rate values for these two scenarios were very similar as are the properties of the substrate. Similar thermal properties between the vinyl substrate and the plywood substrate are assumed given that the vinyl flooring material has a small depth (i.e., 1.2 mm [0.04 in.]) and is backed by the same plywood material used as the plywood substrate. However, as shown in Figure 5.22, the results from the spill scenarios on plywood and vinyl substrates differ significantly from those reported for the coated concrete. The vinyl and plywood 10-second peak heat release rates are approximately 40 percent larger than that achieved in the coated concrete spill fires. Given that the spill depths in these scenarios were all less than 1 mm (0.04 in.), these results are relatively consistent with the findings of the analysis of the fixed area fires which at a depth of 1 mm (0.04 in.) reported differences of approximately 30 percent in peak heat release rate per unit area between the vinyl and coated concrete substrates.

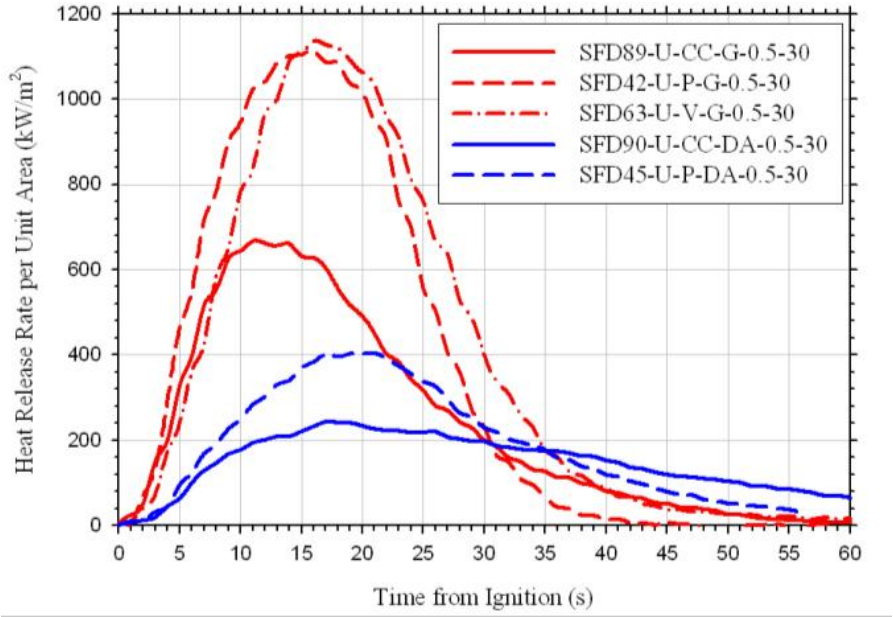

Figure 5.22. Comparison of HRRPUA for 0.5L gasoline spills on various concrete surfaces

5.4.1.4 Carpet Layering Effects

The majority of the carpet tests conducted were composite substrates comprised of carpet, carpet padding, and plywood. However, the potential for the installation of carpet and carpet pad or

simply carpet directly onto a concrete floor does exist. In order to understand the potential effects of these installation variations, a small subset of tests were conducted to assess the impact of the carpet pad and plywood substrates on fire growth and sustained burning in a carpet spill fire scenario. A comparison of the heat release rates for the three substrate scenarios is provided in Figure 5.23. These scenarios include a system comprised of carpet over carpet pad with a plywood subfloor (SFD50A, 56, 56A), carpet over carpet pad with a concrete subfloor (SFD50), and carpet laid directly over a concrete subfloor (SFD 141A). The spill areas for all scenarios were comparable with spill areas ranging from 0.22–0.23 m^2 (2.4–2.5 ft^2).

As shown in Figure 5.23, tests in which carpet and carpet pad were evaluated, two heat release rate peaks were observed. In the test conducted with only carpet present over top of a concrete subfloor (SFD141A), only one peak was measured. The first peak generally occurred within the first minute of burning and was attributed to the burning of the gasoline, carpet, and carpet padding (if present). With padding and plywood substrates, a second peak occurred at about 2–3 minutes. The decay of all fires consisted of residual burning of an annulus of carpet/padding.

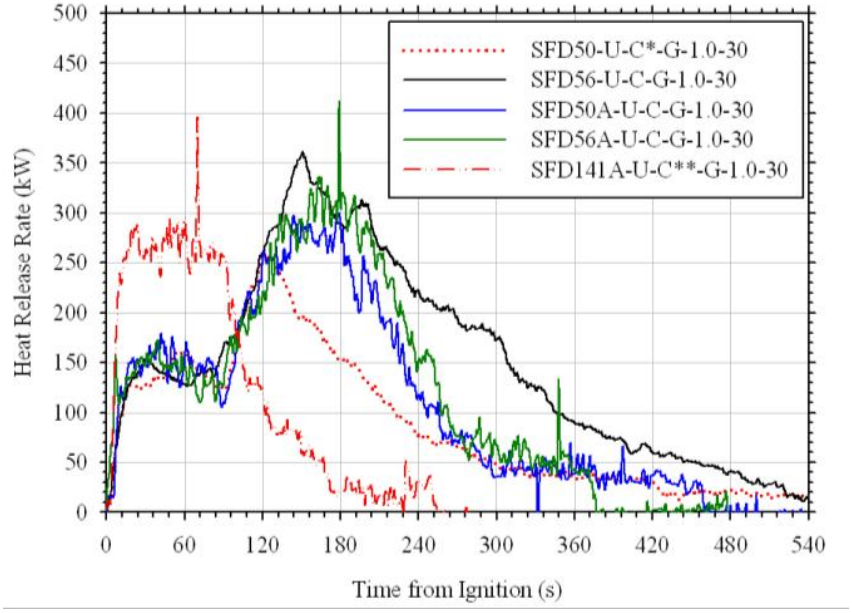

Figure 5.23. Comparison of 1.0 L (0.26 gal.) gasoline spill fire heat release rates on various carpet covered substrates

The tests conducted with the carpet over pad on a plywood substrate were very repeatable with very little deviation from one another, as seen in Figure 5.24 with the overlaying curves for SFD50A and SFD56A. In the absence of a plywood substrate (i.e., replaced with a concrete subfloor), the initial 120 seconds of burning was comparable to that observed with the plywood present. However, after this initial stage, the heat release rate for carpet and pad over concrete began to decay resulting in a peak heat release rate that was approximately 150 kW/m^2 lower than that achieved with the plywood present. This reduction in the peak heat release rate per unit area was primarily attributed to the removal of a significant source of fuel (i.e., burning plywood). After an additional 120 seconds of burning, the heat release rates from tests with and without the plywood substrate converged and remained consistent with one another for the duration of the test. The similar heat release rates measured after approximately 270 seconds are

the result of the outer ring of the spill fire continuing to consume the carpet and carpet padding, which is relatively independent of any potential sub-floor effects. In the absence of both a combustible subfloor material and carpet padding, a spill of 0.5 L of gasoline (SFD141A) results in a fire that is approximately half of that measured in all three other tests with padding present. The carpet only on concrete fire peaked and maintained a steady-state heat release rate for approximately 90 seconds, qualitatively similar to the other three carpet tests with padding. However, after about 90 seconds (associated primarily with the gasoline consumption), the carpet only test decayed whereas the tests with padding started a second growth stage. This data shows that the carpet padding is responsible for approximately half of the heat release rate measured during the initial 90 seconds of burning as well as the continuation of the fire. The padding was a larger contributor to the peak heat release than the wood substrate.

5.4.2 Substrate Temperature Effects

A small set of tests were conducted prior to the establishment of a test start criteria for an initial substrate temperature. Thus, a set of tests were conducted atop the coated concrete while it was at slightly elevated temperatures. For the majority of tests, a substrate temperature less than or equal to 25°C (77°F) was adopted as the minimum temperature at which tests could be conducted. A total of 12 tests were conducted in which the substrate temperature was greater than this threshold. These tests will be used to evaluate the effects of substrate temperature on the mass burning rate/heat release rate of a spill fire.

Due to the unique shapes of the fuel spill fires and the fact that they did not cover the entire substrate surface area, an average temperature over the entire substrate was found to be an inappropriate characterization. Instead, a circular area of 2 m^2 (21 ft^2) centered on the concrete pad was taken via FLIR measurements. This area measurement was found to encompass the majority of all areas heated by preceding spill fires as well as capture areas of the pad that a spill could cover. This average temperature was used as the initial temperature of the substrate for each test. Using this methodology, average concrete substrate temperatures ranged from 18–38°C (64–100°F) for all tests. The maximum temperature difference within any specific group of tests with similar test parameter was 15°C (27°F). When compared to one another, with all other variables held constant, the heat release rates differed with changes in substrate temperature. In some cases the observed differences were as large as a factor of two. In an attempt to correlate the differences observed a plot comparing the 10-second peak heat release rate and initial substrate temperature was created, see Figure 5.24.

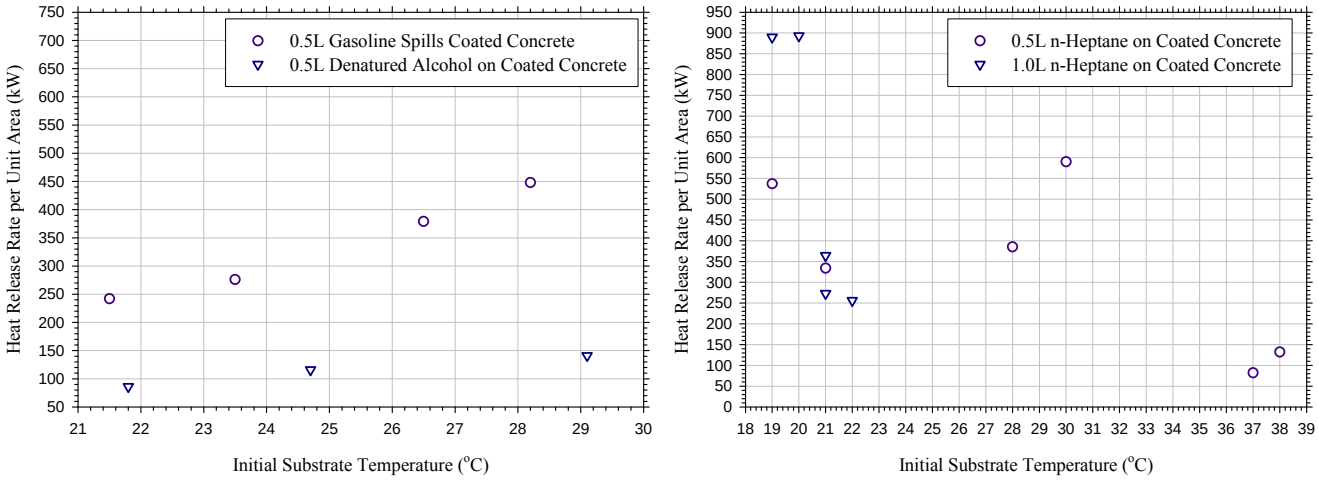

(a) Gasoline and Denatured Alcohol Spills (b) n-Heptane Spills

Figure 5.24. Comparison of 10-second peak heat release rate per unit area and initial substrate temperature for a variety of fuels

As is evident from the scatter presented in Figure 5.24, no consistent correlation between the initial temperature of the substrate, as calculated in this study and the 10-second peak heat release rate was found. However, increasing trends were observed for both the 0.5 L gasoline and 0.5 L denatured alcohol spill scenarios. For these fuels, an increase in substrate temperature of 6–7°C (11–14°F) resulted in differences in heat release rate per unit area of almost a factor of two. These differences are most likely due to either the pre-heating of the fuel by the substrate or potentially the reduction in heat losses to the substrate during combustion. The lack of correlation observed in this limited data set could be the result of the inappropriate averaging of the substrate surface temperatures; however, a better method was not available based upon the data collected in this study. Due to the limited data set analyzed, no conclusive correlation could be identified but the data does indicate that substrate temperature could potentially have a significant role in the development of spill fires and should be looked into further.

5.4.3 Ignition Delay Effects

Ignition delay times of either 30 or 300 seconds were used in the majority of spill fire scenarios tested. The results of these two scenarios, with all other variables held constant, were consistently different. Representative heat release rate plots of 0.5 L gasoline and denatured alcohol spills on coated concrete are provided in Figure 5.25. A summary of the average differences in spill area and 10 s peak heat release rate per unit area are provided in Table 5.7.

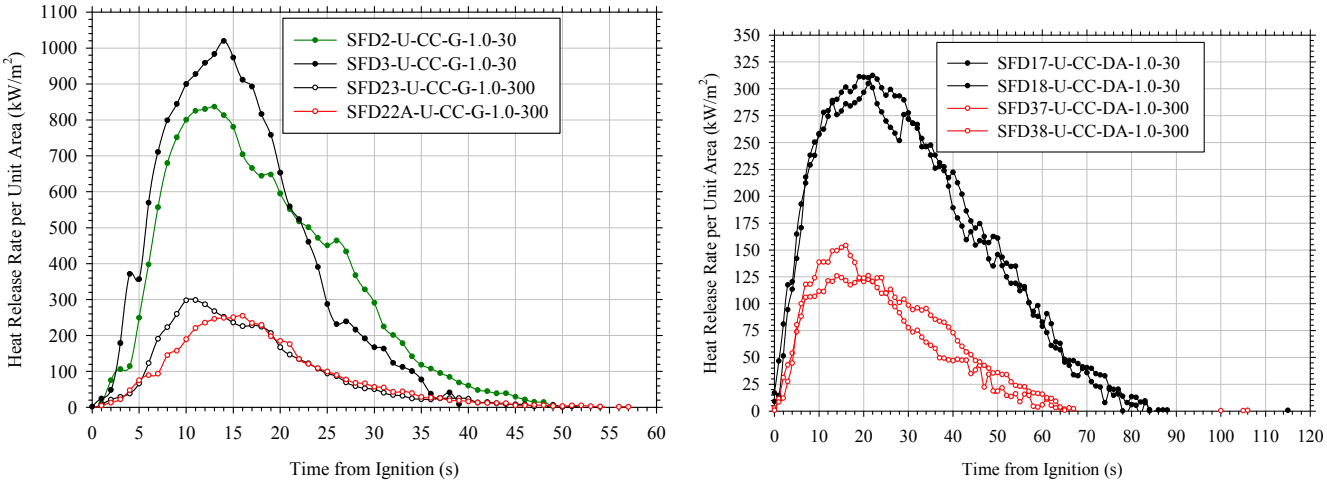

(a) – 0.5 L Gasoline Fires (b) – 0.5 L Denatured Alcohol Fires

Figure 5.25. Heat release rate per unit area for 0.5 L gasoline and denatured alcohol fires with 30 s and 300 s ignition delay times conducted on coated concrete

Table 5.7. Summary of Average Spill Areas and 10-second Peak HRRPUA for Scenarios with Differing Ignition Delay Times

Substrate	Fuel	Qty.	Avg. Spill Area (m^2)			Avg. 10 s Peak HRRPUA (kW/m^2)		
			30 s Ign.	300 s Ign.	% Difference (w.r.t. 300 s)	30 s Ign.	300 s Ign.	% Difference (w.r.t. 30 s)
Coated Concrete	Gasoline	0.5	0.63	0.75	-20	635	303	-52
		1	1.26	1.79	-42	730	244	-67
	DA	0.5	0.58	0.87	-49	238	125	-48
		1	1.08	1.79	-66	300	132	-56
Smooth Concrete	Gasoline	0.5	0.88	0.95	-8	531	136	-74
Brushed Concrete	Gasoline	0.5	0.68	0.86	-27	542	306	-44
		1	1.28	1.47	-14	580	311	-46
Vinyl	Gasoline	0.5	0.58	1.02	-76	958	413	-57
	DA	1	1.095	1.3	-19	417	313	-25

As shown in Table 5.7, the results of these comparisons vary widely. The differences in the average spill area between the 30-second and 300-second ignition delay times range from 8–76 percent with an average value of 36 percent. The differences in the average 10-second peak heat release rates range from 25 percent to as high as 74 percent with an average of 52 percent. Although no direct correlation between the change in area and change in heat release rate could be identified from this data, the data does consistently indicate that increasing the ignition delay from 30 seconds to 300 seconds results in a larger spill area and a decreased peak heat release rate.

The decreased 10-second peak heat release rates for the 300-second ignition delays shown in Table 5.7 are most likely due to several factors including; decreased spill depths due to the

evaporation of volatile fuels at ambient temperatures, a decreased spill depth due to the increasing fuel spill area, and a decreased substrate temperature due to evaporative cooling which once ignited could result in the substrate serving as a larger heat sink. Correlating these individual parameters to the observed heat release rate per unit area differences was attempted but no strong correlations were identified. The analyses of the impacts of each of these variables are shown below using the data collected in these tests.

For the scenarios presented in Table 5.7, both fuels are relatively volatile at ambient temperatures; thus the mass of fuel present in the fuel spill layer decays as a function of time due to evaporation. This evaporative mass loss corresponds to a diminishing fuel spill depth. It is unclear as to whether or not the mass of fuel evaporated in the time frames being considered is substantial with respect to the impacts on the mass burning rate of the fuel. However, given the findings presented earlier in this report regarding the impact of fuel quantity on mass burning rate, the gasoline mass burning rates for the scenarios identified in Table 5.7 were calculated based upon estimates that included losses due to evaporation. It should be noted that denatured alcohol mass burning rates, although presented in Table 5.7 are not considered in this analysis due to the fact that the parameters needed for the empirical correlation [Burgess et al., 1960] are not available.

Based upon small-scale testing conducted on two different substrates, smooth concrete and steel, the evaporation rates of both gasoline and denatured alcohol were determined. It should be noted that these evaporation rates were measured on surfaces whose ambient temperature was approximately 18°C (64°F). This testing was conducted using a 0.09 m^2 (1 ft^2) steel pan and a 0.02 m^2 (0.23 ft^2) smooth concrete pad. In all tests, a 1 mm depth of fuel was placed atop the substrate and the transient mass loss was measured. Evaporative mass loss was characterized using a Sartorius Model FBD-16EDE load cell with a 12 kg (26 lbs.) capacity and 0.1 g resolution. During these tests, ambient air flow conditions and temperatures were nominally the same as those present during all testing. The average evaporation rates measured for the gasoline and denatured alcohol fuels were 0.15 and 0.17 g/s-m^2. Using these evaporation rates along with the spill areas and ignition delays from the spill fires, the quantity of fuel that would have been lost due to evaporation was calculated. For both fuels, the average fraction of fuel lost due to evaporation during the time period of 30–300s (i.e., a total of 270 s) was on the order of 10 ± 1.4 percent. This reduction in fuel volume when applied to the average depths measured for the 30-and 300-second ignition delay tests corresponds to an average difference in fuel depth between the ignition delay time of approximately 32 percent. The 32 percent difference in depth resulting from a 10 percent reduction in fuel volume is a result of the spill areas at 30 and 300 seconds being different. Using the existing correlation of mass burning rate to pool diameter [Burgess et al., 1960] coupled with the depth coefficient (Sections 5.1.2 and 5.1.3), these adjusted fuel spill volumes due to evaporation were used to calculate an expected mass burning rate for each scenario. Assuming a constant effective heat of combustion of 39.5 MJ/kg, these mass burning rates were converted to heat release rate per unit area. A summary of the results from this analysis are provided in Table 5.8. It should be noted that the calculations performed to evaluate the impact of the reduced fuel depth also take into account the reduction in depth due to the increased areas achieved in the 300-second ignition delay tests.

Table 5.8. Analysis of the Impact of Ignition Delay on Mass Burning Rate of Fuels Specifically Considering the Effects of Evaporation

Substrate	Fuel	Qty. (L)	Fuel Depth after 30 s (mm)	Fuel Depth after 300 s (mm)	$HRRPUA_{30s}$ (kW/m^2)	$HRRPUA_{300s}$ (kW/m^2)	% Difference
Coated Concrete	Gasoline	0.5	0.79	0.61	662	554	16
		1	0.78	0.50	721	520	28
Smooth Concrete	Gasoline	0.5	0.56	0.47	535	464	13
Brushed Concrete	Gasoline	0.5	0.73	0.52	631	500	21
		1	0.77	0.62	715	612	14
Vinyl	Gasoline	0.5	0.86	0.43	693	437	37

The heat release rate per unit area values predicted in the analysis presented in Table 5.8 on average show a 22 percent decrease between the 30 and 300 seconds scenarios. The trend observed in this analysis (i.e., decreasing heat release rate per unit area with increasing ignition delay time) is consistent with the spill fire data collected. However, the predicted values only account for approximately one-half of the differences measured for the actual spill fire scenarios. These results indicate that while changes in spill depth due to both evaporation and spreading of a spill have some effects, they are not the only factors causing the reduction of fire size with increasing ignition delay time.

In addition to the factors affecting the physical characteristics of the spill (i.e., reducing the spill depth), the prolonged exposure of a substrate to an evaporating fuel layer will result in some cooling of the material. Furthermore, once the fuel is ignited, heat losses to the 'cool' substrate will initially be greater than those to an ambient temperature substrate due to a larger temperature difference between the fuel and substrate. In order to better understand the effect of the heat transfer occurring during the fire growth, temperatures at the center of the concrete substrate at a depth of 3.2 mm (0.125 in.) were compared for the 30 and 300-second ignition delay scenarios. The concrete temperature at the specified depth did not decrease during the ignition delay period for the 30-second ignition scenario and decreased by less than two degrees during the 300-second ignition delay scenarios. It is possible that the penetration depth of the evaporative cooling of the fuel did not reach a depth of 3.2 mm (0.125 in.) in the time period evaluated; however, these results suggest that the evaporative cooling of the substrate and any consequential heat loss effects after ignition is relatively minimal. This conclusion is based upon the fact that at a temperature difference of 2^oC (3.6^oF), the heat transferred to the substrate would be negligible with respect to the heat being transferred to the fuel surface.

A total of three potential factors were identified as having the potential to cause a reduction in heat release rate per unit area ignition delay times increase. The empirical data collected in this work shows an average difference in HRRPUA for the 30 and 300-second ignition delay times to be approximately 40 percent. When analyzed, two of the factors (evaporation, changes in area) resulted in decreased fuel spill depths which were then correlated to a reduction in the mass

burning rate of the fuel. This reduction in mass burning rate was found to be on the order of 22 percent, which is approximately half of that calculated from the data collected in this study. The remaining fraction of the difference could be a result of experimental uncertainty (i.e., underestimating evaporation rates due to scale or substrate temperature, heat release rate measurement uncertainty, etc.) or other variables that can potentially modify the mass burning rates of the fuels (i.e., changes in fuel chemistry due to evaporation, ambient temperature, etc.).

6.0 CLASS A FIRES AND FORENSIC INDICATORS

6.1 Class A Fires

6.1.1 Class A Fire Procedures

Prior to each Class A fire test, the test material (i.e., PU foam, wood crib, baby seat) was placed at the center of the substrate on which the test was being conducted. For all Class A fire scenarios, the ignition source was two and a half full sheets of newspaper ignited using a small propane flame. For the chair mock-up and baby seat scenarios, the newspaper was crumpled into a nominally 0.15 m (6 in.) diameter ball and placed on top of the center of the fuel package. For the wood crib, the newspaper was twisted and inserted into the center vertical flue of the wood crib. In all configurations, the newspaper was ignited using a 2 second exposure from a propane torch applied to the top of the newspaper. Two minutes of background data (i.e., data acquisition system, cameras, and FLIR camera) were collected prior to each test. After ignition, the fire was permitted to develop naturally. The data, cameras, and FLIR camera continued recording until the last flame extinguished.

6.1.2 Class A Fire Results

A total of three different Class A fuels were evaluated on three different substrates. The purpose of these tests was to characterize the fire patterns resulting from materials representative of fuel packages commonly found in residential and commercial fire scenarios and compare these patterns to those observed during fuel spill fires on identical surfaces. Comparisons of the transient heat release rates for each Class A fuel on a specific substrate are provided in Figure 6.1, Figure 6.3 and Figure 6.5. These plots not only illustrate the severity and duration of the fires resulting from these Class A fuels but also provide insight into the effect of the substrates.

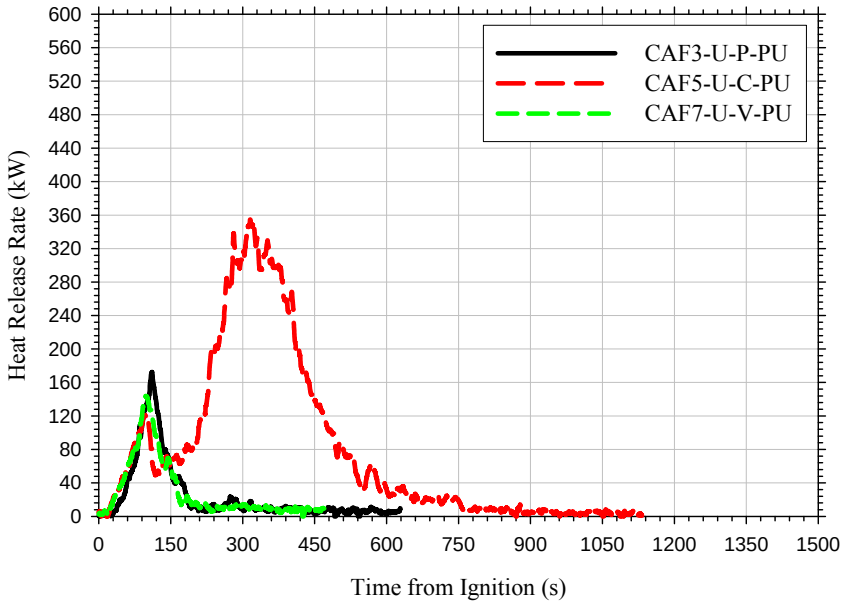

Figure 6.1. Heat release rates from polyurethane foam chair mock-up on plywood, carpet and vinyl substrates

The fire growth curves measured in the polyurethane (PU) foam chair mock-up tests (Figure 6.1) were very repeatable. In these tests, the PU foam produced a peak fire size of approximately 150 kW after two minutes of burning and was consumed approximately 60 seconds after reaching the peak value when burned atop the plywood and vinyl substrates. In these two tests there was very little involvement of the substrate material. However, with the chair mock-up positioned atop carpeting, during the decay phase of the PU burning, the carpet substrate became involved resulting in a second peak with a maximum fire size of approximately 360 kW. The total duration of the fire on carpet was approximately four times longer than the fires on plywood and vinyl (750 vs 180 seconds). Photographs of the burning PU foam chair mock-up on each substrate are presented in Figure 6.2.

Figure 6.3 shows the heat release rates for wood crib fire tests conducted atop plywood, vinyl, and carpet. Photographs of the burning crib on each substrate are presented in Figure 6.4. The wood crib tests conducted on both plywood and vinyl behaved very similarly for the initial 17.5 minutes (1050 s), maintaining a steady state heat release rate of 80 kW. After 17.5 minutes of burning, the heat release rate for the test conducted on plywood increased to 120 kW and maintained this level of burning for an additional five minutes. Over this same period of time, the fire size for the crib on vinyl remained steady at 80 kW. The increased heat release rate measured in the test conducted on plywood is attributed to the increased contribution of the plywood substrate relative to the vinyl substrate. In both tests, approximately 50 percent of the substrate was involved over the course of the wood crib burning. However, the extent of flaming combustion that occurred on the plywood substrate was visibly greater than that observed for the vinyl. As opposed to burning, the vinyl first bubble d, and then charred with only localized area of flaming combustion; the wood underlayment to the vinyl did not become involved. This is most likely the reason for the difference in heat release rate measured for the plywood and vinyl approximately 17 minutes into the test. In the test conducted atop the carpet, the rate of fire development was more rapid and reached a higher peak heat release rate than tests conducted

atop the other substrates. The carpet substrate ignited early in the development of the wood crib fire, resulting in a larger fire size and in turn more rapid development.

(a) – on Plywood

(b) – on Carpet

(c) – on Vinyl

Figure 6.2. Photographs of burning polyurethane foam chair mock-up on various substrates

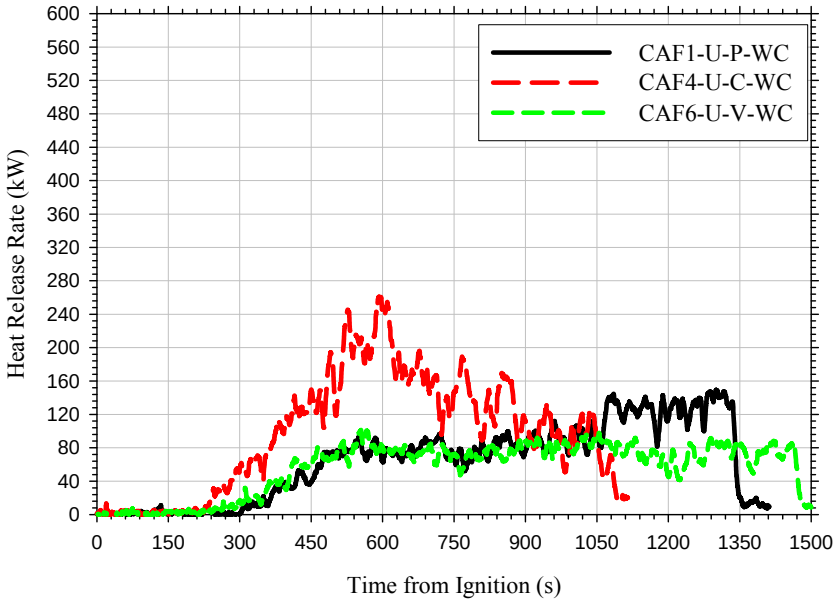

Figure 6.3. Heat release rates from wood crib source on plywood (P, black), carpet (C, red) and vinyl (V, green) substrates

(a) – on Plywood (b) – on Carpet (c) – on Vinyl

Figure 6.4. Photographs of burning wood cribs on various substrates

The third Class A fuel evaluated was the plastic baby seats. A comparison of the burning behavior of these seats atop the plywood, vinyl, and carpet substrates is presented in Figure 6.5. Photographs of the burning baby seats are provided in Figure 6.6. Once ignited, the baby seats quickly became fully-involved and began to melt and form a molten pool of plastic that burned beneath the remnants of the seat. In all cases, the seat was fully consumed with the metal buckles being the only remnant. The test conducted atop the carpet substrate resulted in the largest heat release rate, followed by the plywood, and then the vinyl flooring. This is consistent with the results from the other Class A fuel fires and is a direct result of the contribution of the substrate in the fire.

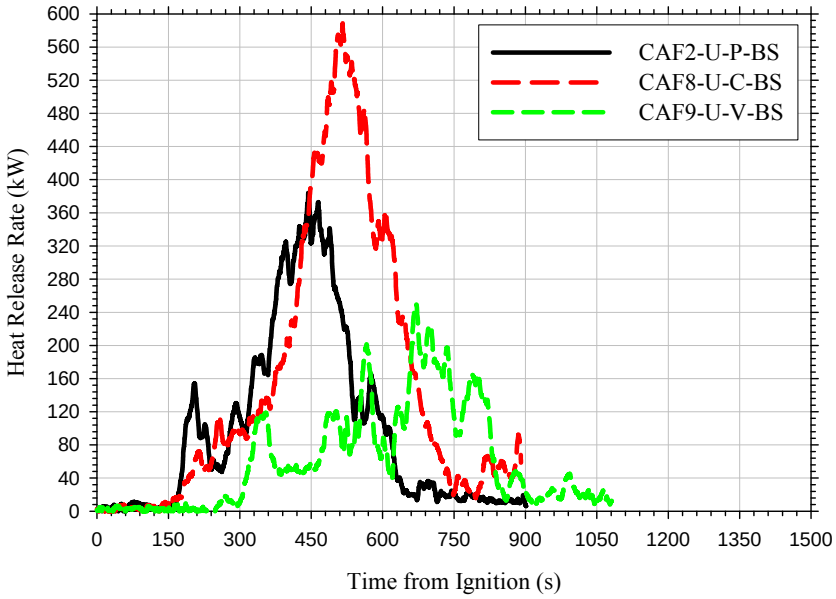

Figure 6.5. Heat release rates from infant baby seat source on plywood (P, black), carpet (C, red) and vinyl (V, green) substrates.

(a) – on Plywood (b) – on Carpet (c) – on Vinyl

Figure 6.6. Photographs of burning plastic baby seats at various times after ignition, on various substrates

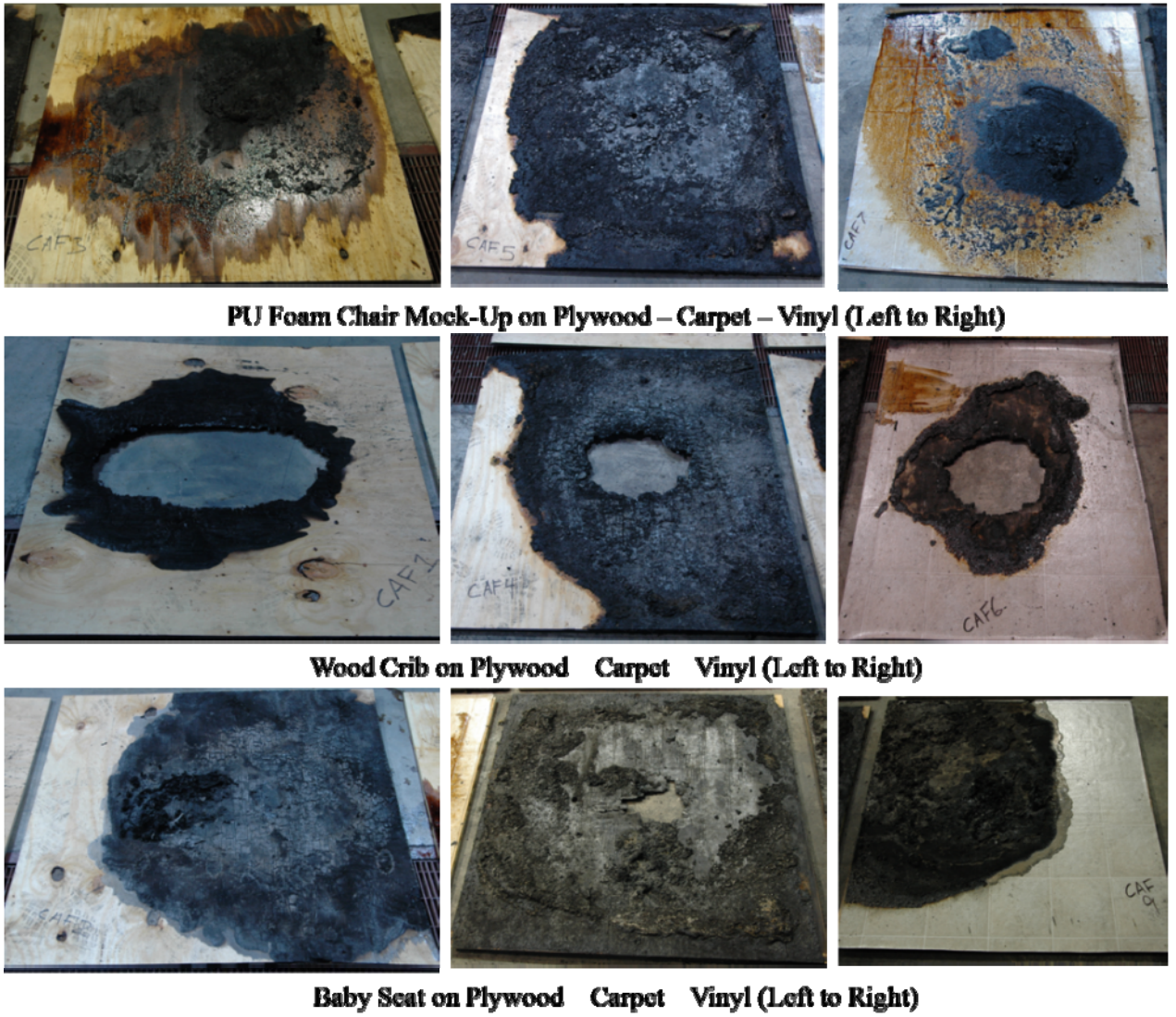

Figure 6.7. Photographs of fire patterns resulting from various Class A material fires

6.1.3 Class A Fire Patterns

In general, the Class A fires conducted on each of the three substrates resulted in burning durations 2–10 times longer than those measured in any of the fuel spill tests conducted. This large range in burning durations resulted in varying fire patterns observed on the substrates. A photograph of each substrate as observed after the Class A fires is provided in Figure 6.7. Furthermore, an average char depth for each of the Class A substrates is provided in Table 6.1.

Table 6.1. Range of Char Depths Measured on Substrates after Class A Fire Exposures

	PU Foam Chair Mock-Up	**Wood Crib**	**Infant Baby Seat**
Plywood	1–2 mm	Burn-through	1–2 mm
Carpet w/ Padding	5–6 mm		Burn-through
Vinyl	1–2 mm		1–2 mm

The infant baby seat fire scenarios resulted in superficial burn patterns for both the plywood and vinyl substrates. Similar to that indicated for the PU foam chair mock-up, the burning plastic chairs are reduced to a burning pool of plastic which prevents radiant energy from the fire from damaging the substrate. The only scenario in which the burning baby seat resulted in significant damage to the substrate was the carpet scenario, and this was attributed to the contribution of the carpet and padding material once involved.

The PU foam fires resulting from the chair mock-up scenario only produced superficial damage on both the plywood and vinyl substrates. These substrates provided a medium on which the molten PU foam could pool and burn. This pooling of the melting PU foam prevented any significant amount of thermal energy from being transferred into the substrate due to the fact that it was being absorbed by the burning pool. As a result of this pooling, the PU foam chair mock-up fires produced significant staining (i.e., discoloration of the substrate) but very little actual thermal damage to the material. PU foam testing conducted on the carpet substrate did, however, result in thermal damage to the substrate (i.e., carpet and padding) as well as the plywood underlayment. In these tests the burning PU foam dripping from the chair involved the carpet and padding material. Visualization of the fire patterns resulting from the PU foam chair mock-up on each substrate are provided in Figure 6.7.

The wood crib fire scenarios all resulted in a similar fire pattern no matter what substrate was used. In these scenarios, the substrates were completely consumed in the area directly beneath the burning crib due to the large degree of radiant energy produced within the internal structure of the burning crib. In general, the area consumed was circular in nature and varied in size ranging from 0.3–0.6 m (1–2 ft) in diameter. The wood crib was 0.3 m (1 ft) square.

The char depths reported in Table 6.1 were measured using a steel center punch with a point diameter of approximately 0.94 mm (0.04 in.). Char depth was consistently measured for all substrates using a 4.5 kg (10 lbs.) mass applied to the back of the punch thus exerting the same amount of force for all measurements. After each measurement, the center punch was removed and the degree of insertion (i.e., char depth) was measured using a Mahr 16ES digital micrometer. It should be noted that these measurements were taken relative to the top layer of

material present after the test, not the top layer of material present at the start of the test. However, the materials were well preserved after each test, thus it is not expected that a significant amount of surface material was lost.

6.2 Spill Fire Patterns on Combustible Substrates

6.2.1 Wood Substrates

6.2.1.1 Oriented Strand Board Fire Patterns

Spill fire tests using three different fuels (gasoline, kerosene, denatured alcohol) were conducted on an oriented strand board (OSB) substrate. These spill scenarios were comprised of 0.5 L (0.13 gal.) of liquid that was permitted to spread over the wood surface for a period of 30-seconds. Resulting fire sizes ranged from 170–570 kW with burning durations ranging from 30–90 seconds. Representative photographs of the gasoline, kerosene, and denatured alcohol fires and the resulting damage to the substrate are provided in Figure 6.8.

As is evident in Figure 6.8, the thermal damage resulting from the spill fire is relatively minimal (i.e., char depths less than 1 mm) for all three fuels considered. However, based upon visual observation, the most damage resulted from the kerosene exposure fire and the least damage resulted from denatured alcohol fires. These differences in thermal damage are consistent with the differences in the heat release rate per unit area (HRRPUA) measured for each of the fuel fires.

The denatured alcohol spill produced a 286 kW/m^2 fire which resulted in the least damage to the OSB substrate with only localized areas of thermal discoloration of the wood material. Char measurements were attempted for this sample, but no quantifiable char depth could be measured. The short duration of this fire coupled with the relatively small fire size and weak radiation fraction did not produce a thermal insult severe enough to char the material to any significant depth. The gasoline spill produced a fire that was approximately 2.5 times larger than that of the denatured alcohol fire (i.e., 805 kW/m^2). Correspondingly, the amount of thermally discolored material was much larger with some localized areas of char depths measuring 1–2 mm. The kerosene spill produced a fire that was twenty percent larger than that of the gasoline (i.e., 961 kW/m^2). This fire resulted in an even larger area of the material being thermally discolored. Although a larger area of the substrate was thermally discolored as a result of the kerosene spill, char depths measured after the tests were still 1–2 mm in very localized areas with the majority of the pattern being immeasurable.

6.2.1.2 Plywood Fire Patterns

Spill fire tests using three different fuels (gasoline, kerosene, denatured alcohol) were conducted on a plywood substrate. These spill scenarios were comprised of 0.5 L (0.13 gal.) of liquid that was permitted to spread over the wood surface for a period of 30-seconds. Resulting fire sizes ranged from 155–595 kW with burning durations ranging from 30–90 seconds. Representative photographs of the gasoline, kerosene, and denatured alcohol fires and the resulting damage to the substrate are provided in Figure 6.9.

SFD126-U-O-G-0.5-30 – During test

SFD126-U-O-G-0.5-30 – Post-fire

SFD150-U-O-K-0.5-30 – During test

SFD150-U-O-K-0.5-30 – Post-fire

SFD132-U-O-DA-0.5-30 – During test

SFD132-U-O-DA-0.5-30 – Post-fire

Figure 6.8. Photographs of gasoline, kerosene, and denatured alcohol fire exposures and resulting fire patterns on oriented strand board (OSB)

SFD41-U-P-G-0.5-30 – During test

SFD41-U-P-G-0.5-30 – Post-fire

SFD43-U-P-K-0.5-30 – During test

SFD43-U-P-K-0.5-30 – Post-fire

SFD45-U-P-DA-0.5-30 – During test

SFD45-U-P-DA-0.5-30 – Post-fire

Figure 6.9. Photographs of gasoline, kerosene, and denatured alcohol fire exposures and resulting fire patterns on plywood, respectively

In general, the characteristics of the damage patterns observed for the fuel spill fires conducted atop the plywood substrate were very consistent with those reported for the OSB. In these tests, the denatured alcohol spill fire resulted in little to no fire pattern, with edge effects observable as with a wetted area. The gasoline fire pattern was more evident with varied areas of thermal discoloration intermixed with areas of wood relatively unchanged. In the case of the kerosene fire patterns on plywood, the severity of the damage to the substrate varied significantly within the pattern. For this pattern, the outermost 'ring' was found to be nothing more than singed plywood showing only minimal evidence of thermal damage, while the interior sixty to seventy percent of the pattern consisted of plywood material that was thermally discolored (i.e., blackened).

6.2.2 Vinyl Substrates

The analysis of fire patterns produced on vinyl flooring considered two different variables. The impact of fuel spill depth on the degree of damage to the substrate was examined using the diked fire and spill fire test series. The impact of the fuel type on the degree of damage to the substrate was examined using the spill fire test series.

6.2.2.1 Vinyl Spill Fire Patterns

Gasoline, kerosene, and denatured alcohol were burned on vinyl substrates using 0.5 L (0.13 gal.) and 1.0 (0.26 gal.) spill quantities that were permitted to spread over the vinyl for a period of 30-seconds. Resulting fire sizes ranged from 387–1687 kW with burning durations ranging from 40–80 seconds. Representative photographs of the various fuel spill fires and resulting damage to the substrate are provided in Figure 6.10.

The fire patterns resulting from both the gasoline and kerosene spills on the vinyl substrate resulted in the thermal discoloration and charring of the vinyl material. However, in these tests, thermal damage to the wood underlayment was never observed. These findings are consistent with those reported in the Putorti [3]. In both cases however, the vinyl material was thermally degraded to the point where the material cracked (see Figure 6.11) and exposed the adhesive layer used to bond the vinyl to the plywood, which in turn became involved in the fire.

6.2.2.2 Vinyl Diked Fire Patterns

Observations were made on each of the diked fire tests conducted on 1.49 m^2 (16 ft^2) vinyl substrates to evaluate the impact of fuel depths (ranging from 1–20 mm) on the thermal damage to the substrate. A photograph of the evolution of the fire patterns and thermal degradation of the vinyl/wood underlayment as a function of fuel thickness are provided in Figure 6.12.

As shown in Figure 6.12, the measured char depths did increase as a function of fuel layer depth. These char rates are relatively consistent with typical char rates reported in the literature [NFPA 921, 2008, EuroCode, 1995] which range from 0.5–4.0 mm/min. On average, the charring rates measured in these tests (0.5–1.0 mm/min) were on the low end of the range provided in the literature. This could be a result of the vinyl substrate being presented during the first stage of the fires.

SFD66-U-V-G-1.0-30 – During test

SFD66-U-V-G-1.0-30 – Post-fire

SFD64-U-V-K-0.5-30 – During test

SFD64-U-V-K-0.5-30 – Post-fire

SFD65-U-V-DA-1.0-30 – During test

SFD65-U-V-DA-1.0-30 – Post-fire

Figure 6.10. Photographs of gasoline, kerosene, and denatured alcohol fire exposures and resulting fire patterns on vinyl substrate

(a) – Degradation of Vinyl due to Gasoline Spill

(b) – Degradation of Vinyl due to Kerosene Spill

Figure 6.11. Photographs of thermal degradation of vinyl substrate due to gasoline and kerosene spill fires

(a) – 1 mm Gasoline Layer
Burning Duration = 55s
Char Depth = Not measureable

(b) – 2 mm Gasoline Layer
Burning Duration = 75s
Char Depth = Not measureable

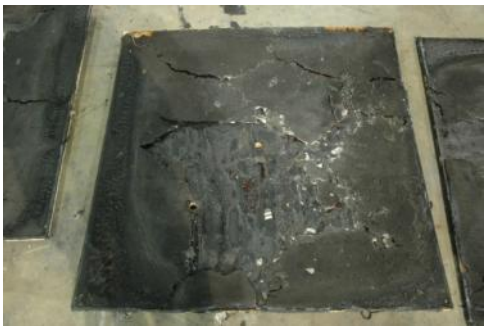

(c) – 3 mm Gasoline Layer
Burning Duration = 110s
Char Depth = 1–2 mm

(d) – 4 mm Gasoline Layer
Burning Duration = 140s
Char Depth = 1–2 mm

(e) – 5 mm Gasoline Layer
Burning Duration = 140s
Char Depth = 1–2 mm

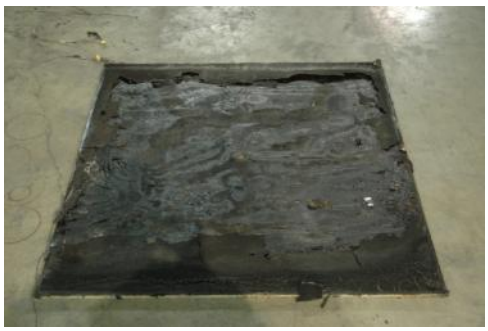

(f) – 20 mm Gasoline Layer
Burning Duration = 315s
Char Depth = 4–5 mm

Figure 6.12. Photographs of thermal degradation of vinyl substrate as a function of gasoline fuel depth

6.2.3 Carpet Substrates

In the carpet tests, three different stages of burning were observed. The first stage consisted of the burning of the liquid fuel over the entire area of the spill. This stage generally lasted between 45–90 seconds. During this stage it was observed that in the center of the spill fire, the carpeting on which the fuel was initially poured remained intact for an extended period of time. This behavior was consistent with the mechanisms that have been attributed to the formation of the

'doughnut' type patterns that have been reported in the literature [3, 23]. After this initial stage, the area involved in the fire expanded due to the involvement of the surrounding combustible carpet/carpet padding material. Based upon visual observations, the degree of involvement of the surrounding carpet was dependent upon the quantity of fuel spilled. As the quantity of fuel spilled increased, so did the area involved during this period of fire growth. This is attributed to the increased amount of incident heat flux imposed upon the surrounding carpet material as the fire size increases with increasing fuel quantity. After two to three minutes of fire growth, the spill fire diminished leaving only the fuel soaked center to continue burning with some flaming around the perimeter. The burning of the fuel soaked center was generally a relatively short event with burning continuing for one to two minutes; however, the progression of the perimeter flaming outward was found to be indefinite. In several tests, this perimeter burning was permitted to burn for extended periods of time (i.e., 60–90 minutes). Consequently, the area of the fire pattern on the carpet substrate evaluated in this work was found to be dependent upon the burning duration; thus, it is possible for carpet fire patterns to be significantly larger than the initial spill area due to extended burning. Photographs documenting the evolution of carpet spill fires resulting from 0.5 L (0.13 gal.) of gasoline and kerosene are provided in Figure 6.13 and Figure 6.14, respectively.

Initial Spill Area

Peak Fire Size

Primary Extinguishment

Final Burn Pattern

Figure 6.13. Progression of gasoline spill fire on carpet (SFD49-U-C-G-0.5-30) from spill to self-extinguishment with resulting burn pattern

Initial Spill Area

Peak Fire Size

Primary Extinguishment

Final Burn Pattern

Figure 6.14. Progression of kerosene spill fire on carpet (SFD52-U-C-K-0.5-30) from spill to self-extinguishment with resulting burn pattern

Post-fire examination of the carpet spill fire burn patterns demonstrated that the patterns generated on the various layers of the substrate (i.e., carpet, carpet pad, and plywood) were very similar in both shape and area. An example of this is provided in Figure 6.15 which illustrates the presence of the 'doughnut' pattern on each layer of the carpet flooring system. In Figure 6.15, the general shape of the burn pattern outlined with a dashed green line while the centrally located less burned area is outlined in a solid red line.

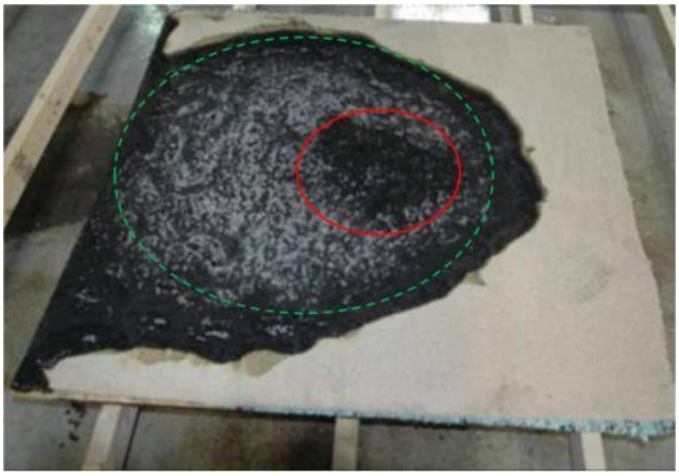

Final Burn Pattern on Carpet Surface

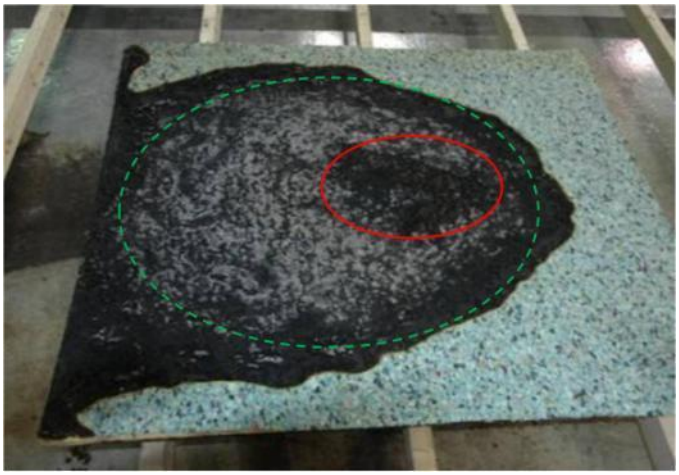

Final Burn Pattern at Padding Interface Surface

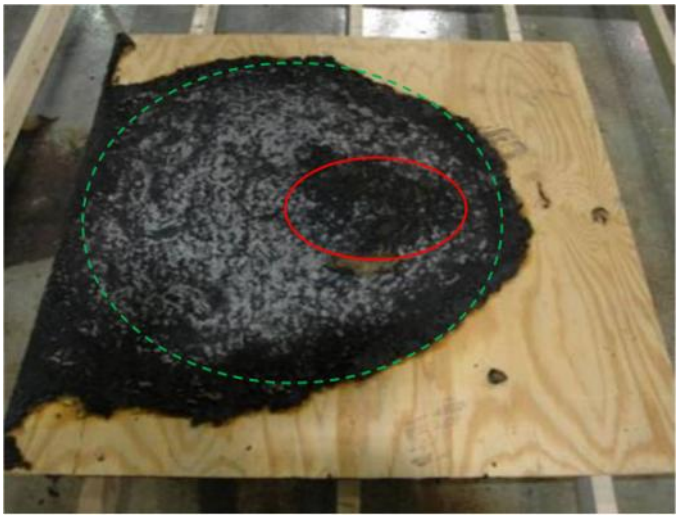

Final Burn Pattern at Plywood Interface

Figure 6.15. Photographs showing the doughnut pattern through all three substrate layers (carpet, pad and wood) from a 1 L kerosene spill fire (SFD-U-C-K-1.0-30)

6.3 Spill Fire Patterns on Concrete Substrates

6.3.1 Smooth, Unfinished Concrete

Gasoline spill fire tests on a smooth, unfinished concrete substrate were conducted using 0.5 and 1.0 L (0.13–0.26 gal.) spill quantities that were permitted to spread over the concrete for a period of 30 or 300 seconds. Resulting fire sizes ranged from 105–600 kW with burning durations ranging from 30–60 seconds. Photographs of the initial spill, the ensuing fire, and the fire patterns resulting from these gasoline fires are provided in Figure 6.16.

Initial Spill Area | Peak Fire Size

Final Fire Pattern | Fire Pattern (zoom)

Figure 6.16. Photographs of initial spill area, peak fire size, and resulting fire patterns from gasoline on smooth, unfinished concrete (SFD-U-SC-G-0.5-30)

Thermal damage to the concrete (i.e., cracking, spalling, pitting, etc.) was not observed during any of the spill fire tests. As shown in Figure 6.16, the patterns resulting from these fires were primarily staining from the decomposition of the fuel and the thermal discoloration of the concrete as a result of the fire. After the fire patterns were documented for each test, the patterns were cleaned using soapy water and a deck mop. However, as can be seen in Figure 6.16, patterns from previous spills remained even after cleaning. Although the gasoline was spilled in a way that ideally would provide a circular spill, the fire patterns were irregular in shape.

6.3.2 Brushed Concrete

Gasoline spill fire tests on a smooth, unfinished concrete substrate were conducted using 0.5 and 1.0 L (0.13 and 0.26 gal.) spill quantities that were permitted to spread over the concrete for a period of 30 or 300 seconds. Resulting fire sizes ranged from 291–633 kW with average burning durations of 60 seconds. Photographs of the initial spill, the ensuing fire, and the fire patterns resulting from these gasoline fires are provided in Figure 6.17.

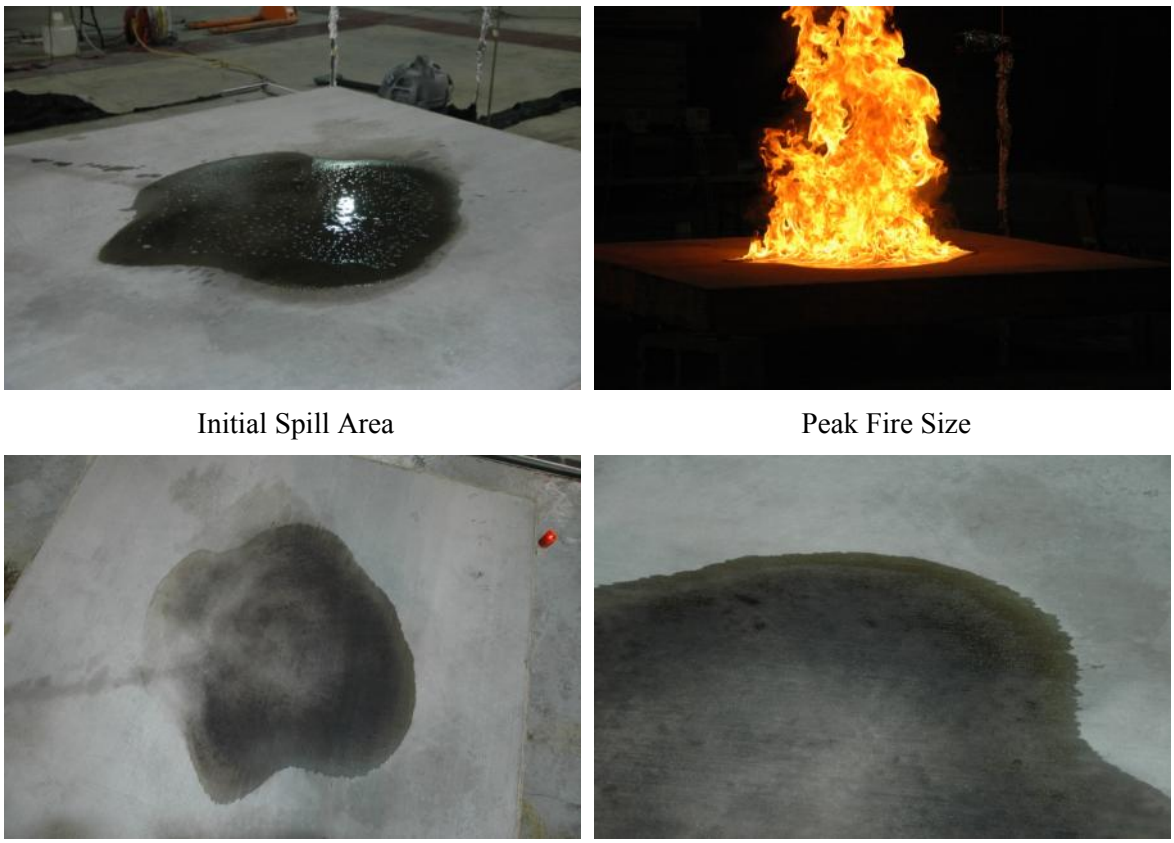

Initial Spill Area | Peak Fire Size

Final Fire Pattern | Final Fire Pattern (zoom)

Figure 6.17. Photographs of initial spill area, peak fire size, and resulting fire patterns from gasoline on brushed concrete (SFD-U-BC-G-0.5-30)

The gasoline fire patterns observed on brushed concrete were comparable to those documented for the smooth concrete substrate. No thermal damage to the concrete (i.e., cracking, spalling, pitting, etc.) was observed, and the patterns resulting from these fires were primarily due to staining from the decomposition of the fuel and to the thermal discoloration of the concrete as a result of the fire. After the fire patterns were documented for each test, the patterns were cleaned using soapy water and a deck mop.

6.3.3 Coated Concrete

Spill fire tests using four different fuels (gasoline, kerosene, denatured alcohol, n-Heptane) were attempted on the coated concrete substrate. However, the kerosene spill fires were unsuccessful due to the inability of the kerosene to support flame spread and sustained burning; only localized

burning was achieved near the ignition source. Consequently, the kerosene fuel was not considered in further spill fire testing on the coated concrete. The spill scenarios were comprised of both 0.5 L (0.13 gal.) and 1.0 L (0.26 gal.) spill quantities that were permitted to spread over the surface for periods of 30 and 300 seconds. Resulting fire sizes ranged from 75–1191 kW with burning durations ranging from 45–90 seconds. Of the three fuels used, only the gasoline spill fires resulted in any visual evidence of a fire pattern on the coated concrete surface. Both the denatured alcohol and n-Heptane fuels burned to completion and left no fuel residue or thermal discoloration of the coated concrete. Representative photographs of a fire and pattern resulting from a gasoline spill conducted on the coated concrete is provided in Figure 6.18.

Peak Fire Size Fire Pattern

Figure 6.18. Photographs of peak fire size and resulting fire pattern from gasoline on coated concrete (SFD-U-CC-G-0.5-30)

6.4 Correlation between Spill and Fire Patterns

The spill fire patterns were analyzed to characterize the relationship between initial spill area and the area contained within a fire pattern. Putorti [3] conducted a similar analysis for wood parquet flooring, vinyl flooring, and carpet. In his work, Putorti developed general correlations that could be used to correlate gasoline spill volume to fire pattern area for these substrates. Given that similar, but not identical substrates were evaluated in this work a series of comparisons were made to understand how applicable these correlations are to different materials. Comparisons were made for each of the three flooring materials for which correlations were developed and the results are provided in Tables 6.2, 6.3, and 6.4.

Table 6.2. Comparison of Gasoline Spill Area and Fire Burn Pattern Areas on Wood Substrates as Predicted by Putorti and Measured In This Study

Spill Qty (mL)	Predicted Wood Spill Area (m^2)	Predicted Wood Burn Pattern Area (m^2)	Plywood Spill Area (m^2)	Plywood Burn Pattern Area (m^2)	OSB Spill Area (m^2)	OSB Burn Pattern Area (m^2)
500	0.75	0.93	0.46	0.52	0.58	0.66
	24% increase		13% increase		14% increase	

Table 6.3. Comparison of Gasoline Spill Area and Fire Burn Pattern Areas on Vinyl as Predicted by Putorti and Measured In This Study

Spill Qty (mL)	Ignition Delay Time (s)	Predicted Vinyl Spill Area (m^2)	Predicted Vinyl Burn Pattern Area (m^2)	Measured Vinyl Spill Area (m^2)	Measured Vinyl Burn Pattern Area (m^2)
500	30	0.9	0.9	0.58	0.59
	300			1.0	1.02
Average difference between spill and burn area				2% increase	
1000	30	1.8	1.7	1.3	1.3
	150			1.9	1.9
Average difference between spill and burn area				<1% increase	

Table 6.4. Comparison of Gasoline Spill Area and Fire Burn Pattern Areas on Carpet as Predicted by Putorti and Measured In This Study

Spill Qty (mL)	Predicted Carpet Spill Area (m^2)	Measured Carpet Spill Area (m^2)
500	0.06	0.21
1000	0.11	0.23
5000	0.47	0.39

As shown in Table 6.2, the spill and burn pattern areas measured in this work were significantly less than those predicted using the correlations provided by Putorti for wood parquet flooring. The plywood and OSB spill areas were 39 and 23 percent less than that predicted using the Putorti correlation, respectively. Two factors may be the cause: the differing spread times used in the two studies and the differing types of wood substrates that were evaluated. All of the data with which the correlations were developed was collected for a 60 second ignition delay whereas the results in this study, for the wood substrates were all collected with a 30-second ignition delay. It is likely that in the shorter spread time in this study resulted in the liquid spreading over a smaller area. Recall, at 30-seconds, the spread on plywood and OSB substrates was measured to be on average 64% of the maximum spill area; whereas at 60 seconds, it was 76% [Section 4.5.3]. Therefore, the effect of the spread time is estimated to account for about 31 and 53% of the difference observed for plywood and OSB, respectively.

In this study, the wood substrates were raw materials (i.e., unfinished wood) susceptible to liquid absorption, whereas the substrate for which the correlation was developed consisted of wood tiling that was coated with a manufacturer applied polyurethane finish [Putorti, 2001]. This coating would have made the substrate highly impermeable and smoother, which would allow the gasoline to flow to larger spill areas.

The correlation for the wood parquet flooring indicates that the burn pattern area for this substrate should be 24% larger than that of the initial spill area. For plywood and OSB, the burn pattern was measured to be 13 and 14 percent larger. In the case of the finished wood evaluated

by Putorti, the polyurethane finish may have contributed to the larger burn area compared to the unfinished plywood and OSB materials.

For the vinyl substrate, the spill and burn pattern areas measured were consistent with those predicted using the correlations developed by Putorti [2001] as shown in Table 6.3. Similar to the wood substrate, both the substrate type and the ignition delays (e.g., spread times) evaluated in these two studies were different. However, in the case of the vinyl, the ignition delay times evaluated included both 30 and 300-second delays which bounded the 60 second values from which the correlations were developed. The effects of the substrate were generally thought to be negligible because both surfaces provided an impermeable medium through which liquid could not penetrate. The measured spill and burn pattern areas for the 30 and 300-second ignition delays evaluated in this study generally bound the predicted values for both the 0.5 L (0.13 gal.) and 1.0 L (0.26 gal.) quantities. For both of these fuel quantities, the longer ignition delay time was comparable to the predicted spill areas, while the spill area measured after 30-seconds was on average 32 percent smaller.

For the carpet substrate, only comparisons of initial spill area could be made due to the fact that burn pattern areas were not correlated in the literature [Putorti, 2001]. In both the literature [Putorti, 2001] as well as in this work, the burn pattern area was a function of how long the carpet/padding was allowed to burn after the phase where the majority of gasoline was consumed. Consequently, correlation between quantity and burn pattern area could not be developed. As shown in Table 6.4, comparisons between the areas measured and those predicted were generally inconsistent despite the fact that the carpet substrates used appear to be very similar. For the 0.5 L (0.13 gal.) and 1.0 L (0.26 gal.) spills, the spill areas measured in this study were 54 and 71 percent larger than those predicted. While for the 5.0 L (1.3 gal.) spills, the area measured was 17 percent less.

Assuming the carpet and padding to be similar between Putorti's tests and this study, the only other difference between the tests was the mechanism used to spill the liquid. These differences included the height from which the liquid was poured and means by which the liquid was poured. Data provided by Putorti [3] was collected from spills poured from an elevation of 0.5 m (20 in.) by rotating a cylinder ninety degree from vertical. The data collected in this study was obtained from spills poured from an elevation of 0.3 m (12 in.) discharged by opening a ball valve and allowing the liquid to empty from the bottom of a container. It is possible that the differences in the spill areas shown in Table 6.4 are due in part to the two spill mechanisms and also due to uncharacterized differences in the carpet and pad that impact liquid absorption.

In general for wood and vinyl substrates, the area within a fire pattern was comparable to that of the spill area. For the wood substrates, the burn pattern area was consistently about 10–15% larger than the initial spill area. For the vinyl, the results were more similar with average areas being less than 10 percent different. For all tests, the area of the initial burn pattern was found to be larger than the initial spill area.

The carpet fire patterns were dependent on the total duration of time they were allowed to burn due to continued flame spread on the carpet and padding beyond the spill fire. Consequently, a ratio of burn area to spill area is not applicable. Instead, an analysis was conducted to determine an average spread rate for the carpet/padding substrate. This spread rate was determined using

area and perimeter measurements collected at one minute intervals. These rates were collected from the time at which all flaming on the interior of the pattern extinguished until the time at which the test was ended via manual extinguishment. The range of time over which data was collected varied from 5–60 minutes. Average spread rates were calculated for each of the fuels used in the carpet spill fire testing (i.e., gasoline, kerosene). A summary of the measured rates for the carpet/padding system evaluated in this study are presented in Table 6.5. In general, it was found that the spread rates were comparable for both fuels and found to be independent of the quantity of fuel spilled.

Table 6.5. Average Flame Spread Rates for Carpet/Padding System Evaluated In This Study

Fuel	**Spread Rate (m/min. [in/min.])**
Gasoline	0.011 ± 0.004 [0.41 ± 0.16]*
Kerosene	0.014 ± 0.003 [0.55 ± 0.12]*

*It should be noted that these rates are specific to the carpet and padding materials used in this study. While similar rates may be observed for other carpeting systems, the specific values presented are unique to the system evaluated.

Further analysis of the patterns resulting from the carpet spill fires identified a potential means of differentiating between the area involved in the initial spill area and the area involved as a result of the continual burning of the carpet/pad material. An illustration of this difference is provided in Figure 6.19. Two areas were identified within the carpet patterns that could be differentiated by their surface characteristics. The area of initial spill involvement was generally completely consumed and had a relatively flat topography, except the mound of material at the center due to the ‘doughnut’ effect. When moving radially outward from the center of the pattern, the topography transitioned from flat surface to a wavier surface comprised of peaks and valleys, as shown in Figure 6.19. It was also noted that the material from which these peaks and valleys were made was generally less consumed (i.e., charred but not burned to ash) when compared to the material in the center of the pattern.

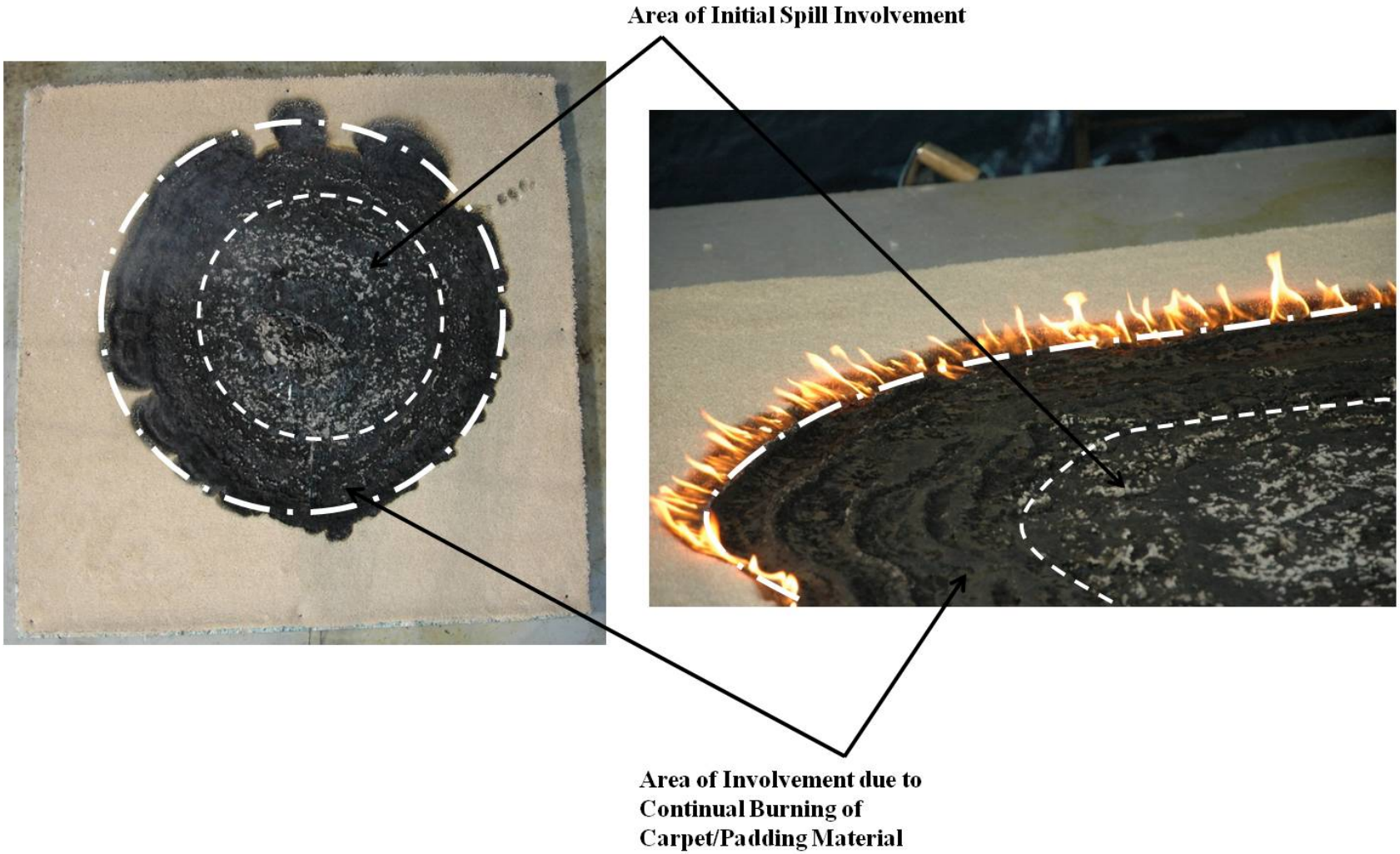

Figure 6.19. Illustration showing the observed differences between the area of initial involvement due to liquid fuel burning and the area involved as a result of the continued burning of the carpet/padding material

6.5 Differentiation between Class A and Liquid Fuel Spill Fire Patterns

One of the primary forensic objectives of this work was to determine whether post-fire indicators exist to differentiate fires with liquid fuel ignition sources and Class A fire sources, particularly those that result in localized burning and/or pooling of burning material. In order to address this objective, three different Class A sources were tested atop three different substrates. The fire patterns resulting from these Class A materials and liquid fuel fires are compared in Figure 6.20, Figure 6.21, and Figure 6.22.

In Figure 6.20, the patterns occurring atop a plywood substrate are presented for six different fuel sources. In these tests, fire patterns varied in severity from superficial charring for the gasoline and kerosene fires to complete burn through for the wood crib. The patterns observed were generally the same size and geometry. In these tests, only the wood crib source resulted in thermal damage to the substrate (i.e., char depths greater than 1 mm). Two of the three fuel spill fires resulted in some thermal discoloration of the plywood substrate but no char depth could be measured. The denatured alcohol spill did not thermally discolor nor thermally damage the plywood, and a residual pattern on the substrate was challenging to accurately identify visually. The only case in which the plywood substrate became involved as a result of the burning fuel was the wood crib; for all other sources, the substrate was only thermally discolored.

In addition to the characterization of the patterns via char depths, qualitative observations were also made in an effort to identify differences between the Class A and flammable liquid fires. As noted above, the shapes of the patterns are not notably distinct. Even the relatively square class A sources produced circular type patterns. The infant baby seat and PU foam chair tests left a visible oily residue, which absorbed into the substrate, thus staining the material.

In Figure 6.21, the patterns occurring atop a vinyl substrate are presented for six different fuel sources. The patterns observed were of generally the same size and geometry. In these tests, the vinyl substrate became involved as a result of all six fuels burning. In all tests, except for the wood crib, the damage to the plywood underlayment was minimal, ranging from no quantifiable thermal damage to superficial damage of depths from 1–2 mm. It should also be noted that in these tests, the denatured alcohol spill fire did result in an easily identified pattern clearly shown from thermal damage to the vinyl. For this substrate, only the PU chair mock-up fire resulted in an oily residue remaining after the fire.

Fire patterns from the tests conducted on the carpet/padding substrate are compared in Figure 6.22. In general, thermal damage to the plywood underlayment was more severe for all fire sources considered than observed for the other substrates. The greater degree of damage is reflective of the contribution of the burning carpet/padding rather than the specific fuels being tested. In these tests, both the infant baby seat and wood crib resulted in complete burn through of the plywood underlayment.

Gasoline

Infant Baby Seat

Kerosene

Wood Crib

Denatured Alcohol

PU Foam Chair Mock-Up

Figure 6.20. Comparative photographs of the plywood fire patterns resulting from 0.5 L liquid fuel spill and Class A material fires

Gasoline

Infant Baby Seat

Kerosene

Wood Crib

Denatured Alcohol

PU Foam Chair Mock-Up

Figure 6.21. Comparative photographs of the vinyl fire patterns resulting from 0.5 L liquid fuel spill and Class A material fires

Gasoline

Infant Baby Seat

Kerosene

Wood Crib (Note: Carpet/padding layers have been removed.)

(Not Tested)

Denatured Alcohol

PU Foam Chair Mock-Up

Figure 6.22. Comparative photographs of the carpet fire patterns resulting from 0.5 L liquid fuel spill and Class A material fires

Several types of patterns were consistently identified for certain fuel types. Examples of these patterns included liquid fuel spill fires consistently resulting in irregularly-shaped burn patterns with minimal thermal damage to the substrate, except in the case of carpet scenarios. Class A fuels constructed from plastic/foam materials consistently left an oily residue on the substrate after self-extinguishing. If there are no other combustibles, it is unlikely that a liquid spill fire will result in thermal damage to wood, vinyl or concrete substrates of more than a millimeter or two. However, it is possible that the aforementioned patterns could be produced via other limited quantity class A sources burning under different conditions or that these patterns could be destroyed when the fire is placed within an enclosure proximate to other burning items.

Therefore based on visual patterns and char depth measurements, no conclusive, objective post-fire indicators were identified to substantiate a fire pattern resulting from a liquid fuel fire. The conclusion of this evaluation is that in order to make assertions regarding the first item ignited, it is also necessary to collect representative samples of the substrate and have these samples analyzed for ignitable liquid residue as recommended in NFPA 921 [2008].

6.6 Ignition Potential of Spill Fire Scenarios

Understanding the thermal environment generated by a liquid fuel fire event can be valuable in that it provides a means of assessing the likelihood of fire spread to neighboring objects. This information can in turn be used by fire investigators to determine area of origin, path of spread, etc. when examining a scene. The heat flux data, summarized in Appendix D, provides quantitative data that can be used to assess the thermal hazard associated with various liquid fuel fire scenarios. As summarized in Table 4.15, spill fire scenarios, even of small volumes of fuel, can produce peak fire sizes ranging from 0.1 – 1.0 MW. Under steady-state conditions, fires of this magnitude can produce a thermal insult sufficient to ignite neighboring combustibles. However, as will be shown in this section, the potential to ignite adjacent combustibles is highly dependent on the thermal exposure time and not just the size of the fire. As shown earlier in this report, spill fire scenarios occur over relatively short time frames. They never achieve a steady-state condition or burn for a duration longer than 60 – 90 seconds, with peak burning generally occurring over a period of 10 – 15 seconds. It should be noted that the heat flux data presented in Appendix D are the 10-second peak average value from each test. These values were calculated in the same manner as the heat release rate presented in Eq. 4-1. The coupling of the fire size and burning duration data provides a means of assessing the thermal exposure to neighboring objects.

However, in order to assess the likelihood that neighboring objects become involved as a result of this exposure, it is necessary to characterize the energy needed to achieve ignition. While numerous studies have been conducted to evaluate the propensity of materials to ignite when exposed to heat, for this discussion, the work of Fleischmann et al. [2001] was considered because it dealt with the radiant ignition of upholstered furniture materials, a common secondary fire material. Fleischmann et al. found minimum ignition times to be 10–15 seconds for heat fluxes of 40 kW/m^2. This data was used to establish ignition criteria for neighboring materials in that the product of the incident flux and exposure duration yields the energy input per surface area of material (kJ/m^2). Using the data provided by Fleischmann et al. [2001] an average value for energy input per unit area was calculated to be 500 kJ/m^2. Using this criterion, combined with the average heat flux data measured in all tests representing liquid fuel fire scenarios (i.e., pan/diked fires with 1 mm fuel depths as well as spill fire scenarios), the required time to ignition was calculated and is presented in Table 6.6. The heat flux data presented in Table 6.6 represents heat fluxes measured at a distance of 1R from the center of the fire (i.e., at the edge of the spill pattern). This distance was selected because any closer proximity to the fire plume would result in sustained flame impingement and the heat fluxes measured at the 2R and 4R locations were far too low to result in the radiant ignition of material (i.e., < 2kW/m^2).

Table 6.6. Summary of Measured Heat Flux and Time Duration Required for Ignition of Combustible Materials with A Minimum Ignition Energy of 500 kJ/m^2

Scenario	10-s Average Peak Heat Flux (kW/m^2)	Time required to Ignite (s)
Pan (1 mm)	5	100
Diked (1 mm)	10	50
Spill (~1 mm)	4	125
Average	**6**	**79**

Based upon the data presented in Table 6.6, materials similar to those used on upholstered furniture would require exposure durations on the order of 79 seconds in order to ignite when exposed to the spill fire scenarios evaluated in this work. However, it should be noted that this exposure duration was determined using 10-second average peak heat flux values which are conservative considering heat fluxes of this severity are only produced during the 10–15 seconds of peak burning. Based upon the heat flux data collected in this work and the assumption of neighboring combustible materials having an energy input per surface area of 500 kJ/m^2 it is not likely that materials outside the flame plume become involved in a liquid fuel spill fire scenario.

7.0 ENGINEERING/FORENSIC ANALYSIS FRAMEWORK

The purpose of this section is to outline an approach that can be used to assess either the fire hazard associated with a given liquid fuel scenario or gain insight into the characteristics of a spill based upon the fire patterns produced by the event. Although the input data available for the two aforementioned scenarios (i.e., fire hazard analysis / forensic analysis) differ, a single framework was developed with various paths requiring various empirical data input.

7.1 Analytical Framework

As described by Beyler [2008], the primary threat associated with liquid fuel fire scenarios is thermal radiation. However, direct impingement to overhead structures can also be significant, and this is governed primarily by convective heating. Regardless of the mechanism, the thermal threat from a fire is known to be dependent upon various parameters including the following:

- Fuel type
- Spill geometry
- Burning duration
- Separation distance between the fire and neighboring objects
- Thermal characteristics of neighboring objects

The framework developed in this work will focus on the first three parameter listed above. The reader is referred to Beyler [2008] for a detailed presentation of currently available techniques

for calculating the thermal radiation threat from large, open hydrocarbon fires. The framework developed is provided two parts, shown in Figure 7.1 and Figure 7.2, were constructed to accommodate a wide range of potential liquid fuel spill/pool scenarios from both a fire hazard and forensic viewpoint, respectively. In total, four different fire hazard analysis paths and two different forensic analysis paths were identified.

7.2 Fire Hazard Analysis Framework

As indicated above, when conducting fire hazard analyses, fuel type and spill/pool configuration parameters are often user selected and/or varied to assess a wide range of fire scenarios. In this case, the user would identify the fuels of interest and obtain the relevant fire property data. Four different scenarios were identified for fire hazard analyses based upon the identification of confined and unconfined spill scenarios and fixed quantity and continuously-fed fuel supplies. These four paths generally encompass the vast majority of potential liquid fuel scenarios and require different analytical approaches to understand the resulting fire threat.

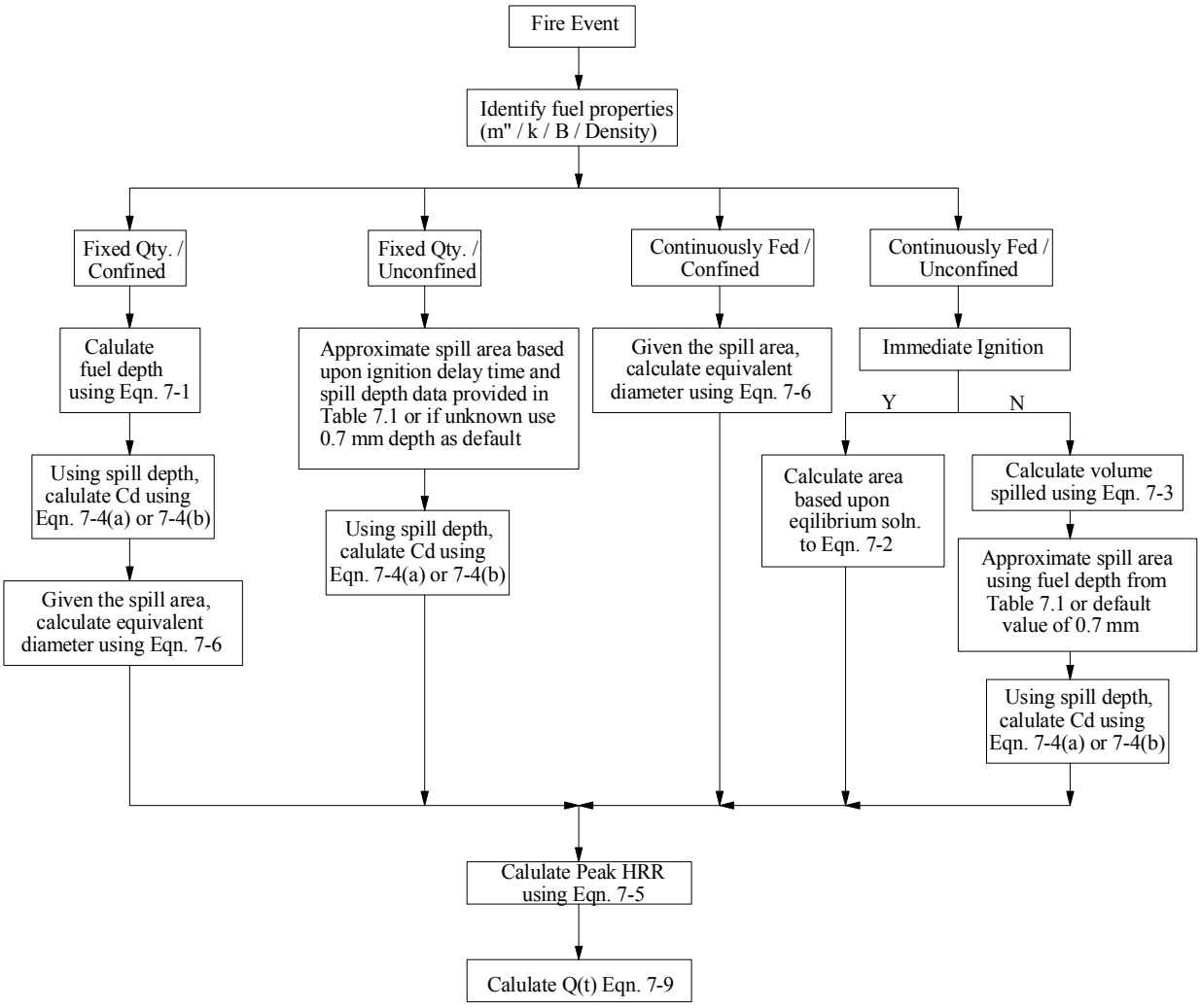

Figure 7.1. Analytical framework developed to characterize fuel spill/pool fire scenarios from a fire hazard viewpoint

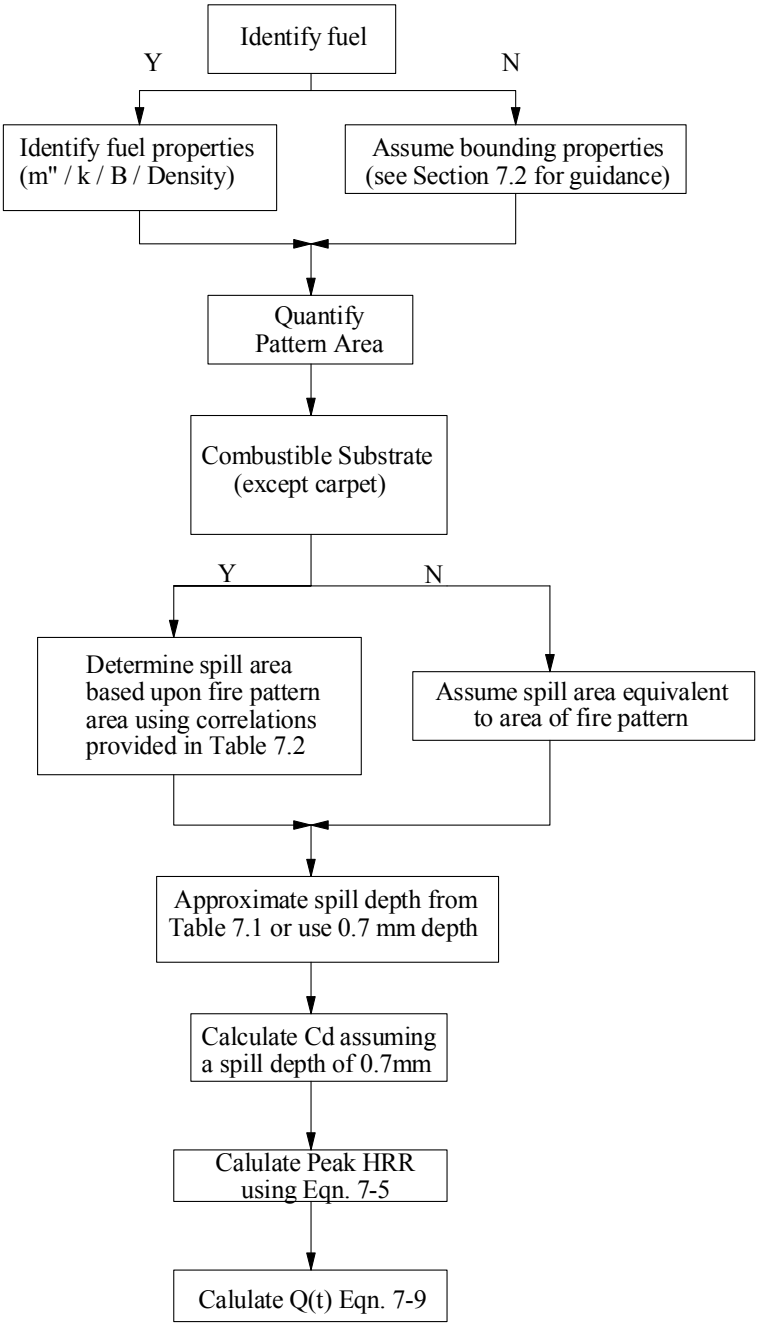

Figure 7.2. Forensic analytical framework developed to characterize fuel spill/pool fire scenarios

The first spill/pool scenario considered was a fixed quantity of fuel in a confined area. For the purposes of this discussion, it is assumed that the quantity of fuel is such that it covers the entire area of confinement otherwise it is considered as a fixed quantity, unconfined scenario. Based upon this assumption, an equilibrium spill depth can be calculated using the known volume of liquid spilled and the area of confinement as shown in Eq. 7-1.

$$\delta = \frac{V_o}{A_o} \qquad \text{Eq. 7-1}$$

where δ is the fuel depth (mm [ft]), V_o is the volume of liquid (L [gal.]), and the A_o is the area of confinement (m^2 [ft^2]).

The second scenario considered is a fixed quantity spill that is unconfined. In this scenario, the bulk flow of the liquid as well as the length of time between the spill and the ignition of the liquid dictates the area covered as opposed to bounding obstacles inhibiting the flow. The fuel depth reached in this type of scenario is generally thought to be on the order 1 mm or less [Gottuk & White, 2008]. This was supported by the data collected in this work for liquids with surface tensions ranging from 17.2–27.2 mN/m, which had an average spill depth of 0.72 $\pm$ 0.34 mm on a variety of substrates (i.e., coated, smooth and brushed concrete; vinyl; plywood and oriented strand board). However, as illustrated by the large standard deviation for the average spill depth presented above, the range of spill depths can vary significantly. The variation in this value is due to the different substrates and ignition delay times evaluated in this work. For a specific spill scenario in which the substrate and/or ignition delay times are known, more representative spill depths can be approximated using the data provided in Table 7.1. The data presented in Table 7.1 is presented in further detail in Section 5.3.1.

In addition to the average spill depths presented in Table 7.1, minimum and maximum spill depths are also provided. These depths can be used to approximate the spill depths resulting from the ignition delay times ranging from 30–300 seconds. In all cases, the minimum spill depth was measured for a 300-second ignition delay and the maximum spill depth was measured for a 30-second ignition delay. It should also be recalled that at 300 s, the spills were generally greater than 90 percent of the maximum spill area.

Table 7.1. Summary of Spill Depths Measured for Various Fuels on Various Substrates

Liquid	**Substrate**	**Average Depth (mm)**	**Standard Deviation (mm)**	**Min. (mm) [300 s ign. delay]**	**Max. (mm) [30 s delay]**
All*	All	0.72	0.34	0.22	2.4
Fuel	All	0.74	0.19	0.45	1.2
Simulants*	All	0.69	0.49	0.22	2.4
All*	Coated Concrete	0.66	0.18	0.32	0.96
All*	Smooth Concrete (NIJ)	0.53	0.08	0.38	0.64
All*	Smooth Concrete (ATF)	0.53	0.20	0.25	0.84
All*	Brushed Concrete	0.76	0.26	0.53	1.5
All*	Vinyl	0.63	0.26	0.22	1.0
All*	Plywood	1.02	0.41	0.38	1.6
All*	Oriented Strand Board	1.04	0.51	0.61	2.4
Gasoline	All	0.71	0.15	0.48	1.1
Denatured Alcohol	All	0.79	0.17	0.56	1.1
Kerosene	All	1.01	0.10	0.91	1.2
3% AFFF	All	0.43	0.15	0.22	0.70
3% FP	All	0.97	0.53	0.37	2.4
Lube Oil	All	1.54	0.55	0.86	2.4

Once an appropriate spill depth has been determined, the area of coverage for a given quantity spill can be calculated using Eq. 7-1. Similarly, if the area of coverage is known and a fuel depth is assumed, one can approximate the quantity of liquid spilled using Eq. 7-1.

The next scenario considered is a continuously-fed, fixed area (i.e., confined) fuel supply. In this scenario, it is assumed that the fuel supply rate is equal to or greater than the mass burning rate, such that a fixed area of some depth is maintained for an extended period of time. It is also assumed that the fuel does not overflow the confined area. In this scenario, the area is known and the depth of fuel is not important given that fuel is continuously supplied, and thus burn-out does not occur (i.e., steady-state burning is allowed to develop).

The final scenario identified is a continuously-fed, unconfined spill scenario. For this scenario, it necessary to identify the time of ignition given that this time will dictate the initial spill area. To address this parameter, two paths are possible. The first path assumes ignition immediately upon release of the liquid. Once ignited, the burning area of fuel will grow in size until an equilibrium spill area is achieved, which will occur when the fuel burning rate equals the fuel supply rate. Equation 7-2 represents the balance between these rates.

$$A_e = \frac{\rho \dot{V}_L}{\dot{m}''} \qquad \text{Eq. 7-2}$$

where A_e is the equilibrium spill fire burning area (m^2 [ft^2]), $\dot{V}_L$ is the volumetric fuel supply rate (m^3/s [ft^3/s]), ρ is the fuel density (kg/m^3 [$lbs./ft^3$]), and $\dot{m}''$ is the mass burning rate per unit area ($kg/s\text{-}m^2$ [$lbs./s\text{-}ft^2$]). Once this equilibrium solution is obtained, the maximum area of the spill is known, and the depth of fuel is not important given that fuel is continuously supplied and burn-out does not occur.

The other path identified for the continuously-fed, unconfined scenario is a delayed ignition (i.e., liquid is permitted to spill and spread for some period of time prior to ignition). As shown in Eq. 7-3, in this scenario, the area of coverage of the spilled liquid prior to ignition can be determined based upon the product of the volumetric flow rate, $\dot{V}_L$, the ignition delay time, and an assumed spill depth.

$$A_t = \frac{\dot{V}_L t}{\delta} \qquad \text{Eq. 7-3}$$

where A_t is the spill area (m^2 [ft^2]) at a given point in time, $\dot{V}_L$ is the volumetric fuel supply rate (kg/s [lbs/s]), t, is the time in seconds after the spill occurs prior to ignition, and δ is the calculated fuel depth (m [ft]). Using a spill depth from Table 7-1 or the average spill depth of 0.72 mm, an initial spill area can be approximated by Eq. 7-3. Once ignited, the initial spill area will grow or regress to the equilibrium spill area, as calculated for the immediate ignition scenario with Eq. 7-2. Consequently, the initial area calculated may provide the maximum fire size, but it will only last for a brief period of time as the fire regresses to the equilibrium area.

Once the spill areas and corresponding spill depths have been calculated, it is necessary in some spill scenarios to calculate the depth coefficient, a parameter developed in this work to modify the fuel burning rate based on small depths causing early burn out before steady-state burning can be achieved. The correlations developed for gasoline and kerosene are provided in Eq. 7-4a and 7-4b.

$$C_\delta = 0.95 * (1 - e^{-0.71\delta}) \quad \text{for gasoline} \quad \text{Eq. 7-4a}$$

$$C_\delta = 0.91 * (1 - e^{-0.58\delta}) \quad \text{for kerosene} \quad \text{Eq. 7-4b}$$

where C_δ is the depth coefficient and δ is the calculated fuel depth (mm). However, to date, depth coefficient correlations have only been developed for gasoline and kerosene fuels. If depth coefficients for other fuels are required it is recommended that Eq. 7-4a and b be used or a coefficient of 0.20 be used for spill depths $\leq$ 5 mm and a coefficient of 1.0 be used for spill depths > 5 mm. These rules of thumb are based upon this study and the spill fire data collected for different fuels in previous research [Gottuk, 2001; Putorti, 2001]. This data can then be used to characterize the transient heat release rate of a spill fire scenario as described below. As indicated above as the fuel depth approaches 5 mm, the depth coefficient approaches unity; thus it is not needed in the calculation of fire size for fuel depths greater than 5 mm.

Once the fuel depth, fuel coverage area, and depth coefficient are determined using the methods described above, the final step in the analysis is the prediction of the heat release rate of the fire scenario. Calculating the peak and/or transient heat release rates requires knowledge of a fuel's mass burning rate per unit area ($\dot{m}''_\infty$), optical properties of the fire plume (kβ), and the heat of combustion of the fuel (ΔH_c). Using this fuel data combined with the spill parameters described above, a transient heat release rate for the given scenario can be calculated. The general form for this calculation is presented in Eq. 7-5, which calculates the peak heat release rate for a given fuel [Gottuk & White, 2008]:

$$\dot{Q}_p = C_\delta \dot{m}''_\infty (1 - e^{-k\beta D}) A \Delta H_C = C_\delta \dot{m}''_\infty (1 - e^{-k\beta D}) \frac{\pi D^2}{4} \Delta H_C \quad \text{Eq. 7-5}$$

where $\dot{Q}_p$ is the peak fire size (kW [Btu/s]), C_δ is the depth coefficient, $\dot{m}''_\infty$ is the peak mass burning rate per unit area for the given fuel (g/s-m^2 [lbs./s-ft^2]), kβ is an empirical constant specific to the fuel, A is the spill area (m^2 [ft^2]), ΔH_c is the heat of combustion of the fuel (MJ/kg [BTU/lbs.]), and D is the effective spill diameter (m [ft]). The effective diameter of non-circular spills can be calculated using Eq. 7-6.

$$D = \sqrt{\frac{4A}{\pi}} \quad \text{Eq. 7-6}$$

Equations 7-5 and 7-6 provide a means of calculating a peak heat release that is both fuel depth and fire diameter dependent. This prediction provides the largest potential fire that a given liquid fuel fire can produce.

In order to assess the thermal threat associated with a fuel spill/pool fire scenario, the peak fire size must be coupled with exposure duration. Estimating exposure duration can be accomplished using one of two techniques. The first technique assumes that the peak fire size is reached instantly and is maintained so long as fuel is present. Using this technique, the burning duration for a given fire scenario can be calculated using Eq. 7-7.

$$t_b = \frac{4m}{\pi D^2 \dot{m}''_\infty} \qquad \text{Eq. 7-7}$$

where t_b is the burning duration for a given scenario (s), m is the mass of fuel available to burn (kg [lbs.]), D is the effective spill diameter (m [ft]), and $\dot{m}''_\infty$ is the peak mass burning rate per unit area for the given fuel (g/s-m^2 [lbs./s-ft^2]). Traditionally, many have assumed that the peak heat release rate of a liquid fuel fire is reached instantaneously and maintained for the duration of the fire as calculated via Eq. 7-7. Consequently, the exposure times associated with this assumption are most likely underestimated as shown in Figure 7.3. In general, this approach tends to over-predict the peak thermal exposure resulting from a fuel spill/pool scenario.

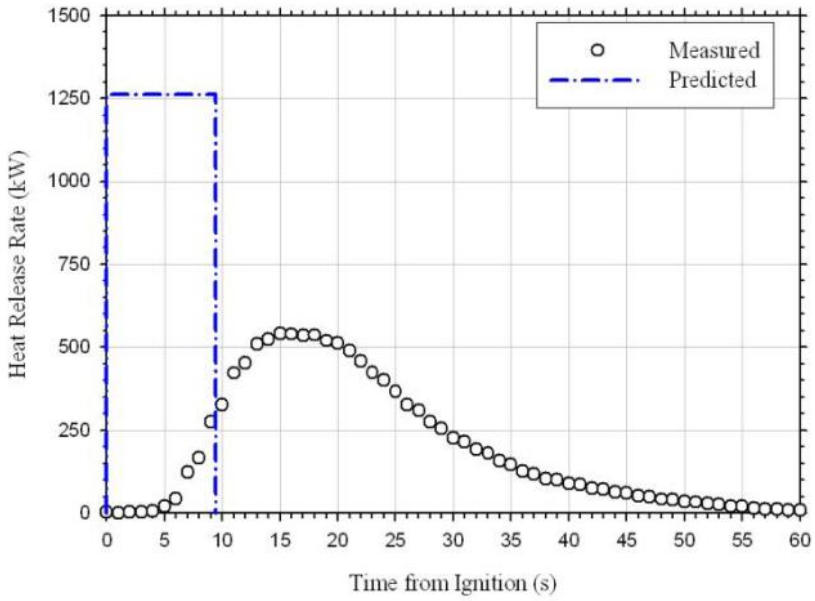

Figure 7.3. Comparison of measured and predicted spill fire heat release rates using assumption that peak heat release rate is achieved instantly

The second technique that can be used to approximate the transient behavior of a fire resulting from the ignition of a liquid fuel spill/pool is to characterize the development, peak, and decay of the fire. This is accomplished by approximating the spread velocity on the hydrocarbon pool surface from the point of ignition, the time to develop maximum burning conditions, and the time to consume all fuel at a given location.

The first step in this process is to characterize the spread of a fire over a fuel surface as a function of time. In general, the spread velocities over the fuel surface are between 0.01–0.1 m/s (0.03–0.3 ft/s) [Gottuk & White, 2008]. As shown in Figure 7.4, these spread velocities will dictate the area of the fuel involved in the fire as a function of time from ignition.

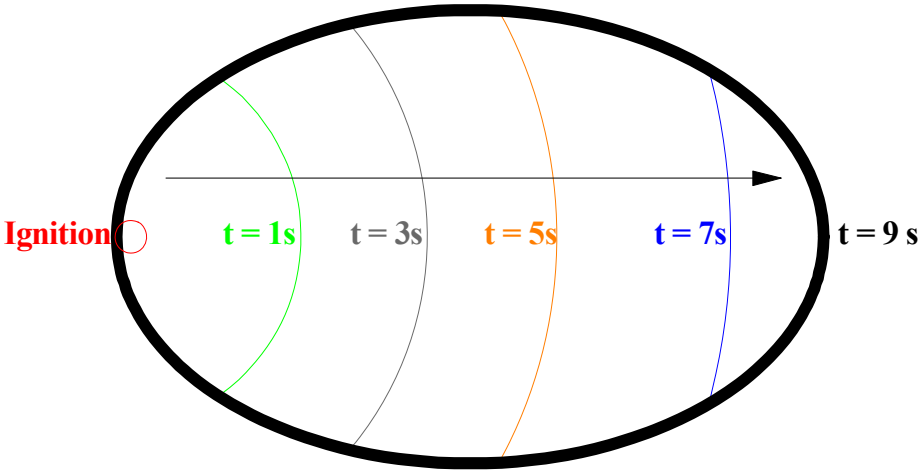

Figure 7.4. Illustration of the progression of a flame front from the point of ignition to complete involvement of a given fuel spill

The transient progression of a flame front over a fuel spill gives rise to a growth rate in the involved area that is proportional to the square of time and results in a constant fire growth rate of ranging from 0.63–63 kW/s² (0.6–60 Btu/s³). Consequently, by assuming a flame spread velocity from the range provided above (i.e., 0.01–0.1 m/s [0.03–0.3 ft/s], it is possible to predict the transient growth rate of a fire to its peak value.

The time to develop a peak burning rate (t_{lag}) can range from 10–60 seconds based upon the results of this study. The time to develop a peak mass burning rate is dependent upon the volatility of the fuel, with less volatile fuels (e.g., kerosene) requiring longer burning durations to reach peak values than was observed for more volatile fuels (e.g., gasoline). This time is then used in conjunction with the fire growth rates discussed previously to dictate the peak fire size achieved for a given scenario. The growth rate and t_{lag} can dictate peak fire size in that it is possible for a fire scenario to burn out prior to reaching peak burning.

Finally, it is necessary to characterize the decay of the fire once available fuel is consumed. The consumption of fuel for a given spill scenario will be dependent upon the rate at which the spill was involved and the rate at which the fuel was consumed. The areas first involved will be the areas first depleted. This is characterized using the equations provided in Eq. 7-8. The burning duration at a given location is determined by integrating the mass loss rate over time and setting this integral equal to the total mass per unit area. The total mass consumed is determined using the following equation:

$$M'' = \int_0^t \frac{\dot{m}''_\infty t}{t_{lag}} dt \qquad t_{burn} < t_{lag}$$

$$M'' = \int_0^{t_{lag}} \frac{\dot{m}''_\infty t}{t_{lag}} dt + \int_{t_{lag}}^{t} m''_b dt \qquad t_{burn} > t_{lag} \qquad \text{Eq. 7-8}$$

where M'' is the total mass of fuel at a fixed location (kg [lb]) and t_{burn} is the time to consume the available mass (s), and t_{lag} is the time differential between ignition and the peak burning rate (s).

The heat release rate as a function of time is determined for a given pool configuration defined by an area and a depth using the following general equation, assuming a circular pool and ignition at the center. An illustration of this scenario is provided in Figure 7.5.

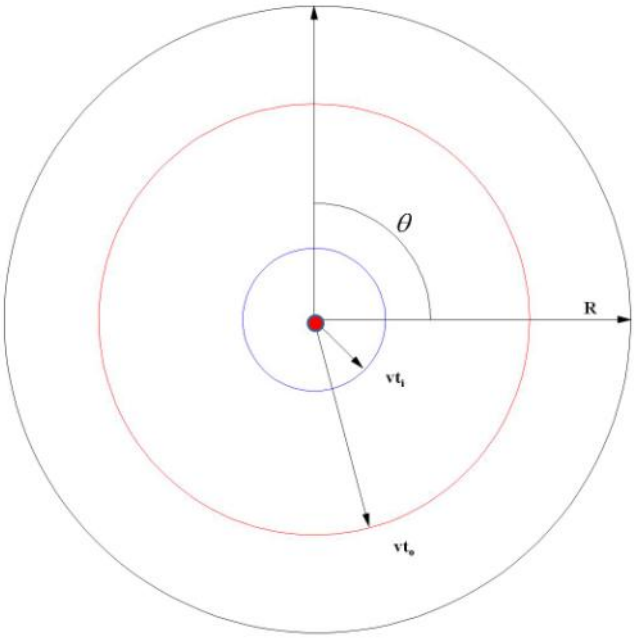

Figure 7.5. Illustration of coordinate system for a circular spill with ignition in the center

Once ignited, the flame front will spread radially outward in all directions (i.e., 0–2π) at a given speed (v) with the area of involvement increasing as a function of time until full involvement of the spill area is achieved. After ignition, the burning rate of the fuel increases as the fuel begins to burn. Whether or not the peak mass burning rate per unit area for a fuel is achieved in a given scenario is dictated by the time required to consume the fuel (t_{burn}) and the time required to reach steady-state burning (t_{lag}). Steady-state burning will be reached if and only if $t_{burn} > t_{lag}$. As the fire spreads over the fuel surface the area involved increases thereby increasing the equivalent diameter of the fire. As described in Eq. 7-5, the equivalent diameter dictates the mass burning rate per unit area ($\dot{m}''_\infty$). Equation 7-9 describes this process.

$$\dot{Q}(t) = \int_0^{2\pi} \int_{vt_i}^{v(t-t_{lag})} C_\partial \dot{m}''_\infty \Delta H_c \, r \, dr \, d\theta + \int_0^{2\pi} \int_{v(t-t_{lag})}^{vt_o} C_\partial \dot{m}''_\infty \Delta H_c \frac{vtr - r^2}{vt_{lag}} dr \, d\theta \qquad \text{Eq. 7-9}$$

where $\dot{Q}(t)$ is the heat release rate (kW [Btu/s]) at time t (s), vt_o is the distance from the point of ignition to the outer edge of burning (m [ft]), vt_i is the distance from the point of ignition to the inner edge of burning, which may be zero (m [ft]), v is the spread velocity on the liquid surface (m/s [ft/s]), $\dot{m}''_\infty$ is the maximum mass burning rate of the liquid (kg/s-m² [lb/s-ft²]), ΔH_c is the heat of combustion of the liquid (kJ/kg [Btu/lb]), r is the position from the point of ignition (m [ft]), t_{lag} is the time differential between ignition and the peak burning rate (s), and θ is the angular coordinate of the liquid pool. Variations arise if the time to locally consume all fuel is less than the lag time. The distance to the outer edge of burning is either equal to vt or vt_e, where t_e is the time to reach the outer edge of the pool, whichever is smaller.

The unknown parameters in Eq. 7-8 and 7-9 are the flame spread velocity, the spill depth, and the total volume of fuel involved. As described earlier, the flame spread velocity is expected to lie between 0.01–1.0 m/s (0.03–3.3 ft/s) [Gottuk & White, 2008]. The spill depth for unconfined spill fires is on average 0.7 ± 0.34 mm (0.028 in.). The maximum spill depth would be constrained by local conditions such as the presence of obstructions (cables, hoses, boxes) as well as degree to which the floor is not perfectly flat. The methods described above were originally developed by Hunt et al. [2010] and were modified to fit the purposes of this report.

7.3 Forensic Analysis Framework

The framework used when assessing a spill/pool fire from a forensic viewpoint was presented in Figure 7.2. For a fire investigation, it is more often than not that neither the fuel type nor spill scenario is known. Consequently, different data sets must be considered in order to enable an investigator to develop an understanding of the fuel spill fire scenario based upon the fire patterns. Barring other evidence, the only methods available to determine a fuel type maybe through analytical test methods [e.g., ASTM E1618, 2010] for examining the ignitable liquid residues present on a sample of substrate from the scene. However, even if the results from analytical test methods are inconclusive, bounding data for different fuel types can be used.

The next step is to determine a spill area. This requires analysis of the fire patterns left by the event on the substrate. Depending on the extent of damage, an approximation of the fire pattern area may be obtained through physical measurements of the pattern or through image analysis of photographs taken of the patterns. Once an area is obtained, it is necessary to distinguish whether or not the substrate was combustible. This is an important distinction because on combustible substrates, the pattern area is not necessarily the same as the spill area; whereas on non-combustible substrates, the spill area and fire pattern area are nominally the same. Based upon data collected in this study as well as that presented in the literature [Putorti, 2001], fire pattern areas on combustible substrates are nominally the same or up to 24 percent larger than the initial spill area. A summary of the measured percent increases between fire pattern and spill areas relative to specific substrates is presented in Table 7.1.

Table 7.2. Summary of Differences between Spill and Fire Pattern Areas for Various Substrates

Flooring Material	Measured Increase in Area from Spill Pattern to Fire Pattern (%)
Raw Wood (Plywood/OSB)	13–14
Finished Parquet	24
Vinyl	<2
Non-Combustible	None

Adjusting the measured fire pattern area according to these increases will provide an approximation of the initial spill area. Carpet flooring is not incorporated into the list above due to the variety of parameters independent from the liquid fuel spill parameters (i.e., carpet combustibility, carpet sub-layer combustibility, time permitted to burn, etc.) that affect the burn pattern. A methodology to analyze the impact of carpet parameters is presented in Section 6.4. The depth of the spill can be approximated using the data presented in Table 7.1 or by assuming a default depth of 0.7 mm. Using this depth a depth coefficient can be calculated using Eq. 7-4(a) and (b) if the fuel is either gasoline or kerosene, respectively. With these inputs it is possible to calculate either a peak or transient heat release rate.

7.4 Framework Verification

The ability of the engineering/fire analysis frameworks described above to predict the heat release rate for a given fire scenario was verified using empirical data collected from tests representing several of the liquid fuel scenarios identified in Figure 7.1 and Figure 7.2. Three different scenarios were used as verification cases. Two different spill scenarios were used to evaluate the fire hazard analysis framework: a fixed quantity/unconfined gasoline spill and a continuously-fed/unconfined spill. The forensic framework was evaluated for a single gasoline spill fire scenario conducted atop a plywood substrate.

The first scenario evaluated was a 0.5 unconfined, fixed volume spill of gasoline on an unspecified substrate. For this example, the ignition time is not specified. The data used for comparison was that collected in SFD89-U-CC-G-0.5-30. In this scenario, 0.5 L (0.13 gal.) of gasoline was spilled over a coated concrete substrate and permitted to spread for a period of 30 seconds before being ignited. The spill was ignited at the edge and burned for approximately 60 seconds. However, approximately 15–20 seconds after ignition, the burning surface of the spill separated into several smaller areas of burning fuel as a result of localized fuel burn out. The 10-second peak heat release rate measured in this test was 412 kW. Using the framework described above and input data from the aforementioned test, the transient heat release rate from the SFD89-U-CC-G-0.5-30 spill fire was predicted. In order to properly assess the capability of the framework as a predictive tool, test specific data (i.e., measured spill area and measured lag time) were not used because these data generally would not be available to an engineer performing a fire hazard analysis. Instead, various assumptions were made just as would be done in real-world scenarios. The first step in the analysis is to identify the fuel type, which is gasoline, and the relevant properties for this fuel. The gasoline properties used in this analysis are listed below:

- ρ (kg/m^3) = 742
- ΔH_c (MJ/kg) = 37.6
- $\dot{m}''_\infty$ = 55 g/s-m^2
- Kβ = 2.1

Fuel properties for a number of fuels can be found in [Babrauskas, 2008] and in this report.

The next step is to characterize the area of the spill and the resulting fuel depth. Given a spill volume of 0.5 L (0.13 gal.), Eq. 7-1 is used to calculate a nominal spill area of 0.71 m^2 (7.6 ft^2), based on an assumed average spill depth of 0.7 mm. For this example, the average spill depth is used because substrate material and ignition delay times were not specified; otherwise a more refined spill depth value could have been selected from Table 7.1. From these data and the use of Eq. 7-4a and 7-6a, the depth coefficient C_δ is calculated to be 0.38 and the equivalent spill diameter is calculated to be 0.95 m (3.1 ft). Finally, in order to characterize the transient heat release rate for the given scenario using Eq. 7-9, it is necessary to approximate the spread rate (v) and time to reach peak burning (t_{lag}). However, given that these inputs are case dependent and often unknown, a range of values were evaluated for this scenario. The range of values evaluated is listed below. The results from these ranges are provided in Figure 7.6, compared to the measured transient heat release rate for this scenario.

- t_{lag} (s) = 10–30
- v (m/s) = 0.05–1.0

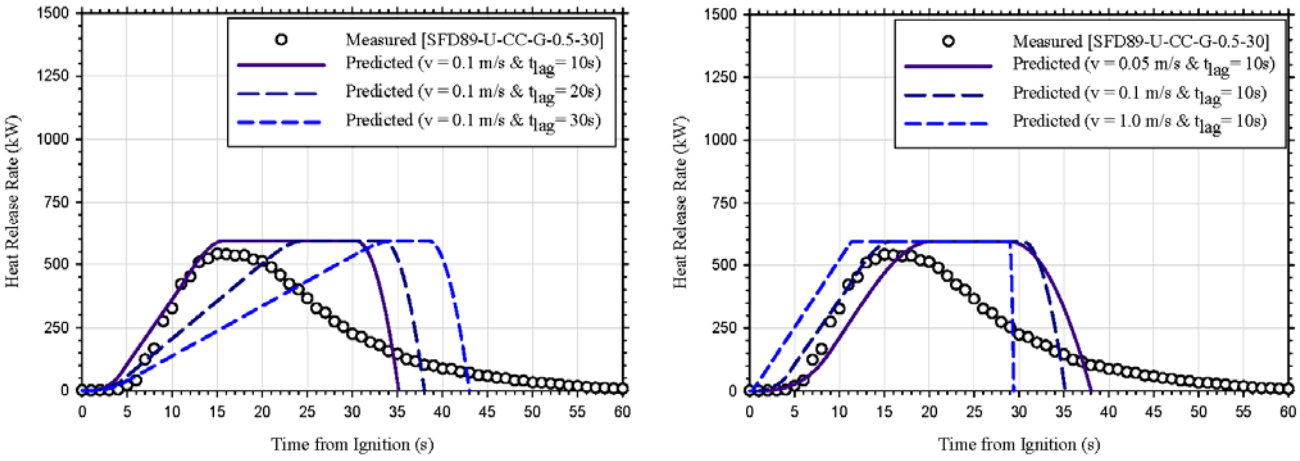

(a) (b)

Figure 7.6. Comparison of measured (SFD89-U-CC-G-0.5-30) and predicted fixed quantity/unconfined fuel spill fire scenarios

In general, the measured and predicted peak heat release rates were found to be very comparable for all spread rate/lag time permutations considered. As shown in Figure 7.6a, increasing the lag time, decreased the rate at which the fire grew to its peak fire size. For the scenario evaluated, this increase in lag time resulted in deviation from the measured heat release growth. For this example, it was found that a lag time of 10-seconds best matched the measured growth rate.

Figure 7.6b illustrates the impact of varying the flame spread rate across the fuel surface from 0.05 up to 1.0 m/s (0.16–3.3 ft/s). In general, the variations in flame spread rates evaluated had only marginal impact on the predicted heat release rates, shifting the growth rate by approximately 10-seconds for an order of magnitude difference in flame spread values. Larger flame spread values resulted in the fire reaching the peak heat release rate sooner which resulted in a decreased burning duration for the scenario. A flame spread rate of 0.1 m/s best represented the measured heat release rate.

As shown in Figure 7.6, the measured and predicted heat release rates diverge after peak heat release rates are achieved with the measured heat release rate beginning to decay and the predicted heat release rate maintaining the peak for an additional 10 seconds. This divergence is due to the models inability to predict localized burnout of the fuel spill which was observed in the test. This phenomenon reduces the total area of burning liquid, thus reducing the heat release rate and extending the burning duration as shown in Figure 7.6. The opposite is true for the model prediction, which neglects burnout and thus assumes a continuous burning layer until all fuel is consumed. As shown in Figure 7.6, this assumption results in an extended period of peak heat release rate burning followed by an immediate burnout condition.

The second spill scenario evaluated using the framework described in Figure 7.1 was a 0.5 L (0.13 gal.) fixed quantity, confined area gasoline scenario. The data used for comparison was that collected in DSF22-C-CC-G-20-1.5. In this scenario, 0.5 L (0.13 gal.) of gasoline was poured onto a 1.5 m (4 ft) square diked, coated concrete pad to form a 20 mm deep pool. The fuel was ignited at the edge and burned for approximately seven minutes. In this test quasi-steady-state burning was achieved 20–30-seconds after ignition and maintained for a period of approximately 3.5 minutes followed by a decay phase that lasted for an additional 2–3 minutes. The 10-second average peak heat release rate measured in this test was 2,450 kW.

Since the fuel used in this scenario was gasoline, the fuel properties identified above were used. The fuel depth is calculated from the given volume and area using Eq. 7-1. Next, the depth coefficient and equivalent fire diameter were calculated using Eq. 7-4a and 7-6. The values calculated were 0.95 for C_δ and 1.38 m (4.5 ft) for an equivalent diameter. Finally, the transient heat release rate for this scenario was calculated using Eq. 7-9 with a range of values for the flame spread rate (v) and time to reach peak burning (t_{lag}). The range of values was the same as those evaluated in the previous case, and results similar to those described above were obtained. In general, increased lag times resulted in slower growth rates and loner periods of burning before a peak heat release rate was reached. Increased flame spread rates resulted in faster growing fires that peaked earlier and burned out sooner than the measured heat release rate. For this scenario a flame spread rate of 0.1 m/s and a t_{lag} of 25 seconds was found to best characterize the measured heat release rate. This flame spread rate was the same as that used in the previous gasoline spill fire scenario but the t_{lag} was 15 seconds larger than that used in the previous scenario. This additional lag time could be due to the slightly larger surface area of the scenario thus the time required for the flame to spread over the fuel surface would be longer. The predicted heat release rate using these parameters is compared to the measured transient heat release rate for this scenario in Figure 7.7.

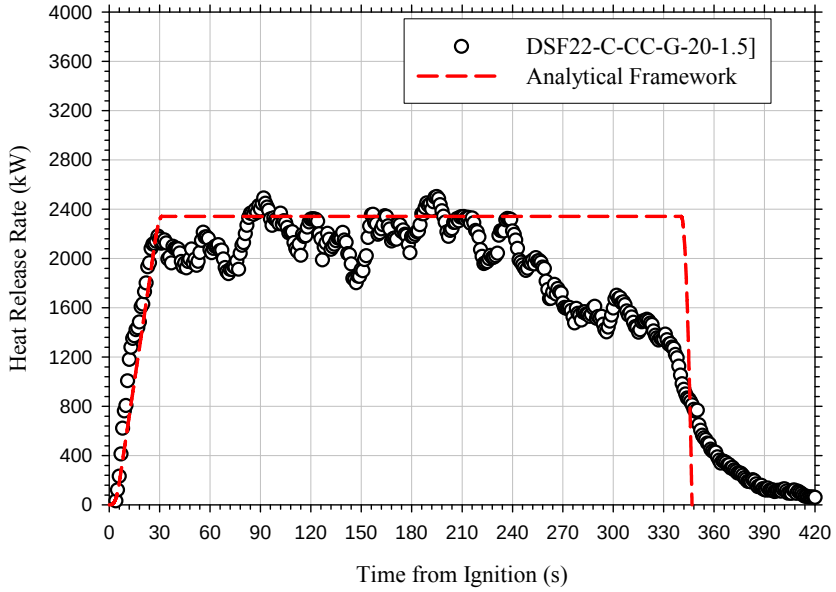

Figure 7.7. Comparison of measured (DSF22-C-CC-G-20-1.5) and predicted 0.5 L (0.13 gal.) fixed quantity, confined area gasoline fire

As shown in Figure 7.7, the measured and predicted peak heat release rates are generally comparable during the initial growth phase and quasi- steady-state portions of the fire. The predicted heat release rate peaks at a 2,504 kW which is less than five percent higher than the 10-second peak heat release rate measured in the test. The primary difference between the measured and predicted heat release rates is the behavior that occurs after 240 seconds of burning. At this point, the measured heat release rate begins to gradually decay and does so over the next 180 seconds before self-extinguishing. However, at this point in the test the predicted heat release rates maintain the peak heat release rate and do so for an additional 90 seconds before rapidly decreasing and burning out. This behavior is very similar to that observed for the fixed quantity/unconfined spill modeling work presented in Figure 7.6. In both cases, the divergence is due to the models inability to predict localized burnout of the fuel which was observed in the test.

The final validation case was a 0.5 L (0.13 gal.) gasoline spill onto a plywood substrate that was permitted to spread for 30-seconds prior to ignition (SFD42-U-P-0.5-30). In an effort to assess the utility of the proposed forensic analysis tool, the only input data used was the fire pattern area since this may be the only data available to a fire investigator. The first step in this analysis would be to determine the type of fuel used. This could be accomplished analytically, using ignitable liquid reside (ILR) testing, or through inference, if additional evidence (e.g., gas can or eyewitness testimony) suggests the use of a certain fuel. If there are no strong indicators of fuel type and ILR testing is not conclusive, this could also be accomplished using a bounding data set. Once a fuel has been identified, it is necessary to characterize the spill.

For this test, the fire produced a fire pattern with an area approximately 0.6 m^2 (6.5 ft^2). Using this data and the fact that the fire occurred on plywood, an initial spill area of 0.52 m^2 (5.6 ft^2) was calculated using the 13 percent reduction specified for plywood substrates (Table 7.1). Once this area was determined, a spill volume was approximated to be 0.37 L (0.1 gal.) by assuming

an average spill depth of 0.7 mm (Table. 7.1). Quick discussion of why we use 0.7 mm as opposed to plywood specific data. Applying Eq. 7-1, a spill volume of 0.37 L (0.1 gal.) is calculated based upon the spill area and assumed spill depth. These results were then used to calculate a depth coefficient (C_δ) of 0.38 and an equivalent diameter of 0.94 m (3.1 ft) using Eq. 7-4a and 7-6. Finally, the transient heat release rate for this scenario was calculated using Eq. 7-9 with a range of values for the spread rate (v) and time to reach peak burning (t_{lag}). The range of values was the same as those evaluated in the previous cases, and results similar to those described above were obtained. For this scenario, a flame spread rate of 0.1 m/s and a t_{lag} of 10-seconds was found to best characterize the measured heat release rate. These values are the same as those found to produce the best match for the first gasoline spill fire scenario evaluated. The predicted heat release rate using these parameters is compared to the measured transient heat release rate for this scenario in Figure 7.8.

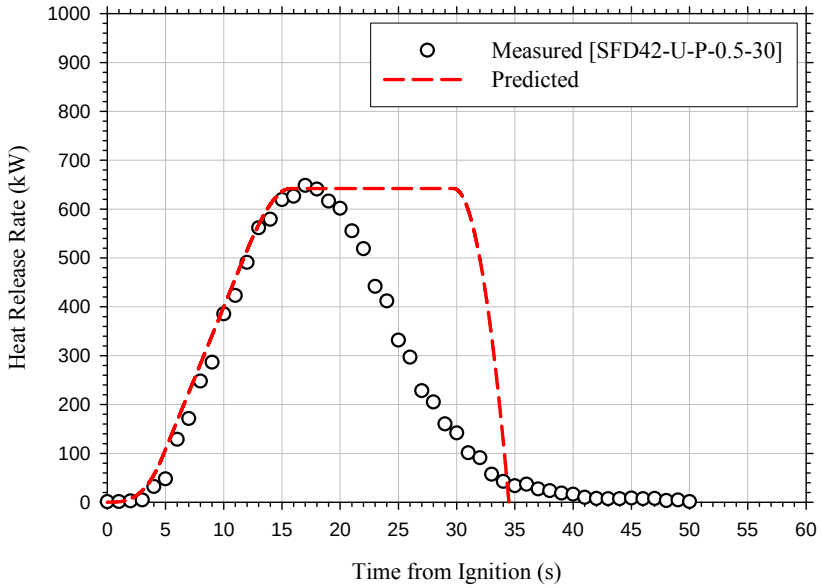

Figure 7.8. Comparison of measured (SFD42-U-P-0.5-30) and predicted heat release rates calculated based upon forensic fire pattern analysis from a 0.5 L (0.13 gal.) gasoline spill onto a plywood substrate

As was observed in the previous two cases, the peak heat release rate predicted using the framework agreed well to that experimentally measured. Furthermore, just as was observed in the previous two validation cases, the measured and predicted heat release rates diverge after peak heat release rates are achieved with the measured heat release rate beginning to decay and the predicted heat release rate maintaining the peak heat release rate for an additional period of time. As described earlier, this divergence could be due in part to the models inability to predict localized burnout of the fuel spill.

In general, the framework predicted peak heat release rates that were in very good agreement with the measured values. Furthermore, the time frame in which the peak heat release rate is achieved as well as the total burning duration for the predicted scenarios were generally acceptable, particularly in a bounding manner to those obtained experimentally. However, it should be noted that the rate of increase in and duration of the growth period of the predicted fuel

fires are dependent upon both the flame spread rate (v) and lag time (t_{lag}) which are generally not well defined for most fuels and highly scenario dependent. Consequently a range of values for each of these inputs was considered. The decay phases of the measured and predicted heat release rate profiles differed for all three scenarios evaluated. The differences observed in the decay phase of these comparisons are an artifact of the models inability to account for localized fuel burnout within the fuel spill fire which was noted in a majority of the tests conducted in this study. As a result of this, the model assumes a uniform, continuous fuel layer burning, when in reality after the peak is reached, the spill can break up into several smaller areas of localized burning, thus reducing the total heat release rate measured for the test. This is consistent with the fact that the model over-predicts the decay phase of the scenarios evaluated (i.e., the peak mass burning rate is maintained for a longer period of time than was observed experimentally).

When compared to the predictions provided by current pool fire models [NUREG, 2003], the results of this new analysis framework show a marked improvement in accurately characterizing the peak heat release and burning duration for a variety of fuel spill scenarios. A comparison of the heat release rates measured in this study, those predicted using the framework outlined in Figure 7.1, and the predictions of a historical model are provided in Figures 7.8 and 7.9. Traditionally, the burning rates measured in deep pool fire scenarios are applied to spill fire scenarios. The application of these burning rates results in the over-prediction of peak heat release rates by as much as five times. Furthermore, the historical model assumes an instantaneous growth and decay. The results these assumptions are shown in Figures 7.9 and 7.10.

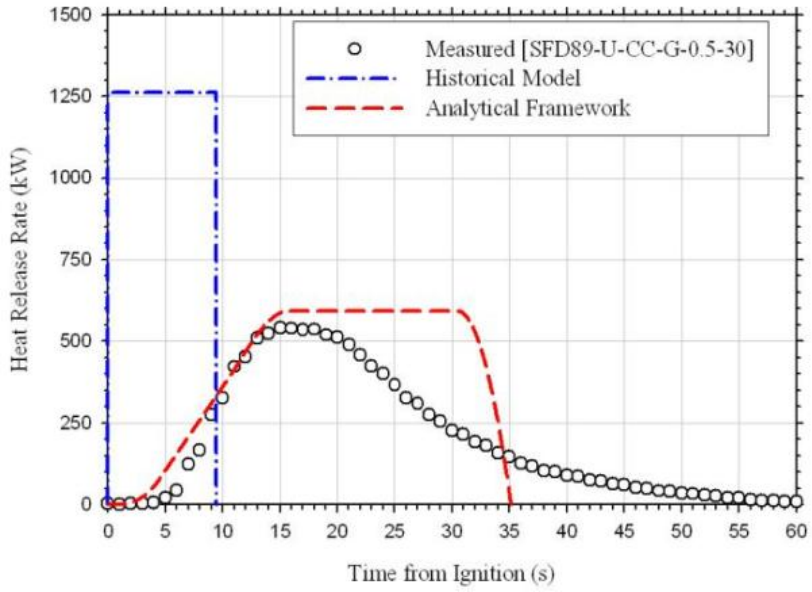

Figure 7.9. Comparison of measured heat release rate for a 0.5 L gasoline spill on coated concrete (SFD89-U-CC-G-0.5-30), prediction from a historical model, and prediction from the analytical framework

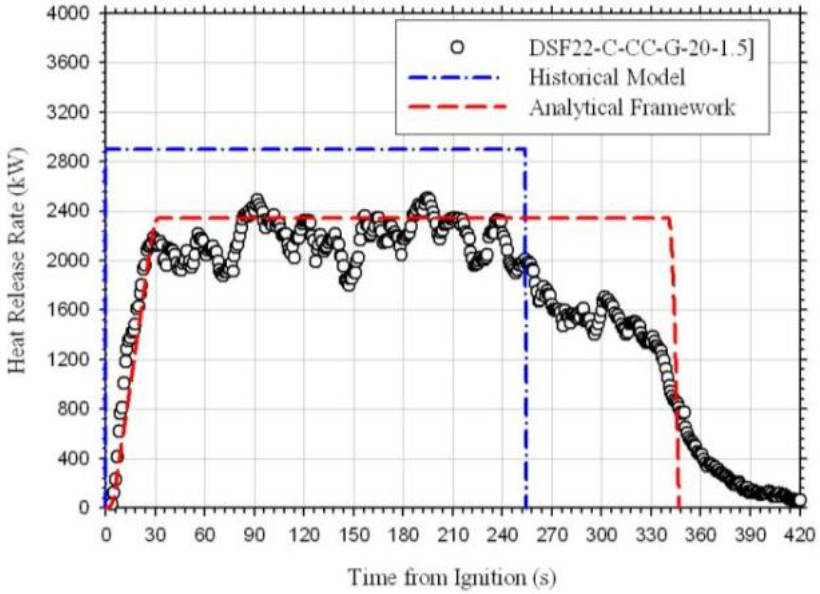

Figure 7.10. Comparison of measured heat release rate for a 20 L gasoline spill on coated concrete (DSF22-C-CC-G-20-1.5), prediction from a historical model, and prediction from the analytical framework

In general, the historical model over-predicts the peak heat release rate for both cases and under-predicts the burning duration when compared to the measured heat release rate. For the spill fire scenario (Figure 7.9), the historical model predicted a peak heat release rate that is a factor of two larger than that measured experimentally and a burning duration one-sixth of that measured. For the deep pool scenario (Figure 7.10), the historical model over-predicted the peak heat release rate by 17 percent with a burning duration that was approximately 75 percent of that measured experimentally. As shown in Figures 7.9 and 7.10, the predictions from the analytical framework were generally more comparable to that measured experimentally. The differences in peak heat release rates predicted by the new framework and measured in both scenarios were within five percent of each other. The framework did under-predict the burning duration but to a lesser extent than by the historical model predictions.

7.5 Conclusions

An analytical framework was developed to serve as a tool for the fire protection and forensic fire communities when assessing fuel spill fire scenarios. The framework was developed in such a way that it can be used to assess the fire hazard for a variety of potential fuel spill scenarios or be used to develop a better understanding of a specific fuel spill fire event based upon forensic patterns created by the event. Historically, the assessment of fuel spill fire scenarios is performed using data collected from fixed area, 'deep' pool fire scenarios which may or may not be appropriate depending upon the scenario being evaluated. The framework presented in this work distinguishes between the varieties of potential spill/pool scenarios and outlines appropriate methodologies that should be used to assess these different types of liquid fuel fires. In this work, a limited number of verification cases were evaluated using the framework, and in general, the predicted values were comparable to those measured, specifically the peak heat release rates that were within five percent for all three cases evaluated. This is a marked improvement over

the existing tools used to characterize the fire size resulting from a fuel spill scenario, which has over-predicted peak heat release rates by as much as a factor of five. Although good agreement with respect to peak heat release rate predictions were realized using the framework, deficiencies were identified. The primary deficiency is the models inability to accurately model the decay phase of these types of scenarios. In general, it was found that the framework over-predicts the duration of the steady state burning which was identified as an artifact of the occurrence of localized fuel burn out in the experimental results which are not accurately captured in the predicted results.

8.0 SUMMARY OF FINDINGS

The results of these tests allowed for the examination of the effects of various parameters (i.e., fuel quantity, substrate, ignition delay) on both the spill and fire dynamics of scenarios resulting from the release of various quantities of liquid. This work also provided insight into the forensic fire patterns developed from both liquid and Class A fuel fires atop a variety of surfaces.

Based upon a statistical analysis of the fluid depths measured in the spill dynamics testing for all spill quantities, liquid types, and substrates, an average depth of 0.72 mm with a standard deviation of 0.34 mm was determined. This value is consistent with the values currently recommended in the literature for liquid spill analysis. The range of spill depths measured was from 0.22 mm up to 2.4 mm depending upon the specific liquid/substrate scenario. This relatively wide range of empirical depths demonstrates the importance of understanding key variables governing fluid spread such that an appropriate spill depth is used when performing an engineering analysis. The primary two factors governing the spread of a fuel and the equilibrium spill depth reached are the surface tension of the liquid and the surface characteristics of the substrate. However, given that the surface tensions of most fuels are relatively similar; this parameter is generally not as influential, when considering the characteristics of a spill. The more dominant variable to consider is the surface topography which can have a substantial impact on the spread and equilibrium spill depth, both of which play an important role in predicting the fire hazard resulting from the spill. It is for this reason that an understanding of the surface on which a spill occurs is far more important than understanding the fuel that was spilled, from a spill dynamics standpoint. This data set was also used to investigate correlations between both liquid properties and initial spill volumes when compared to equilibrium spill depth. Equilibrium spill depth correlated relatively well with the surface tension of the liquid and as surface tension decreased, so did the equilibrium spill depth. When examining the relationship between initial spill volume and equilibrium spill depth, an increasing trend was also observed (i.e., as spill volume increased, so did the measured equilibrium spill depth). Currently, there are inconsistencies between the empirical and theoretical data presented in the literature. These inconsistencies are an artifact of the variability in the surface characteristics that are not accounted for in the theoretical solution. These differences could lead to ancillary affects that cause the spilled liquid to slow in its progression or stop all together leading to localized pooling of the liquid.

Based upon the testing conducted it was determined that, in addition to fire diameter, the burning rate of a fuel is dependent upon several factors including, but not limited to; fuel quantity, substrate, and ignition delay. Fuel quantity was identified as a factor because it can be directly related to the depth of fuel for fixed quantity/fixed area fires and can be applied to scenarios in

which the fires are continuously-fed. For fixed quantity scenarios, the volume of liquid spilled is proportional to the depth of liquid within the area of coverage. For these scenarios, a depth of 5 mm was established as the minimum depth for which a peak mass burning rate comparable to the diameter dependent maximum mass burning rate provided in the literature can be achieved. This was true for steel, water, concrete, and vinyl substrates. At depths less than 5 mm the peak burning rates were consistently less than the diameter dependent maximum burning rate. The reduction in mass burning rate associated with fixed quantity 1mm fuel depths was on the order of 70–80 percent. Based upon the data collected, correlations were developed for both gasoline and kerosene that can be used to predict the reduction on peak mass burning rate as a function of fuel depth. The product of these correlations when coupled with the diameter dependent mass burning rate correlation available in the literature can be used to predict more appropriate mass burning rate for thin, fuel layer scenarios. Although this 5 mm depth criterion was found to be appropriate for all fixed quantity scenarios the same was not true for continuously-fed fire scenarios. In these scenarios fuel depths on the order of 1 mm were maintained while still achieving peak mass burning rates that were comparable to the diameter dependent maximum mass burning rates. These results demonstrated that it is not the depth of fuel that impacts the peak mass burning rate but that it is the quantity of fuel available to burn. In addition to the impact of fuel quantity on burning rate it was also found that for a combustible fuels, specifically, kerosene the ignitability and flame spread potential of the fuel at thin depths is very small making the fuel very challenging to ignite and burn in these scenarios.

The second parameter identified as having an impact on the mass burning rate of a fuel was the substrate on which the fuel is burning. To date, the reduction in the mass burning rate of a fuel associated with a thin layer of fuel has been attributed to heat transfer occurring between the substrate and the fuel layer. The data collected in this work supports this statement in that differences in the mass burning rates of a fuel for given spill scenarios were found to be different when burned atop surfaces with differing thermal properties. The rank order of the mass burning rates for each fire size were consistent with the highest burning rates occurring on the vinyl flooring and the lowest on concrete. For the scenarios evaluated, no specific thermal property of the substrates (i.e., thermal conductivity, thermal inertia, thermal effusivity, and thermal diffusivity) could be directly correlated to the rank order of burning rates. In general, less thermally conductive materials (i.e., vinyl and water) produced mass burning rates higher than those achieved in tests with more thermally conductive substrates (i.e., steel and concrete). However, the ranking of mass burning rates with respect to the thermal conductivity of the substrates was not appropriate when evaluating the case of the concrete and steel. In this case, the mass burning rates measured on the concrete were consistently lower than those measured on the steel despite the fact that the thermal conductivity of the steel is an order of magnitude larger than that of the concrete. This discrepancy may be attributed to the reflectivity of the steel and the resulting re-radiation from the steel substrate to the fuel layer. This reflected heat was then transferred into the fuel layer thus raising the mass burning rate of the fuel. In general, the influence of the substrate was only found to be significant for fuel depths less than 5 mm.

Typically, when discussing the impact of the substrate on the mass burning rate of a fuel and the associated heat transfer it is assumed that the substrate is acting as a heat sink (i.e., removing heat from the fuel layer) thus reducing the peak burning rate achieved. However, a small subset of tests in which the fuel substrate was heated to temperatures greater than ambient conditions demonstrates that an opposite affect can occur. These tests, while limited, generally show that an

elevated substrate temperature can in fact increase the peak mass burning achieved during a fire scenario. A hypothesis resulting from this limited data set is that, when heated, the substrate no longer acts as a heat sink and in fact transfers heat to the fuel thus pre-heating the fuel layer prior to ignition. This pre-heating reduces the amount of energy required to volatize the fuel thus more fuel can be evaporated more readily.

The findings of the spill dynamics and fixed area (i.e., pan and diked) fire tests were generally supported by the results from the spill fire dynamics testing conducted. In these tests, the impact of fuel depth and substrate were evident and comparable to that measured for the fixed area scenarios. The results from these tests also identified the third parameter impacting the peak mass burning rate achieved. This parameter was the ignition delay time (i.e., the time between the initial spill and ignition of the spilled liquid). In these tests, ignition delay times of 30 and 300 seconds were evaluated and when compared the results varied widely. In general, the 300-second ignition delay resulted in larger areas with reduced peak mass burning rates. However, the differences in the average spill area between the 30-second and 300-second ignition delay times range from 8–76 percent with an average value of 36 percent and the differences in the average 10-second peak heat release rates range from 25 percent to 74 percent with an average of 52 percent. Although no direct correlation between the change in area and change in heat release rate could be identified from this data, the data does consistently indicate that increasing the ignition delay from 30-seconds to 300 seconds results in a larger spill area and a decreased peak heat release rate. Although this effect could not be fully explained using the data collected, substrate cooling and evaporative fuel losses were characterized and found to support the decrease in peak mass burning rate.

It should be noted that for all tests conducted on all substrates and all fuel depths, the impact of diameter on peak mass burning rate was evident and did follow the power-law correlation provided in the literature. Furthermore, it was found that on average the maximum mass burning rate achieved by the multi-constituent fuels (i.e., gasoline and kerosene) evaluated were approximately 20 percent lower than the data currently available in the literature while for the pure fuel evaluated the mass burning rate was equivalent. The reduction in mass burning rate for the multi-constituent fuels was attributed to the reduction in volatility and inclusion of more alcohols in the multi-constituent blends.

Using the data collected in this study an analytical framework was developed. The framework can be used in two capacities; 1) to predict the fire hazard associated with a fuel spill fire scenario, and 2) provide a tool that can be used to gain insight into a fuel spill scenario based upon the forensic patterns produced by the event. In general, the framework was found to predict the fuel spill fire scenarios evaluated in this study relatively well.

With respect to the forensic analysis of both the fuel spill and Class A fires it was found that the fuel spill fire patterns were generally comparable in area to the areas measured for the spills prior to ignition. For non-combustible substrates the pre- and post-fire pattern areas were nearly identical while for the combustible substrates, except carpet, increases in area of up to 14 percent were observed. For carpet scenarios, the area of pattern involvement was time dependent due to the fact that the pattern areas continued to increase as the flame front moved outwards with the combustion of the carpet and carpet padding. For these scenarios, flame spread rates over the carpet surface, after the liquid fuel was consumed, ranged from 0.011–0.014 m/min.

(0.41–0.55 in./min.). Substrate damage from the liquid fuel spill fires was generally minimal primarily consisting of thermal discoloration and staining of the material. The damage to the substrate was mostly superficial with some evidence of the early stages of thermal decomposition of the wood. Damage resulting from the Class A fuel varied depending upon the fuel with some fuels resulting in complete burn-through of the substrate and other resulting in thermal damage with large quantities of oily residue being deposited atop the substrate.

Several types of patterns were consistently identified for certain fuel types. Examples of these patterns included; liquid fuel spill fires consistently resulting in irregularly-shaped burn patterns with minimal thermal damage to the substrate, except in the case of carpet scenarios and Class A fuels constructed from plastic/foam materials consistently left an oily residue on the substrate after self-extinguishing. However, based on visual patterns as well as via char depth measurements, no real, objective post-fire indicators were consistently identified to differentiate the fire patterns resulting from the various Class A and flammable liquid fuel fires. It is possible that the aforementioned patterns could be produced via other fire sources burning under different conditions or that these patterns could be destroyed when the fire is placed within an enclosure proximate to other burning items. The conclusion of this evaluation is that in order to make assertions regarding the first item ignited it is necessary to collect representative samples of the substrate and have these samples analyzed for ignitable liquid residue.

9.0 REFERENCES

1. SFPE, 2008, "Liquid Fuel Fire," SFPE Handbook for Fire Protection Engineering, Section 2–15, Society of Fire Protection Engineers, 2008, p. 2–297.

2. Gottuk, D., Scheffey, J., Williams, F., Gott, J., and Tabet, R., "Optical Fire Detection for Military Aircraft Hangars: Final Report on OFD Performance to Fuel Spill Fires and Optical Stresses," NRL/MR/6180--00-8457, Naval Research Laboratory, Washington, DC, 2001.

3. Putorti, A., "Flammable and Combustible Liquid Spill Burn Patterns," National Institute of Justice, NIJ-604-00, 2001.

4. Joulain, P., "The Behavior of Pool Fires: State of the Art and New Insights," *Twenty-Seventh Symposium (International) on Combustion*, The Combustion Institute, 1998 pp. 2691–2706.

5. Steinhaus, T, Welch, S., Carvel, R., and Torrero, J., "Large-Scale Pool Fires," *Thermal Science Journal*, **11** (3), 2000.

6. Blinov, V. and Khudiakov, G., "Diffusion Burning of Liquids," U.S. Army Translation, NTIS No. AD296762, 1961.

7. Hottel, H., "Certain Laws Governing Diffusive Burning of Liquids," *F. Res. Abs. and Rev*., **1**, p. 41, 1959.

8. Babrauskas, V., "Estimating Large Pool Fire Burning Rates," *Fire Tech*., **19**, 1983, p. 251.

9. Burgess, D. and Zebatakis, M., "Research on the Hazards Associated with the Production and Handling of Liquid Nitrogen," Bureau of Mines, Department of the Interior, WADD TR 60-141, 1960.

10. Emmons, H., deRis, J., and Orloff, L., "A Dimensionless Correlation of Pool Burning Data," *Combustion and Flame*, **18**, 1972, pp. 381–388.

11. deRis, J., "Fire Radiation – A Review," *Proceedings of the Seventeenth International Symposium on Combustion*, 1978, pp. 1003–1016.

12. Modak, A., "Ignitability of High Fire Point Liquid Spills," Factory Mutual Research Corporation, NP-1731, Research Project 1165-1, 1981.

13. Raj, K., Phani, P., and Kelelkar, A., "Assessment Models in Support of Hazard Assessment Handbook," Department of Transportation, 74685-40, 1974.

14. Grimaz, S., Allen, S., Stewart J., and Docetti, G., "Predictive Evaluation of Surface Spreading Extent for the Case of Accidental Spillage of Oil on the Ground," 2007.

15. Simmons, C., Keller, J., and Hylden, J., "Spills on Flat Inclined Surfaces," Pacific Northwest National Laboratory, PNNL-14457, 2004.

16. Bradley, D., "Model for Pool Fires following Chemical Agent Spills," Science Applications International Corporation, 2002.

17. Batchelor, G. K., *An Introduction to Fluid Dynamics*, Cambridge: U.P., 1967.

18. Keller, J. and Simmons, C., "The Influence of Selected Liquid and Soil Properties on the Propagation of Spills Over Flat Permeable Surfaces," Pacific Northwest National Laboratory, PNNL-15058, 2005.

19. Belore, R. and Buist, I., "Modeling of Oil Spills in Snow," S.L. Ross Environment Research Limited, 1988.

20. Chambers, G., "Flight Line Extinguisher Evaluation," U.S. Air Force Report DOD-AGFSRS-76-9, 1977.

21. Hill, S., Scheffey, J., Walker, F., and Williams, F., "Tests of Alternative Fire Protection Methods for USAF Hangars," Memorandum Report 8337, Naval Research Laboratory, Washington, DC, 1999.

22. NFPA 921, "Guide for Fire and Explosion Investigations," National Fire Protection Research Foundation, 2008.

23. Garo, J., Koseki, H., Vantelon, J., and Fernandez-Pello, C., "Combustion of Liquid Fuels Floating on Water," BIBLID: 0354-9836, 11, 2007.

24. Beyler, C., "Analysis of the Fire Investigation Methods and Procedures Used in the Criminal Arson Cases against Ernest Ray Willis and Cameron Todd Willingham," submitted to the Texas Forensic Science Commission, 2009.

25. ASTM E1354, "Standard Test Method for Heat and Visible Smoke Release Rates for Materials and Products Using an Oxygen Consumption Calorimeter," American Society for Testing and Materials, 2009.

26. HEATING 7.2, "Multidimensional Finite-Difference Heat Conduction Analysis Tool," Oak Ridge National Laboratory, ORNL/TM-12262, 1993.

27. Okamoto, K., Watanabe, N., Hagimoto, Y., Miwa, K., and Ohtani, H., "Changes in Evaporation Rate and Vapor Pressure of Gasoline with Progress Evaporation," *Fire Safety Journal*, **44**, 2009, pp. 756–763.

28. Okamoto, K., Watanabe, N., Hagimoto, Y., Miwa, K., and Ohtani, H., "Evaporation Characteristics of Multi-Component Liquid," *Journal of Loss Prevention in the Process Industries*, **23**, 2010, pp. 89–97.

29. Nuclear Regulatory Commission, "Fire Dynamics Tools (FDT^{s}) Quantitative Fire Hazard Analysis Methods for the U.S. Nuclear Regulatory Commission Fire Protection Inspection Program," NUREG-1805, 2004.

30. Mackinven, R., Hansel, J.G., and Glassman, I., "Influence of Laboratory Parameters on Flame Spread across Liquid Fuels," *Combustion Science and Technology*, **1**, 1970, pp. 293–306.

31. Burgoyne, J.H. and Roberts, A.F., "The Spread of Flame across a Liquid Surface, II. Steady-State Conditions," *Proc. Roy. Soc. A,* **308**, 1968, pp. 55–68.

32. IAAI, "Pocket Guide to Accelerant Evidence Collection," International Association of Arson Investigators, 2nd Edition, 1999.

33. Dolan, J., Stauffer, E., and Newman, R., *Fire Debris Analysis*, Academic Press, 2008.

34. Shanley, J.H., "USFA Fire Burn Pattern Tests," United States Fire Administration, 1997.

35. Eurocode 5-1.2, *Design of Timber Structures*, 1995.

36. Compliance and Innovative Strategies Division (2008), "Fuel Trends Report: Gasoline 1995-2005," Washington, DC: U.S. EPA.

37. Ma T., Olenick, S., Klassen, M., Roby, R., and Torrero, J., "Burning Rate of Liquid Fuel on Carpet (Porous Media)," *Fire Technology*, **40**, 2004, pp. 227–246.

38. ASTM D7334-08, "Standard Practice for Surface Wettability of Coatings, Substrates and Pigments by Advancing Contact Angle Measurement," 2008.

39. ASTM E1412-07, "Standard Practice for Separation of Ignitable Liquid Residues from Fire Debris Samples by Passive Headspace Concentration with Activated Charcoal," 2007.

40. ASTM E1618-10, "Standard Test Method for Ignitable Liquid Residues in Extracts from Fire Debris Samples by Gas Chromatography-Mass Spectrometry," 2010.

41. ASTM D93-08, "Standard Test Methods for Flash Point by Pensky-Martens Closed Cup Tester," 2008.

42. ASTM D86-09, "Standard Test Method for Distillation of Petroleum Products at Atmospheric Pressure," 2009.

43. ASTM D287-10, "Standard Test Method for API Gravity of Crude Petroleum and Petroleum Products (Hydrometer Method)," 2006.

44. Incropera, F.P. and DeWitt, D.P., *Fundamentals of Heat and Mass Transfer*, 5th Edition, John Wiley & Sons, Inc., 2002.

45. International Energy Agency, "Condensation and Energy – Catalog of Material Properties," Report Annex XIV, **3**, March 1991.

46. Eaton, T.E., "Physical Properties of Gasoline," Journal of Applied Fire Science, **1** (2), pp. 175–183, 1991.

47. Cameo Chemicals MSDS, "Diesel," 1999.

48. IBC, *International Building Code*, Chapter 19 – Concrete, 2009.

49. ASTM D7433-08, "Standard Test Method for Measuring Surface Water Absorption of Overlaid Wood-Based Panels," 2008.

50. C. Beyler, "Fire Hazard Calculations for Large Open Hydrocarbon Fires," *The SFPE Handbook of Fire Protection Engineering,* NFPA, Quincy, MA, Chapter 3-11, 2008.

51. Hunt, S. P, Tomecek, D. T, and Campbell, B. C., "Analysis of Passive Fire Protection Needs in the Cylinder Receipt and Dispatch Building at the LES Facility in Eunice, New Mexico," report prepared by Hughes Associates, Inc. for Hukari Technical Services, Revision A, Baltimore, MD, April 30, 2010.

52. NUREG, "Fire Dynamics Tools (FDT^{S}) Quantitative Fire Hazard Analysis Methods for the U.S. Nuclear Regulatory Commission Fire Protection Inspection Program," NUREG-1805, 2003.

APPENDIX A – TEST MATRICES

Table A.1. Pan Fire Test Series

Test ID	Side Length (m [ft])	Fuel Area	Fuel	Fuel Depth (mm)	Substrate
PF1B - C - W - G - 1 - 0.093	0.31 [1]	0.093	Gasoline	1	Water
PF2 - C - W - G - 5 - 0.093	0.31 [1]	0.093		5	
PF3 - C - W - G - 10 - 0.093	0.31 [1]	0.093		10	
PF4 - C - W - G - 20 - 0.093	0.31 [1]	0.093		20	
PF5 - C - W - G - 1 - 0.372	0.61 [2]	0.372		1	
PF6 - C - W - G - 5 - 0.372	0.61 [2]	0.372		5	
PF7 - C - W - G - 10 - 0.372	0.61 [2]	0.372		10	
PF8 - C - W - G - 20 - 0.372	0.61 [2]	0.372		20	
PF13 - C - W - K - 1 - 0.093	0.31 [1]	0.093	Kerosene	1	Water
PF14 - C - W - K - 5 - 0.093	0.31 [1]	0.093		5	
PF15 - C - W - K - 10 - 0.093	0.31 [1]	0.093		10	
PF16 - C - W - K - 20 - 0.093	0.31 [1]	0.093		20	
PF17 - C - W - K - 1 - 0.372	0.61 [2]	0.372		1	
PF18 - C - W - K - 5 - 0.372	0.61 [2]	0.372		5	
PF19 - C - W - K - 10 - 0.372	0.61 [2]	0.372		10	
PF20 - C - W - K - 20 - 0.372	0.61 [2]	0.372		20	
PF20A - C - W - K - 20 - 0.372	0.61 [2]	0.372		20	
PF25 - C - W - G - 1 - 0.093	0.31 [1]	0.093	Gasoline	1	Water
PF26 - C - W - G - 5 - 0.093	0.31 [1]	0.093		5	
PF27 - C - W - G - 10 - 0.093	0.31 [1]	0.093		10	
PF28 - C - W - G - 20 - 0.093	0.31 [1]	0.093		20	
PF29 - C - W - G - 1 - 0.372	0.61 [2]	0.372		1	
PF30 - C - W - G - 5 - 0.372	0.61 [2]	0.372		5	
PF31 - C - W - G - 10 - 0.372	0.61 [2]	0.372		10	
PF32 - C - W - G - 20 - 0.372	0.61 [2]	0.372		20	
PF37 - C - W - K - 1 - 0.093	0.31 [1]	0.093	Kerosene	1	Water
PF38 - C - W - K - 5 - 0.093	0.31 [1]	0.093		5	
PF39 - C - W - K - 10 - 0.093	0.31 [1]	0.093		10	
PF40 - C - W - K - 20 - 0.093	0.31 [1]	0.093		20	
PF41 - C - W - K - 1 - 0.372	0.61 [2]	0.372		1	
PF42 - C - W - K - 5 - 0.372	0.61 [2]	0.372		5	
PF43 - C - W - K - 10 - 0.372	0.61 [2]	0.372		10	
PF49 - C - S - G - 1 - 0.093	0.31 [1]	0.093	Gasoline	1	Steel
PF49B - C - S - G - 1 - 0.093	0.31 [1]	0.093		1	
PF50 - C - S - G - 5 - 0.093	0.31 [1]	0.093		5	
PF50A - C - S - G - 5 - 0.093	0.31 [1]	0.093		5	
PF51 - C - S - G - 10 - 0.093	0.31 [1]	0.093		10	
PF51A - C - S - G - 10 - 0.093	0.31 [1]	0.093		10	
PF52 - C - S - G - 20 - 0.093	0.31 [1]	0.093		20	
PF52A - C - S - G - 20 - 0.093	0.31 [1]	0.093		20	

Table A.1. Pan Fire Test Series (Continued)

Test ID	Side Length (m [ft])	Fuel Area	Fuel	Fuel Depth (mm)	Substrate
PF53 – C – S – G - 1 - 0.372	0.61 [2]	0.372	Gasoline	1	Steel
PF53A – C – S – G - 1 - 0.372	0.61 [2]	0.372	Gasoline	1	Steel
PF54 – C – S – G - 5 - 0.372	0.61 [2]	0.372	Gasoline	5	Steel
PF54A – C – S – G - 5 - 0.372	0.61 [2]	0.372	Gasoline	5	Steel
PF55 – C – S – G - 10 - 0.372	0.61 [2]	0.372	Gasoline	10	Steel
PF55A – C – S – G - 10 - 0.372	0.61 [2]	0.372	Gasoline	10	Steel
PF56 – C – S – G - 20 - 0.372	0.61 [2]	0.372	Gasoline	20	Steel
PF57 – C – W- G - 1 - 1.488	1.22 [4]	1.488	Gasoline	1	Water
PF58 – C – S – DA - 2 - 1.488	1.22 [4]	1.488	Denatured Alcohol	2	Steel
PF60 – C – W- G - 20 - 1.488	1.22 [4]	1.488	Gasoline	20	Water
PF61 – C – S – K - 1 - 0.093	0.31 [1]	0.093	Kerosene	1	Steel
PF61A – C – S – K - 1 - 0.093	0.31 [1]	0.093		1	
PF62 – C – S – K - 5 - 0.093	0.31 [1]	0.093		5	
PF62A – C – S – K - 5 - 0.093	0.31 [1]	0.093		5	
PF63 – C – S – K - 10 - 0.093	0.31 [1]	0.093		10	
PF63A – C – S – K - 10 - 0.093	0.31 [1]	0.093		10	
PF64 – C – S – K - 20 - 0.093	0.31 [1]	0.093		20	
PF64A – C – S – K - 20 - 0.093	0.31 [1]	0.093		20	
PF65 – C – S – K - 1 - 0.372	0.61 [2]	0.372		1	
PF66 – C – S – K - 5 - 0.372	0.61 [2]	0.372		5	
PF67 – C – S – K - 10 - 0.372	0.61 [2]	0.372	Kerosene	10	Steel
PF68 – C – S – K - 20 - 0.372	0.61 [2]	0.372	Kerosene	20	Steel
PF69 – C – S – DA - 1 - 1.488	1.22 [4]	1.488	Denatured Alcohol	1	Steel
PF70 – C – S – DA - 5 - 1.488	1.22 [4]	1.488	Denatured Alcohol	5	Steel
PF72 – C – S – G - 1 - 1.488	1.22 [4]	1.488	Gasoline	1	Steel
PF73 – C – S – G - 1 - 0.093	0.31 [1]	0.093		1	
PF73A – C – S – G - 1 - 0.093	0.31 [1]	0.093		1	
PF74 – C – S – G - 5 - 0.093	0.31 [1]	0.093		5	
PF74A – C – S – G - 5 - 0.093	0.31 [1]	0.093		5	
PF75 – C – S – G - 10 - 0.093	0.31 [1]	0.093		10	
PF75A – C – S – G - 10 - 0.093	0.31 [1]	0.093		10	
PF76 – C – S – G - 20 - 0.093	0.31 [1]	0.093		20	
PF76A – C – S – G - 20 - 0.093	0.31 [1]	0.093		20	
PF77 – C – S – G - 1 - 0.372	0.61 [2]	0.372		1	
PF77A – C – S – G - 1 - 0.372	0.61 [2]	0.372		1	
PF78 – C – S – G - 5 - 0.372	0.61 [2]	0.372		5	
PF78A – C – S – G - 5 - 0.372	0.61 [2]	0.372		5	
PF79 – C – S – G - 10 - 0.372	0.61 [2]	0.372		10	
PF79A – C – S – G - 10 - 0.372	0.61 [2]	0.372		10	
PF80 – C – S – G - 20 - 0.372	0.61 [2]	0.372		20	

Table A.1. Pan Fire Test Series (Continued)

Test ID	Side Length (m [ft])	Fuel Area	Fuel	Fuel Depth (mm)	Substrate
PF81 - C - W- G - 1 - 1.488	1.22 [4]	1.488	Gasoline	1	Water
PF82 - C - W- G - 5 - 1.488	1.22 [4]	1.488	Gasoline	5	Water
PF84 - C - W- G - 20 - 1.488	1.22 [4]	1.488	Gasoline	20	Water
PF85 - C - S - K - 1 - 0.093	0.31 [1]	0.093	Kerosene	1	Steel
PF85A - C - S - K - 1 - 0.093	0.31 [1]	0.093		1	
PF86 - C - S - K - 5 - 0.093	0.31 [1]	0.093		5	
PF86A - C - S - K - 5 - 0.093	0.31 [1]	0.093		5	
PF87 - C - S - K - 10 - 0.093	0.31 [1]	0.093		10	
PF87A - C - S - K - 10 - 0.093	0.31 [1]	0.093		10	
PF88 - C - S - K - 20 - 0.093	0.31 [1]	0.093		20	
PF88A - C - S - K - 20 - 0.093	0.31 [1]	0.093		20	
PF89 - C - S - K - 1 - 0.372	0.61 [2]	0.372		1	
PF90 - C - S - K - 5 - 0.372	0.61 [2]	0.372		5	
PF91 - C - S - K - 10 - 0.372	0.61 [2]	0.372		10	
PF92 - C - S - K - 20 - 0.372	0.61 [2]	0.372		20	
PF93 - C - S - DA - 1 - 1.488	1.22 [4]	1.488	Denatured Alcohol	1	Steel
PF94 - C - S - DA - 5 - 1.488	1.22 [4]	1.488	Denatured Alcohol	5	
PF96 - C - S - G - 5 - 1.488	1.22 [4]	1.488	Gasoline	5	
PF98 - C - S - K - 40 - 0.093	0.31 [1]	0.093	Kerosene	40	
PF99 - C - S - H - 20 - 0.093	0.31 [1]	0.093	Heptane	20	
PF104 - C - S - G - 40 - 0.093	0.31 [1]	0.093	Gasoline	40	Steel
PF106 - C - S - G - 40 - 0.093	0.31 [1]	0.093		40	
PF107 - C - S - G - 40 - 0.093	0.31 [1]	0.093		40	
PF108 - C - S - K - 40 - 0.093	0.31 [1]	0.093	Kerosene	40	Steel
PF109 - C - W- G - 2 - 1.488	1.22 [4]	1.488	Gasoline	2	Water
PF110 - C - W- G - 3 - 1.488	1.22 [4]	1.488		3	
PF111 - C - W- G - 4 - 1.488	1.22 [4]	1.488		4	
PF112 - C - W- G - 5 - 1.488	1.22 [4]	1.488		5	
PF113 - C - S - DA - 3 - 1.488	1.22 [4]	1.488	Denatured Alcohol	3	Steel
PF114 - C - S - DA - 4 - 1.488	1.22 [4]	1.488	Denatured Alcohol	4	Steel
PF115 - C - W- G - 2 - 1.488	1.22 [4]	1.488	Gasoline	2	Water
PF116 - C - W- G - 3 - 1.488	1.22 [4]	1.488		3	
PF117 - C - W- G - 4 - 1.488	1.22 [4]	1.488		4	
PF118 - C - S - DA - 2 - 1.488	1.22 [4]	1.488	Denatured Alcohol	2	Steel
PF119 - C - S - DA - 3 - 1.488	1.22 [4]	1.488		3	
PF120 - C - S - DA - 4 - 1.488	1.22 [4]	1.488		4	
PF121 - C - W- G - 5 - 1.488	1.22 [4]	1.488	Gasoline	5	Water
PF122 - C - S - G - 5 - 1.488	1.22 [4]	1.488	Gasoline	5	Steel
PF123 - C - S - G - 1 - 1.488	1.22 [4]	1.488	Gasoline	1	Steel

Table A.2. Diked Fire Test Series

Test ID	Side Length (m [ft])	Fuel	Fuel Depth (mm)	Substrate
DSF1 - C - CC - G - 1 - 0.093	0.31 [1]	Gasoline	1	Coated Concrete
DSF2 - C - CC - G - 5 - 0.093	0.31 [1]	Gasoline	5	Coated Concrete
DSF3 - C - CC - G - 10 - 0.093	0.31 [1]	Gasoline	10	Coated Concrete
DSF4 - C - CC - G - 20 - 0.093	0.31 [1]	Gasoline	20	Coated Concrete
DSF5 - C - CC - K - 1 - 0.093	0.31 [1]	Kerosene	1	Coated Concrete
DSF6 - C - CC - K - 5 - 0.093	0.31 [1]	Kerosene	5	Coated Concrete
DSF7 - C - CC - K - 10 - 0.093	0.31 [1]	Kerosene	10	Coated Concrete
DSF8 - C - CC - K - 20 - 0.093	0.31 [1]	Kerosene	20	Coated Concrete
DSF9 - C - CC - G - 1 - 0.372	0.61 [2]	Gasoline	1	Coated Concrete
DSF10 - C - CC - G - 5 - 0.372	0.61 [2]	Gasoline	5	Coated Concrete
DSF11 - C - CC - G - 10 - 0.372	0.61 [2]	Gasoline	10	Coated Concrete
DSF12 - C - CC - G - 20 - 0.372	0.61 [2]	Gasoline	20	Coated Concrete
DSF13 - C - CC - K - 1 - 0.372	0.61 [2]	Kerosene	1	Coated Concrete
DSF14 - C - CC - K - 5 - 0.372	0.61 [2]	Kerosene	5	Coated Concrete
DSF15 - C - CC - K - 10 - 0.372	0.61 [2]	Kerosene	10	Coated Concrete
DSF16 - C - CC - K - 20 - 0.372	0.61 [2]	Kerosene	20	Coated Concrete
DSF17 - C - CC - G - 1 - 1.488	1.22 [4]	Gasoline	1	Coated Concrete
DSF18 - C - CC - G - 2 - 1.488	1.22 [4]	Gasoline	2	Coated Concrete
DSF19 - C - CC - G - 3 - 1.488	1.22 [4]	Gasoline	3	Coated Concrete
DSF20 - C - CC - G - 4 - 1.488	1.22 [4]	Gasoline	4	Coated Concrete
DSF21 - C - CC - G - 5 - 1.488	1.22 [4]	Gasoline	5	Coated Concrete
DSF22 - C - CC - G - 20 - 1.488	1.22 [4]	Gasoline	20	Coated Concrete
DSF23 - C - CC - K - 1 - 1.488	1.22 [4]	Kerosene	1	Coated Concrete
DSF24 - C - CC - K - 2 - 1.488	1.22 [4]	Kerosene	2	Coated Concrete
DSF25 - C - V - G - 1 - 0.093	0.31 [1]	Gasoline	1	Vinyl
DSF26 - C - V - G - 5 - 0.093	0.31 [1]	Gasoline	5	Vinyl
DSF27 - C - V - G - 10 - 0.093	0.31 [1]	Gasoline	10	Vinyl
DSF28 - C - V - G - 20- 0.093	0.31 [1]	Gasoline	20	Vinyl
DSF29 - C - V - K - 1 - 0.093	0.31 [1]	Kerosene	1	Vinyl
DSF30 - C - V - K - 5 - 0.093	0.31 [1]	Kerosene	5	Vinyl
DSF31 - C - V - K - 10 - 0.093	0.31 [1]	Kerosene	10	Vinyl
DSF32 - C - V - K - 20 - 0.093	0.31 [1]	Kerosene	20	Vinyl
DSF33 - C - V - G - 1 - 0.372	0.61 [2]	Gasoline	1	Vinyl
DSF34 - C - V - G - 5 - 0.372	0.61 [2]	Gasoline	5	Vinyl

Table A.2. Diked Fire Test Series (Continued)

Test ID	Side Length (m [ft])	Fuel	Fuel Depth (mm)	Substrate
DSF35 - C - V - G - 10 - 0.372	0.61 [2]	Gasoline	10	Vinyl
DSF36 - C - V - G - 20 - 0.372	0.61 [2]	Gasoline	20	Vinyl
DSF37 - C - V - K - 1 - 0.372	0.61 [2]	Kerosene	1	Vinyl
DSF38 - C - V - K - 5 - 0.372	0.61 [2]	Kerosene	5	Vinyl
DSF39 - C - V - K - 10 - 0.372	0.61 [2]	Kerosene	10	Vinyl
DSF40 - C - V - K - 20 - 0.372	0.61 [2]	Kerosene	20	Vinyl
DSF41 - C - V - G - 1 - 1.488	1.22 [4]	Gasoline	1	Vinyl
DSF42 - C - V - G - 2 - 1.488	1.22 [4]	Gasoline	2	Vinyl
DSF43 - C - V - G - 3 - 1.488	1.22 [4]	Gasoline	3	Vinyl
DSF44 - C - V - G - 4 - 1.488	1.22 [4]	Gasoline	4	Vinyl
DSF45 - C - V - G - 5 - 1.488	1.22 [4]	Gasoline	5	Vinyl
DSF46 - C - V - G - 20 - 1.488	1.22 [4]	Gasoline	20	Vinyl

Table A.3. Spill Dynamics Test Series

Test ID	Substrate	Liquid Type	Qty. (L)
SD1 - U - V - FS1 - 0.1	Vinyl	3% AFFF	0.1
SD2 - U - V - FS1 - 0.1			
SD3 - U - V - FS1 - 0.1			
SD4 - U - V - FS2 - 0.25		3% FP	0.25
SD5 - U - V - FS2 - 0.25			
SD6 - U - V - FS2 - 0.25			
SD7 - U - V - L - 0.5		Lube Oil	0.5
SD8 - U - V - L - 0.5			
SD9 - U - V - L - 0.5			
SD10 - U - C - FS1 - 0.5	Carpet	3% AFFF	0.5
SD11 - U - C - FS1 - 0.5			
SD12 - U - C - FS1 - 0.5			
SD13 - U - C - FS2 - 0.5		3% FP	0.5
SD14 - U - C - FS2 - 0.5			
SD15 - U - C - FS2 - 0.5			
SD19 - U - P - FS1 - 0.5	Plywood	3% AFFF	0.5
SD20 - U - P - FS1 - 0.5			
SD21 - U - P - FS1 - 0.5			
SD22 - U - P - FS2 - 0.5		3% FP	0.5
SD23 - U - P - FS2 - 0.5			
SD24 - U - P - FS2 - 0.5			
SD25 - U - P - L - 0.5		Lube Oil	0.5
SD26 - U - P - L - 0.5			
SD27 - U - P - L - 0.5			
SD28 - U - CC - FS1 - 0.5	Coated Concrete	3% AFFF	0.5
SD29 - U - CC - FS1 - 0.5			
SD30 - U - CC - FS1 - 0.5			
SD31 - U - CC - FS2 - 0.5		3% FP	0.5
SD32 - U - CC - FS2 - 0.5			
SD33 - U - CC - FS2 - 0.5			
SD34 - U - CC - L - 0.5		Lube Oil	0.5
SD35 - U - CC - L - 0.5			
SD36 - U - CC - L - 0.5			
SD37 - U - SC - FS1 - 0.5	Smooth Concrete (NIJ)	3% AFFF	0.5
SD38 - U - SC - FS1 - 0.5			
SD39 - U - SC - FS1 - 0.5			
SD40 - U - SC - FS2 - 0.5		3% FP	0.5
SD41 - U - SC - FS2 - 0.5			
SD42 - U - SC - FS2 - 0.5			
SD43 - U - SC - L - 0.5		Lube Oil	0.5
SD44 - U - SC - L - 0.5			
SD45 - U - SC - L - 0.5			

Table A.3. Spill Dynamics Test Series (Continued)

Test ID	Substrate	Liquid Type	Qty. (L)
SD46 - U - BC - FS1 - 0.5	Brushed Concrete	3% AFFF	0.5
SD47 - U - BC - FS1 - 0.5			
SD48 - U - BC - FS1 - 0.5			
SD49 - U - BC - FS2 - 0.5		3% FP	0.5
SD50 - U - BC - FS2 - 0.5			
SD51 - U - BC - FS2 - 0.5			
SD52 - U - BC - L - 0.5		Lube Oil	0.5
SD53 - U - BC - L - 0.5			
SD54 - U - BC - L - 0.5			
SD55A - U - P - FS1 - 0.5	Plywood	3% AFFF	0.25
SD56A - U - P - FS1 - 0.5			
SD57 - U - P - FS1 - 0.5			
SD58 - U - O - FS1 - 0.5	Oriented Strand Board (OSB)	3% AFFF	0.35
SD59 - U - O - FS1 - 0.5			
SD60 - U - O - FS1 - 0.5			
SD61 - U - O - FS2 - 0.5		3% FP	0.5
SD62 - U - O - FS2 - 0.5			
SD63 - U - O - FS2 - 0.5			
SD64 - U - V - FS1 - 0.5	Vinyl	3% AFFF	0.5
SD65 - U - V - FS1 - 0.5			
SD66 - U - V - FS1 - 0.5			
SD67 - U - C - FS1 - 0.5	Carpet	3% AFFF	2
SD68 - U - C - FS1 - 0.5			
SD69 - U - SC - FS1 - 0.5	Smooth Concrete (ATF)	3% AFFF	0.5
SD70 - U - SC - FS1 - 5			5
SD71 - U - SC - FS1 - 20			20
SD72 - U - SC - FS1 - 0.5			0.5
SD73 - U - SC - FS1 - 5			5
SD74 - U - SC - FS1 - 20			20
SD75 - U - SC - FS1 - 0.5			0.5
SD76 - U - SC - FS1 - 5			5
SD77 - U - SC - FS1 - 20			20
SD78 - U - SC - FS2 - 0.5		3% FP	0.5
SD79 - U - SC - FS2 - 5			5
SD80 - U - SC - FS2 - 20			20
SD81 - U - SC - FS2 - 0.5			0.5
SD82 - U - SC - FS2 - 5			5
SD83 - U - SC - FS2 - 20			20
SD84 - U - SC - FS2 - 0.5			0.5
SD85 - U - SC - FS2 - 5			5
SD86 - U - SC - FS2 - 20			20

Table A.4. Spill Fire Dynamics Test Series

Test ID	Substrate	Fuel	Qty. (L)	Spread Time (s)
SFD1 - U - CC - G - 0.5 - 300	Coated Concrete	Gasoline	0.5	300
SFD2 - U - CC - G - 1 - 30		Gasoline	1	30
SFD3 - U - CC - G - 1 - 30		Gasoline	1	30
SFD11 - U - CC - K - 0.5 - 300		Kerosene	0.5	300
SFD11 - U - CC - K - 0.5 - 0		Kerosene	0.5	0
SFD11A - U - CC - K - 0.5 - 300		Kerosene	0.5	300
SFD16 - U - CC - DA - 0.5 - 300		Denatured Alcohol	0.5	300
SFD17 - U - CC - DA - 1 - 30		Denatured Alcohol	1	30
SFD18 - U - CC - DA - 1 - 30		Denatured Alcohol	1	30
SFD21 - U - CC - G - 0.5 - 300		Gasoline	0.5	300
SFD21A - U - CC - G - 0.5 - 300		Gasoline	0.5	300
SFD22 - U - CC - G - 1 - 150		Gasoline	1	150
SFD22A - U - CC - G - 1 - 300		Gasoline	1	300
SFD23 - U - CC - G - 1 - 300		Gasoline	1	300
SFD31 - U - CC - K - 0.5 - 0		Kerosene	0.5	0
SFD36 - U - CC - DA - 0.5 - 300		Denatured Alcohol	0.5	300
SFD36A - U - CC - DA - 0.5 - 300		Denatured Alcohol	0.5	300
SFD36B - U - CC - DA - 0.5 - 300		Denatured Alcohol	0.5	300
SFD37 - U - CC - DA - 1 - 300		Denatured Alcohol	1	300
SFD38 - U - CC - DA - 1 - 300		Denatured Alcohol	1	300
SFD41 - U - P - G - 0.5 - 30	Plywood	Gasoline	0.5	30
SFD42 - U - P - G - 0.5 - 30		Gasoline	0.5	30
SFD43 - U - P - K - 0.5 - 30		Kerosene	0.5	30
SFD44 - U - P - K - 0.5 - 30		Kerosene	0.5	30
SFD45 - U - P - DA - 0.5 - 30		Denatured Alcohol	0.5	30
SFD46 - U - P - DA - 0.5 - 30		Denatured Alcohol	0.5	30
SFD49 - U - C - G - 0.5 - 30	Carpet/Pad/ Plywood	Gasoline	0.5	30
SFD50 - U - C - G - 1 - 30	Carpet/Pad/ Concrete	Gasoline	1	30
SFD50A - U - C - G - 1 - 30	Carpet/Pad/ Plywood	Gasoline	1	30
SFD51 - U - C - G - 5 - 30		Gasoline	5	30
SFD52 - U - C - K - 0.5 - 30		Kerosene	0.5	30
SFD53 - U - C - K - 1 - 30		Kerosene	1	30
SFD53A - U - C - K - 1 - 30		Kerosene	1	30
SFD54 - U - C - K - 5 - 30		Kerosene	5	30
SFD55 - U - C - G - 0.5 - 30		Gasoline	0.5	30
SFD56 - U - C - G - 1 - 30	Carpet/Pad/ Plywood	Gasoline	1	30
SFD56A - U - C - G - 1 - 30		Gasoline	1	30
SFD57 - U - C - G - 5 - 30		Gasoline	5	30
SFD58 - U - C - K - 0.5 - 30		Kerosene	0.5	30
SFD59 - U - C - K - 1 - 30		Kerosene	1	30
SFD60 - U - C - K - 5 - 30		Kerosene	5	30
SFD61 - U - V - G - 0.5 - 30	Vinyl	Gasoline	0.5	30
SFD62A - U - V - G - 1 - 30		Gasoline	1	30
SFD63 - U - V - G - 0.5 - 30		Gasoline	0.5	30

Table A.4. Spill Fire Dynamics Test Series (Continued)

Test ID	Substrate	Fuel	Qty. (L)	Spread Time (s)
SFD64 - U - V - K - 0.5 - 30	Vinyl	Kerosene	0.5	30
SFD65 - U - V - DA - 1 - 30		Denatured Alcohol	1	30
SFD66 - U - V - G - 1 - 30		Gasoline	1	30
SFD67 - U - V - G - 0.5 - 300		Gasoline	0.5	300
SFD68 - U - V - G - 1 - 150		Gasoline	1	150
SFD69 - U - V - G - 1 - 167		Gasoline	1	167
SFD71 - U - V - DA - 1 - 300		Denatured Alcohol	1	300
SFD73 - U - CC - H - 0.5 - 300	Coated Concrete	Heptane	0.5	300
SFD74 - U - CC - H - 1 - 30		Heptane	1	30
SFD78 - U - CC - H - 0.5 - 300		Heptane	0.5	300
SFD78A - U - CC - H - 0.5 - 300	Coated Concrete	Heptane	0.5	300
SFD79 - U - CC - H - 1 - 300		Heptane	1	300
SFD79A - U - CC - H - 1 - 300		Heptane	1	300
SFD83 - U - BC - G - 0.5 - 30	Brushed Concrete	Gasoline	0.5	30
SFD84 - U - BC - G - 1 - 30		Gasoline	1	30
SFD86 - U - BC - G - 0.5 - 300		Gasoline	0.5	300
SFD87 - U - BC - G - 1 - 300		Gasoline	1	300
SFD89 - U - CC - G - 0.5 - 30	Coated Concrete	Gasoline	0.5	30
SFD89A - U - CC - G - 0.5 - 30		Gasoline	0.5	30
SFD89B - U - CC - G - 0.5 - 30		Gasoline	0.5	30
SFD90 - U - CC - DA - 0.5 - 30		Denatured Alcohol	0.5	30
SFD91 - U - CC - G - 0.5 - 30		Gasoline	0.5	30
SFD92 - U - CC - DA - 0.5 - 30		Denatured Alcohol	0.5	30
SFD93 - U - CC - H - 0.5 - 30		Heptane	0.5	30
SFD94 - U - CC - H - 0.5 - 30		Heptane	0.5	30
SFD95 - U - CC - G - 1 - 30		Gasoline	1	30
SFD96 - U - CC - G - 1 - 30	Coated Concrete	Gasoline	1	30
SFD100 - U - CC - G - 0.5 - 300	Coated Concrete	Gasoline	0.5	300
SFD115 - U - V - DA - 1 - 30	Vinyl	Denatured Alcohol	1	30
SFD117 - U - V - DA - 1 - 300	Vinyl	Denatured Alcohol	1	300
SFD119 - U - CC - H - 1 - 30	Coated Concrete	Heptane	1	30
SFD121 - U - CC - H - 1 - 300	Coated Concrete	Heptane	1	300
SFD122 - U - SC - G - 0.5 - 30	Smooth Concrete	Gasoline	0.5	30
SFD123 - U - SC - G - 1 - 30		Gasoline	1	30
SFD124 - U - SC - G - 0.5 - 300		Gasoline	0.5	300
SFD126 - U - O - G - 0.5 - 30	OSB	Gasoline	0.5	30
SFD127 - U - O - G - 0.5 - 30		Gasoline	0.5	30
SFD128 - U - O - DA - 0.5 - 30		Denatured Alcohol	0.5	30
SFD129 - U - O - DA - 0.5 - 30		Denatured Alcohol	0.5	30
SFD130 - U - O - G - 0.5 - 30		Gasoline	0.5	30
SFD131 - U - O - G - 0.5 - 30		Gasoline	0.5	30
SFD132 - U - O - DA - 0.5 - 30		Denatured Alcohol	0.5	30
SFD133 - U - O - DA - 0.5 - 30		Denatured Alcohol	0.5	30
SFD134 - U - BC - G - 0.5 - 30	Brushed Concrete	Gasoline	0.5	30

Table A.4. Spill Fire Dynamics Test Series (Continued)

Test ID	Substrate	Fuel	Qty. (L)	Spread Time (s)
SFD135 - U - BC - G - 1 - 30	Brushed Concrete	Gasoline	1	30
SFD136 - U - CC - G - 0.5 - 0	Coated Concrete	Gasoline	0.5	0
SFD136 - U - BC - G - 0.5 - 300	Brushed Concrete	Gasoline	0.5	300
SFD137 - U - BC - G - 1 - 300	Brushed Concrete	Gasoline	1	300
SFD139 - U - CC - H - 0.5 - 300	Coated Concrete	Heptane	0.5	300
SFD140 - U - SC - G - 0.5 - 30	Smooth Concrete	Gasoline	0.5	30
SFD141 - U - SC - G - 1 - 30	Smooth Concrete	Gasoline	1	30
SFD141A - U - C - G - 1 - 30	Carpet/Concrete	Gasoline	1	30
SFD142 - U - SC - G - 0.5 - 300	Smooth Concrete	Gasoline	0.5	300
SFD150 - U - O - K - 0.5 - 30	OSB	Kerosene	0.5	30
SFD151 - U - O - K - 0.5 - 30	OSB	Kerosene	0.5	30
SFD152 - U - C - G - 1 - 300	Carpet/Pad/ Plywood	Gasoline	1	300
SFD153 - U - O- K - 0.5 - 30	OSB	Kerosene	0.5	30
SFD154 - U - O - K - 0.5 - 30	OSB	Kerosene	0.5	30
SF156 - U - V - K - 0.5 - 30	Vinyl	Kerosene	0.5	30
SFD157 - U - V - G - 0.5 - 300	Vinyl	Gasoline	0.5	300
SFD158 - U - SC - G - * - 0	Smooth Concrete	Gasoline	*	0
SFD159 - U - SC - G - * - 0		Gasoline	*	0
SFD160 - U - SC - DA - * - 0		Denatured Alcohol	*	0

Table A.5. Class A Fire Test Series

Test ID	Substrate	Class A Combustible
CAF1 - U - P	Plywood	Wood Crib
CAF2 - U - P	Plywood	Car Seat
CAF3 - U - P	Plywood	Polyurethane Foam Chair
CAF4 - U - C	Carpet	Wood Crib
CAF5 - U - C	Carpet	Polyurethane Foam Chair
CAF6 - U - V	Vinyl	Wood Crib
CAF7 - U - V	Vinyl	Polyurethane Foam Chair
CAF8 - U - C	Carpet	Car Seat
CAF9 - U - V	Vinyl	Car Seat

APPENDIX B – HOOD CALORIMETER CONFIGURATION AND CALIBRATION

All tests in this series were conducted in the ATF Fire Research Lab's Medium Burn Room (MBR). This room is approximately 46.2 m (151 ft) long by 24.5 m (80 ft) wide. The average height from floor to ceiling of the MBR is approximately 10.2 m (33.5 ft). The MBR contains five hood calorimeters, three of which were used in this test series and will be described. A 4 MW square shaped hood calorimeter is located in the northern side of the MBR. The southwest and southeast sides of the MBR contain a 1 MW square hood and a 1 MW round hood, respectively. In order to optimize air flow conditions in the MBR, tarps were placed from the floor to approximately 1.0 m (3 ft) from the ceiling to create separate compartments for each of the three hood calorimeters. The 1 MW (square and round) hoods are located off-center in compartments approximately 17 m (56 ft) deep by 12.2 m (40 ft) wide. The 4 MW hood area takes up the rest of the MBR and is approximately 29 m (95 ft) deep by 24.5 m (80 ft) wide. In addition to these hoods, exhaust vents are placed at the ceiling in the four corners of the MBR in the event that smoke escapes from under one of the hoods during a test.

All three hoods used in testing are of steel construction. The 4 MW hood has a square curtain around the bottom of a conical shaped transition, leading to a circular exhaust duct. The 1 MW square hood has a square curtain and a pyramidal shaped transition leading to a circular exhaust duct. The 1 MW round hood has no curtain and only consists of a conical shaped transition leading to a circular exhaust duct. The dimensions of the hood capture areas as well as the hood heights are shown in Table B.1.

Table B.1. Hood Capture Areas and Dimensions

	4 MW Hood	**1 MW Square**	**1 MW Round**
Hood Diam. or Square Area – meters [ft]	5.63 x 5.63 [18.4 x 18.4]	3.0 x 3.03 [9.84 x 9.94]	3.22 [10.6]
Distance from floor to bottom of hood – meters [ft]	0.713 [2.34]	0.289 [0.95]	0.381 [1.25]

For each of the hoods in the MBR, the exhaust duct runs vertical from the top of the hood transition through the ceiling and into the plenum space above. The ducts then make a 90 degree turn and run horizontally for a distance before entering the scrubber. For the 4 MW hood, the 90 degree turn is accomplished using an elbow connection. However, for the 1 MW square and 1 MW round hoods, the 90 degree turn is accomplished with a miter bend. The hood duct diameters are shown in Table A.2.

Table B.2. Hood Duct Diameters

	4 MW Hood	**1 MW Square**	**1 MW Round**
Duct Diameter – meters [ft]	1.35 [4.42]	0.653 [2.14]	0.655 [2.15]

Hood calorimetry instrumentation consists of either one (for 1 MW hoods) or two (for 4 MW hood) bi-directional velocity probes with collocated thermocouples, a set of oxygen consumption sample lines, and white light and laser smoke sensors. The bi-directional velocity probes are connected to Setra Model 267 differential pressure transducers. Collocated thermocouples are Omega type-K, inconel sheathed models. Oxygen consumption sample lines run to a Servomex

4100 gas analyzer that measures O_2, CO_2, and CO concentrations. The basic elements of the laser system are a Heluim-Neon (HeNe) laser and two photodiode detectors. The basic elements of the white light system are a control unit, a light source and a light receiver. The white light system is manufactured by Fire Testing Technology (FTT), and conforms to DIN 50055.

For the 1 MW round and square hoods, the velocity probes and sample lines are located in the duct at heights of 9.5 m (31 ft) and 8.5 m (28 ft) above the ground, respectively. For the 1 MW hoods, the white light and laser sensors are located between 14.5 m (47 ft) and 14.8 m (48 ft) above the floor MBR in the plenum space. For the 4 MW hood, the two velocity probes and sample lines are located in the duct approximately 10.9 m (36 ft) after the 90 degree bend in the plenum space. The nominal exhaust flow rates used in testing can be seen in Table B.3.

Table B.3. Nominal Hood Exhaust Flow Rates

4 MW Hood	**1 MW Square**	**1 MW Round**
35000 cfm	8000 cfm	11000 cfm

For each individual hood, the exhaust flow rates varied from test to test as expected fire sizes changed. In addition, the exhaust flow rate was set using building HVAC velocity probes and not those used for calorimetry calculations. This does not affect the accuracy of the measured exhaust flow rates, but can impact the test-to-test repeatability of the initial exhaust flow rate. The numbers reported in Table B.3 are the nominal exhaust flow rates measured and used in the calorimetry calculations.

Prior to using the hood calorimeters for testing, each was calibrated with a series of tests to determine its c-factor. These tests were conducted using an appropriately sized natural gas burner. The 1 MW hoods were calibrated using a 0.3 m (1 ft) square sand burner capable of a 500 kW heat release rate. The 4 MW hood was calibrated using a unique natural gas tube burner capable of producing fires ranging in size from 0.2–4 MW. For the 1 MW hood calibration, the burner heat release rate was increased from 0 to 500 kW in steps of 100 kW for periods of 5 minutes each, resulting in a 25 minute test. A representative 1 MW calibration test heat release rate curve can be seen in Figure B.1. This figure shows both the burner heat release rate as well as the adjusted measured heat release rate.

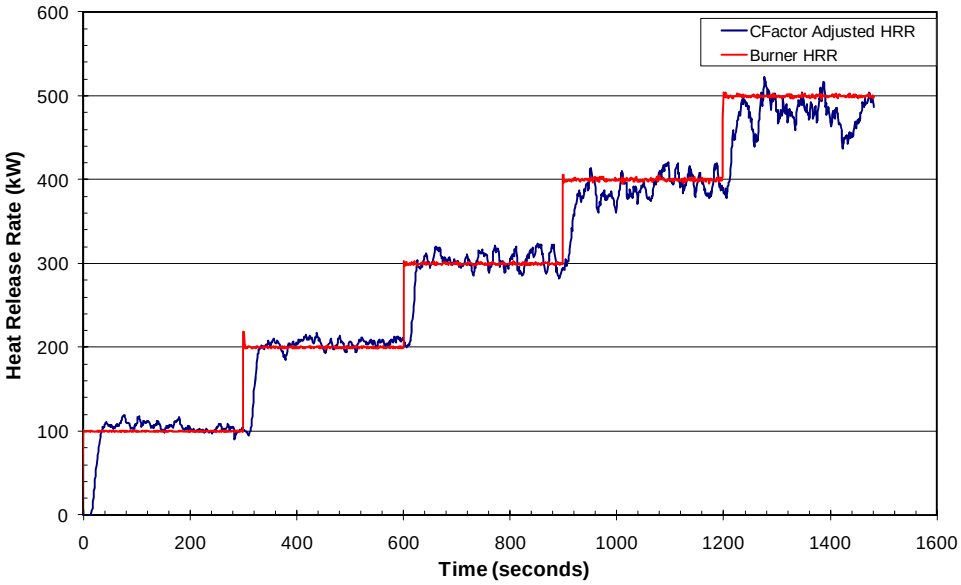

Figure B.1. Representative 1 MW calibration test heat release rate curve

The 4 MW hood calibration used a similar stepped heat release rate, increasing from 0 to 4 MW by increments of 1 MW for periods of 5 minutes and then decreasing by increments of 1 MW for periods of 5 minutes, resulting in a 35 minute calibration test. Figure B.2 shows a representative 4 MW calibration test's heat release rate curve including the burner heat release rate and the c-factor adjusted heat release rate.

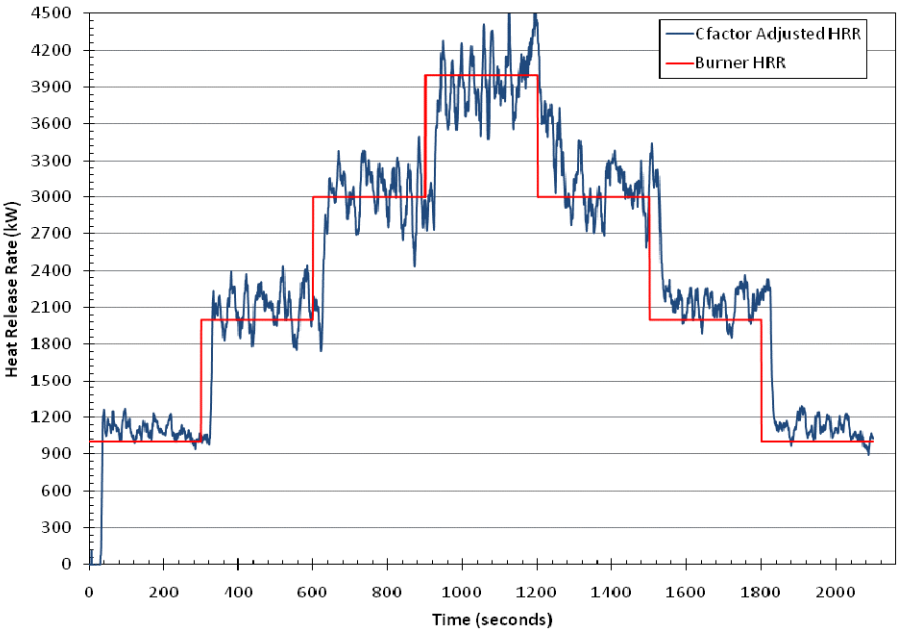

Figure B.2. Representative 4 MW calibration test heat release rate curve

APPENDIX C – VIDEO ANALYSIS METHODOLOGY AND CALIBRATION

For this work a video analysis methodology was developed to quantify the progression and equilibrium spill depths of the spills evaluated. This methodology consisted of scaling the images collected and measuring the area covered by the spilled liquid. The purpose of this appendix is to provide a description of the methodology used and the calibration data collected to validate the methodology.

Image analysis was performed on both standard and infrared video images. Standard video images were collected using a Sony Model HVR-A1U video camera and infrared video images were collected using a FLIR ThermaCAM Model P640 infrared camera. Due to the varying experimental test setups, video images were collected from one of two viewpoints. The first viewpoint analyzed was taken from directly above the spill (i.e., camera lens parallel to the spill substrate) thus no image adjustment was necessary. This viewpoint was used in the majority of the spill dynamics tests. As shown in Figure C.1, for this setup the cameras were positioned 8.9 m (29 ft - 4 in.) above the spill substrate.

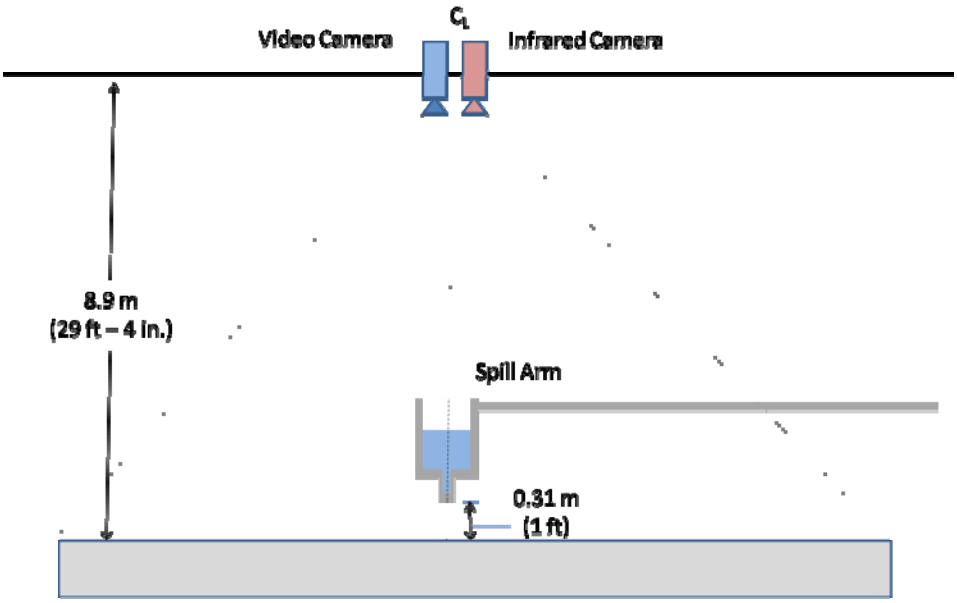

Figure C.1. Illustration of overhead camera setup

The second viewpoint analyzed was taken from an off-axis perspective due to the fire plume resulting from the ignition of the fuel spill fires. In this scenario, shown in Figure C.2, the cameras were located 11.6 m (38 ft) away from the center of the spill substrate and 7.9 m (26 ft) above the substrate. This viewpoint was used in the majority of the spill fire tests as well as some of the large quantity spill dynamics tests.

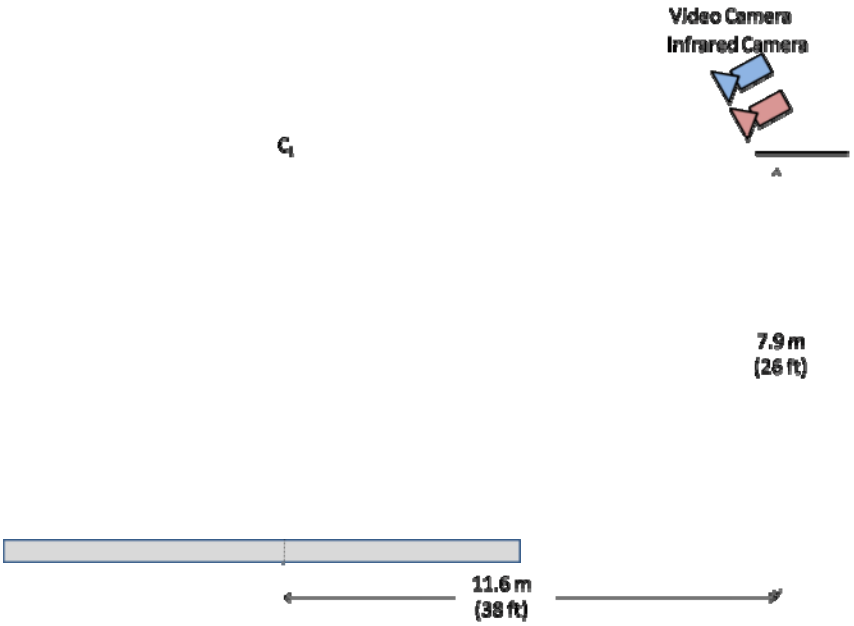

Figure C.2. Illustration of off-axis camera setup

Standard video images were used when the leading edge of the liquid flow could be easily identified and tracked for the duration of a test. Infrared images were used when the flowing liquid could not be easily tracked. The infrared imaging capability of the camera made it possible to track a visually unidentifiable liquid flow based upon the emissivity differences between the flooring materials and the fuels. Examples of the images collected from both the standard and thermal imaging cameras are presented in Figure C.3. Also shown in this figure are the two viewpoints used.

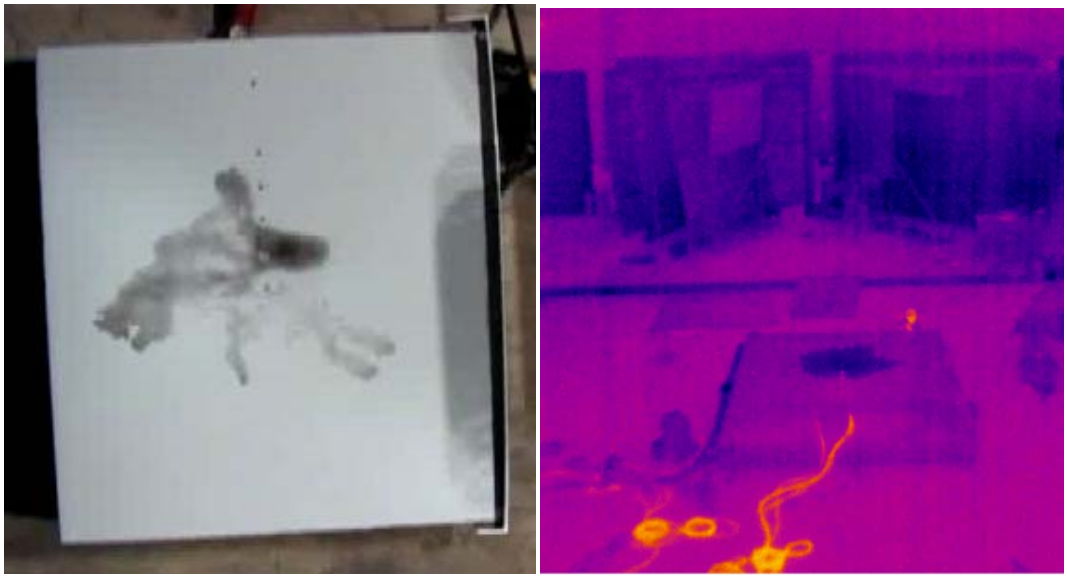

Figure C.3. Example images from the standard video camera taken from overhead (left) and the thermal imaging camera taken from the off-axis location

Video images were then analyzed using several software packages that were used to extract stills from the videos, perform keystone correction on images taken from an off-axis vantage point, and take area measurements whereby the transient and equilibrium area covered by the spilled liquid could be quantified. The progression of a spill and/or nominal depth of the spill was then determined. Spill depth was determined based upon the quotient of the known spill volume and the measured spill area.

As indicated above, both standard video and thermal imaging video were used to record all tests in which spill area was calculated. Test video was then converted to a sequence of still images using VirtualDub 1.5.10. Using this software the images collected by the video and thermal imaging cameras were extracted at a rate 1 frame per second and 1 frame every 5 seconds, respectively. The next step in the procedure was dependent upon the camera location for the test being analyzed. For images collected from overhead, no modification to the image was needed and the image sequence could be processed for area measurements. Liquid spill areas were determined from the test photographs using a National Institute of Health image analysis program called ImageJ. ImageJ is a very sophisticated program that, among other functions, can calculate the area of objects in a photograph. ImageJ uses a pixel counting algorithm to determine area of an object within a boundary. The process begins by opening each photograph with ImageJ. The calibration length was then identified and used to scale the image. Generally, the side length of the spill substrate was used as the calibration scale in all analyses. Once scaled, the spill area was outlined and the software calculated the area identified using the scale provided.

A similar approach was taken when analyzing off-axis images with the exception of one additional set that was required to account for the parallax effect resulting from the off-axis image. In order to compensate for parallax a keystone correction was performed on all off-axis images. Keystone corrections were performed using the Hugin 0.7.0 image analysis software package. Once corrected, the image was scaled and analyzed using an approach identical to that described above. Due to the fact that the images were being scaled and keystone corrections were being performed, once cameras were installed the cameras were not moved and the focal length of the cameras remained constant.

Prior to testing, a series of calibration images were collected in order to validate the image analysis methodology and to determine the accuracy at which area data could be collected using the stated approach. The calibration images consisted of the placement of objects with known areas at various locations on the spill substrates and using the methodology described above to measure the areas of these objects. The measured and known areas were then compared to evaluate the validity of the approach as well as the overall accuracy with which area could be measured. The results of these calibration efforts are provided in Figure C.4.

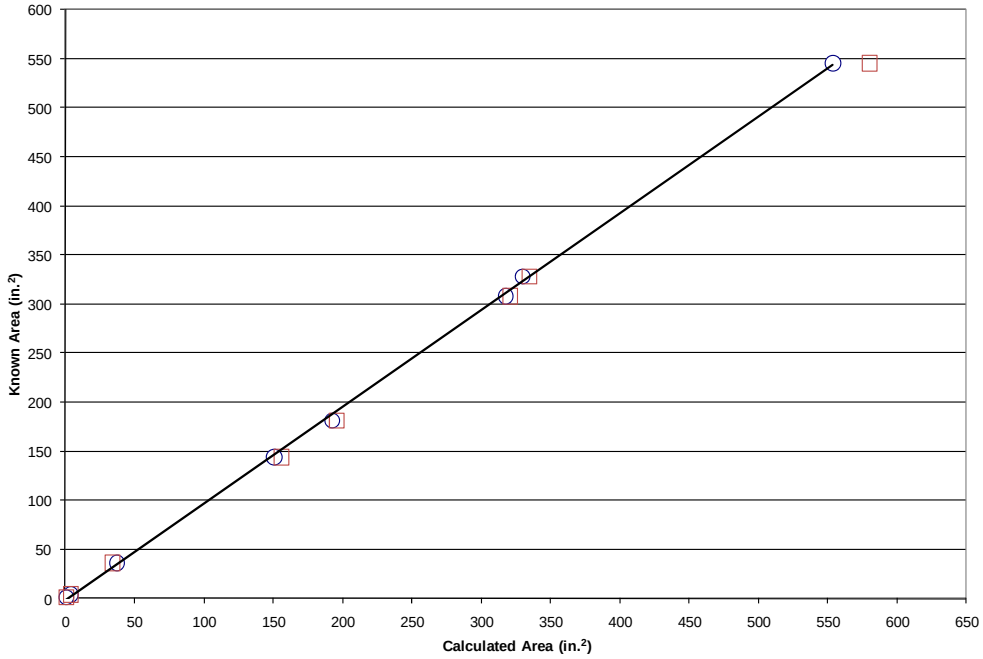

Figure C.4. Comparison between known and measured object areas for both overhead and off-axis image calibration

On average, the measured spill area was within 5.5 percent of the known area for both camera locations, as shown in Figure C.4. The largest difference in measured and known areas was observed when attempting to measure objects whose areas were 0.0006 m^2 (1 $in.^2$). At this size, the differences between measured and known areas were between 12 to 14 percent. However, objects with known areas of 0.0026 m^2 (4 $in.^2$) were measured reliably (i.e., within 5 percent). Based upon this break point between the accuracy of the 0.0006 m^2 (1 $in.^2$) and 0.0026 m^2 (4 $in.^2$) objects it was concluded the methodology described above was capable of accurately measuring spill areas to within 0.0026 m^2 (4 $in.^2$).

APPENDIX D – TABULATED HEAT FLUX DATA

Table D.1. Heat Fluxes Measured in Pan Fire Scenarios

Test ID	Pan Size	Equiv. Dia.	Fuel	Fuel Depth	Substrate	Heat Flux (kW/m^2)						
						4 R	2 R	1 R	Center above Fuel	0.5 R above Water	0.5 R above Fuel	Center above Water
PF25	0.30	0.34	Gasoline	1	Water	2	3	5	51	33	54	
PF1B				1	Water	2	3	5	53	20	46	
PF2				5	Water	3	6	12	58	40	65	
PF26				5	Water	3	5	9	58	37	64	
PF27				10	Water	3	5	9	55	43	65	
PF3				10	Water	3	6	11	57	1	63	
PF4				20	Water	3	7	13	55	37	62	
PF28				20	Water	3	6	12	54	37	60	
PF49				1	Steel	1	3	4	48	44	45	
PF73				1	Steel	1	3	4	48	48	42	
PF73A				1	Steel	1	3	6	48	37		
PF49B				1	Steel	1	3	6	41	39		
PF50				5	Steel	3	5	9	62	65	59	
PF74				5	Steel	3	6	10	61	62	61	
PF50A				5	Steel	3	6	15	65	38		
PF74A				5	Steel	3	7	14	65	34		
PF51A				10	Steel	3	7	14	53	7		
PF75A				10	Steel	3	6	14	50	7		
PF51				10	Steel	3	6	11	62	64	57	
PF75				10	Steel	3	6	10	62	63	60	
PF52				20	Steel	3	6	11	61	59	50	
PF76				20	Steel	3	5	10	62	59	64	
PF52A				20	Steel	3	6	13	48	2		
PF76A				20	Steel	3	6	13	49	2		
PF13	0.30	0.34	Kerosene	1	Water	1	1	2	8	27	29	
PF37				1	Water	0	1	1	18	32	16	
PF14				5	Water	2	4	6	57	38	58	
PF38				5	Water	3	5	9	59	47	60	
PF39				10	Water	2	5	8	56	45	65	
PF15				10	Water	2	4	10	57	46	63	
PF16				20	Water	4	5	6	55	49	64	
PF40				20	Water	2	5	8	53	48	61	
PF61				1	Steel	1	1	2	39	44	36	
PF85				1	Steel	1	1	2	41	41	35	

Test ID	Pan Size	Equiv. Dia.	Fuel	Fuel Depth	Substrate	Heat Flux (kW/m^2)						
						4 R	2 R	1 R	Center above Fuel	0.5 R above Water	0.5 R above Fuel	Center above Water
PF61A				1	Steel	0	1	1	12	46		
PF85A				1	Steel	0	1	1	14	42		
PF62A				5	Steel	2	5	10	62	20		
PF86A				5	Steel	2	5	11	62	18		
PF62				5	Steel	2	5	8	56	60	73	
PF86				5	Steel	3	5	9	56	60	76	
PF63				10	Steel	3	5	9	56	58	69	
PF87				10	Steel	4	5	6	57	57	69	
PF63A	0.30	0.34	Kerosene	10	Steel	2	5	10	63	6		
PF87A				10	Steel	2	5	10	65	7		
PF64				20	Steel	2	6	16	59	53	71	
PF88				20	Steel	2	5	8	58	54	66	
PF64A				20	Steel	2	5	11	58	3		
PF88A				20	Steel	2	5	10		3		
PF99	0.31	0.34	Heptane	20	Steel	2	5	10		3		
PF5				1	Water	2	5	9	42	33	62	38
PF29				1	Water	2	5	9	28	29	74	41
PF30				5	Water	4	9	14	43	30	76	43
PF6				5	Water	4	9	16	26	31	71	42
PF7				10	Water	4	10	18	12	27	74	45
PF31				10	Water	4	11	20	14	41	68	46
PF8				20	Water	6	14	40	67	30	69	51
PF32				20	Water	6	16	44	64	29	66	48
PF77				1	Steel	2	4	7	86	53	65	74
PF53	0.61	0.69	Gasoline	1	Steel	2	4	5	81	48	65	73
PF53A				1	Steel	2	4	7	82	34	70	50
PF77A				1	Steel	2	5	7	84	36	70	52
PF78A				5	Steel	4	10	19	65	55	77	59
PF54A				5	Steel	4	10	19	93	57	71	62
PF54				5	Steel	4	8	14	101	60	72	82
PF78				5	Steel	4	9	14	96	58	71	72
PF79A				10	Steel	4	10	20	92	58	70	64
PF55A				10	Steel	4	10	19	85	53	72	65
PF55				10	Steel	4	9	14	90	53	72	69
PF79				10	Steel	4	9	16	94	143	74	0

Test ID	Pan Size	Equiv. Dia.	Fuel	Fuel Depth	Substrate	Heat Flux (kW/m^2)						
						4 R	2 R	1 R	Center above Fuel	0.5 R above Water	0.5 R above Fuel	Center above Water
PF80				20	Steel	6	14	35	96	43	74	61
PF56				20	Steel	6	16	40	95	43	76	59
PF41				1	Water	1	1	2	60	44	53	39
PF18				5	Water	3	6	12	66	38	77	54
PF42	0.61	0.69	Kerosene	5	Water	3	6	11	63	32	77	48
PF19				10	Water	4	9	16	52	35	72	50
PF43				10	Water	3	8	12	63	32	75	48
PF20				20	Water	7	13	37	68	31	70	44
PF65				1	Steel	1	2	2	77	43	62	54
PF89				1	Steel	1	2	3	45	46	69	59
PF66				5	Steel	3	7	12	94	55	72	62
PF90				5	Steel	3	8	12	94	48	73	67
PF67	0.61	0.69	Kerosene	10	Steel	4	8	14	86	60	76	65
PF91				10	Steel	4	9	17	83	56	75	57
PF68				20	Steel	6	15	40	89	58	65	66
PF92				20	Steel	6	17	44	94	63	67	66
PF20A				20	Water	6	13	31	70	45	-	60
PF57				1	Water	4	8	12	58	80	57	88
PF81				1	Water	4	8	12	64	81	55	94
PF109				2	Water	5	11	17	49	87	36	52
PF115				2	Water	5	11	18	55	78	56	23
PF110				3	Water	5	12	18	51	74	48	28
PF116				3	Water	6	12	19	53	19	49	91
PF117				4	Water	5	12	18	63	79	52	96
PF111				4	Water	6	13	20	52	78	53	91
PF112	1.22	1.38	Gasoline	5	Water	6	14	21	53	89	46	104
PF82				5	Water	6	14	21	56	81	50	90
PF121				5	Water	6	13	21	56	73	40	85
PF60				20	Water	6	16	30	90	82	101	102
PF84				20	Water	7	17	31	85	85	103	105
PF72				1	Steel	3	7	10	63	74	79	92
PF123				1	Steel	3	6	9	63	72	63	87
PF96				5	Steel	6	15	26	69	76	95	97
PF122				5	Steel	6	14	26	80	89	95	102

Test ID	Pan Size	Equiv. Dia.	Fuel	Fuel Depth	Substrate	Heat Flux (kW/m^2)						
						4 R	2 R	1 R	Center above Fuel	0.5 R above Water	0.5 R above Fuel	Center above Water
PF69	1.22	1.38	DA	1	Steel	0	1	1	32	38	26	26
PF93				1	Steel	0	1	1	32	35	32	33
PF58				2	Steel	1	1	2	40	42	31	37
PF118				2	Steel	1	1	2	42	41	35	29
PF113				3	Steel	1	2	2	46	44	47	41
PF119				3	Steel	1	1	2	41	36	38	38
PF114				4	Steel	1	1	2	43	47	37	46
PF120				4	Steel	1	2	2	35	46	43	44
PF70				5	Steel	1	2	2	43	48	44	47
PF94				5	Steel	1	2	2	46	46	44	45

Table D.2. Heat Fluxes Measured in Diked Fire Scenarios

Test ID	Pan Size	Equiv. Dia.	Fuel	Fuel Depth	Substrate	Heat Flux (kW/m^2)				
						4 R	2 R	1 R	Center	0.5 R
DSF25	0.31	0.34	Gasoline	1	Vinyl	2	4	6	40	39
DSF26				5	Vinyl	3	7	14	11	27
DSF27				10	Vinyl	3	6	12	13	6
DSF28				20	Vinyl	4	9	20	2	2
DSF1				1	Concrete	1	1	2	36	15
DSF2				5	Concrete	3	6	11	45	20
DSF3				10	Concrete	2	6	11	19	7
DSF4				20	Concrete	2	6	10	2	1
DSF29	0.31	0.34	Kerosene	1	Vinyl	2	6	11	63	52
DSF30				5	Vinyl	3	6	15	26	12
DSF31				10	Vinyl	3	7	13	8	7
DSF32				20	Vinyl	3	7	14	4	3
DSF5				1	Concrete	1	2	3	64	45
DSF6				5	Concrete	3	6	12	29	14
DSF7				10	Concrete	3	6	10	10	5
DSF8				20	Concrete	2	5	7	3	2
DSF33	0.61	0.69	Gasoline	1	Vinyl	4	9	19	72	55
DSF34				5	Vinyl	4	10	22	79	48
DSF35				10	Vinyl	4	10	21	-	-
DSF36				20	Vinyl	4	11	25	4	3
DSF9				1	Concrete	2	3	6	59	50
DSF10				5	Concrete	4	10	25	74	52
DSF11				10	Concrete	5	10	24	21	21
DSF12				20	Concrete	5	11	28	8	12
DSF37	0.61	0.69	Kerosene	1	Vinyl	4	8	16	89	61
DSF38				5	Vinyl	4	8	17	-	-
DSF39				10	Vinyl	4	8	16	13	9
DSF40				20	Vinyl	4	8	17	5	4
DSF13				1	Concrete	1	2	4	69	41
DSF14				5	Concrete	4	9	23	90	43
DSF15				10	Concrete	4	8	18	13	15
DSF16				20	Concrete	4	9	20	5	4
DSF41	1.22	1.38	Gasoline	1	Vinyl	4	10	16	94	145
DSF42				2	Vinyl	6	13	23	85	155
DSF43A				3	Vinyl	6	17	34	103	133
DSF44				4	Vinyl	7	17	31	121	131

Test ID	Pan Size	Equiv. Dia.	Fuel	Fuel Depth	Substrate	Heat Flux (kW/m^2)				
						4 R	2 R	1 R	Center	0.5 R
DSF45				5	Vinyl	7	17	33	89	142
DSF46				20	Vinyl	7	19	37	102	106
DSF17				1	Concrete	3	9	15	72	83
DSF18				2	Concrete	5	12	22	65	75
DSF19	1.22	1.38	Gasoline	3	Concrete	6	15	27	75	81
DSF20				4	Concrete	7	17	32	80	102
DSF21				5	Concrete	7	17	33	71	104
DSF22				20	Concrete	7	18	34	77	95

Table D.3. Heat Fluxes Measured in Spill Fire Scenarios

Test ID	Substrate	Fuel	Qty. (L)	Spread Time (s)	Spill Area (m^2)	Equiv. Dia. (m)	Heat Flux (kW/m^2)							
										Embedded				
							4 R	2 R	1 R	Loc 1	Loc 2	Loc 3	Loc 4	Loc 5
SFD136	Coated Concrete	Gasoline	0.5	0	0.52	0.82	0	0	0	0	0	0	0	0
SFD89A				30	0.61	0.88	1	2	3	68	60	38	6	3
SFD89B				30	0.62	0.89	1	2	4	73	66	22	7	5
SFD91				30	0.62	0.89	1	2	3	68	65	16	5	3
SFD89				30	0.65	0.91	1	2	4	73	66	34	5	3
SFD21				300	0.69	0.94	1	1	2	70	67	38	3	1
SFD1				300	0.72	0.96	0	1	2	63	48	6	2	1
SFD100				300	0.77	0.99	1	1	2	63	69	46	10	4
SFD21A				300	0.82	1.02	1	1	2	70	64	46	4	2
SFD3			1	30	1.11	1.19	2	4	9	65	72	53	15	9
SFD2				30	1.17	1.22	1	3	7	66	70	56	14	9
SFD95				30	1.37	1.32	2	4	7	75	64	52	11	6
SFD96				30	1.41	1.34	2	4	7	85	64	45	10	5
SFD22				150	1.89	1.55	1	3	5	70	54	14	7	6
SFD22A				300	1.77	1.50	0	1	3	52	58	45	8	7
SFD23				300	1.81	1.52	1	2	4	57	57	43	9	13
SFD11		Kerosene	0.5	0	**LOCALIZED OR NO IGNITION OBSERVED**		0	0	1	44	63	32	2	1
SFD31				0			0	0	1	58	51	35	2	1
SFD11				300			0	0	1	38	62	10	3	1
SFD11A				300			0	0	0	2	45	27	2	0
SFD93		Heptane	0.5	30	0.87	1.05	1	2	4	83	72	18	6	4
SFD94				30	0.91	1.08	1	2	3	76	67	29	5	3
SFD78				300	0.98	1.12	0	1	2	47	55	48	33	4
SFD73				300	1.06	1.16	0	1	2	36	54	55	28	7
SFD139				300	1.10	1.18	0	1	3	51	51	16	8	11
SFD78A				300	1.12	1.19	1	1	3	55	62	36	8	3
SFD74			1	30	1.30	1.29	2	5	12	87	84	56	48	32
SFD119				30	1.33	1.30	2	5	12	83	90	62	49	37
SFD79				300	1.90	1.56	1	2	4	49	42	18	15	22
SFD121				300	1.92	1.56	1	2	5	52	45	15	8	7
SFD79A				300	1.94	1.57	1	1	3	54	57	15	7	4
SFD92		DA	0.5	30	0.57	0.85	0	0	0	29	26	1	0	0
SFD90				30	0.59	0.86	0	0	0	29	27	1	0	0
SFD16				300	0.84	1.04	0	0	0	30	36	15	1	0
SFD36				300	0.84	1.03	0	0	0	33	41	29	1	0

Test ID	Substrate	Fuel	Qty. (L)	Spread Time (s)	Spill Area (m^2)	Equiv. Dia. (m)	Heat Flux (kW/m^2)							
										Embedded				
							4 R	2 R	1 R	Loc 1	Loc 2	Loc 3	Loc 4	Loc 5
SFD36B	Coated Concrete	DA	1	300	0.86	1.05	0	0	0	19	33	2	1	1
SFD36A				300	0.87	1.05	0	0	0	28	26	19	1	0
SFD18			1	30	1.06	1.16	0	0	1	35	34	31	4	9
SFD17			1	30	1.09	1.18	0	0	1	32	35	35	24	3
SFD38			1	300	1.78	1.51	0	0	0	21	35	2	1	1
SFD37			1	300	1.79	1.51	0	0	0	18	33	2	1	2
SFD140	Smooth Concrete	Gasoline	0.5	30	0.86	1.05	1	1	3	NO HEAT FLUX DATA RECORDED				
SFD122			0.5	30	0.89	1.06	1	1	3					
SFD142			0.5	300	0.93	1.09	0	0	0					
SFD124			0.5	300	0.96	1.11	0	0	1					
SFD141			1	30	1.57	1.41	2	3	7					
SFD123			1	30	1.61	1.43	2	3	7					
SFD83	Brushed Concrete	Gasoline	0.5	30	0.67	0.92	0	1	3	NO HEAT FLUX DATA RECORDED				
SFD134			0.5	30	0.69	0.93	0	1	3					
SFD136			0.5	300	0.52	0.82	0	1	2					
SFD86			0.5	300	0.88	1.06	0	1	2					
SFD84			1	30	1.28	1.28	1	2	5					
SFD135			1	30	1.28	1.28	1	2	5					
SFD87			1	300	1.45	1.36	0	1	3					
SFD137			1	300	1.48	1.37	0	1	3					
SFD49	Carpet/ Pad/ Plywood	Gasoline	0.5	30	0.20	0.51	0	0	1	1	1	0	1	0
SFD55			0.5	30	0.22	0.53	0	0	1	0	1	0	1	0
SFD56			1	30	0.22	0.53	1	1	3	0	1	1	3	2
SFD50			1	30	0.22	0.52	0	1	2	11	57	10	2	1
SFD50A			1	30	0.22	0.53	0	1	3	NO HEAT FLUX DATA RECORDED				
SFD56A			1	30	0.24	0.56	0	1	3					
SFD152			1	300	0.21	0.52	0	1	3					
SFD51			5	30	0.38	0.69	2	5	13					
SFD57			5	30	0.39	0.70	2	5	13					
SFD58		Kerosene	0.5	30	0.20	0.51	0	1	1	1	1	0	1	0
SFD52			0.5	30	0.21	0.51	0	1	1	1	1	0	1	1
SFD53			1	30	0.23	0.54	1	1	3	0	1	0	0	0
SFD59			1	30	0.23	0.54	0	1	3	NO HEAT FLUX DATA RECORDED				
SFD53A			1	30	0.24	0.55	0	1	3					
SFD54			5	30	0.39	0.70	2	5	11					
SFD60			5	30	0.41	0.72	2	5	12					

Test ID	Substrate	Fuel	Qty. (L)	Spread Time (s)	Spill Area (m^2)	Equiv. Dia. (m)	Heat Flux (kW/m^2)							
										Embedded				
							4 R	2 R	1 R	Loc 1	Loc 2	Loc 3	Loc 4	Loc 5
SFD141A	Carpet/ Concrete	Gasoline	1	30	0.22	0.53	0	1	2	**NO HEAT FLUX DATA RECORDED**				
SFD63	Vinyl	Gasoline	0.5	30	0.56	0.85	1	3	7	53	67	36		
SFD61	Vinyl	Gasoline	0.5	30	0.59	0.87	2	4	7	56	68	25		
SFD67			0.5	300	0.99	1.12	0	0	0	0	0	0	0	0
SFD157			0.5	300	1.04	1.15	0	0	0	0	0	0	0	0
SFD62A			1	30	1.25	1.26	2	5	10	58	60	17	8	5
SFD66			1	30	1.32	1.30	2	5	11	62	71	32	11	8
SFD68			1	150	1.89	1.55	2	4	8	75	69	10	7	6
SFD69			1	167	1.81	1.52	2	5	9	71	41	14	6	5
SF156		Kerosene	0.5	30	0.50	0.80	1	3	6	91	69	35		
SFD64			0.5	30	0.52	0.81	1	3	6	64	78	42		
SFD65		DA	1	30	1.08	1.17	0	1	1	48	38	3	1	0
SFD115	Vinyl	DA	1	30	1.11	1.19	0	0	1	43	34	1	1	0
SFD117			1	300	1.28	1.28	0	0	1	53	8	1	0	0
SFD71			1	300	1.32	1.30	0	0	1	43	6	1	0	0
SFD126	OSB	Gasoline	0.5	30	0.53	0.82	0	0	0	**NO HEAT FLUX DATA RECORDED**				
SFD130			0.5	30	0.53	0.82	0	0	0					
SFD127			0.5	30	0.70	0.95	0	0	0					
SFD131			0.5	30	0.71	0.95	0	0	0					
SFD150		Kerosene	0.5	30	0.47	0.77	1	2	5	**NO HEAT FLUX DATA RECORDED**				
SFD154			0.5	30	0.49	0.79	1	3	7					
SFD151			0.5	30	0.54	0.83	1	2	5					
SFD153			0.5	30	0.55	0.84	1	2	5					
SFD128		DA	0.5	30	0.55	0.84	0	0	0	**NO HEAT FLUX DATA RECORDED**				
SFD132			0.5	30	0.57	0.85	0	0	1					
SFD133			0.5	30	0.63	0.90	0	0	1					
SFD129			0.5	30	0.65	0.91	0	0	1					
SFD41	Plywood	Gasoline	0.5	30	0.46	0.76	2	4	8	55	52	33	–	
SFD42			0.5	30	0.51	0.81	1	3	6	43	58	35		
SFD44		Kerosene	0.5	30	0.42	0.73	1	2	4	55	68	29	–	
SFD43			0.5	30	0.43	0.74	1	2	5	66	77	35		
SFD46		DA	0.5	30	0.45	0.76	0	0	1	24	23	39	–	
SFD45			0.5	30	0.49	0.79	0	0	1	21	24	9		